CHARACTERISATION OF RELA DYNAMICS IN PANCREATIC DUCTAL ADENOCARCINOMA

Francesca Butera

The Institute of Cancer Research

The University of London

A thesis submitted for the degree of Doctor of Philosophy

2022

Declaration

I, Francesca Butera, declare that the work presented in this thesis is my own. Where information has been derived from other sources, or work has been performed by or with assistance from others, I confirm that this has been indicated in the thesis.

Abstract

The NF-κB transcription factor RELA is a master regulator of the immune response and cell survival. Numerous studies have determined the parameters and configuration of single cell RELA translocation dynamics, with various cell types displaying oscillations in RELA localisation. Nonetheless, single cell RELA dynamics in Pancreatic Ductal Adenocarcinoma (PDAC) cells are uncharacterised, even though RELA is constitutively active in PDAC and RELA is a prognostic marker for poor survival. Additionally, the Bakal lab has shown that RELA localisation is regulated by cell shape, but the mechanistic basis is unknown.

Using live imaging of CRISPR-CAS9 fluorescently tagged RELA, I characterised single cell endogenous RELA responses in two human PDAC cell lines in response to TNFα levels physiologically relevant to PDAC. PDAC cells responded atypically and with high sensitivity to TNFα, as RELA dynamics are sustained, non-oscillatory and cell cycle independent. Remarkably, single cells with higher RELA nuclear localisation are more likely to undergo TNFα-induced cell death, adding complexity to prior understanding of RELA as a pro-survival factor.

To pinpoint the molecular mechanism of cell shape control of RELA, I incorporated measures of geometry and cytoskeletal proteins into Bayesian network models and identified actin dynamics as a source of heterogeneity in RELA translocation with TNFα. Using small molecule inhibitors, I discovered that the nucleation of actin stress fibres and branched actin function in RELA responses to TNFα.

I then used RNA sequencing and Co-IP with protein mass spectrometry to identify effectors and interactors of RELA in PDAC. Notably, RELA significantly upregulates the non-canonical NF-κB pathway, as well as the actin regulators ARHGAP31 and NUAK2. Furthermore, I found evidence that negative feedback by IκBβ and ε govern RELA dynamics in PDAC cells.

Finally, I characterised RELA responses to reovirus infection, in combination with PARP inhibition based on a screen result, providing the first temporal resolution of single cell RELA responses to oncolytic viruses. PDAC cells responded to the reovirus T3D with continuous RELA dynamics while melanoma cells displayed a switch-like response. Moreover, cells with high RELA nuclear localisation with reovirus infection underwent cell death. Notably, PARP inhibition enhanced reovirus-induced RELA nuclear translocation and cell death.

These discoveries confirm RELA hyperactivity in PDAC on the single cell level and identify positive feedback loops between RELA and actin, in addition to perturbation of negative feedback, as underlying mechanisms. I also provide evidence that elevated RELA nuclear localisation is associated with cell death in multiple immune-related settings.

Acknowledgements

Growing up, I had no clear indication of what path to take in life. Until, at the age of 18, I first stepped into a lab (in this case in the ageing research department at King's College London) and felt that I had entered a marvellous world of wonder, creativity, and innovation. I have felt very fortunate to maintain that feeling and to be able to pursue my interests in science and call it a career. I am thankful for the opportunity to learn about what makes us human, the chance to test out my ideas, and the potential to discover something new.

I thank my supervisor Chris Bakal for hiring me as a wide-eyed undergraduate and seeing the potential in me for a PhD. Thank you for sharing your passion for science across diverse fields and for showing me the beauty and value of microscopy.

Thank you to Silvia Santos and Roy Wollman for examining my PhD and providing invaluable feedback to improve my thesis and scientific approach.

To my colleagues in the Bakal lab, thank you for making the past 4+ years exciting and for helping me to persevere through the stressful times, while being ready with a bottle of prosecco in times of celebration. I am grateful for all of your input into my work and our day-to-day scientific (and casual!) discussions. You have been a joy to work with.

Thank you to Kevin Harrington for your support and for allowing me to contribute to your lab's incredible work on oncolytic viruses. Your faith in your team's work and its translation into the clinic are inspirational.

To the strong women past and present in the ICR who have mentored me: Alexis Barr*, Julia Sero, Vicky Bousgouni, Chloe Simpson, Patricia Pascal-Vargas, Mar Arias Garcia, Louise Evans, Jo Kyula, and Vic Roulstone. Thank you for teaching me how to be driven while kind. You have and always will be great role models to me.

*who very generously supervised me during my undergraduate placement year and taught me how to culture cells, perform molecular biology techniques, and generate cell lines. A massive thank you!

I owe a great deal of gratitude to Lucas Dent, who has imparted countless hours to helping and teaching me. Your altruism, dedication to science, and never-ending capacity motivate me to be a better scientist. You will make a wonderful team leader.

I gratefully acknowledge Cancer Research UK for funding this project and the many discoveries improving lives across the world. Thank you to the Institute of Cancer Research for hosting my PhD and everyone in the ICR community (scientific and support) for your support and sharing of ideas.

A particular thank you to my wonderful collaborators Theo Roumeliotis, Jo Kyula and Vic Roulstone. Theo - thank you for performing the proteomics experiments and for patiently walking through the statistical analysis with me. Jo and Vic - thank you for your positive attitudes and for teaching me about viruses.

I am grateful to Vicky Bousgouni, Lucas Dent, Melina Beykou and Matt De Vries for comments on my thesis, and to Tencho Tenev, Kai Betteridge and Ian Jones for advice on my project.

To my friends and my brother Rai, thank you for being there for me and keeping me going through the years.

Most of all, I thank my parents for their unconditional love and support.

Abbreviations

Abbreviation	Full word	Abbreviation	Full word
5-FU	5-Fluorouracil	LPS	Lipopolysaccharide
ACTN4	Alpha-actinin-4	LT-β	Lymphotoxin β
ADM	Acinar to ductal metaplasia	MACF1	Microtubule actin cross-linking factor
AI	Artificial intelligence	MAL	Myelin and lymphocyte protein
ALPK1	Alpha-protein kinase 1	MAPK	Mitogen-activated protein kinase
AP1	Activator protein 1	mDIA	Diaphanous
ARC	Activity-regulated cytoskeleton-associated protein	MEF	Mouse embryonic fibroblast
ARF	ADP-ribosylation factor	MHC	Major histocompatibility complex
ARHGAP31	Rho GTPase activating protein 31	MLC	Myosin light chain
ARP2/3	Actin related protein 2/3	MLKL	Mixed lineage kinase domain-like protein
AUC	Area under curve	MS	Mass spectrometry
BCL-XL	B-cell lymphoma-extra large	MT	Microtubule
BCL2/3	B-cell lymphoma 2/3	MTOC	Microtubule organising center
BCR	B cell receptor	Nab	Nanoparticle albumin-bound
BID	BH3 interacting domain death agonist	NDUFA4	NDUFA4 Mitochondrial Complex Associated
BIRC3	Baculoviral IAP repeat-containing protein 3	NEMO (IKKγ)	NF-κB essential modulator (IκB kinase gamma)
Blebb	Blebbistatin	NES	Nuclear export signal
BMDM	Bone marrow derived macrophage	NF-κB	Nuclear factor kappa B
BSA	Bovine serum albumin	NIK	NF-κB-inducing kinase
C/EBP	CCAAT/enhancer binding proteins	NLS	Nuclear localisation signal
CAPE	Caffeic acid phenethyl ester	NOXA	Phorbol-12-myristate-13-acetate-induced protein 1
CAR	Chimeric antigen receptor	NPC	Nuclear pore complex
CAS9	CRISPR associated protein 9	NSAID	Non-steroidal anti-inflammatory drugs
CASP3/8/9/10	Caspase 3/8/9/10	NUAK2	NUAK family kinase 2
CBP	CREB-binding protein	OIS	Oncogene induced senescence
CD137 (4-1BB)	Cluster of differentiation 137	OV	Oncolytic virus
CD19	Cluster of differentiation 19	P4HA1	Prolyl 4-hydroxylase subunit alpha 1
CD28	Cluster of differentiation 28	PAM	Protospacer adjacent motif
CD3ζ	Cluster of differentiation 3 zeta	PAMP	Pathogen associated molecular pattern
CDC42	Cell division cycle 42	PARP	Poly (ADP-ribose) polymerase
CDK	Cyclin-dependent kinase	PBS	Phosphate-buffered saline

CDKN2A	Cyclin dependent kinase inhibitor 2A	PCA	Principal component analysis
cFLIP	Cellular FLICE (FADD-like IL-1β-converting enzyme)-inhibitory protein	PCNA	Proliferating cell nuclear antigen
ChIP	Chromatin immunoprecipitation	PD1	Programmed cell death protein 1
Chk1	Checkpoint kinase 1	PDAC	Pancreatic ductal adenocarcinoma
Co-IP	Co-immunoprecipitation	PF228	PF573228
COX2	Cyclooxygenase 2	PFA	Paraformaldehyde
CRISPR	Clustered regularly interspaced short palindromic repeats	PKA	Protein kinase A
CTLA4	Cytotoxic T-lymphocyte-associated protein 4	PKR	Protein kinase R
CXCL1/2	C-X-C motif chemokine ligand 1/2	PMA	Phorbol 12-myristate 13-acetate
Cyto D	Cytochalasin D	Poly(I:C)	Polyinosine:polycytidylic acid
DAAM	Disheveled-associated activator of morphogenesis	PRKDC	Protein kinase DNA-activated catalytic subunit
DAMP	Damage-associated molecular pattern	PRR	Pattern recognition receptors
DC	Dendritic cell	PTX	Paclitaxel
dCTP	Deoxycytidine triphosphate	PUMA	p53 upregulated modulator of apoptosis
Defact	Defactinib	RAC1	Ras-related C3 botulinum toxin substrate 1
Dem	Demecolcine	Ran	Ras-related nuclear protein
DLBCL	Diffuse large B-cell lymphoma	RANKL	Receptor activator of nuclear factor kappa-B ligand
DMEM	Dulbecco's modified eagle medium	RANTES	Regulated on activation, normal T cell expressed and secreted
DMSO	Dimethyl sulfoxide	RB	Retinoblastoma
DNAH1/3	Dynein axonemal heavy chain 1/3	RFP	Red Fluorescent Protein
DR4/5	Death receptor 4/5	RHA	Right homology arm
E2F	E2 factor	RHD	Rel homology domain
EBV	Epstein-Barr virus	RIGI	retinoic acid-inducible gene I
ECM	Extracellular matrix	RIPK1/3	Receptor-interacting serine/threonine-protein kinase 1/3
EGF	Epidermal growth factor	RLR	RIG-I-like receptor
EGFR	Epidermal growth factor receptor	RNA-FISH	RNA fluorescence in situ hybridization
EIF3B	Eukaryotic translation initiation factor 3 subunit B	RNAi	RNA interference
EMSA	Electrophoretic mobility shift assay	ROCK	Rho-associated kinase
EMT	Epithelial-to-mesenchymal	RT3D	Reovirus type 3 Dearing

	transition		
ER	Endoplasmic reticulum	SLC25A	Solute carrier family 25
FA	Focal adhesion	SMAC	Second mitochondria-derived activator of caspases
FADD	FAS-associated death domain protein	SMAD4	Mothers against decapentaplegic homolog 4
FAK	Focal adhesion kinase	SNAI2	Snail family transcriptional repressor 2
FBS	Fetal bovine serum	SOX9	SRY-box transcription factor 9
FdUMP	Fluorodeoxyuridine monophosphate	SQSTM1 (p62)	Sequestosome 1
FdUTP	Fluorodeoxyuridine triphosphate	SRF	Serum response factor
FMN1/2	Formin 1/2	STAT	Signal transducer and activator of transcription
FOXO	Forkhead box class o	t-SNE	t-distributed stochastic neighbor embedding
FP	Fluorescent protein	TAD	Transactivation domain
FUCCI	Fluorescent ubiquitination-based cell cycle indicator	TAK1	Transforming growth factor beta-activated kinase 1
FUTP	Fluorouridine triphosphate	TAM	Tumour associated macrophages
GAP	GTPase activating protein	TBK1	TANK-binding kinase 1
GAPDH	Glyceraldehyde 3-phosphate dehydrogenase	TCI	Time course inspector
GDP	Granosine diphosphate	TCR	T cell receptor
GEF	Guanine nucleotide exchange factor	TGF	Transforming growth factor
GFP/eGFP	Green fluorescent Protein/enhanced green fluorescent protein	TIMM23B	Translocase of inner mitochondrial membrane 23 homolog B
GTP	Granosine triphosphate	TIMMDC1	Translocase of inner mitochondrial membrane domain containing 1
H/RS	Hodgkin/Reed-Sternberg (lymphoma)	TLR4	Toll-like receptor 4
HAT	Histone acetyltransferase	TNFAIP3 (A20)	TNF alpha induced protein 3
HDAC	Histone deacetylase	TNFR1	Tumor necrosis factor receptor 1
HSV1	Herpes simplex virus 1	TNFRSF1A	Tumour necrosis factor receptor superfamily member 1A
IAP	Inhibitor of apoptosis protein	TNFα/TNF-a	Tumour necrosis factor α
ICR	Institute of Cancer Research (London, UK)	TNPO1	Transportin1
IF	Immunofluorescence	TOMM40	Translocase of outer mitochondrial membrane 40
IFN	Interferon	TP53	Tumour protein 53
IKK	IκB kinase	TRADD	TNFR1-associated death domain
IL	Interleukin	TRAF2/3	TNF receptor associated factor 2/3

IRAK1/4	Interleukin 1 receptor associated kinase 1/4	TRAIL	Tumour necrosis factor-related apoptosis-inducing ligand
IRF	Interferon regulatory factor	TS	Thymidylate synthase
IκB	Inhibitor of nuclear factor kappa B	TUFM	Tu Translation Elongation Factor, Mitochondrial
IκB-SR	Inhibitor of κB super repressor	UBR4	Ubiquitin protein ligase E3 component n-recognin 4
JAM-A	Junctional adhesion molecule A	VEGF	Vascular endothelial growth factor
KLF4	Krüppel-like factor 4	Vin	Vinblastine
KRAS	Kirsten rat sarcoma viral oncogene homolog	WNT	Wingless-related integration site
L1CAM	L1 cell adhesion molecule	WT	Wild-type
LED	Light emitting diode	YAP	Yes associated protein
LHA	Left homology arm	ZEB1/2	Zinc finger E-box-binding homeobox 1/2
lncRNA	Long non-coding RNA		

Chapter Outline

List of Figures

Chapter 1

Chapter 3

Chapter 4

Chapter 5

Chapter 6

List of Tables and Appendices

Tables

Appendices

Chapter 1: Introduction

1.1 NF-κB transcription factors

1.1.1 Overview - members, structures, and interactions

The nuclear factor kappa B (NF-κB) family of transcription factors are master regulators of the stress response, with hundreds of target genes involved in a broad spectrum of processes, including cell death (Antwerp et al., 1996; Barkett and Gilmore, 1999), proliferation (Zhang et al., 2004; Li et al., 2014), senescence (Lesina et al., 2016) and differentiation (Liou et al., 2013; Stein and Baldwin, 2013; Sero et al., 2015). NF-κB transcription factors also play multiple roles within the immune system, in particular lymphoid organogenesis (Caamaño et al., 1998; Alcamo et al., 2002), pathogen recognition (Alcamo et al., 2001; Alexopoulou et al., 2001), and inflammatory responses (Yang et al., 1998; Miagkov et al., 1998; Chen et al., 2003; Monaco et al., 2004).

NF-κB transcription factors are expressed in all mammals and *Drosophila* but are absent in *C. elegans* and yeast (Steward, 1987; Pujol et al., 2001; Wang et al., 2006; Gilmore, 2006; Gilmore and Wolenski, 2012). NF-κB proteins were discovered by Ranjan Sen and David Baltimore in 1986 from a mobility shift assay identifying nuclear factors binding to the heavy- and κ light-chain enhancers. NF-κB was found to have strong binding affinity to the enhancer of the immunoglobulin κ light-chain gene in B cells but not in the other tested cell lines (Sen and Baltimore, 1986). Nonetheless, NF-κB proteins have since been reported as not specific to B cells nor critical regulators of the κ light chain gene, since NF-κB knockout B cells can produce κ light-chain containing antibodies. In addition, the intronic κ enhancer, which contains the NF-κB binding site, is not necessary for the production of κ light chain-containing antibodies (Xu et al., 1996; Hoffmann and Baltimore, 2006). The presence of cytoplasmic NF-κB in unstimulated conditions was also discovered (Baeuerle and

Baltimore, 1988a), in addition to cytoplasmic NF-κB inhibition by a protein called Inhibitor of nuclear factor kappa B (IκB) (Baeuerle and Baltimore, 1988b).

There are five NF-κB transcription factors: RELA (p65), RELB, REL (c-REL), NF-κB1 (p105) and NF-κB2 (p100) (Wilhelmsen and Temin, 1984; Ghosh et al., 1990; Schmitz and Baeuerle, 1991; Ryseck et al., 1992). p50 and p52 are the processed forms of phosphorylated p105 and p100 respectively (Blank et al., 1991; Rivière et al., 1991; Mercurio et al., 1993). NF-κB family members function as homodimers and heterodimers, with most combinations detected and all combinations believed to exist under certain conditions (Nolan et al., 1991; Ghosh et al., 2012). However, the heterodimer containing RELA and p50 is the best characterised, ubiquitously expressed, and functions in the canonical NF-κB pathway, which is described in Section 1.1.2 (Kunsch et al., 1992; Ramsey et al., 2019; Gilmore and Wolenski, 2012). For these reasons, the RELA:p50 heterodimer is commonly referred to as NF-κB.

RELA, RELB, REL, p50 and p52 harbour a common Rel Homology domain (RHD): a 300 amino acid domain that contains sequences essential for dimerisation, nuclear import, and DNA binding to sequences in the promoters of target genes termed ‘κB’ sites (Ghosh et al., 1990; Kieran et al., 1990; Nolan et al., 1991; Ryseck et al., 1992). κB sites are around 10 bp in length and are diverse in sequence with the consensus ‘5'-GGGRNYYYCC-3', where R is a purine; Y is a pyrimidine; and N is any nucleotide (Chen et al., 1998). Another crucial component of NF-κB structure is the C-terminal transactivation domain (TAD), which is present in RELA, RELB and REL but not p52 and p50. (Schmitz and Baeuerle, 1991; Ryseck et al., 1992; Martin and Fresno, 2000). Therefore, RELA, RELB and REL need to be present in an NF-κB dimer for the dimer to be transcriptionally active. Consequently, p50-p50 and p52-p52 homodimers typically repress transcription (Cheng et al., 2011). In addition to the TAD, RELB requires an N-terminal leucine zipper domain for activation (Dobrzanski et al., 1993). IκB molecules are a subfamily of the large Ankyrin Repeat Domain superfamily, with 5-7 ankyrin repeats that mediate interaction with the RHD of NF-κB proteins to prevent

NF-κB nuclear translocation (Jacobs and Harrison, 1998). p105 and p100 also have ankyrin repeats and can function as IκB proteins before proteolytic processing (Fan and Maniatis, 1991).

The most C-terminal region of the RHD (~100 amino acids) is responsible for dimer formation, with each subunit of an NF-κB dimer providing a symmetrical β-strand element that combine to form a β-sheet at the interface, with approximately 12 side chains per subunit mediating contact (Ghosh et al., 1995; Huxford et al., 1998). There are 15 possible combinations of NF-κB subunits for homo or heterodimers, though certain combinations occur more frequently, in particular the RELA:p50 and the RELB:p100 heterodimers (Hoffmann et al., 2006). Subunits also bind with different affinities, for instance, the RELA:p50 heterodimer interface is stronger than that of either homodimer (Chen et al., 1998). Interestingly, subunit specificity is not significantly correlated with the sequence of κB binding sites, suggesting that dimer selection is not due to the κB sequence alone. This was shown by Hoffmann et al. by generating cell lines with deficiencies for NF-κB proteins (either single or multiple knockouts) and assaying endogenous gene expression following exposure to the cytokine Tumour Necrosis Factor α (TNFα), which identified the contribution of each subunit to target gene expression (Hoffmann et al., 2003). Nonetheless, studies have looked into the binding site preferences of different NF-κB subunits and identified general preferences in terms of target sequence length. One study identified that p50 has an affinity for 11 bp sites while RELA and REL select for 10 bp sites (Kunsch et al., 1992). Another study identified that RELA:p50 dimers bind to 10 bp and 11 bp sequences with similar affinities and 10-fold more strongly than RELA or c-REL homodimers, which themselves bind with high affinity to 9 bp sequences (Phelps et al., 2000).

NF-κB proteins are known to co-operate with and, in some cases, directly bind to other transcription factors to regulate target gene expression, including IRFs (Tong et al., 2016), STATs (Yang et al., 2007; Lee et al., 2009), C/EBPs (Stein et al., 1993a), AP1 members (Stein et al., 1993b), and p53 (Webster and Perkins, 1999). NF-κB proteins also recruit

non-specific chromatin modifiers to aid transcriptional activation. Histone acetyltransferase complexes (HATs) and histone deacetylases (HDACs) regulate the addition and removal of acetyl residues to lysines of histones respectively, where lysine acetylation is associated with active transcription (Allfrey et al., 1964; Bannister and Kouzarides, 1996; Taunton et al., 1996). NF-κB factors are particularly associated with the HAT CBP/p300 (Berghe et al., 1999) and HDACs 1 and 2 (Ashburner et al., 2001), which in turn impact NF-κB-directed gene transcription. κB target sequences (Leung et al., 2004) and the phosphorylation status of NF-κB subunits (Zhong et al., 1998, 2002) affect which cofactors interact with the NF-κB dimer bound to a target gene. Finally, NF-κB factors can interact with atypical IκB proteins such as Bcl3 and IκBζ, which are reported to act as anti-repressors of p50 and p52 homodimers (Bours et al., 1993; Yamamoto et al., 2004).

1.1.2 The canonical and non-canonical NF-κB signalling pathways

There are two major NF-κB signalling pathways, referred to as ‘canonical’ and ‘non-canonical’ (Figure 1.1). The canonical NF-κB pathway is responsive to most physiological NF-κB stimuli, including the potent activators TNFα, interleukin 1 (IL1), and lipopolysaccharide (LPS) (Bonizzi and Karin, 2004). Meanwhile, selective stimuli activate the non-canonical pathway, including some TNFα family cytokines like lymphotoxin-β (Dejardin et al., 2002) and the costimulatory molecule CD40 on B cells (Hömig-Hölzel et al., 2008). Moreover, there are only a few identified functions of the non-canonical pathway, with the best-studied role in lymphoid organogenesis (Siebenlist et al., 2005)

Figure 1.1

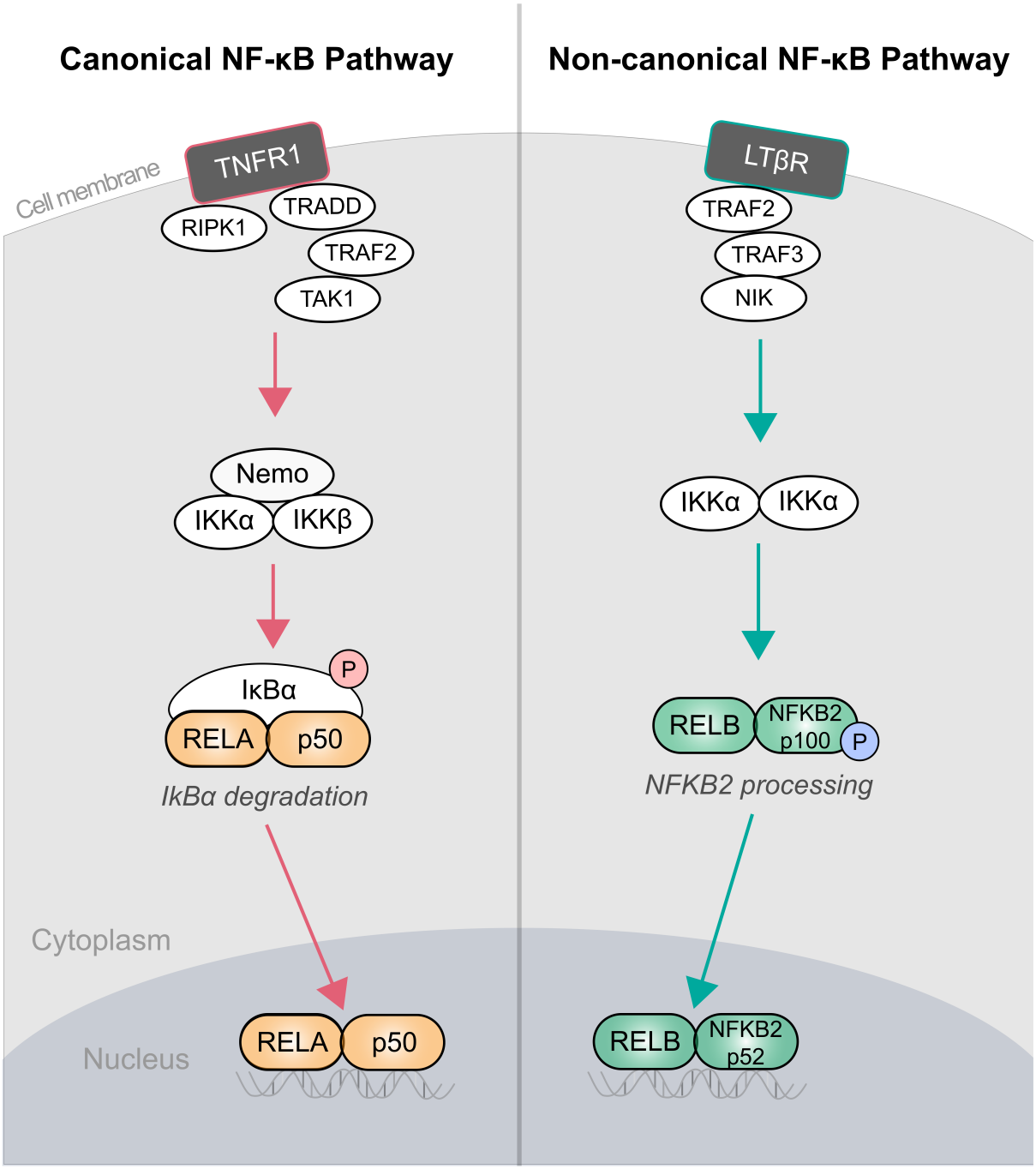
Canonical NF-κB Pathway
Non-canonical NF-κB Pathway
Cell membrane
TNFR1
RIPK1
TRADD
TRAF2
TAK1
Nemo
IKKα
IKKβ
IκBα
P
RELA
p50
IkBα degradation
LTβR
TRAF2
TRAF3
NIK
IKKα
IKKα
RELB
NFKB2
p100
P
NFKB2 processing
Cytoplasm
Nucleus
RELA
p50
RELB
NFKB2
p52

Figure 1.1 Canonical and non-canonical NF-κB signalling pathways

In the canonical NF-κB pathway (left of figure), RELA:p50 heterodimers are sequestered in the cytoplasm by IκBα in basal conditions. TNFα ligand binding to its receptor stimulates the assembly of a multimeric complex (TRADD, FADD - not shown, TRAF2, RIPK1 and TAK1). TAK1 phosphorylates and activates the IKK complex consisting of two catalytic subunits IKKα and IKKβ with the regulatory subunit NEMO (also known as IKKγ). The IKK complex phosphorylates IκBα, targeting IκBα for degradation via the proteasome and releasing the RELA:p50 complex. Free RELA:p50 translocates to the nucleus where it binds to DNA at κB sites to regulate target gene transcription. In the non-canonical NF-κB pathway in unstimulated conditions, RELB is in a complex with p100, which acts as an IκB protein holding the complex in the cytoplasm. Activation of the non-canonical pathway (right of figure) occurs by select stimuli, including LT-β, which stimulates NIK phosphorylation and activation of an IKK complex of two IKKα subunits, which in turn phosphorylate p100 to trigger its cleavage into p52. The RELB:p52 heterodimer is then able to translocate to the nucleus.

The canonical NF-κB signalling pathway involves the NF-κB heterodimer RELA:p50 (Baeuerle and Baltimore, 1989). In basal conditions, RELA:p50 is actively exported from the nucleus and sequestered in the cytoplasm by IκBα, which masks the nuclear localisation signal (NLS) of RELA and other NF-κB proteins (Arenzana-Seisdedos et al., 1997; Beg et al., 1992). One well-understood route for canonical NF-κB pathway activation is through TNFα binding to its receptor, leading to the formation of a multimeric complex including the adaptor protein TRADD, the kinase RIPK1, and the ubiquitin ligase TRAF2 (Kelliher et al., 1998; Micheau and Tschopp, 2003). This receptor complex recruits the IκB kinase (IKK) complex, consisting of IKKα, IKKβ, and NEMO/IKKγ in the canonical NF-κB pathway (Mercurio et al., 1997; Rothwarf et al., 1998). IKKβ is then phosphorylated and activated by TAK1, a member of the MAPK protein kinase family (Wang et al., 2001). Activated IKK complexes phosphorylate IκBα proteins, leading to ubiquitination and degradation of IκBα via the proteasome (Chen et al., 1995; DiDonato et al., 1997). IκBα removal exposes the NLS of the NF-κB heterodimer, which enters the nucleus and regulates target gene transcription (Latimer et al., 1998).

The non-canonical pathway is dependent on the kinase NIK, which is regulated by TRAF3 and TRAF2 (Vallabhapurapu et al., 2008). NIK phosphorylates and activates an IKK complex consisting of two IKKα subunits, which phosphorylate p100 (*NFKB2*) associated with RELB. p100 is then processed into p52, generating the transcriptionally competent RELB:p52 complex (Senftleben et al., 2001a; Xiao et al., 2001).

1.1.3 RELA nuclear import and export

The nuclear envelope has nuclear pore complexes (NPCs) through which import and export systems transport large molecules (> 40 kDa) including RELA and p50, which each have a classical arginine and lysine-rich NLS that bind to importin α/β heterodimers (Fagerlund et al., 2005). In basal conditions, IκBα limits RELA nuclear translocation by masking the NLS of RELA (Beg et al., 1992), while IκBα degradation and subsequent NLS exposure enable

initial binding of importin α3 and α4 proteins to the NLS, followed by recruitment and binding of importin-β to transport the RELA:p50 heterodimer through NPCs (Fagerlund et al., 2005). The GTPase Ran supplies the energy for nuclear transport. In the nucleus, importin-bound Ran-GDP is converted to Ran-GTP, which triggers dissociation of importin-β from RELA and results in free RELA that can bind to DNA (Görlich et al., 1996). Nuclear RELA can be ubiquitinated and degraded via the proteasome (Saccani et al., 2004) or exported from the nucleus. The latter involves binding of newly synthesised IκBα to RELA and removal of RELA from gene promoters, followed by binding of exportin-1 to RanGTP and the nuclear export signal (NES) of IκBα in complex with RELA (Brown et al., 1993; Scott et al., 1993; Sun et al., 1993; Richards et al., 1997; Huang et al., 2000; Kashyap et al., 2016). After the passage of exportin with its cargo through NPCs into the cytoplasm, RanGTP is hydrolysed to RanGDP by RanGAP, thus stimulating cargo release (Dahlberg and Lund, 1998).

1.1.4 Post-translational modifications of RELA

Protein phosphorylations are mediated by protein kinases that transfer a phosphate to the hydroxyl group of serine, threonine or tyrosine on a target protein. In the case of RELA, phosphorylations predominantly affect transactivation. Two important phosphorylations for RELA activity occur on serine 276 (S276) and serine 536 (S536). S276 is in the RHD of RELA and is predominantly phosphorylated by Protein Kinase A (PKA) (Zhong et al., 1997, 1998), but is a target of multiple other kinases including MSK1 and MSK2 (Vermeulen et al., 2003; Jacks and Koch, 2010). S276 phosphorylation occurs in response to IκBα degradation since the catalytic subunit of PKA is masked by the IκBα:RELA complex (Zhong et al., 1997). S276 phosphorylation is involved in coactivator recruitment to target gene promoters, as phosphorylation causes a conformational change in RELA that enhances interaction with CBP/p300 and enables acetylation of K310 on RELA, which impacts transcriptional specificity (Zhong et al., 1998; Buerki et al., 2008). Meanwhile, S536 is located in the TAD of RELA and is mediated by multiple kinases, including TBK1 and the IKKs α, β and ε (Sakurai

et al., 1999; Buss et al., 2004a). Similar to S276, S536 phosphorylation increases CBP/p300 binding and K310 acetylation of RELA, however, S536 is not associated with IκBα degradation but may promote RELA nuclear translocation (Sasaki et al., 2005). Other characterised phosphorylation sites on RELA include threonine 254, which controls IκBα binding (Ryo et al., 2003), and serine 468, which is involved in negatively regulating basal RELA activity (Buss et al., 2004b).

1.1.5 RELA and the immune system

The immune system encompasses the interconnected innate and adaptive responses. The innate response is a rapid response to pathogens and involves soluble factors, including cytokines and chemokines, and several effector cell types, such as macrophages, dendritic cells (DCs), and natural killer (NK) cells. In contrast, adaptive immunity develops more slowly and is mediated by CD4+ (helper, effector, regulatory and memory) T cells and CD8+ (cytotoxic) T cells (reviewed by Dranoff, 2004). The adaptive response is subdivided into the humoral and cell-mediated immune responses. Humoral immunity is characterised by B cell antibody production and the formation of immunologic memory (Slifka et al., 1998). Humoral immunity requires helper T cells to promote B cell differentiation to produce neutralising antibodies against specific antigens (Parker, 1993). Meanwhile, cellular immunity focuses on the elimination of pathogens that invade intracellularly and culminates in cytotoxic T cell destruction of infected cells (Dennert and Lennox, 1972).

NF-κB signalling is involved in the development and homeostasis of hematopoiesis - the generation of the lymphoid, myeloid and granulocytic lineages. Myeloid stem cells give rise to macrophages, neutrophils, basophils, mast cells and eosinophils, while the common lymphoid progenitor gives rise to T cells, B cells and NK cells. DC cells can arise from either myeloid or lymphoid lineage (Hayden et al., 2006). Neutrophils, eosinophils and basophils are also referred to as granulocytes as they harbour protein-containing granules key to their function (Borregaard and Cowland, 1997). Notably, RelA knockout mice are embryonic lethal

so the role of RelA in hematopoiesis in adult animals needs to be studied by other means, typically involving the use of non-degradable IκBα (IκB-SR), or through rescue of murine RelA or IKKβ knockout by deletion of TNFα or the TNFα receptor (Beg et al., 1995a; Hayden et al., 2006). Interestingly, p50-deficient mice are not embryonic lethal but have immune deficiencies and are particularly susceptible to infection (Sha et al., 1995).

RELA is responsive to diverse stimuli attached to the innate immune system, including pattern recognition receptors (PRRs) such as toll-like receptors and RIG-I-like receptors (Medzhitov and Janeway, 1997). Cells expressing PRRs detect microbial components called pathogen-associated molecular patterns (PAMPs), in addition to detecting damage-associated molecular patterns (DAMPs), which are released by damaged and necrotic tissues (Scaffidi et al., 2002; El Mezayen et al., 2007). In response to PAMPs and DAMPs, macrophages become activated and secrete diverse cytokines and chemokines, many of which are regulated by NF-κB, including TNFα, IL-1β, IL-6, IL-8 and IL-12 (Collart et al., 1990; Libermann and Baltimore, 1990; Hiscott et al., 1993; Kunsch and Rosen, 1993; Murphy et al., 1995).

In the innate immune response, NF-κB signalling regulates the development of multiple cell types, including DCs and granulocytes. A body of research has shown that DC development depends on canonical NF-κB signalling, with a particular study finding that RelA/p50 double knockout mice lack CD8a+ and CD8a- DCs, with other DC lineages reportedly unaffected (Wang et al., 2007). Meanwhile, the CD8a- subset of DCs are believed to rely on RELB (Wu et al., 1998). NF-κB inhibition also downregulates expression of MHC class II and B7 co-stimulatory molecules in DC cells (McLellan et al., 2000; Yoshimura et al., 2001). In mature granulocytes, RELA promotes homeostasis through anti-apoptotic signalling (Beg et al., 1995b), while RELA appears to function in the protection of neutrophils from apoptosis specifically during the inflammatory response (François et al., 2005).

In the adaptive immune system, NF-κB signalling functions during several stages of lymphopoiesis. Out of all NF-κB signalling molecules, the generation of mature lymphocytes is most severely disrupted by single knockout of the IKK complex subunit NEMO (Schmidt-Supprian et al., 2000). However, combined loss of p52 and p50 or RelA and c-Rel disrupts lymphopoiesis at early stages in mice (Franzoso et al., 1998; Grossmann et al., 1999). Moreover, lymphocytes in the bone marrow and the thymus are selected in an NF-κB dependent process reliant on apoptosis. The selection of CD4+CD8+ T cells depends on the ability of their T cell receptor to recognise peptide:MHC complexes presented on antigen-presenting cells, which are largely dendritic cells. The presence and strength of this interaction determine which T cells are selected (Hayden et al., 2006). Notably, T cells with too high affinity interactions are also removed as this occurs when T cells bind self peptide:MHC - the hallmark of autoimmunity (Maynard et al., 2005). RELA is a downstream effector of both the T cell receptor (TCR) and B cell receptor (BCR), which converge on IKK activation and IκBα degradation (Khoshnan et al., 2000; Weil et al., 2003; Shinohara et al., 2005). RELA functions in the positive selection of T cells through induction of antiapoptotic genes and is also believed to promote apoptosis as a part of negative selection, following high affinity TCR ligation (Hettmann et al., 1999; Mora et al., 2001). Furthermore, upon activation, CD4+ T cells differentiate into different subsets of effector T cells, including Th1 and Th2 among others, and NF-κB signalling functions in CD4+ T cell differentiation through cytokine production and T-cell intrinsic methods (Zhu et al., 2010). In particular, the T cell subtype Th1 requires RELA and c-Rel expression (Aronica et al., 1999; Hilliard et al., 2002), while Th2 responses involve p50 (Das et al., 2001). Conversely, NF-κB signalling functions in the development of T regulatory cells, which suppress the immune response to prevent autoimmunity and are generated with thymocyte development or with CD4+ T cell differentiation (Sakaguchi et al., 1995). Mice deficient in the murine equivalents of TAK1, IKK and the IKK-regulating signalling molecules CARMA1 and BCL10 have reduced T regulatory cell production (Barnes et al., 2009; Chang et al., 2015; Gückel et al., 2011; Yang et al., 2021).

In addition to T cells, NF-κB factors regulate the selection of B cells, as shown by the impaired humoral responses of mice deficient in any of the five NF-κB factors or those expressing IκB-SR in B cells (Bendall et al., 1999). In B cells, NF-κB functions as a pro-survival factor during negative selection, as immature B cells have constitutive NF-κB activity that is downregulated following BCR ligation (Wu et al., 1996). Interestingly, during B cell maturation there is a shift in RELA:p50 dimers to cREL:p50 dimers, which likely functions to alter NF-κB targets to those appropriate at each stage of B cell development (Liou et al., 1994).

Lastly, NF-κB signalling functions in the generation of primary lymphoid tissue (bone marrow and thymus) as well as secondary lymphoid tissues, which include the lymph nodes, Peyer's patches and the spleen. Early stages of lymphoid organogenesis involve an interaction between lymphotoxin α1β2-expressing hematopoietic cells and VCAM1-expressing stromal cells that initiates a positive feedback loop involving RELA-activating and RELA-induced cytokines, including lymphotoxin α1β2 itself, RANKL and TNFα (Iademarco et al., 1992; Jiang et al., 2003; Mouri et al., 2011; Yamashita and Passegué, 2019). In addition, double knockout mice for RelA and Tnfr1 lack Peyer's patches and lymph nodes, and have disordered spleens (Alcamo et al., 2002). The non-canonical NF-κB pathway also plays a prominent role in maintaining splenic architecture, as shown by mice deficient for NIK or RelB (Burkly et al., 1995; Kajiura et al., 2004).

1.2 Single cell RELA dynamics

1.2.1 Assays of NF-κB activity

Assessment of NF-κB activity can be approached by diverse biochemical and image-based methods (Figure 1.2A). The most direct assays of RELA activity use nuclear extracts and quantify DNA binding. In electrophoretic mobility shift assays (EMSA), also known as gel shift assays, solutions of nucleic acids and a protein of interest are combined and subjected

to electrophoresis to resolve protein-DNA complexes from free linear DNA, since protein-bound DNA has slower mobility compared to free DNA. DNA binding activity can also be assayed using luciferase reporters, whereby a luciferase gene is placed downstream of a promoter controlled by multiple κB binding sites and luminescence is quantified (for examples see Alexopoulou et al., 2001 [Figure 1A]; Arlt et al., 2003 [Figure 2B]; Turner et al., 2010 [Figure 1A]). Alternatively, the level of binding to specific genomic regions can be analysed by Chromatin Immunoprecipitation (ChIP) using a RELA antibody. EMSA and ChIP can be followed up with next generation sequencing for whole-genome analysis, or ChIP can be tested by qPCR with primers against promoters for target genes.

Figure 1.2

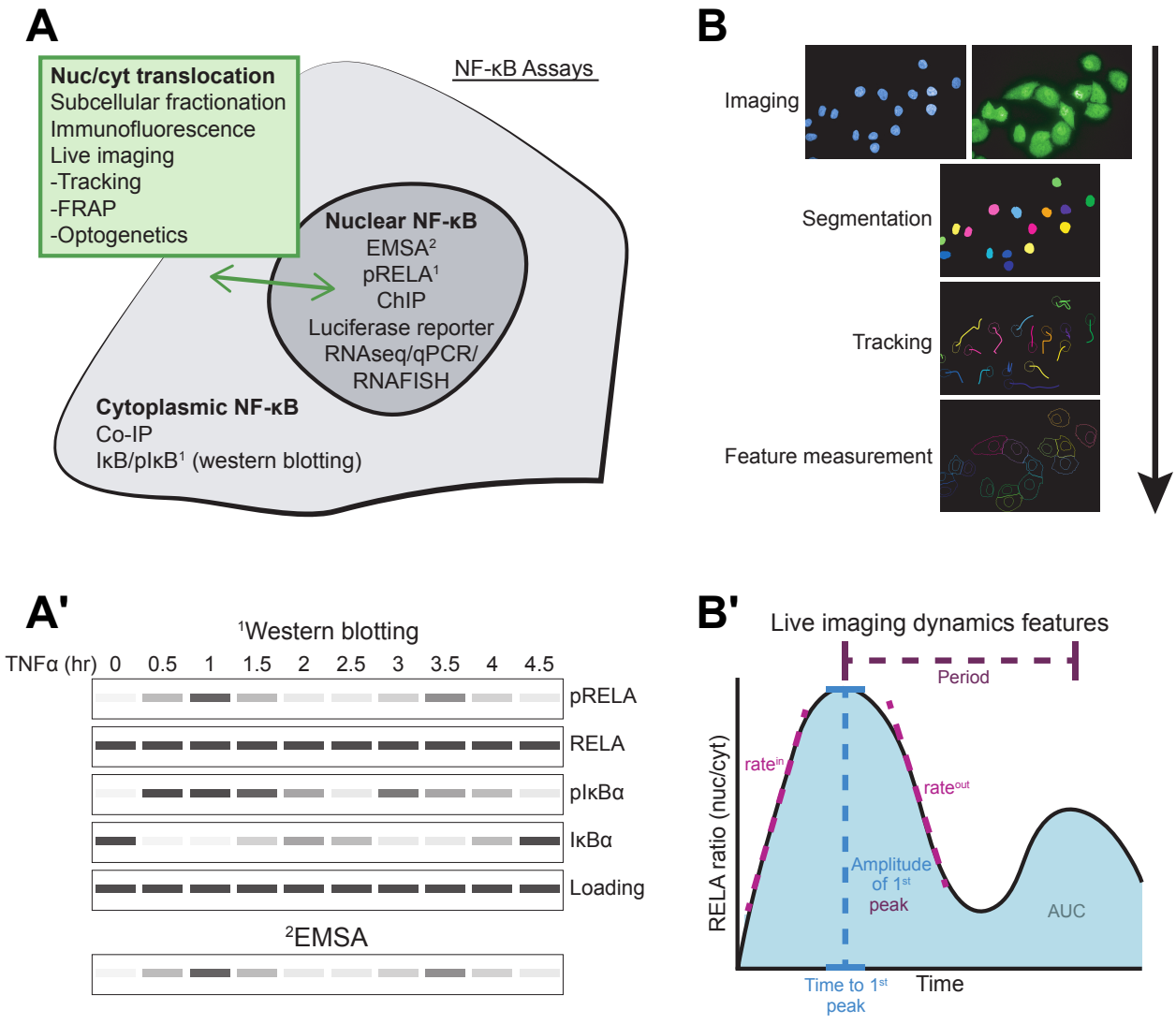
A
NF-κB Assays
Nuc/cyt translocation
Subcellular fractionation
Immunofluorescence
Live imaging
-Tracking
-FRAP
-Optogenetics
Nuclear NF-κB
EMSA2
pRELA1
ChIP
Luciferase reporter
RNAseq/qPCR/
RNAFISH
Cytoplasmic NF-κB
Co-IP
IκB/pIκB1 (western blotting)
B
Imaging
Segmentation
Tracking
Feature measurement
A'
1Western blotting
TNFα (hr) 0 0.5 1 1.5 2 2.5 3 3.5 4 4.5
pRELA
RELA
pIκBα
IκBα
Loading
2EMSA
B'
Live imaging dynamics features
Period
rate^in
rate^out
Amplitude of 1st peak
AUC
RELA ratio (nuc/cyt)
Time to 1st peak
Time
C
Categories of RELA translocation dynamics
Continuous TNFα
Continuous TNFα
Continuous TNFα
RELA ratio (nuc/cyt)
Time
RELA ratio (nuc/cyt)
Time
RELA ratio (nuc/cyt)
Time
1. Peak followed by damped oscillations
2. Peak followed by sustained oscillations
3. Single pulse

Figure 1.2 Common in vitro assays of NF-κB activity

(A) Types of assays to assess nuclear NF-κB levels (pRELA immunofluorescence or western blotting), DNA binding (EMSA, ChIP or luciferase reporter), or activation of target genes by RNA quantification (RNA-seq/RT-qPCR/RNA-FISH). Alternatively, cytoplasmic NF-κB can be assayed by Co-IP or measurement of the ratio of phosphorylated IκBα (a measure of IκBα degradation) to total IκBα and as a measure of NF-κB inhibition. The ratio of cytoplasmic to nuclear NF-κB localisation can be assayed using subcellular fractionation, immunofluorescence or live imaging with fluorescent reporters. (A') Schematic cartoon representation of a western blot of activated versus total RELA and phosphorylated IκBα versus total IκBα (top) and RELA EMSA (bottom) of simulated measurements are shown over time following cell stimulation with TNFα (e.g. 10 ng/ml). Peak RELA activation occurs ~1 hr after TNFα addition followed by oscillations in IκBα and activated RELA levels over time. The western blot is based on results from Nelson et al., 2004 (Figure 4D) and the EMSA from Hoffmann et al., 2002 (Figure 2E). (B) General pipeline for image-based assessment of NF-κB subcellular localisation. Fluorescently labelled nuclei in microscopy images are segmented and tracked using automated image analysis (e.g. using Fiji, Nuclitrack or CellProfiler). Features, including geometric and intensity measurements, are measured in the segmented regions on a single cell basis. (B') Commonly measured features of live RELA dynamics. (C) Categories of frequently observed RELA translocation dynamics in response to continuous TNFα stimulation. In all cases, peak RELA nuclear localisation occurs rapidly after TNFα addition. The most commonly observed RELA dynamics profile has damped oscillations of RELA nuclear localisation (1), while persistent RELA oscillations have also been observed (2). In a subset of cell types, RELA is transiently in the nucleus with a single pulse (3).

Using whole-cell extracts, RELA activity can be analysed using western blotting by comparing the level of pRELA (Ser536), which indicates IKK activity (Sakurai et al., 1999), against total RELA; or pIκBα (Ser32 or Ser36) against total IκBα, which informs on the proportion of IκBα targeted for degradation (Traenckner et al., 1995). Oscillations, a common profile of RELA dynamics discussed further in Section 1.2.2, were initially identified by EMSA (Hoffmann et al., 2002) then by western blotting for pRELA and RELA and live imaging (Nelson et al., 2004) (Figure 1.2A').

Most modern studies quantify cytoplasmic to nuclear RELA translocation as a measure of RELA activity. Although not commonly employed, assays can assess the population average subcellular RELA relocalisation response to stimuli using subcellular fractionation (Hayashi et al., 1993). However, a more popular approach is to assay RELA localisation with single cell resolution using immunofluorescence, or augmented further to include temporal resolution by using live imaging. Importantly, single cell assays have revealed wide interline and intraline heterogeneity in RELA responses to various cell stresses (Nelson et al., 2004; Sero et al., 2015; Martin et al., 2020). Analysis of RELA activity by subcellular localisation relies on the assumption that NF-κB factors are always inactive in the cytoplasm and more likely to be active when nuclear. However, live imaging may be carried out in concert with NF-κB activity luciferase reporters or measurement of target gene expression by RNA-seq or RNA Fluorescence In-Situ-Hybridization (RNA-FISH) to confirm NF-κB activity. A prime example of a combined live imaging and gene expression approach is by Lane et al. (2017), who live imaged p65-Clover in mouse macrophages treated with lipopolysaccharides and collected at three timepoints for transcriptome sequencing. Live imaging can also be combined with endpoint immunofluorescence, which has been upgraded by the development of the iterative indirect immunofluorescence imaging technique by Lucas Pelkman's lab (Gut et al., 2018), which has significantly elevated the ability to retest samples with antibodies.

Live translocation analysis has successfully been applied to multiple signalling molecules, including ERK (Santos et al., 2007), STAT1 (Mudla et al., 2020), FOXO3 (Sampattavanich et

al., 2018), p21 (Barr et al., 2017), and p53 (Batchelor et al., 2011). The field of single cell dynamics has revealed pivotal information about the configuration of molecule components, stimuli requirements, heritability, and cell cycle dependence of signalling pathways (Santos et al., 2007; Barr et al., 2017; Martin et al., 2020). In addition, live imaging can reveal the deregulation of various pathways in diseases and therefore suggest clinical vulnerabilities (Gerosa et al., 2020; Klomp et al., 2021). The majority of studies carry out single cell tracking using fluorescent markers but label-free approaches have also been developed (Edlund et al., 2021). Moreover, live imaging can be combined with light (optogenetics) (DeFelice et al., 2019) or chemically inducible promoters for temporal control of gene expression (Meylan et al., 2009), or FRAP for determining the diffusion kinetics of proteins of interest (Sung et al., 2009).

Optimisation of imaging techniques has shed light on several factors improving image quality and representation of wildtype conditions, balanced against limiting cell toxicity (Table 1.1). Furthermore, live imaging requires recapitulation of environmental conditions (temperature, humidity, and CO_2).

Table 1.1 Considerations for timelapse imaging

Tool	Benefits	Drawbacks
Endogenous tagging	Detection of target in natural genomic context	Weak signal, time to generate cell lines
Exogenous constructs	Stronger signal	Overexpression and associated perturbation of feedback loops
Lasers (versus LED)	More powerful (can pick up weaker signals)	Toxicity
Confocal microscopy (versus widefield)	Blocks out-of-focus light improving signal to noise	Signal can be weaker
Glass substrate (versus plastic)	Lower refractive index (clearer image)	Cost
Increasing the laser power and exposure time	Stronger signal	Photobleaching and toxicity

Far-red fluorescent proteins (versus GFP)	Less autofluorescence	Availability
Shorter time intervals	Easier to track cells	Photobleaching and toxicity
Phenol red-free medium	Reduced background fluorescence	Inability to detect pH changes
Microfluidics	Ability to refresh medium or expose cells to conditions (e.g. drug treatments) without disruption to imaging	Cost

The experiment itself and microscopy often account for a minor fraction of the time needed to carry out live dynamics assays, due to the necessity of several stages of post-imaging computational processing that can be computationally demanding. These stages include basic image processing (e.g. renaming, cropping, background subtraction), segmentation of cell regions, tracking of single cells, and measurement of quantitative features such as intensity and geometric measurements (Figure 1.2B). Remarkably, each stage is carried out by different laboratories in a bespoke manner, as there is no consensus on the optimal method for automated image analysis and many steps need to be modified according to the specific assay.

Image segmentation typically begins with delineating the borders of the nucleus, which are easier to segment compared to the whole cell due to more cell-to-cell consistency in shape and size, availability of strong nuclear markers (e.g. DAPI and Hoechst), and less likelihood of overlap between cells. Cell segmentation can then be obtained by propagation and expansion of the nucleus. In fixed images, the actin-binding dye phalloidin or antibody staining against α-tubulin are effective methods for consistently outlining the cell, as are the live imaging equivalents for actin and tubulin visualisation, such as Spirochrome's SiR-Actin and SiR-Tubulin. Fluorescent protein expression under a strong and constitutive promoter, such as the CMV promoter, can also be used for cell segmentation. Different types of segmentation algorithms, including clustering and probabilistic-based methods, have been

reviewed in detail by Nketia et al., 2017. From segmented nuclei, cells can be tracked over time when allowed for by the time intervals, the field of view, and cell mobility.

Currently, faithful tracking is the most challenging hurdle to overcome with live imaging analysis in the 2D realm. Tracking can be carried out manually using Fiji (Schindelin et al., 2012) or Ilastik's 'Manual Tracking' workflow (Berg et al., 2019), or automated with the opportunity to correct tracks, which is enabled by the Fiji plugin TrackMate (Tinevez et al., 2017), Nuclitrack (Cooper et al., 2017) and specific Ilastik workflows. Many labs have also developed custom MATLAB scripts for single cell tracking for RELA analysis (Selimkhanov et al., 2014; Kellogg and Tay, 2015; Lane et al., 2017; Martin et al., 2020). Nonetheless, new techniques employing deep learning with neural networks for object recognition are being rapidly developed and will dramatically expand the number of cells that can be tracked (Krizhevsky et al., 2017; Chen et al., 2021; Wen et al., 2021), thus removing one of the key limiting factors of live imaging assays.

There are a number of popular software platforms that combine segmentation and quantification, including Fiji (ImageJ), CellProfiler (Carpenter et al., 2006) and Columbus (PerkinElmer). From intensity measurements output from these programs, several time series features can be calculated, including peak amplitude, number of peaks, the time to peak, activity duration, oscillation frequency, oscillation period, maximal and mean rate of nuclear entry and exit, and the area under the curve (Figure 1.2B'). Time series data can also be analysed for non-classical features, as exemplified by Lubba et al. who reduced 4791 features to 22 time series signatures (implementable using 'catch22' software), including measurements of linear and non-linear autocorrelation, with the aim of optimising computational efficiency of time series analysis (Lubba et al., 2019).

The capacity and efficiency of information transmission is an established field in itself, in which dynamics features are assessed by how much information they hold - technically described in 'bits' - and how well they inform on phenotypes or gene expression. This may

consider the loss of information from receptors through RELA dynamics to gene expression, which is affected by noise and ligand specificity (Maity and Wollman, 2020). Information capacity appears to be context-dependent, for instance, in the human rhabdomyosarcoma cell line KYM1, AUC and the maximum fold-change harbour the highest transmission capacity (each around 1.4 bits) from RELA dynamics in response to TNFα (Zhang et al., 2017b). Meanwhile, gene expression correlates most strongly with murine RelA nuclear duration in both mouse macrophages and fibroblasts, as well as time to peak RelA in fibroblasts, across various NF-κB stimuli including LPS and Poly(I:C) (Martin et al., 2020). Furthermore, dynamic RELA responses to LPS have reduced noise-induced information loss compared to static RELA responses (Selimkhanov et al., 2014)

Notably, assays of RELA localisation may present the absolute nuclear abundance or, more often, the ratio of nuclear to cytoplasmic (or whole-cell) RELA. The advantage of the latter is providing an internal control on a cell-to-cell basis, which accounts for experimental differences in laser strength or the z plane being captured relative to the centre of the cell. This can be taken a step further by restricting the cytoplasmic measurement to the ring (perinuclear) region, which prevents signal disturbance due to overlapping between cells or cell differences in curvature. Furthermore, studies have found significant overlap in the distributions of nuclear RELA abundance between basal and TNFα-stimulated populations, suggesting that nuclear RELA abundance is insufficient to determine whether a specific cell has responded to TNFα (Cheong et al., 2011; Lee et al., 2014).

1.2.2 Profiles of RELA translocation dynamics in response to TNFα

Multiple studies have characterised single cell RELA dynamics in a plethora of cell types responding to TNFα. Notably, variation on the single cell level has been frequently identified, despite the use of genetically identical monoclonal populations (Kellogg and Tay, 2015). The major RELA dynamics profiles are summarised in Figure 1.2C.

Oscillatory RELA translocation patterns were the first described single cell RELA dynamics profile. Nelson et al. (2004) demonstrated these patterns using a cervical cancer cell line (HeLa) and a neuroblastoma cell line (SK-N-AS) transfected with RelA-dsRed. In response to 10 ng/ml TNFα, 97 % of SK-N-AS cells responded with 91 % displaying oscillations, while 86 % of HeLa cells responded with 30 % displaying oscillations. With both cell lines, oscillations were ‘damped’, whereby the first peak of RelA nuclear localisation has the highest amplitude and successive peaks have progressively decreasing amplitude (Nelson et al., 2004). A related study by Turner et al. (2010) using SK-N-AS cells transiently transfected with RelA-dsRed assayed RelA dynamics with lower TNFα doses. TNFα doses 100 pg/ml and above induced synchronous RelA nuclear translocation while intermediate TNFα dose (30 pg/ml) reduced synchrony in the time to nuclear translocation and reduced the amplitude of nuclear to cytoplasmic RelA. TNFα doses < 30 pg/ml further delayed initial RelA nuclear translocation, with RelA only translocating into the nucleus after 200 min TNFα exposure in several individual cells (Turner et al., 2010).

Similarly, a study by Tay et al., (2010) identified oscillations in RelA-/- 3T3 mouse fibroblasts expressing RelA-dsRed, under control of the endogenous mouse RelA promoter, and treated with 0.005-100 ng/ml TNFα. Higher concentrations (10 ng/ml) stimulated oscillations with successive peaks of equal amplitude and a time to first peak around 20 min, while lower concentrations showed damped RelA oscillations and a time to first peak around 50 min. In addition, Sero et al. (2015) identified damped RELA oscillations in MCF10A human breast epithelial cells stimulated with continuous 10 ng/ml TNFα. In MCF10A cells, peak RELA nuclear localisation occurs around 30 min after TNFα stimulation. Overall, RELA oscillations are observed in diverse cell types of human and mouse origin but the TNFα dose required for sustained oscillations appears to be cell-line specific. Moreover, TNFα dose appears to affect synchrony in RELA translocation between cells and also affects how rapidly RELA translocates to the nucleus relative to TNFα stimulation.

Sustained oscillations can also be achieved using pulsatile TNFα stimulation, which may be representative of the pulsatile exposure to inflammatory signals by cell neighbours (Ashall et al., 2009). Ashall et al. exposed SK-N-AS cells to 5 min TNFα pulses at various intervals. 200 min pulses induced sustained RELA oscillations with successive peaks of equal magnitude, while 100 min or 60 min intervals induced RELA oscillations with successive peaks having increasingly damped amplitude. Therefore, the timing of TNFα pulses affects whether oscillations are damped or sustained. Kellogg and Tay (2015) also identified that TNFα pulsing reduces variability in the oscillation period within cells. They showed that mouse 3T3 fibroblasts have oscillations out of sync and irregular periods in the presence of continuous TNFα. Meanwhile, 120 min TNFα pulses entrained the oscillations, resulting in periods between successive peaks, but 60 min TNFα pulses failed to entrain oscillations. Overall, TNFα pulsing reduces between-cell and within-cell variability depending on the matching of the timing of the pulse to the natural oscillatory periods.

Finally, some studies have identified that single cells can respond to TNFα with transient RELA nuclear localisation. For instance, a 30 ng/ml TNFα induces a rapid single pulse of RELA nuclear localisation in Jurkat T cells imaged for 250 min, with the first peak occurring 20-30 min after TNFα addition (Bagnall et al., 2015). Similarly, a study using a range of tumour cell types, including KYM1 and A549, imaged for 200-300 min with 0.01-50 ng/ml TNFα show a single pulse of RELA nuclear translocation in the average RELA tracks, although whether oscillations are present in individual tracks is unclear (Zhang et al., 2017b). A single pulse of RELA activity can also be induced by a single pulse of TNFα stimulation, as shown by Ashall et al. using a single 5 min pulse of TNFα with SK-N-AS and HeLa cells (Ashall et al., 2009).

Nonetheless, most research considering RELA dynamics has used exogenous RELA reporter constructs. However, select studies have assayed endogenous RELA using knock-in cells, with the advantage of retaining the natural genomic context of RELA, ensuring that all molecules are imaged, and eliminating artifacts due to RELA

overexpression. Oscillations in endogenous RELA were initially shown on the population level using EMSA and western blotting (Nelson et al., 2004). Similarly, oscillations have been shown with endogenous RELA on the single cell using live imaging. For instance, GFP-RelA knock-in MEFs display TNFα-induced asynchronous damped oscillations with 1-7 cycles, though a subset of cells display a single cycle followed by minor and irregular fluctuations (Sung et al., 2009). Using the same cell model, pulsed TNFα stimulation of 90 min periods were shown to induce synchronous oscillations close to the intrinsic period (Zambrano et al., 2016). Similarly, C-terminal fused RELA oscillates in response to TNFα in MCF7 breast cancer cells with intrinsic 90 min periods (Stewart-Ornstein and Lahav, 2016). Accordingly, endogenously tagged RELA in MEFs and MCF7 cells also display oscillations in nuclear localisation, indicating that this is an aspect of intrinsic RELA dynamics.

In summary, cell populations responding to TNFα display a mixture of RELA responses, with the majority of cells displaying damped oscillations. Nonetheless, all RELA translocation profiles show common rapid RELA nuclear translocation initiated immediately after TNFα addition and peaking around 30-60 min after TNFα stimulation, with TNFα doses 0.01 ng/ml and above. However, lower TNFα doses induce more delayed RELA nuclear translocation.

1.2.3 Profiles of RELA dynamics in response to LPS

Lipopolysaccharides are glycolipid macromolecules that are a major component of the outer membrane of gram-negative bacteria, such as *Escherichia coli* and *Salmonella*, providing structural support and protection from toxic molecules (Rietschel et al., 1994; Raetz and Whitfield, 2002). LPS recognition by human host cells is primarily mediated by the TLR4 pathway that can activate RELA nuclear translocation via TAK1 and IKK or by alternative pathways, with signalling generally converging on IκBα degradation (Kawai and Akira, 2007; Park et al., 2009).

Since both the outer carbohydrates and lipid A portions of LPS are variable (Heinrichs et al., 1998), Gutschow et al. were interested in whether LPS response depends on its source and

preparation. To this end, they looked at nuclear intensity changes of p65-dsRed under the endogenous mouse RelA promoter normalised to cytoplasmic intensity before LPS stimulation in mouse 3T3 fibroblasts, in response to three LPS preparations (Sigma, Invitrogen/EB and Ultrapure/UP) extracted from *E. coli* (Gutschow et al., 2013). In general, single cell RelA responses showed transient nuclear translocation and some cells showed oscillations, however, multiple differences were observed depending on LPS source. Sigma LPS stimulated longer nuclear localisation compared to EB and UP, while the time to peak nuclear localisation was longest for EB LPS stimulated cells. Gutschow et al. also tested 9 orders of magnitude in LPS concentration and found that Sigma and EB LPS induced murine RelA nuclear localisation at a wide range of concentrations, while UP LPS was ineffective at the lowest concentrations. Further testing identified that the difference in potency between the preparations is related to TNFα signalling, though the exact mechanism remains a source for further study. Therefore, LPS induces heterogeneous, transient and sometimes oscillatory single cell RelA nuclear translocation in mouse fibroblasts, with the parameters of RelA activation varying by LPS source.

A study in 2014 by Sung et al. focused on how LPS affects RELA activation in immune cells using quantitative live imaging of mouse macrophages. The results showed that 10 ng/ml LPS induced maximal nuclear RELA localisation by 1 hr post-stimulation followed by a decrease in RELA nuclear localisation to near basal levels by 5 hours post-stimulation. Interestingly, some cells sustained high levels of murine RelA abundance despite reduction in the ratio of nuclear to whole-cell RelA, suggesting an increase in the total amount of RelA over time. Further investigation found that LPS induces a positive feedback loop involving RelA activation of its own gene *RelA*, which was confirmed using Co-IP. Using genome-wide siRNA screening, Sung et al. identified that the transcription factor Ikaros is crucial for RELA positive feedback, with Ikaros found to also bind to the *RelA* promoter. Overall, Sung et al.'s findings show that increases in LPS dose promote a RELA positive feedback loop that

overcomes negative feedback between RELA and IκBα, enabling more sustained RelA activation in macrophages in response to LPS (Sung et al., 2014).

Single cell comparisons in RELA activation between LPS and TNFα stimulated cells were carried out by Kellogg et al. (2015) who tested the effects of changing LPS and TNFα dose and duration on RELA responses. They identified that the percentage of cells responsive to either stimulus was controlled by the stimulus integral (concentration and duration), signifying 'switch-like' activation of RELA that enables a robust response in the presence of noise in the stimulus. However, Kellogg et al. also found heterogeneity in the timing of RELA activation and level of target gene expression depending on the dose. Low LPS dose led to heterogeneous RELA responses, with median peak RELA nuclear localisation at 80 min post-stimulation. Consequently, low LPS dose stimulates delayed RELA nuclear translocation compared to high LPS dose, which had a median peak of 35 min after stimulation with a more homogenous response (Kellogg et al., 2015). Interestingly, Gutschow et al. noted that the inverse relationship between the peak amplitude of RELA nuclear intensity and time to peak previously observed with TNFα (Tay et al., 2010) is also present with LPS-stimulated cells when the source is Ultrapure, however, Sigma LPS maintained the same peak amplitude irrespective of time to peak (Gutschow et al., 2013).

Overall, LPS and TNFα both elicit heterogeneous single cell responses that are affected by stimulus dose and duration and are additionally determined by positive feedback loops with RELA and cytokine production and negative feedback loops with IκBα. However, RELA nuclear translocation appears to be more delayed and transient in LPS compared to TNFα, though both stimuli can induce oscillatory behaviour.

1.2.4 Encoding single cell RELA translocation dynamics

The signalling components dictating RELA responses have been elucidated by combining live cell imaging with high throughput single cell analysis, mathematical modelling, and genetic knockouts. The major determinants of RELA dynamics are the intrinsic RELA

inhibitor IκBα and RELA activating IKK proteins (Hoffmann et al., 2002; Nelson et al., 2002; Werner et al., 2005), while IκBε, IκBα and A20 are believed to fine-tune RELA responses (Hoffmann et al., 2002; Kearns et al., 2006; Werner et al., 2008). In addition, RELA activation is influenced by mechanical factors, including cell geometry, matrix stiffness, and actin and tubulin polymerisation (discussed in Section 1.2.6 and Section 4.1.5). Work by Neil Perkins and Mike White's groups, in particular, have also connected RELA responses to the cell cycle (Section 3.1.2).

The autoregulatory loop between RELA and IκBα was identified by studies in 1993 that described the cycle of TNFα-induced IκBα degradation and NF-κB activation followed by IκBα synthesis and NF-κB inhibition (Brown et al., 1993; Scott et al., 1993; Sun et al., 1993). A study by Nelson et al. (2002) explored the effect of expressing RELA-dsRed with or without IκBα-EGFP expression on RELA dynamics. Expression of both RELA and IκBα reduced IκBα degradation and increased RELA translocation compared to RELA-dsRed expression alone, suggesting that the ratio of IκBα to RELA influences RELA dynamics (Nelson et al., 2002)

In the same year, stochastic modelling linked the negative feedback loop between NF-κB and specifically the IκBα member of the IκB family with oscillations in NF-κB DNA binding assessed by EMSA (Hoffmann et al., 2002). This was deduced by the loss of NF-κB oscillations in IκBα knockout cells but the continued presence of NF-κB oscillations in IκBβ and IκBε double knockout cells. From mathematical modelling, the authors concluded that IκBα functions in rapid attenuation of RELA activity and induction of RELA oscillations, while IκBβ and IκBε reduce oscillatory potential and stabilise NF-κB binding during prolonged TNFα. This is supported by a further study revealing that NF-κB-induced IκBε transcription is delayed compared to IκBα (Kearns et al., 2006). Thus, IκB proteins play distinct roles in determining RELA dynamics. In addition, TNFAIP3/A20, a deubiquitinase that binds to and inactivates IKK, is implicated in damping the prolonged response of NF-κB activation but has no effect on the initial NF-κB response to TNFα (Werner et al., 2008).

In line with the findings above, a recent study identified that IκBα levels pre-TNFα stimulation affect the RELA response to TNFα (Patel et al., 2021). In this study, image-based machine learning was used to predict which cells will activate NF-κB (RELA:p50) in response to TNFα (0.005-5 ng/ml) and achieved this with 79.4 % accuracy. Nuclear RELA before stimulation (referred to as 'leaky' RELA localisation) was the most predictable feature for cell activation, though features of the histone marker H2B used for nuclear segmentation were also highly predictive. Moreover, the ratio of IκBα to NF-κB determined cell leakiness and subsequently the activation probability of cells. Interestingly, cells with high initial IκB levels required less TNFα for NF-κB activation, due to anti-correlation between the IκBα:NF-κB ratio and total IκBα level.

A study by Werner et al. (2005) also highlighted the link between IKK activity and NF-κB DNA binding by comparing cell responses to TNFα and LPS. TNFα induced rapid IKK activity and rapid NF-κB DNA binding, with IKK activity returning to baseline within 60 min of TNFα stimulation. Conversely, LPS induced delayed but more slowly attenuated IKK activity and NF-κB DNA binding. Accordingly, the majority of genes induced at late timepoints (8 hours post-stimulation) were more highly induced by LPS than TNFα, indicating that the timing of TNFα or LPS-induced gene expression corresponds to the timing of IKK activity.

1.2.5 Decoding single cell RELA translocation dynamics

Specificity in RELA transcriptional output is encoded by the parameters of RELA translocation dynamics. This is demonstrated by the presence of 'early', 'intermediate'/'middle' and 'late' groups of RELA target genes. These were first identified by Tian et al. (2005) by carrying out quantitative RT-PCR at 1, 3 and 6 hr post-TNFα stimulation and sorting 74 putative NF-κB dependent genes by the timepoint of their peak expression, with NF-κB binding confirmed by chromatin immunoprecipitation. The early group encodes several cytokines and negative regulators of NF-κB signalling, while the late group encodes cell surface receptors, signal adaptors, and adhesion molecules (Tian et al., 2005).

Work by Tay et al. (2010) linked the classes of temporally expressed TNFα-induced genes to RELA dynamics captured by live imaging under the same TNFα stimulation conditions. Using a set of 23 NF-κB targets, early genes were found to closely match NF-κB nuclear localisation dynamics due to rapid upregulation of gene expression followed by high degradation rates. In addition, early genes were found to have relatively constant expression across TNFα doses. On the other hand, late genes required high TNFα doses for expression and accumulated in expression over time. Similar to Tian et al., the RELA regulators *Nfkbia* (encoding IκBα) and *Tnfaip3* were identified as early genes, while Tay et al. additionally identified a subset of late genes involved in the regulation of apoptosis, suggesting that RELA only regulates apoptosis after persistent nuclear localisation (Tay et al., 2010).

Finally, work by Ashall et al. (2009) demonstrated the effect of pulsatile TNFα stimulation on RELA target gene expression. The classic early gene *NFKBIA* responded equally in expression to a single 5 min TNFα pulse to pulses with 60, 100 or 200 min intervals. Meanwhile, the late gene CCL5 (RANTES) has negligible expression with a 5 min TNFα pulse and increases in expression with higher frequency pulses, with maximal expression in the presence of continuous TNFα stimulation (Ashall et al., 2009). Therefore, RELA oscillation parameters have the greatest impact on the expression of late responding RELA target genes.

While prior studies carried out live imaging and qPCR under the same conditions and compared results, Lane et al. (2017) performed single cell RNA-seq on the same population of cells after live imaging, retaining cell identity to match RELA dynamics to gene expression. This study identified three distinct clusters of RELA dynamics in RAW264.7 cells in response to LPS and confirmed that the populations have distinct transcriptional profiles. Another study quantified RELA dynamics and the transcription of *IL8*, *TNFAIP3* (A20), and *NFKBIA* using single-molecule fluorescent in situ hybridisation in HeLa cells treated with TNFα. Gene transcription correlated more highly with the fold-change of nuclear RELA over time, in particular maximum fold-change (R^2 = 0.52-0.67), rather than nuclear RELA

abundance at any timepoint (R^2 = 0.15-0.3) (Lee et al., 2014). Therefore, descriptors of RELA dynamics correlate with RELA target gene expression.

To summarise, the fold-change in RELA activation over time correlates with RELA target gene expression, which can be classed into patterns of temporal expression. Early responding transcripts to RELA activation tend to be positive and negative regulators of RELA that maintain NF-κB pathway homeostasis and peak around 1 hr after TNFα stimulation. Meanwhile, late responding transcripts to TNFα are involved in more specific processes and build in abundance over time.

1.2.6 Mechanical regulation of RELA nuclear translocation

RELA nuclear translocation is regulated by a repertoire of mechanical properties including cell geometry, contractility, substrate stiffness, and shear stress. Sero et al., 2015 showed that geometric cues regulate RELA nuclear translocation downstream of TNFα in a panel of breast cancer lines. Cells with mesenchymal-type morphology, including flat and protrusive cell shape, were found to have high RELA nuclear localisation that is predicted to reinforce this mesenchymal cell shape, as RELA drives the expression of genes involved in the epithelial to mesenchymal transition (EMT) (Chua et al., 2007). Meanwhile, Sero et al. demonstrated that less spread cells with high neighbour contact, which is typical of epithelial morphology, have low RELA nuclear localisation that in turn suppresses EMT. Manipulation of cell shape using the chemical inhibitor of Rho-associated protein kinase (ROCK) Y27 or inhibition of tubulin with nocodazole alters cytoskeletal dynamics and, in turn, modulates RELA dynamics. In particular, the amplitude of RELA oscillation was enhanced and suppressed by Y27 and nocodazole respectively. Sero et al. also demonstrated that RELA activation is sensitive to extracellular matrix (ECM) stiffness, as breast cells seeded on glass or polyacrylamide gels of 16 kPa or 35 kPa Young's moduli have distinct cell morphology and higher RELA ratio with increased substrate stiffness. Thus, cell geometry and ECM stiffness affect RELA dynamics in breast cancer cells.

A related study by Sailem & Bakal used RNAi screening data in 18 breast cancer cells lines. To identify relationships between cell shape and gene expression, data were incorporated into multilinear regression models. Interestingly, RELA activity, tumour grade and patient survival could be predicted from cell shape parameters. Specifically, RELA response was predicted to be higher in basal and HER2 breast cancer tumours compared to luminal tumours and this was confirmed using IF. Their findings suggest that cell shape changes drive RELA activity that promotes breast cancer progression.

Similarly, a study analysed the effect of manipulating cell shape on TNFα and RELA induced gene expression (Mitra et al., 2017). To do this, they seeded NIH 3T3 fibroblasts on fibronectin micropatterns to attain cells with two mechanical states: 1) rectangles with an anisotropic and stretched shape with well-spread morphology and a high degree of actin polymerisation and myosin contractility; 2) circles with isotropic/symmetrical cell shape, relaxed and well-spread morphology, and a low degree of actin polymerisation and myosin contractility. 30 min stimulation of the two cell shape types with 20 ng/ml TNFα resulted in a significantly higher fold-increase in RELA nuclear localisation in circular cells compared to rectangular cells. Notably, Mitra et al. showed that TNFα induces geometry-dependent actin depolymerisation, which enhances IκBα degradation, and causes geometry-dependent changes in gene expression.

In addition to changes in gene expression, melanoma cells with different shapes have distinct RELA-regulated cytokine production, which is important for immune modulation in cancer. This was demonstrated in a study assaying cytokine production in the human melanoma cell lines A375P and A375M2 (Georgouli et al., 2019). A375M2 cells are derived from A375P and are highly metastatic melanoma cells with high myosin II activity and ~90 % of A375P have round morphology. In contrast, A375P cells are poorly metastatic and about 50 % of the population have rounded morphology, with the remaining having elongated cell shape. Georgouli et al. used a protein array of 274 human chemokines, growth factors and matrix metalloproteinases and identified 155 proteins that are highly secreted by A375M2

compared to A375P cells. Differences in the secretome were revealed to be dependent on cell contractility, as MLC2 or ROCK perturbation resulted in the reduction of cytokine and chemokine secretion by A375M2 cells. Following on from this, Georgouli et al. identified involvement of RELA activity in this model, as A375M2 melanoma cells have higher RELA nuclear localisation compared to A375P and depletion of MLC2 in A375M2 led to decreased pIκBα levels. Moreover, myosin II activity is involved in a positive feedback loop with IL-1 induced by RELA activation. Therefore, ROCK-myosin II activity in melanoma cells controls the production of immune molecules by RELA activation.

The effects of shear stress on RELA activation have also been investigated in a range of cell types. Shear stress refers to a force that is applied parallel to the surface of a cell. An example of shear stress in vivo is blood flow against the vascular endothelium. Culturing endothelial cells under shear stress was found to raise the production of cytoprotective transcripts, including Bcl-2, and reduced the transcript levels of pro-inflammatory cytokines such as IL-8 (Partridge et al., 2007). This emphasises how the impact of mechanotransduction on transcriptional output is gene-specific, allowing a single input to result in complex and coordinated responses. Partridge et al. also found that shear stress moderates the transcription of RELA targets involved in negative feedback loops (IκBα, IκBε and A20), which could affect the long-term translocation dynamics of RELA itself.

Shear stress and RELA activation have also been studied in bone maintenance. Mechanical stress is applied to the bone as a result of interstitial fluid moving across the membranes of osteoblasts and osteocytes (Robling and Turner, 2009). Focal adhesions are complexes connecting the ECM to intracellular signalling and have been studied as mechanotransducers of fluid shear stress in osteoblasts (Lee et al., 2017). Interestingly, Focal adhesion kinase (FAK), which regulates focal adhesion turnover, was found to be essential for RELA nuclear translocation in unstimulated osteoblasts exposed to fluid shear stress (Gerard-O'Riley et al., 2010). Therefore, mechanotransduction of shear stress may

lead to gene expression changes via alteration in RELA activity, which may contribute to bone homeostasis.

1.3 NF-κB and cancer

1.3.1 Overview - activation and functions of NF-κB in cancer

NF-κB transcription factors are upregulated in multiple cancers and can promote oncogenesis by diverse methods, such as by enhancing cell survival during physiological stress (Meylan et al., 2009), promoting the epithelial to mesenchymal transition (Huber et al., 2004; Min et al., 2008), or upregulating VEGF to control vascularisation (Xie et al., 2010).

NF-κB activation can occur through mutations in the NF-κB pathway, which are rare in solid tumours but common in lymphoid malignancies (Hoesel and Schmid, 2013; Nagel et al., 2014). In 1997, constitutive activation of RELA:p50 was identified in Hodgkin/Reed-Sternberg (H/RS) cells, in addition to the dependence of proliferation and survival of these cells on NF-κB activity (Bargou et al., 1997). Importantly, depletion of constitutive NF-κB activity in Hodgkin's lymphoma cells impaired tumour growth in mouse models, indicating the NF-κB signalling functions in the maintenance of Hodkin's lymphoma. Subsequent genetic analysis for the basis of NF-κB hyperactivation in Hodgkin's lymphoma has identified several routes. For instance, Emmerich et al. demonstrated that HR/S cell lines patient samples can harbour mutations in IκBα, such as a missense mutation causing C-terminal truncation of IκBα resulting in constitutive overexpression of IκBα, however, this did not appear to affect NF-κB activity (Emmerich et al., 1999). In a follow-up study, Emmerich et al. identified somatic mutations in IκBε in the same patients, including a frameshift causing severe IκBε truncation (Emmerich et al., 2003). Although the authors do not comment on the effect on NF-κB activity, it is possible that mutations in the genes encoding IκB proteins contribute to NF-κB activation in H/RS. Another way in which NF-κB activation may occur in Hodgkin's lymphoma is through Epstein-Barr virus (EBV), which

infects up to half of classical Hodgkin's lymphoma (Kapatai and Murray, 2007). EBV encodes LMP1 (Kulwichit et al., 1998), which is a potent activator of both the canonical and non-canonical NF-κB pathways irrespective of ligand stimulation (Luftig et al., 2004; Wu et al., 2006).

Diffuse large B-cell lymphoma (DLBCL) also shows constitutive activity of the canonical NF-κB signalling pathway, which was initially shown to result from constitutive IKK activity (Davis et al., 2001) or by a deleterious IκBα mutation (Thomas et al., 2004). However, a study analysing 238 B-cell lymphomas, including 64 DLBCL and 52 follicular lymphomas, additionally identified frequent occurrence of A20 inactivation, the re-expression of which suppresses cell growth and induces apoptosis (Kato et al., 2009). Gene expression analysis focusing on activated B cell-like (ABC) DLBCL identified that > 50 % of cases have somatic mutations in multiple NF-κB regulators, including TNFAIP3/A20, TAK1, TRAF2, and RANKL. In particular, A20 inactivation was identified in 30 % of patients (Compagno et al., 2009). Similar to the diverse mutations found to stimulate NF-κB activation in H/RS and DLBCL, two studies in 2007 identified that mutations in *NFKB1*, *NFKB2*, *TRAF3* and *NIK* occur in multiple myeloma (Annunziata et al., 2007; Keats et al., 2007). Therefore, upregulation of RELA in lymphomas can arise from diverse aberrations in NF-κB pathways that ultimately aid both tumour cell survival and proliferation.

An example of how a genetic event may lead to development of a solid cancer was provided by Pflueger et al., who used RNA-seq to identify cancer-specific gene fusions in 25 human prostate cancer samples and identified a fusion placing *IKBKB* (IKKβ) next to *TNPO1* (Transportin 1), with samples containing the fusion to have 9-fold higher expression of IKKβ than other samples. The produced IKKβ is expected to be wildtype as the fusion does not affect the translation start site of *IKBKB*. Moreover, small molecule inhibition of IKKβ resulted in a reduction of phospho-RELA (Ser536) and cell viability compared to control treatment (Pflueger et al., 2011).

Somatic and germline mutations in the *CYLD* gene can also upregulate the NF-κB pathway in multiple tumours types, as wildtype CYLD is a negative regulator of NF-κB signalling by deconjugating K63-linked ubiquitin chains on NF-κB activators (Brummelkamp et al., 2003; Kovalenko et al., 2003). *CYLD* mutations are common in the skin adnexal tumours cylindroma and mutant CYLD upregulates NF-κB signalling, resulting in increased survival and proliferation of cylindroma cells (Leonard et al., 2001). Interestingly, Rashid et al. identified that *CYLD* mutations are rare in the other skin adnexal tumour types spiradenoma (mutations in 5/17 tumours) and spiradenocarcinoma (mutations in 2/24 tumours). The authors identified that spiradenomas and spiradenocarcinomas instead harbour a missense mutation in the kinase domain of the *ALPK1* gene (Rashid et al., 2019). In this paper, I collaborated with the authors to show that the identified hotspot *ALPK1* mutation is associated with enhanced nuclear RELA translocation in several cancer cell lines (Figure 1.3). Thus, hyperactivation of RELA is associated with skin adnexal solid tumours through alteration of genes connected to the NF-κB pathway.

Figure 1.3

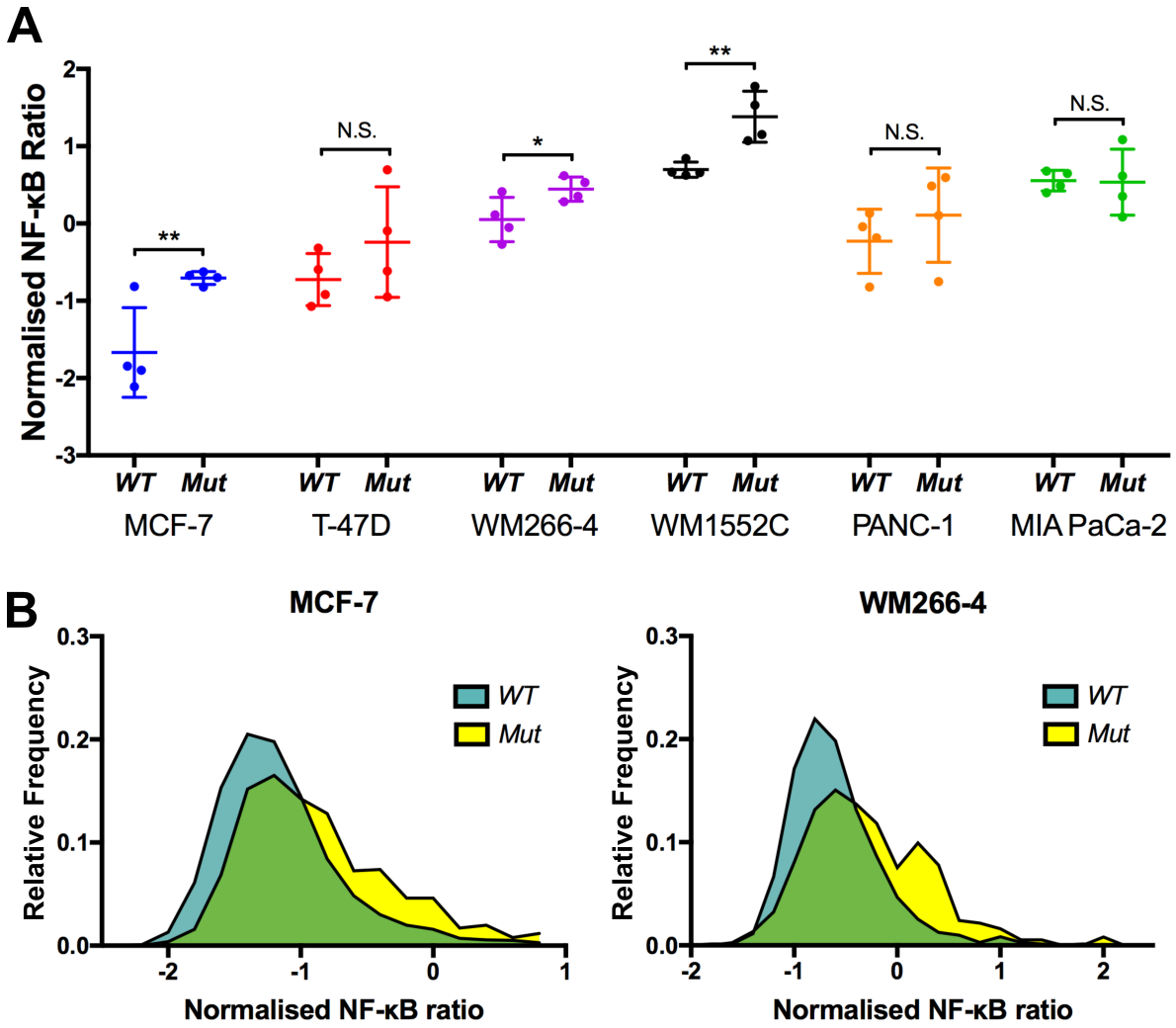
A
Normalised NF-κB Ratio
2
1
0
-1
-2
-3
**
N.S.
*
**
N.S.
N.S.
WT Mut
MCF-7
T-47D
WM266-4
WM1552C
PANC-1
MIA PaCa-2
B
MCF-7
WM266-4
Relative Frequency
0.3
0.2
0.1
0.0
WT
Mut
-2
-1
0
1
2
Normalised NF-κB ratio

Figure 1.3 ALPK1 mutation is associated with enhanced RELA nuclear localisation

Figure shows my results published in Rashid et al., 2019 (Supplementary Figure 6) assaying the effects of the p.V1092A ALPK1 mutation on RELA nuclear translocation in cancer cell lines. Cells were transfected with a wildtype or an ALPK1 p.V1092A cDNA construct together with a red fluorescent protein (RFP) construct and NF-κB (RELA) ratios (nuclear to ring region intensity) were measured in RFP-positive cells. Each data point is the mean of 6 technical replicates (each 500 RFP-positive cells) and the experiment was replicated four times (independent biological replicates). Y Axis is a log scale. (A) NF-κB (RELA) ratios by cell line. N.S. = non-significant, *p < 0.05, **p < 0.01, one-tailed t-test; bars, standard deviation. (B) Frequency distributions of NF-κB (RELA) ratios in MCF-7 and WM266-4 cells.

In general, upregulation of NF-κB activity in solid tumours is achieved through exposure to cytokines in the tumour microenvironment, as several cancers are inflammation-associated, including pancreatic cancer (discussed in Section 1.3.3), colon cancer, and melanoma (Pikarsky et al., 2004). In the case of colon cancer, Greten et al. showed that IKKβ deletion in intestinal epithelial cells decreased tumour incidence but, interestingly, did not affect inflammation or tumour size. However, the change in tumour incidence was attributed to heightened apoptosis with IKKβ deletion. Meanwhile, the same study impaired IKKβ in myeloid cells which did affect tumour size by reducing expression of proinflammatory cytokines that may function as growth factors (Greten et al., 2004). Another study showed that inhibition of the NF-κB pathway in colon cancer cells can affect cell cycle progression. This is because curcumin, which suppresses phosphorylation and degradation of IκBα, inhibits thymidylate synthase and the transcription factor E2F-1, subsequently causing cells to arrest at the G0/G1 boundary (Rajitha et al., 2016). Furthermore, curcumin significantly reduced tumour growth from the colorectal cancer cell lines HCT116 and HT29 in nude mice. Conversely, Sakamoto et al. knocked down NEMO/IKKγ, the regulatory subunit within the IKK complex, and found no difference in WT and knockdown cells in the proliferation of colorectal cancer cells. However, NEMO knockdown cells had higher apoptosis rates following TNFα and 5-FU treatment, lower expression of angiogenic chemokines, and suppressed subcutaneous tumour expansion and vessel formation (Sakamoto et al., 2009). Sakamato et al. assayed nuclear RELA staining colorectal cancer tissue by immunohistochemistry and found nuclear RELA in 40 % (35/88) of samples, as well as constitutive NF-κB activation in 6/9 colorectal cancer cell lines by EMSA.

In melanoma, NF-κB activity is believed to promote tumorigenesis through constitutive expression of a repertoire of chemokines that enforce NF-κB activity through autocrine and paracrine feedback loops (Ueda and Richmond, 2006). These chemokines include CXCL8/IL8 (Scheibenbogen et al., 1995; Wood and Richmond, 1995; Schaider et al., 2003), CXCL1 (Dhawan and Richmond, 2002), and CCL5/RANTES (Mrowietz et al., 1999). There

is also evidence that mutant BRAF (V600E), which is present in 45 % of melanoma cases, increases IKK activity, IκBα degradation and resistance to TNFα or cycloheximide-induced apoptosis (Liu et al., 2007).

However, the role that NF-κB factors play in regulating innate immune cells and the impact on cancer development is complex (Biswas and Lewis, 2010; Lalle et al., 2021). Tumour-associated macrophages (TAM) are immune cells that infiltrate solid tumours and are associated with a poor prognosis regardless of whether they are in the M1 or M2 state (Leek et al., 1996; Lissbrant et al., 2000). M1 (classically activated) TAMs are pro-inflammatory while M2 (alternatively activated) TAMs promote anti-inflammatory response and tissue repair (Mills et al., 2000; Mantovani et al., 2004). As the M1 state can be stimulated by the pro-inflammatory cytokines TNFα and IFNγ, which are transcriptionally upregulated by NF-κB signalling, NF-κB activity is believed to polarise TAM1 towards an M1 state (Collart et al., 1990; Martinez and Gordon, 2014). However, in an ovarian cancer model, IKKβ was found to polarise TAMs to the M2 state, with IKKβ depleted macrophages displaying reduction in TNFα and IL-10 production and reduced tumour burden (Hagemann et al., 2008). TNFR signalling via NF-κB also promotes tumour immune escape via myeloid-derived suppressor cells (MDSC), which are heterogeneous immune cells with immunosuppressive functions (Hu et al., 2014). Therefore, NF-κB activation can affect TAM function to promote both inflammatory and anti-inflammatory responses.

On the other hand, NF-κB proteins have putative tumour suppressor roles that are primarily associated with the promotion of anti-tumour immunity (He et al., 2010). For example, canonical NF-κB signalling is involved in the maturation and survival of dendritic cells (DCs), which function as antigen-presenting cells that link innate and adaptive immunity (Steinman and Hemmi, 2006). Accordingly, NF-κB activity is commonly repressed in DCs in the tumour microenvironment through Programmed cell death protein 1 (PD1) expression (Karyampudi et al., 2016). RELA is also required for the proliferation of several immune cell types,

including natural killer cells (Tato et al., 2003), B cells (Milanovic et al., 2017) and CD8+ T cells (Shifrut et al., 2018), as well as being involved in T-cell activation (Li et al., 1994).

Notably, NF-κB signalling affects the response of tumours to immunotherapy. Cytotoxic T-lymphocyte-associated protein 4 (CTLA4) and PD1 are receptors expressed by T cells as inhibitory checkpoints to prevent autoimmunity (Freeman et al., 2000; Schwartz et al., 2001; Stamper et al., 2001). However, cancers co-opt these pathways by expressing the ligands for these receptors for immune escape (Leach et al., 1996). Checkpoint blockade is a type of immunotherapy in which CTLA4 and PD1 and their ligands are inhibited and has proven successful in targeting multiple cancer types, particularly melanoma (Robert et al., 2015). Interestingly, whole exome sequencing of tumours in 52 patients pre-immunotherapy to identify differences between responders and non-responders to anti-PD1 therapy identified that *NFKBIE* mutations, specifically variants in codons G34 and G41, are exclusive to tumours of responders. Moreover, Gene Set Enrichment Analysis identified that TNFα signalling via NF-κB is one of the top pathways differentially expressed by response (Amato et al., 2020). NF-κB also appears to be actively damped by CTLA4 signalling in tumours, as CTLA4 increases the cytoplasmic levels of IκBα and reduces nuclear RELA levels, as well as reducing RELA DNA-binding activity (Pioli et al., 1999). Accordingly, CTLA4-/- mice have spontaneous NF-κB activity in T cells (Harlin et al., 2002).

CAR T cells are a part of an immunotherapy in which T cells are genetically engineered to express a chimeric antigen receptor (CAR) that enables targeting of the T cell to a specific protein, which is used to enhance T cell recognition of cancer cells (Kuwana et al., 1987; Eshhar et al., 1993; Lamers et al., 2006). Two approved CAR therapies have T cell receptor subunit CD3ζ and one of the costimulatory domains CD28 or 4-1BB. A 2018 study identified that 4-1BB enhancement of CAR T cells targeting CD19 relies on NF-κB activation, in part through TRAF regulation (Li et al., 2018). A more recent study attributes these findings to the non-canonical NF-κB pathway, which promotes CAR T cell survival and persistence that is

positively correlated with CAR T cell efficacy in targeting CD19+ hematologic malignancies (Philipson et al., 2020).

Finally, NF-κB signalling affects the potency of oncolytic viruses (OV), which are viruses that preferentially replicate in tumour cells (reviewed by Harrington et al., 2019). With reoviruses, a dsRNA-based OV, there is evidence that NF-κB signalling can support cell death (Connolly et al., 2000). Consequently, inhibition of NF-κB activation of PUMA expression has been shown to prevent oncolysis that is necessary for the OV process (Thirukkumaran et al., 2017). NF-κB signalling also promotes the recruitment of immune cells following reovirus infection through the generation of pro-inflammatory factors (IL-8 and IFN-β) that induce a chemotactic response in NK cells, DC cells, and anti-melanoma cytotoxic T cells (Steele et al., 2011).

1.3.2 Pancreatic Ductal Adenocarcinoma

Pancreatic Ductal Adenocarcinoma (PDAC) is the fifth leading cause of death from cancer in the UK, with a 5-year survival rate below 4 % (Vincent et al., 2011). The pancreas contains cells of exocrine (acinar), epithelial (ductal) and endocrine origin. PDAC occurs in the exocrine portion of the pancreas and most commonly in the pancreas head (van Erning et al., 2018) (Figure 1.4). The exocrine portion comprises the bulk of the pancreas mass (~80 %) and contains a branching network of acinar and ductal cells (Pandol, 2010). Ductal cells form the epithelium lining the ducts that deliver zymogens (enzyme precursors) produced by the acinar cells into the gastrointestinal tract. The endocrine tissue of the pancreas consists of clusters of cells called the Islets of Langerhans, which regulate glucose homeostasis and metabolism through the secretion of hormones such as insulin and glucagon (Hezel et al., 2006).

Figure 1.4

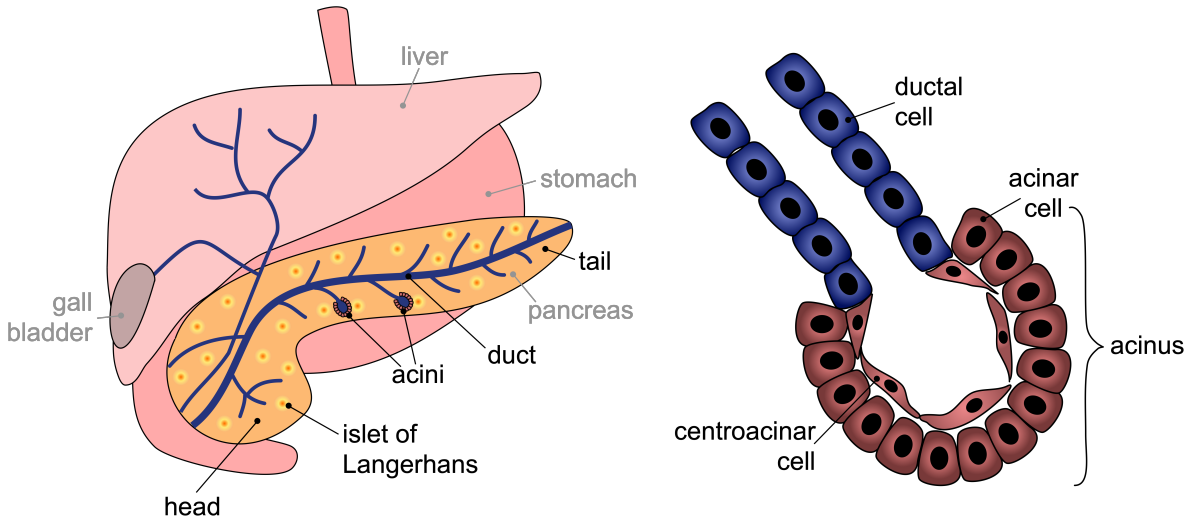
liver
stomach
tail
pancreas
gall
bladder
duct
acini
islet of
Langerhans
head
ductal
cell
acinar
cell
acinus
centroacinar
cell

Figure 1.4 PDAC anatomy

Schematic diagram of the pancreas. The pancreas (left of figure) is divided into the head, neck and body. The majority of the pancreas has an exocrine function and consists of acini and ducts that produce and transport digestive juices respectively. The endocrine function of the pancreas is carried out by the islets of Langerhans, which are distributed throughout the pancreas. Acini (right of figure) are situated at the end of small intercalated ducts, which drain into larger ducts. Acini also contain centroacinar cells, which are spindle-shaped cells that are an extension of the intercalated duct.

PDAC is characterised by upregulated desmoplastic reaction (fibrosis). The stroma encompasses most of the PDAC tumour mass (Chu et al., 2007; Erkan et al., 2012) and is composed of ECM, including the most abundant ECM component collagen, as well as a variety of non-cancerous cells (Pandol et al., 2009). The highly fibrotic stroma causes difficulties in treating PDAC, as the stroma appears to drive oncogenesis (Butcher et al., 2009; Laklai et al., 2016; Rice et al., 2017) and therapeutic resistance by acting as a physical and chemical barrier to drug delivery (Erkan et al., 2012; Liang et al., 2017). Moreover, the early stages of PDAC are overlooked due to a lack of symptoms or presence of non-specific symptoms that are common in the ageing demographic the PDAC predominantly affects, with almost half of new pancreatic cancer cases diagnosed in patients aged 75 or over (Office for National Statistics, 2017). A significant consequence of late detection is that the majority of PDAC patients present metastasis - the spread of cancer from the primary to secondary sites - or considerable local spread at first presentation (Werner et al., 2013). As a result, only a minority (less than 20 %) of PDAC cases are potentially resectable (Huang et al., 2019).

Other than advancing age, the main risk factors for PDAC are chronic pancreatitis, smoking, second-hand smoke exposure, diet-related factors (including obesity, red meat consumption and new onset of diabetes), and familial predisposition (Yeo and Lowenfels, 2012). However, over 90 % of pancreatic cancer cases are linked to sporadic mutations (Chari et al., 2015).

In 2008, the pancreatic cancer exome was published in a study that analysed the transcriptome of 24 PDACs (Jones et al., 2008) and identified that the four most frequently mutated genes in PDAC are *KRAS*, *CDKN2A* (*p16*), *TP53* and *SMAD4* (*DPC4*), which all had previously well-studied roles in PDAC (Almoguera et al., 1988). RAS proteins are intracellular membrane-bound proteins belonging to the small GTPase superfamily that have key roles in the regulation of proliferation, differentiation and cell survival (Hall et al., 1983; Bar-Sagi and Hall, 2000). There are three *RAS* genes encoding four RAS isoforms that share 82-90 % amino acid sequence homology: HRAS, NRAS and two KRAS splice variants

(Hobbs et al., 2016). Specific *RAS* genes are expressed and mutated at varying rates in different cancers, with *KRAS* being the most commonly mutated gene across all cancers and the gene mutated exclusively in PDAC, occurring in > 90 % of PDACs with estimates varying according to the study, e.g. 93 % in 142 stage I/II PDACs (Biankin et al., 2012) and 100 % of 42 PDACs at varying grades (Rozenblum et al., 1997). G12D is the most common *KRAS* mutation for PDAC (41 % of *KRAS* mutations), followed by G12V (34 %) and G12R (16 %), while other mutations are rare in PDAC, including G12C, which occurs in 1 % of all *KRAS* mutations (Sausen et al., 2015; Waddell et al., 2015; Witkiewicz et al., 2015; Waters and Der, 2018). In general, KRAS is activated early during PDAC development and often followed by loss of the tumour suppressors p53, SMAD4 or CDKN2A later in PDAC progression. Nonetheless, only ~38 % of PDAC patients have mutations in all four driver genes (Rozenblum et al., 1997; Yachida et al., 2012)

The two current first-line standard of care treatments for advanced PDAC are 1) FOLFIRINOX and 2) gemcitabine combined with nanoparticle albumin-bound (nab-) paclitaxel (Fong et al., 2019). FOLFIRINOX is a combination treatment consisting of 5-FU, leucovorin, irinotecan, and oxaliplatin. 5-FU was developed in the 1950s and has since been used to treat a range of cancers including colorectal and breast cancers (Duschinsky et al., 1957; Heidelberger et al., 1957; Longley et al., 2003). 5-FU is administered intravenously and metabolises intracellularly into fluorodeoxyuridine monophosphate (FdUMP), fluorodeoxyuridine triphosphate (FdUTP), and fluorouridine triphosphate (FUTP) (Diasio and Harris, 1989). The most effective function of 5-FU in chemotherapy is disruption of thymidylate synthase (TS) (Longley et al., 2003), which is essential for all de novo synthesis of the pyrimidine nucleotide thymidylate required in DNA replication (Maley and Maley, 1960). 5-FU additionally functions as an analogue for the nucleotide uracil and can be misincorporated into DNA (FdUTP) or RNA (FUTP), with the latter disrupting pre-RNA processing, post-transcriptional modification and splicing of RNAs (Doong and Dolnick, 1988; Ghoshal and Jacob, 1994; Kanamaru et al., 1986). Incorporation into DNA or TS

inhibition by 5-FU metabolites both interfere with DNA replication and are therefore cytotoxic to proliferating cells (Heidelberger et al., 1957; Ingraham et al., 1982). Leucovorin is used to enhance 5-FU efficacy (Park et al., 1988), while Irinotecan and oxaliplatin do not directly alter 5-FU function but also interfere with DNA replication (Kunimoto et al., 1987; Fan et al., 1998; Woynarowski et al., 2000).

The gemcitabine/nab-paclitaxel combination was approved as treatment for PDAC in 2013, following a Phase III clinical trial (MPACT) with 861 patients randomised to receive gemcitabine monotherapy or gemcitabine/nab-paclitaxel. The MPACT trial reported a median overall survival of 8.5 and 6.7 months and progression-free survival of 3.7 months and 5.5 months for the Gemcitabine monotherapy and Gemcitabine/nab-paclitaxel treatment arms respectively (Von Hoff et al., 2013). Gemcitabine is administered intravenously and the key metabolite of Gemcitabine (dFdCTP) functions similarly to 5-FU as a nucleotide analogue, as dFdCTP can be incorporated into DNA instead of deoxycytidine triphosphate (dCTP) during replication (Hertel et al., 1988; Ruiz van Haperen et al., 1993). Gemcitabine monotherapy is currently used as an adjuvant for resectable PDAC (Oettle et al., 2007; Saung and Zheng, 2017), or as a palliative care option for patients with poor performance status (Fong et al., 2019). The standard of care combination employs the taxane Paclitaxel, which is a commonly used chemotherapy that prevents disassembly of microtubules (MTs) at low concentrations and promotes MT polymerisation at high concentrations (Schiff et al., 1979). Consequently, paclitaxel suppresses MT dynamics and causes incorrect spindle assembly during mitosis that triggers cell cycle arrest (Schiff and Horwitz, 1980; Long and Fairchild, 1994).

Nonetheless, the survival rate for PDAC has not improved over the last 30 years and new strategies to target PDAC are essential, with particular promise in targeted therapies modulating signalling pathways aberrant in a patient-specific manner (Ostrem et al., 2013; Vyas et al., 2015; Waddell et al., 2015), therapies that modify the PDAC tumour microenvironment (Provenzano et al., 2012; Jiang et al., 2016), and therapies mobilising the

immune system (Beatty et al., 2011; Hardacre et al., 2013; Kimura et al., 2012; Fan et al., 2020).

1.3.3 Hyperactivation and roles of NF-κB in Pancreatic Ductal Adenocarcinoma development and progression

Multiple studies have identified hyperactivation of RELA in PDAC tumours compared to healthy pancreatic tissue. This was first demonstrated by Wang et al. (1999) using a monoclonal antibody to detect activated RELA by recognising an epitope overlapping the RELA NLS, which is the binding region for IκBα, in paired healthy and tumour tissue samples from PDAC patients taken at the time of surgery. Activated RELA was identified in 67 % (16/24) of PDAC samples but not in normal pancreatic ductal epithelial cells or surrounding stroma. The pancreatic tissue samples were also tested for RELA activation using EMSA with nuclear extracts, identifying activity in 70 % (14/20) of PDAC tissue samples and absent in paired healthy tissues. Wang et al. additionally tested commonly used human PDAC cell lines by EMSA and reported RELA DNA binding activity in 82 % (9/11) of cell lines (Wang et al., 1999). Independent analysis by Vimalachandran et al. (2005) observed moderately lower rates of RELA activity in PDAC samples, reporting nuclear RELA staining in 58 % (23/40) of PDAC tumour samples and in 26 % (7/27) of benign ducts. Similarly, another study found strong nuclear expression of RELA in 45 % (37/82) of cases and strong cytoplasmic RELA expression in 51 % (42/82) of pancreatic adenocarcinomas by immunohistochemistry (Weichert et al., 2007). Interestingly, high RELA expression was associated with a poorer prognosis for 2 year survival but whether RELA was nuclear or cytoplasmic had a similar prognosis, provided that RELA staining was considered high. Elevated RELA expression, regardless of subcellular localisation, was also significantly associated with increased expression of the RELA targets *NFKBIA* and *CCND2* (Cyclin D2), suggesting that RELA may function in cell cycle regulation in PDAC (Weichert et al., 2007)

Overall, nuclear RELA localisation appears to occur in > 50 % of PDAC tumours, although whether RELA is transiently or always nuclear has not been elucidated.

Two studies by Paul J Chiao's lab identified that RELA can function in PDAC development or metastasis using orthotopic PDAC mouse models (Fujioka et al., 2003a, 2003b). With the human PDAC cell line AsPc-1, expression of an IκBα phosphorylation mutant (S32, 36A) blocked RELA activity and downstream expression of VEGF and IL-8, in addition to inhibiting PDAC metastasis to the lungs. Meanwhile, expression of defective IκBα in the human PDAC cell line PANC1 prevented tumour formation altogether, potentially due to a significant reduction in expression of the anti-apoptotic RELA targets Bcl-xL and Bcl-2. Similar results were attained in a study using a PDAC mouse model with p53 deficiency and TGFα overexpression (Greten et al., 2002). NF-κB and STAT3 activation was found to promote Bcl-xL expression in premalignant pancreatic lesions and in tumour cells, with high Bcl-xL levels observed throughout tumorigenesis. Moreover, expression of phosphorylation defective IκBα, combined with STAT3 inhibition, induced cell death in mouse pancreatic tumour cells, suggesting that RELA plays a role in the survival of PDAC cells from early stages of PDAC development.

A common theme in research assessing the basis for RELA hyperactivation in PDAC and the impact on PDAC progression is the dependence on exposure to cytokines, in particular the pro-inflammatory interleukin IL-1α, as revealed by a series of studies also by the Chiao lab. The first study identified that maintenance of RELA activity in orthotopic nude PDAC mouse models relies on IL-1α secretion in cells, while IL-1α expression is contingent on the activity of the transcription factor dimer Activator protein 1 (AP1) (Niu et al., 2004). A follow-up study identified the importance of IL-1α stimulation on persistent RELA activity in PDAC metastasis using the human PDAC cell line MIA PaCa2. MIA PaCa2 cells stably expressing IL-1α have constitutive RELA activity and enhanced cell invasion compared to control MIA PaCa2 cells in vitro, as well as higher incidence of liver metastasis in vivo in a mouse model. Importantly, this metastatic phenotype was blocked by phosphorylation

defective IκBα and subsequent NF-κB inactivation (Melisi et al., 2009). Perhaps the greatest understanding of RELA interaction with IL-1α in PDAC was provided by the lab's 2012 study, which incorporated the signalling adaptor and autophagy receptor p62 (SQSTM1: Sequestosome 1), as well as oncogenic KRAS, into their model (Ling et al., 2012). In this study, the Chiao lab generated mice with pancreas-specific oncogenic KRAS (G12D) and found that *Kras*^{G12D} activates AP1, which in turn induces IL-1α production that upregulates murine RelA. They also identified that the NF-κB target p62 is required for constitutive RelA activity and RelA, IL-1α and p62 are more highly expressed in PanIN and PDAC than in healthy pancreatic tissue in KRAS^{G12D} mice. These findings indicate that IL-1α upregulation of RELA in PDAC involves a positive feedback loop between RELA and p62.

There is evidence that the inflammatory signals from the tumour microenvironment crosstalk with mechanical signals to upregulate RELA in PDAC. A study by Kiefel et al. showed that Expression of full-length L1 Cell Adhesion Molecule (L1CAM), as transmembrane protein, in PDAC cells leads to constitutive activation of NF-κB via upregulation of IL-1β expression, while knocking down α5-integrin and integrin-linked kinase attenuates IL-1β production and NF-κB activation (Kiefel et al., 2010). Thus, cell adhesion molecules collaborate with inflammatory signals to upregulate RELA in PDAC cells.

Surprisingly, there is limited evidence about positive feedback between TNFα and RELA in PDAC, although TNFα is a RELA target (Collart et al., 1990) and TNFα and RELA are identified as both upregulated in PDAC and usable as prognostic markers for poor survival (Weichert et al., 2007; Zhao et al., 2016). In 2016, Zhao et al. detected high TNFα levels in 58 % (58/100) of pancreatic cancer patient samples. As TNFα levels were high in PanIN (PDAC precursors) in addition to PDAC lesions, but not in healthy pancreatic tissue, TNFα is believed to be relevant to PDAC development. TNFα expression is also higher in the subpopulations within the human PDAC lines MIA PaCa2 and PANC1 that are resistant to gemcitabine and paclitaxel therapy, suggesting that TNFα is associated with chemoresistance. In support of this hypothesis, anti-TNFα treatment reduced desmoplasia in

vivo and improved responsiveness to chemotherapy. Although the authors do not comment on the involvement of NF-κB signalling, TNFα treatment versus anti-TNFα therapy correlated with changes in several cytokines that are known RELA targets, including IFNγ, IL-2, IL-6, IL-9, IL-10 and TNFα itself (Zhao et al., 2016).

Although genetic mechanisms for RELA activation are not typically associated with PDAC, regulation by microRNAs has been suggested as a possible means for RELA hyperactivation in PDAC. For example, miR-301a downregulates NF-κB repressing factor (Nkrf) and upregulates NF-κB reporter activity (Lu et al., 2011). As miR-301a is a transcriptional target of the RELA:p50 heterodimer, miR-301a and RELA function in a positive feedback loop that can lead to constitutive RELA activation. Importantly, Nkrf is downregulated while miR-301a is upregulated in human PDAC tissues, with miR-301a inhibition halting xenograft tumour growth. Likewise, the microRNA miR-1266 is significantly upregulated with pancreatic cancer and associated with chemoresistance of pancreatic cancer cells to gemcitabine in vitro and in vivo. miR-1266 promotes resistance in part by inhibiting negative regulators of the NF-κB pathway (Zhang et al., 2018b). In contrast, the microRNA miR-146a-5p is significantly depleted in PDAC compared to normal tissue and is reported to downregulate RELA, as well as impact PDAC cell growth and chemoresistance (Meng et al., 2020).

Another route for RELA upregulation in PDAC is the activation of Interleukin 1 Receptor Associated Kinase 4 (IRAK4). The four members of the IRAK family are involved in signal transduction in the interleukin-1 and Toll-like receptor signalling pathways (Suzuki et al., 2002). Briefly, a signalling cascade results in IRAK4 phosphorylation of IRAK1, which then binds to and activates TAK1, followed by phosphorylation and activation by TAK1 of the IKK complex in the canonical NF-κB pathway (Jiang et al., 2002; Cushing et al., 2017). Activated IRAK4 is associated with a negative prognosis in PDAC and has a strong correlation with activated RELA staining. Moreover, IRAK4 perturbation by CRISPR-CAS9, small molecule inhibition or RNAi interference reduces RELA activity, PDAC cell proliferation, and the

production of multiple pro-inflammatory cytokines, including IL-1β, IL-6, IL-8 and CXCL1/2 (Zhang et al., 2017a).

In addition, RELA is linked to the pathogenesis of chronic and hereditary pancreatitis, which are risk factors for PDAC development (Zhang and Rigas, 2006). Chronic pancreatitis is most commonly caused by excessive alcohol consumption and accounts for up to 3 % of pancreatic cancer cases (Lowenfels et al., 1999), with approximately 5 % of patients with chronic pancreatitis developing PDAC with a 1-2 decade lag between diagnosis of chronic pancreatitis and PDAC (Raimondi et al., 2010). The majority of evidence linking RELA to pancreatitis involves the use of cerulein, which is an oligopeptide long known to cause pancreatitis and administered to rodents to induce acute pancreatitis for study (Sato et al., 1989; Yang et al., 2020). High cerulein concentrations can activate NF-κB activity, via ROS production, and in turn stimulate inflammation (Yu et al., 2002). Mice overexpressing RELA and injected with cerulein have higher RELA and inflammation levels, as well as more severe pancreatitis, compared to mice with cerulein injections alone. Furthermore, sustained RELA activation by constitutive expression of IKK2 in pancreatic acinar cells induces RELA activity and several aspects of chronic pancreatitis in mice, including activation of stellate cells and elevation of fibrosis (Huang et al., 2013). More recently, inhibition of RELA activity by Resveratrol in KC PDAC mouse models was found to reduce the severity of cerulein-induced pancreatitis and hindered the formation of PanINs (Qian et al., 2020). Therefore, RELA is involved in a positive feedback loop with chronic pancreatitis that may contribute to PDAC initiation.

Although the bulk of literature pertaining to RELA activity in PDAC provides examples of the oncogenic roles of RELA, RELA has been shown to present tumour suppressor functions in rare and specific contexts. A key instance of this oncogene-induced senescence (OIS), which limits the progression of PDAC precursors to invasive neoplasms (Guerra et al., 2011). In 2016, Lesina et al. showed that deletion of murine RelA reduces lifespan and causes significantly earlier development of PDAC in *Kras*^{G12D} mouse models of pancreatic

cancer, which express RelA in preneoplastic and PDAC lesions. Paradoxically, significantly lower proliferation was identified in the PDAC tumours of mice lacking RelA. It was then discovered that OIS was blocking proliferation in the presence of RelA, which impeded the progression of premature lesions to full-blown PDAC. This was supported by the loss of senescence-associated β-galactosidase staining in PDAC mouse models with RelA deletion. Furthermore, senescence was identified as dependent on RelA-mediated CXCL1 (mouse orthologue of human IL-8) production, with PanIN lesions with RelA deletion no longer displaying accelerated progression to PDAC with CXCL1 expression. Therefore, Lesina et al. found that RelA has a tumour suppressor role early on during PDAC development through the promotion of senescence by CXCL1 production, but may still promote tumour proliferation in advanced tumours (Lesina et al., 2016).

1.3.4 Therapies targeting NF-κB signalling for cancer treatment

The root of modern targeting of NF-κB signalling lies historically in the modulation of TNFα (see Balkwill, 2009 for an in-depth account). In the 1970s, TNFα was shown to cause necrosis in tumours (Carswell et al., 1975) and was later found to promote T cell-mediated immunity (Havell et al., 1988; Kashii et al., 1999). Consequently, TNFα was implemented in several clinical trials as a hopeful new drug for targeting cancer. However, TNFα therapy did not cause significant effects on tumour reduction in the clinic and were universally associated with severe toxic side effects with systemic administration (Selby et al., 1987; Kuei et al., 1989). Meanwhile, local TNFα administration appeared to be more tolerable and effective in eradicating tumours in patients, but the benefits of TNFα were limited to the primary tumour and ineffectual against metastases (Grunhagen et al., 2006; Balkwill, 2009). To the surprise of the scientific community, it was discovered in the 1990s, by Frances Balkwill in collaboration with George Kollias, that knocking out TNFα in mice reduced tumour formation from carcinogens (Moore et al., 1999). Subsequently, tumour promoting roles of TNFα were identified, such as induction of oxidative damage causing mutagenesis in mouse

tissues in vivo (Yan et al., 2006). Moreover, TNFα levels were found to be elevated in malignant cells compared to normal cells (Ferrajoli et al., 2002; Kulbe et al., 2007) and in advanced cancer compared to non-metastatic tumours (Karayiannakis et al., 2001). In 1993, Anti-TNFα was initially shown to reduce metastasis of fibrocarcinoma cells in mice to the lungs (Orosz et al., 1993). Significantly, Egberts et al. demonstrated that TNFα inhibition with etanercept or infliximab caused reduction of orthotopic PDAC tumour growth in mice by 30 % and reduction of metastasis by 50 %, despite mild effects on proliferation and invasiveness in vitro. Moreover, the in vivo effects were heightened in a PDAC resection model (Egberts et al., 2008).

Evidence of anti-tumour effects of inhibiting, rather than administering, TNFα led to a number of phase II clinical trials using anti-TNFα antibodies for the treatment of breast cancer (Madhusudan et al., 2004), ovarian cancer (Madhusudan et al., 2005) and renal cell carcinoma (Harrison et al., 2007), which each showed potential for the clinical efficacy of anti-TNFα therapy. Nonetheless, a phase I/II clinical trial assessing the effect of combined anti-TNFα treatment (etanercept) with gemcitabine in PDAC patients found no clinical benefit of the addition of anti-TNFα treatment in terms of duration of patient survival (Wu et al., 2013). Similarly, a phase III clinical trial testing the effect of TNFα delivery to PDAC tumour cells by gene transfer identified no difference in patient survival between standard care and standard care with TNFα (Herman et al., 2013).

Since the early 2000s, direct inhibition of the NF-κB pathway has been explored preclinically (Giridharan and Srinivasan, 2018), including inhibition of RELA:p50 nuclear import by targeting importin α and β (Stelma and Leaner, 2017), or by using a peptide encompassing the p50 NLS sequence to competitively inhibit the interaction of endogenous p50 with importins (Lin et al., 1995). RELA binding to DNA can also be approached by competitive inhibition by providing cells with dsDNA fragments, termed ‘decoy’ oligodeoxynucleotides, containing κB sequences that RELA binds to instead of native κB sequences (Morishita et al., 1997). Other strategies for inhibition of RELA activity include targeting RELA

transactivation (Takada et al., 2004), post-translational modification (Park et al., 2015), and cofactors (Choi et al., 2008).

Alternatively, RELA activity can be inhibited by enhancing the stability of IκB proteins, which are degraded through the 26S proteasome following IκB phosphorylation and poly-ubiquitination (Chen et al., 1995). Bortezomib is a reversible and selective inhibitor of the proteasome that has been shown to inhibit RELA and completely suppress proliferation, in addition to causing cell death in diverse cancer cell lines (Kane et al., 2003; Chen et al., 2011). Bortezomib has also been shown to potentiate the effects of cell death by the topoisomerase I inhibitor irinotecan in pancreatic and colorectal cancer cell lines (Shah et al., 2001; Cusack et al., 2001), as well as improve gemcitabine-mediated cytotoxicity and tumour growth inhibition of MIA PaCa2 pancreatic cancer xenografts (Bold et al., 2001). However, bortezomib therapy has only proved to be efficacious and well-tolerated in haematological cancers in the clinic (Richardson et al., 2003), but has limited efficacy and severe toxicity in solid tumours, as demonstrated by phase II clinical trials in malignant melanoma (Amiri et al., 2004; Croghan et al., 2010) and metastatic breast cancer (Yang et al., 2006).

In 1994, the non-steroidal anti-inflammatory drug (NSAID) aspirin was shown to inhibit NF-κB signalling (Kopp and Ghosh, 1994) and there is compelling evidence that aspirin functions by inhibiting IKKβ (Yin et al., 1998). However, it is unclear whether aspirin's effect on NF-κB or in tumour reduction functions in part through inhibition of the enzyme cyclooxygenase 2 (COX2), since aspirin irreversibly acetylates COX2 (Vane, 1971) and COX2 is upregulated in multiple cancers (Williams et al., 1999). Interestingly, COX2 is believed to be an NF-κB target, causing COX2 inhibition to downregulate COX2 synthesis via NF-κB inhibition (Shishodia et al., 2004). Regardless of the mechanism, aspirin inhibits constitutive RELA activity in pancreatic cell lines and prevents pancreatic tumour formation in mice injected with PANC1 cells (Sclabas et al., 2005). An independent study similarly found that nitric oxide-releasing aspirin reduces PDAC tumour weight, incidence and spread

in $KRAS^{G12D}$ mouse models (Rao et al., 2012). A phase III UK trial (Add-Aspirin) seeking to recruit 11,000 participants aims to test the effects of aspirin on the treatment of early-stage breast, colorectal, gastro-oesophageal, and prostate cancer (Coyle et al., 2016).

Other routes currently under investigation in the clinic include targeting the RELA regulators IL-1R and IRAK4 (Khurana et al., 2020). The IL-1R inhibitor anakinra is an FDA-approved drug that has shown promising preclinical results in PDAC models, causing reduction of RELA activity and significantly reducing tumour burden *in vivo* when combined with gemcitabine, compared to gemcitabine treatment alone (Zhuang et al., 2016). Anakira is in a clinical trial (NCT02550327) by the Baylor Research Institute to test the effect of combination with nab-paclitaxel, gemcitabine, and cisplatin in patients with resectable or potentially resectable PDAC. Meanwhile, IRAK4 is expressed in most (60 %) PDAC tumours and strongly correlates with RELA expression by immunohistochemical analysis, with IRAK4 believed to drive RELA activation and promote chemoresistance in PDAC cells (Zhang et al., 2017a), as well as promote tumour fibrosis and PDAC cell survival when highly expressed in cancer-associated fibroblasts (Zhang et al., 2018a). The specific IRAK4 inhibitor CA-4948 is currently being tested in patients with relapsed or refractory haematological malignancies as a single agent (Younes et al., 2019). Several of the aforementioned studies have described a reduction of chemoresistance associated with inhibition of NF-κB signalling. This concept was also explored in PDAC cell lines by antibody blocking of IL-1R, which reduced high basal NF-κB activity and decreased resistance of PDAC cell lines to etoposide treatment (Arlt et al., 2002) (Arlt et al., 2003).

In contrast to other agents targeting NF-κB signalling, the NF-κB inhibitor curcumin is considerably well tolerated at high doses and has minimal toxicity (Lao et al., 2006). Curcumin is a naturally occurring compound and the active component of turmeric (*Curcuma longa*), which was discovered in the 1800s (Gupta et al., 2012). In 1995, a study by Singh and Aggarwal revealed that curcumin inhibits NF-κB activity (Singh and Aggarwal, 1995) and a follow up study by the Aggarwal lab showed that curcumin functions by inhibiting IKK

proteins (Bharti et al., 2003). Subsequently, it was demonstrated that curcumin inhibits the proliferation of pancreatic cell lines, promotes gemcitabine-induced cell death through the inhibition of RELA activity, and reduces PDAC tumour volume in vivo (Kunnumakkara et al., 2007). Furthermore, 8 g/day curcumin, as a single agent or in combination with gemcitabine, has proved to have beneficial effects in a subset of PDAC patients (Dhillon et al., 2008; Kanai et al., 2011). Consequently, curcumin remains a viable route for safely targeting RELA signalling in PDAC, although further exploration in the clinic has not been carried out in the last decade.

Overall, systemic inhibition of NF-κB signalling has encountered numerous pitfalls and has generally failed to progress in the clinic, primarily due to complex, unpredictable and often toxic effects, as well as issues with prolonged immune suppression (Karin, 2009). Therefore, research is underway to develop delivery systems to target NF-κB signalling in a tissue-specific manner, such as through the use of cell-penetrating nanocarriers (Kanazawa et al., 2015). A more comprehensive understanding of distinctions in RELA signalling between tissues may also reveal new routes for targeting RELA. Furthermore, issues with RELA inhibition may be overcome by modulating, rather than completely ablating, RELA activity or by controlling RELA dynamics to control certain transcripts.

1.4 Summary and PhD Aims

In this chapter I have summarised the basic configuration of the canonical NF-κB signalling pathway, which functions in immune signalling, cell survival, and proliferation (Collart et al., 1990; Antwerp et al., 1996; Zhang et al., 2004). The NF-κB factor RELA forms a heterodimer with p50 and is held inactive in the cytoplasm by IκBα in basal conditions (Baeuerle and Baltimore, 1988b; Kunsch et al., 1992). However, the potent cytokine TNFα stimulates activation of the IKK complex, which phosphorylates and causes degradation of IκBα (Chen et al., 1995). Upon destruction of IκBα, importin proteins mediate translocation of free

RELA:p50 to the nucleus, where RELA:p50 binds to κB sequences in DNA (Chen et al., 1998; Fagerlund et al., 2005).

Studies have assayed RELA localisation, using live imaging and fluorescent tagging of RELA, as a measure of RELA activity. In all cell types, RELA rapidly translocates to the nucleus following high dose TNFα stimulation, with peak RELA nuclear localisation occurring 30-60 min after TNFα treatment (Tay et al., 2010; Sero et al., 2015). In several cell types, RELA oscillates between the nucleus and the cytoplasm with damped peaks or, in some cases, with successive peaks of equal amplitude (Nelson et al., 2004; Sung et al., 2009). Alternatively, RELA can be unresponsive to TNFα or respond with a single pulse of nuclear localisation (Bagnall et al., 2015). In addition to inflammatory stimuli, RELA dynamics are encoded by mechanical cues - including cell shape, myosin activity, and matrix stiffness (Georgouli et al., 2019; Sero et al., 2015) - as well as the cell cycle (Ankers et al., 2016). Moreover, RELA induces transcription of *NFKBIA* (the gene encoding IκBα), which is believed to cause oscillations in RELA activity (Sun et al., 1993; Hoffmann et al., 2002). Importantly, RELA dynamics appear to dictate the specificity and timing of transcriptional output, which may enable context-dependent RELA activation of specific target genes (Ashall et al., 2009; Lane et al., 2017).

Finally, this chapter detailed the reported hyperactivity of RELA in PDAC patients and the putative functions RELA has in PDAC oncogenesis. RELA is upregulated in > 50 % of PDAC tumours and is associated with poor survival (Wang et al., 1999; Weichert et al., 2007). RELA activation appears to primarily result from positive feedback with inflammation in the PDAC tumour microenvironment (Melisi et al., 2009), in addition to regulation by mechanical signalling (Kiefel et al., 2010) and microRNAs (Meng et al., 2020). PDAC survival is often diagnosed at a late stage and has a 5-year survival rate of < 4 % in the UK (Vincent et al., 2011). Targeting RELA in PDAC appears to be an attractive route for reducing tumour burden and chemoresistance (Bold et al., 2001; Kanai et al., 2011; Rao et al., 2012), but there exist clinical limitations in targeting NF-κB signalling due to toxic side effects (Karin,

2009). A better comprehension of RELA signalling and identification of novel mechanisms regulating RELA hyperactivity may expose new vulnerabilities in NF-κB signalling that can be exploited therapeutically.

The overall objectives of this PhD project are to improve understanding of RELA translocation dynamics in PDAC on the single cell level, to understand factors influencing these dynamics, and to elucidate the role that RELA plays in PDAC cells. These are dissected into four key aims addressed in this thesis:

Aim 1: To characterise endogenous single cell RELA dynamics in PDAC cells in response to TNFα and oncolytic virus infection.

Aim 2: To identify whether features of RELA single cell dynamics are associated with cell survival.

Aim 3: To identify whether cell shape, actin and tubulin features correlate with heterogeneity in single cell RELA localisation with TNFα in PDAC cells.

Aim 4: To identify changes in the transcriptome in PDAC cells induced by TNFα-mediated RELA nuclear translocation.

Chapter 2: Materials and Methods

Cell lines and cell culture

Cell lines were maintained at 37 °C and 5 % CO_2 in Dulbecco's Modified Eagle Medium (DMEM; Gibco) supplemented with 10 % heat-inactivated Fetal Bovine Serum (Sigma) and 1 % Penicillin/Streptomycin (Gibco).

MIA PaCa-2, PANC-1, Capan-1, SW-1990, Panc05.04 and hTERT-RPE1 were obtained from ATCC. A375 cells were provided by the Harrington lab (ICR).

Cell lines were confirmed as mycoplasma-negative by PCR (e-Myco Mycoplasma PCR Detection Kit; iNtRON Biotechnology).

CRISPR-CAS9 endogenous tagging

RELA and PCNA were tagged endogenously at each C-terminus using CRISPR-CAS9-mediated gene editing in MIA PaCa2 and PANC1 cells. RELA was tagged with enhanced GFP (Zhang et al., 1996) and PCNA was tagged with mScarlet-I (Bindels et al., 2017), abbreviated throughout this thesis as RELA-GFP and PCNA-Scarlet respectively. RELA-GFP was first introduced into wildtype cell lines then PCNA-mScarlet was added to validated RELA-GFP clones.

Homology constructs were generated by extracting the region around the stop codon of each gene by PCR. The product was used as a template to amplify the left homology arm (LHA) and right homology arm (RHA) by PCR. PCRs were carried out using High-Fidelity Q5 DNA Polymerase (NEB) according to the manufacturer's protocol. The RHA contains a mutation corresponding to the gRNA protospacer adjacent motif (PAM) to prevent repeat targeting by the Cas9 nuclease. Primers used to amplify the homology arms included overlaps for 1) a DNA cassette encoding a linker protein, the fluorescent protein, and antibiotic resistance

(kindly donated by Francis Barr); 2) the pBluescript II SK (-) vector (Agilent) following EcoRV digestion. The final homology construct was generated from the four DNA oligos by Gibson assembly using the NEB Gibson Assembly Master Mix and according to the NEB protocol.

gRNA oligos were designed using CRISPR.mit.edu. Forward and reverse oligos were phosphorylated, annealed and ligated into a BbsI-digested pX330 U6 Chimeric hSpCas9 plasmid, gifted from Feng Zhang (Cong et al., 2013).

Custom oligos were synthesised by Sigma-Aldrich. A list of the custom oligos used to extract the genomic region around the RELA C-terminus and gRNA oligos are summarised in Table 2.1. Oligos were synthesised by Sigma-Aldrich.

Cells were transfected with homology and gRNA constructs using Lipofectamine 2000 (ThermoFisher) according to the manufacturer's protocol. Cells were expanded and selected for antibiotic resistance for three weeks. FP-positive cells were selected using FACS and sorted into single cells per well in 96-well plates and clones were expanded and tested for FP presence by amplifying and sequencing the C-terminus of the RELA and PCNA genes from genomic DNA, in order to confirm the presence of the linker and eGFP or mScarlet DNA.

Table 2.1: Oligos for CRISPR-CAS9 genome editing

Target	Oligo	Sequence
RELA	C-Terminus gDNA extraction forward	TGGGTCAGATGGGGTAAGAG
RELA	C-Terminus gDNA extraction reverse	CCAGCTTGGCAACAGATTTA
RELA	Homology construct (eGFP & neomycin resistance) LHA forward	ACGGTATCGATAAGCTTGATT GGGTCAGATGGGGTAAGAG
RELA	Homology construct (eGFP & neomycin resistance) LHA reverse	CGCCACCACCGCTCCCACC GGAGCTGATCTGACTCAGCA
RELA	Homology construct (eGFP & neomycin resistance) RHA forward	TTCTTGACGAGTTCTTCTGAG GAGGTGACGCCTGCCCTCC
RELA	Homology construct (eGFP & neomycin resistance) RHA reverse	CCGGGCTGCAGGAATTCGAT CAAGGAAGTCCCAGACCAAA

RELA	gRNA forward	TGAGTCAGATCAGCTCCTAA
RELA	gRNA reverse	TTAGGAGCTGATCTGACTCA
PCNA	C-Terminus gDNA extraction forward	GCCCTGGAGCCTTGATATTC A
PCNA	C-Terminus gDNA extraction reverse	TCTCACTTGTTCCTTGAGCTC A
PCNA	Homology construct (mScarlet-I & blasticidin resistance) LHA forward	ACGGTATCGATAAGCTTGATG AGTTTGCAGAGCTGAAATTA
PCNA	Homology construct (mScarlet-I & blasticidin resistance) LHA reverse	CGCCACCACCGCTCCCACCA GATCCTTCTTCATCCTCGA
PCNA	Homology construct (mScarlet-I & blasticidin resistance) RHA forward	GTTATGTGTGGGAGGGCTAA GCATTCTTAAAATTCAAGAA
PCNA	Homology construct (mScarlet-I & blasticidin resistance) RHA reverse	CCGGGCTGCAGGAATTCGAT TCTCACTTGTTCCTTGAGCT
PCNA	gRNA forward	CACCGCGAGGATGAAGAAGG ATCTT
PCNA	gRNA reverse	AAGATCCTTCTTCATCCTCGC GGTG

Lentiviral cell line generation

HEK-293T cells were transduced using Effectene (Qiagen) with the lentiviral plasmid pTRIPZ-IκB-SR (mouse), kindly gifted from Tencho Tenev (Pascal Meier Lab), with the packaging plasmid psPAX2 (Addgene) and envelope expressing plasmid pMD2.G (Addgene).

After 48 hr, supernatant from transduced HEK-293T cells was filtered using 0.45 µm syringe filters then immediately added to target cells.

After 72 hr, target cells were selected with puromycin for 2-4 weeks then single cell sorted using FACS into 96 well plates. Clones were expanded and tested for retention of RELA-GFP in the cytoplasm in the presence of 10 ng/ml TNFα when pre-treated with doxycycline (dox) for 24 hr and normal nuclear translocation of RELA-GFP without dox

treatment. In all experiments involving IκB-SR, cells were treated with dox at a final concentration of 0.1 μg/ml.

TNFα treatment

Cells were treated with human recombinant TNFα diluted in complete medium at a final concentration of 0.1 ng/ml, or 1 ng/ml and 10 ng/ml when specified. TNFα sourced from Sino Biological was diluted in water and used to treat the panel of PDAC lines for Bayesian analysis (Figure 4.3 and Figure 4.4). Due to lack of availability, TNFα was sourced from R&D Systems and diluted in 0.1 % BSA/PBS for all other experiments.

Drug treatments

The reagents in Table 2.2 were used at the listed concentrations unless specified.

Table 2.2: Drugs

Name	Company	Product code	Concentration
Paclitaxel	Sigma	T7402	50 nM
Vinblastine	Sigma	V1377	25 nM
Nocodazole	Sigma	M1404	400 nM
Demecolcine	Sigma	D7385	100 nM
Cytochalasin D	Sigma	C8273	2 μM
CK666	Sigma	SML0006	200 μM
H1152	Tocris	2414	20 μM
Blebbistatin	Sigma	203390	20 μM
PF573228	Tocris	S7654	1 μM
Defactinib	Selleckchem	S7654	10 μM
SMIFH2	Abcam	Ab218296	25 μM

Talazoparib (BMN-673)	Selleckchem	S7048	0.1, 1, 10 nM
Olaparib	Selleckchem	S1060	0.1, 1, 10 nM
Veliparib	Selleckchem	S1004	0.1, 1, 10 nM

Reovirus infection

Reovirus Dearing type 3 (RT3D) stocks diluted in PBS were provided by Oncolytics Biotech at $3x10^9$ tissue culture infectious dose 50 (TCID50/ml). Cells were infected with RT3D at MOI 10 unless specified. The original screen for synthetic lethal interactions between chemotherapeutic drugs and RT3D was carried out by Joan Kyula and Victoria Roulstone (Harrington lab, ICR).

Immunofluorescence staining

Cells were fixed with warm formaldehyde dissolved in PBS at a final concentration of 4 % for 15 min at 37 °C then washed three times with PBS. At RT (room temperature), cells were permeabilised for 10 min in 0.2 % TritonX-100 (Sigma Aldrich) dissolved in PBS and blocked for 1 hr in 2 % BSA/PBS. Cells were stained with 1 µg/ml Hoechst (Sigma Aldrich) in PBS for 15 min at RT, washed three times and left in PBS/azide before imaging.

Cells were incubated with primary antibodies (Table 2.3) for 2 hr at RT or overnight at 4 °C, washed three times with PBS, and incubated with secondary antibodies (Table 2.4) for 90 min at RT. Where relevant, Alexa 568 Phalloidin (Invitrogen; A12380; 1:1000) was added simultaneously with secondary antibody incubation.

Table 2.3: Primary antibodies for immunofluorescence

Target	Company	Code	Working dilution
NF-κB p65 (RELA)	Abcam	16502	1:500
α-Tubulin	Bio-Rad	MCA78G	1:1000

pFAK (Tyr397)	Invitrogen	44-624G	1:250

Table 2.4: Secondary antibodies for immunofluorescence

Product	Company	Code	Working dilution
Alexa 488/568/647 goat anti-mouse IgG (H+L)	Invitrogen	A11029, A11004, A21235	1:500
Alexa 488/568/647 goat anti-rabbit IgG (H+L)	Invitrogen	A11034, A11036, A21246	1:500
Alexa 647 goat anti-rat IgG (H+L)	Invitrogen	A21247	1:500

Confocal spinning disk microscopy

Images were taken using the PerkinElmer Opera confocal microscope or the Zeiss Axio Observer Z1 Marianas Microscope with a CSUX1 confocal spinning disk unit built by 3i (Intelligent Imaging Innovations, Denver, CO).

The PerkinElmer microscope was used with a 20 x air objective. For fixed cell imaging, a minimum of 21 fields of view were captured per well. For live cell imaging, MIA PaCa2 RELA-GFP PCNA-Scarlet and PANC1 RELA-GFP PCNA-Scarlet cells were seeded at a density of 1,000 cells per well in a 384-well plate one day prior to imaging. Images were taken of 4 fields per well at 10 min intervals using the Opera QEHS imaging system with an environmental control chamber set to 80 % humidity, 5 % CO_2 and 37 °C.

Images taken on the 3i confocal microscope were captured using 3i Slidebook (Version 6) software with a 20 x air objective. The microscope is maintained at 37 °C with > 60 % humidity, and a flow regulator was used to set CO_2 to 5 % for live imaging experiments.

Image analysis

Images from the PerkinElmer Opera microscope were analysed using custom image analysis scripts with PerkinElmer's Columbus 2.6.0 software platform. Scripts detected and segmented individual nuclei using Hoechst and the cytoplasm using Tubulin, or RELA when Tubulin is not included in the staining set. Cells touching the image border are filtered out and neighbour contact (% cell border touching another cell) for each remaining cell is calculated. The nuclear region is reduced by 1 px from the nuclear outer border from Hoechst segmentation and the ring region is set as the area 2 px to 6 px outside of the nuclear outer border. Intensities of all stains are calculated in all segmented regions on a single-cell level. A total of 32 geometric, cytoskeletal and Hoechst features were measured in addition to measurements of RELA/RELA-GFP. RELA Ratio is calculated by dividing the mean nuclear intensity of RELA/RELA-GFP by the mean ring region intensity of RELA/RELA-GFP. Texture features were calculated using SER methods with region normalisation. Bright and Spot textures were smoothed to a kernel of 4 px to detect large patches (bundles) of actin/tubulin. Ridge texture was non-smoothed to detect sharp ridges (filaments) of actin/tubulin. Elongatedness was calculated as $((2 * \text{Cell Length})^2 / \text{Cell Area})$. Actin Filament Area was measured using Columbus's 'Find Spots' function applied to the actin channel. Neighbour contact was calculated using an inbuilt Columbus algorithm calculating the percentage of a cell's border in contact with other cell borders. Grouped neighbour contact measurements were generated from non-normalised data rounded to the nearest multiple of ten.

For analysis of live cell imaging from the PerkinElmer Opera microscope, nuclear and ring region measurements of RELA and PCNA over time were carried out using Nuclitrack software (Cooper et al., 2017), with 50-60 cells tracked per treatment, cell line and biological repeat (n = 2 biological repeats). Nuclitrack tracking was carried out by myself with assistance from Andrea Brundin (Imperial College London). Cells were imaged 2 hr prior to TNFα treatment, to capture basal RELA localisation, and 48 hr following 0.01 ng/ml, 0.1

ng/ml or 10 ng/ml TNFα. Cells were tracked for only 10 hr following TNFα treatment while the total 48 hr imaging period was used to ascertain cell fate (survival or death). Intensity measurements in the second biological repeat were normalised to the first based on control well measurements (absence of TNFα) to account for changes in intensity over time due to photobleaching and laser power changes. Each biological repeat consisted of eight technical (well) replicates per cell line and treatment. For each cell line, tracks from all treatments and biological repeats were collated and trimmed to 120 min prior to until 600 min following TNFα treatment then clustered using Time Course Inspector (Dobrzyński et al., 2020) in R, with Ward D2 linkage and the Manhattan dissimilarity measure. RELA ratio peaks were detected in Excel as RELA ratios fitting either of two criteria: 1) > 0.02 above both the mean RELA ratio of the previous two time points and the mean RELA ratio of the following three timepoints; 2) > 1 and the maximum RELA ratio in the surrounding 40 min window, and > 0.01 above the mean RELA ratio of the previous two time points and the mean RELA ratio of the following two timepoints. The ‘first peak’ is the peak that occurs at the earliest timepoint following TNFα addition.

All imaging for cells infected with reovirus (Chapter 6) was carried out on the 3i microscope. Unsegmented nuclei were segmented and tracked using Nuclitrack for live imaging data.

For all other data, nuclei were segmented in FIJI (Schindelin et al., 2012) using the StarDist Plugin (Schmidt et al., 2018). Nuclei in the TNFα washout experiment (Figure 3.9) were tracked using TrackMate with StarDist-segmented nuclei. Quantification of intensity and cell shape features were carried out in CellProfiler (Carpenter et al., 2006).

Data from tracks analysed in CellProfiler (Figure 3.9 and all live imaging in Chapter 6) were processed in R. Data were converted to wide format and missing RELA ratio measurements in tracks were imputed using the imputeTS package and smoothed using savitzky-golay filtering with the sgolayfilt function in the ‘signal’ package. The peak RELA ratio was identified by the maximum RELA ratio per track. The first and second derivatives were

calculated using the sgolayfilt function. First derivative values around the peak RELA ratio were used to calculate the maximum rate of RELA ratio change (max 1^{st} derivative = max $rate_{in}$, min 1^{st} derivative = max $rate_{out}$). The duration of RELA nuclear localisation by track was identified by the maximum of the second derivative.

Cell spreading assay

MIA PaCa2 RELA-GFP PCNA-Scarlet and PANC1 RELA-GFP PCNA-Scarlet cells were seeded at a density of 1,000 cells per well in 384-well plates in DMEM with 100 nM SiR-Actin and 10 μM Verapamil (Spirochrome). Cells were treated with BSA/PBS (control) or 0.1 ng/ml TNFα diluted in DMEM, then immediately imaged for 12 hr at 10 min intervals. The intensity and cell morphology measurements were calculated for five cells per treatment/cell line on a single cell level using Columbus software (PerkinElmer). For reference values in adhered cells, the well average RELA ratio over time aligned to the time of 0.1 ng/ml TNFα addition was calculated using Columbus for at least 5 wells per cell line and treatment.

TNFα washout assay

40,000 MIA PaCa2 RELA-GFP PCNA-Scarlet cells were seeded in 2 ml phenol red-free DMEM in a glass-bottom dish (MatTek; P35G-1.5-14-C) coated with fibronectin (Sigma; f0895) diluted 1:100 in PBS from stock. The following day, cells were imaged on the 3i confocal spinning disk microscope with 20 fields of view at 10 min intervals for 1 hr prior to TNFα addition. Cell medium was aspirated and replaced with 0.1 ng/ml TNFα for 60 min, then aspirated and replaced with fresh DMEM using a perfusion system (designed by Kai Betteridge, ICR). Cells were imaged for a further 47 hours following TNFα removal.

Co-immunoprecipitation

MIA PaCa2 cells were cultured in 15 cm dishes to 80 % confluence then treated with TNFα at a final concentration of 0.01 ng/ml, 0.1 ng/ml or 10 ng/ml, or with a BSA/PBS control.

Co-immunoprecipitation (Co-IP) was carried out using GFP-Trap Agarose beads (Chromotek; gta-10) or with binding control agarose beads (Chromotek; bab-20) using RIPA lysis buffer and according to the manufacturer's protocol. Original sample, flow-through and elution from the agarose beads were checked by western blotting with an anti-RELA antibody (abcam; 16502). Samples were analysed by mass spectrometry (methods in the 'Proteomics' section below).

IκB-SR with TNFα treatment for proteomics and RNA-seq analysis

MIA PaCa2 and PANC1 cells stably expressing doxycycline (dox)-inducible lentiviral IκB-SR were seeded in t25s (for RNA-seq) or t75s (for proteomics) to attain 30 % confluence the following day. At 30 % confluence, cells were treated with 1 µg/ml dox or DMSO. After 48 hr dox, cells were treated with TNFα at a final concentration of 0.01 ng/ml, 0.1 ng/ml or 10 ng/ml, or with a BSA/PBS control for 1 hr or 5 hr.

Proteomics

Sample preparation for proteomic analysis through to database searching and quantification were carried out by Theo Roumeliotis (ICR, Prof Jyoti Choudhary), who kindly provided the protocols.

Sample preparation for proteomic analysis

Cell pellets were lysed in 150 µL lysis buffer of 100 mM triethylammonium bicarbonate (TEAB), 1 % sodium deoxycholate (SDC), 50 mM NaCl, 10 % isopropanol and Halt protease and phosphatase inhibitor cocktail (100X) (Thermo, #78442) on ice, with 15 second pulsed probe sonication followed by heating at 90 °C for 5 min and another 5 second sonication. Protein concentration was measured with the Quick Start™ Bradford protein assay (BioRad) according to the manufacturer's instructions. Protein aliquots of 100 or 60 µg were reduced with 5 mM tris-2-carboxyethyl phosphine (TCEP) for 1 h at 60 °C and alkylated with 10 mM iodoacetamide (IAA) for 30 min in dark. Proteins were digested overnight with trypsin at a

final concentration 75 ng/µL (Pierce). Peptides were labelled with the TMT-11plex or TMTpro-16plex reagents (Thermo) according to the manufacturer's instructions. SDC was removed by acidification with 1 % formic acid and centrifugation, and supernatant was SpeedVac dried. For the immunoprecipitation (IP) samples, 100 µL of 100 mM TEAB were added to the beads followed by reduction and alkylation as above and overnight digestion with trypsin at a final concentration 50 ng/µL. Supernatant was dried with a centrifugal vacuum concentrator and stored at -20 °C until the mass spectrometry (MS) analysis (label-free analysis) or peptides were labelled with the TMT-11plex reagents, combined, dried and C18 cleaned-up using the Pierce™ High pH Reversed-Phase Peptide Fractionation Kit before the MS analysis.

High-pH Reversed-Phase peptide fractionation and phosphopeptide enrichment

For the total proteome and phosphoproteome analysis, peptides were fractionated with high-pH Reversed-Phase (RP) chromatography using the XBridge C18 column (2.1 x 150 mm, 3.5 µm, Waters) on a Dionex UltiMate 3000 HPLC system. Mobile phase A was 0.1 % v/v ammonium hydroxide and mobile phase B was acetonitrile, 0.1 % v/v ammonium hydroxide. The TMT labelled peptides were fractionated at 0.2 mL/min with the following gradient: 5 min at 5 % B, for 35 min gradient to 35 % B, gradient to 80 % B in 5 min, isocratic for 5 min and re-equilibration to 5 % B. Fractions were collected every 42 sec, combined in 28 fractions and SpeedVac dried.

Phosphopeptide enrichment of up to 20 peptide fractions was performed with the High-Select™ Fe-NTA Phosphopeptide Enrichment Kit (Thermo) using a modified protocol in a well plate array format. A volume of 50 µL resin/buffer was transferred on top of 10 µL filter tips that were fitted on a 96-well plate using a suitable tip rack. The resin was washed three times with 40 µL wash/binding solution and centrifugation at 500 g for 1 min. Peptides were reconstituted in 30 µL wash/binding solution and were loaded onto the tip-columns with the resin. After 30 min, the flow-through from three washes with wash/binding solution were

collected in a clean 96-well plate with centrifugation at 500 g for 1 min each time. Phosphopeptides were eluted twice with 40 µL elution buffer in a clean 96-well plate with centrifugation at 500 g for 1 min, transferred in glass vials (Waters, P/N 186005669CV) and SpeedVac dried.

LC-MS analysis

LC-MS analysis was performed on a Dionex UltiMate 3000 UHPLC system coupled with the Orbitrap Lumos Mass Spectrometer (Thermo Scientific). Peptides were loaded onto the Acclaim PepMap 100, 100 µm × 2 cm C18, 5 µm, trapping column at flow rate 10 µL/min. Samples were analysed with the EASY-Spray C18 capillary column (75 µm × 50 cm, 2 µm) at 50 °C. Mobile phase A was 0.1 % formic acid and mobile phase B was 80 % acetonitrile, 0.1 % formic acid. The separation method was: for 90 min gradient 5 % - 38 % B, for 10 min up to 95 % B, for 5 min isocratic at 95 % B, re-equilibration to 5 % B in 5 min, for 10 min isocratic at 5 % B at flow rate 300 nL/min.

The precursor ions between 375-1,500 m/z were selected with mass resolution of 120 k, AGC 4×10^5 and IT 50 ms for CID fragmentation with isolation width 0.7 Th in the top speed mode (3sec). The collision energy was set at 35 % with AGC 1×10^4. MS3 quantification was obtained with HCD fragmentation of the top 5 most abundant CID fragments isolated with Synchronous Precursor Selection (SPS). Quadrupole isolation width was set at 0.7 Th, collision energy was applied at 55 % or 65 % and the AGC setting was 1×10^5 or 5×10^4. The HCD MS3 spectra were acquired for the mass range 100-500 with 50 k resolution. Targeted precursors were dynamically excluded for further isolation and activation for 45 seconds. Phosphopeptides and label-free IP samples were analysed at the MS2 level with HCD-38 % at 50K Orbitrap or Rapid Iontrap detection respectively.

Database search and quantification

Raw mass spectrometry data were analysed in Proteome Discoverer 2.4 (Thermo Scientific) with the SequestHT search engine for peptide identification and quantification. The precursor

and fragment ion mass tolerances were 20 ppm and 0.02 Da (Orbitrap)/0.5 Da (Iontrap) respectively. Spectra were searched for fully tryptic peptides with maximum of 2 miss-cleavages. TMT6plex or TMTpro at N-terminus/K and Carbamidomethyl at C were selected as static modifications. Oxidation of M, Deamidation of N/Q and Phosphorylation of S/T/Y (for phospho-enriched samples only) were selected as dynamic modifications. Spectra were searched against reviewed UniProt human protein entries, peptide confidence was estimated with the Percolator node and peptides were filtered at q-value < 0.01 based on decoy database search. The reporter ion quantifier node included a TMT quantification method with an integration window tolerance of 15 ppm. Only peptides with average reporter signal-to-noise > 3 were used and phosphorylation localization probabilities were estimated with the IMP-ptmRS node.

Data were analysed using Perseus (MaxQuant) software (Tyanova et al., 2016) using the pipeline recommended for cancer research analysis (Tyanova and Cox, 2018).

RNA-seq

Samples were processed and reads aligned by the Tumour Profiling Unit at the ICR. Statistical analysis was carried out using the DEseq2 package (Love et al., 2014) in R. Normalised counts from DEseq were $\log_2$ transformed. The $\log_2$ value for the DMSO control (without dox) for the corresponding cell line (MIA PaCa2 or PANC1) and timepoint (1 hr or 5 hr) was negated from transformed counts. Counts were then z-scored by cell line or across all samples as indicated. Genes with < 10 counts across all samples were removed prior to statistical analysis and genes with 0 counts for any sample were omitted from results. Advice for statistical analysis of RNA-seq data was kindly provided by Gareth Muirhead (ICR).

Statistical analysis

All statistical analysis was carried out using R software. Statistical tests were carried out using the ‘Rstatix’ package and Principal Component Analysis (PCA) was carried out using

the inbuilt ‘prcomp’ function using z-score data. Graphs were generated in R using the ‘ggplot’ package (Wickham, 2016) unless specified.

To analyse cell-to-cell differences in the 35 geometric, cytoskeletal and Hoechst features within and between PDAC and RPE1 cell lines (Chapter 4.2.1), single cell and well (mean) data were collated from all cell lines and treatments from three biological repeats. Features were normalised to the mean across all treatments and cell lines for each biological repeat. Features were reduced for Bayesian analysis by clustering normalised single cell measurements into ten clusters using the ‘ComplexHeatmap’ package in R (Gu et al., 2016), clustering by the Spearman’s Rank coefficient with average linkage. Bayesian network models and arc strengths were generated in R using normalised single cell data for the ten reduced features via the ‘bnlearn’ R package (rsmax2 method) (Scutari, 2010). This algorithm depicts unidirectional arcs, so reverse relationships can exist but are not as statistically likely as the directional relationships indicated.

Z-scores in Figure 4.2 were calculated per technical replicate using the mean and standard deviation for control measurements for each feature across all lines for each biological repeat (n = 3). Mean z-scores per feature and cell line were calculated by averaging z-scores for technical replicates across all biological repeats.

In Figure 4.5, MIA PaCa2 and PANC1 RELA-GFP cells fixed after 1 hr 0.1 ng/ml TNFα were allocated to RELA translocation clusters based on RELA ratio, using the mean RELA ratio +/- (0.6 * standard deviation) for live tracked cells at 60 min for each RELA translocation cluster (M1-M4 and P1-P4) to define RELA ratio limits per cluster. Fixed cells were stained for actin and tubulin and z-scores for the ten independent cytoskeletal and cell shape features used in Bayesian analysis were calculated by cell line. t-SNE analysis was carried out in R (“Rtsne” package) using z-score data. Statistical differences between RELA translocation clusters for each cell feature by cell line were identified by ANOVA.

Chapter 3: Live RELA translocation dynamics in PDAC cells

3.1 Introduction

3.1.1 Effects of TNFα dose and duration on RELA translocation responses

Section 1.2.2 discussed the different profiles of RELA translocation dynamics in response to TNFα. Briefly, several cell types display oscillatory RELA dynamics with constant TNFα stimulation, but single cells can be unresponsive or present a single transient pulse of RELA nuclear localisation (Nelson et al., 2004; Sung et al., 2009; Tay et al., 2010). Here, I focus on the effects of altering TNFα dose and stimulus duration on the amplitude and heterogeneity of RELA nuclear translocation.

Due to the importance and pleiotropic nature of its activity, RELA needs to function correctly in the face of noise in extrinsic signals, such as transient bursts of cytokine production by macrophages (Baer et al., 1998) or genotoxic stress (Piret and Piette, 1996). This is necessary in order for RELA to upregulate the appropriate output, such as inflammation or cell death. How cells process fluctuating inputs through modulation of RELA activity has been extensively studied in the last two decades. Research has explored whether RELA has a switch-like or continuous response, with each category bearing distinct merits. 'All or nothing' RELA responses describe when signal strength does not affect the intensity of RELA activation but could affect the likelihood of a cell activating. The binary presence of factors required for RELA activation could achieve this response, which may be the case in multiple myeloma tumours with constitutive RELA activation due to mutations in *NFKB1*, *NFKB2*, *TRAF3* or *NIK* (Annunziata et al., 2007; Keats et al., 2007). This would elicit a more robust RELA response in the presence of signal variability, at the cost of limiting information

processing to discrete output (Selimkhanov et al., 2014; Kellogg and Tay, 2015). Another scenario involves continuous RELA responses, in which the stimulus dosage or duration correlates with RELA activity, achievable by cell-to-cell variability in intrinsic factors like IKK or IκBα expression. This latter model would be more likely to enable RELA induction of a spectrum of cell fates within the same cell population (Lane et al., 2017; Spencer et al., 2009).

The first experiments to test how RELA responds to various TNFα concentrations and duration were carried out by Alexander Hoffman, Shannon Werner, David Baltimore, and colleagues, using EMSA to assay NF-κB DNA binding activity. At the population level, NF-κB activity duration was constant across TNFα stimulation durations (5, 15, 30 or 60 min), suggesting that RELA has a bimodal response to TNFα stimulation (Hoffmann et al., 2002). Moreover, while continuous TNFα stimulation provided oscillations at the population level, a single TNFα pulse led to a single pulse in NF-κB activity. Hoffman et al.'s 2002 model of NF-κB activation described switch-like NF-κB activation in response to short-duration stimulation, while stimulation longer than 1 hr results in an NF-κB response proportional to stimulation duration. Translation of NF-κB responses into transcriptional output was observed in a subset of genes (e.g. the chemokine IP-10) expressed soon after continuous TNFα stimulation or after a 15 min TNFα pulse. Meanwhile, other genes were only induced after prolonged NF-κB activity, including the chemokine RANTES.

A follow-up study by Werner et al. tested shorter duration TNFα pulses (1, 2, 5, and 15 min) and concurred that TNFα pulse duration does not affect the profiles of IKK and NF-κB activities by both computational simulation and experiments (Werner et al., 2008). Similarly, a 1 min TNFα pulse could induce expression of specific target genes, including IκBα, IκBε, IP10 and MCP1, which had expression independent of TNFα duration and concentration. Thus, initial research into NF-κB activity on the population level provided evidence that NF-κB responses are robust to extrinsic noise.

Importantly, Hoffman et al. (2002) and Werner et al. (2008) primarily describe the importance of negative feedback by IκBα, IκBε and A20 in regulating NF-κB activation, which I discuss in section 5.1.5. Notably, IκBα is crucial to both oscillatory NF-κB dynamics and cessation of NF-κB following activation.

Mike White's group pioneered the analysis of single-cell heterogeneity in RELA responses (Nelson et al., 2004; Ashall et al., 2009). SK-N-AS neuroblastoma cells expressing RELA-dsRed, subjected to continuous TNFα stimulation, display oscillatory RELA dynamics out of sync on the single-cell level. However, 5 min TNFα pulses synchronise RELA translocation between cells, with stimulation frequency affecting RELA translocation amplitude. The closest amplitude of RELA nuclear translocation to continuous TNFα stimulation was achieved with 200 min intervals (low frequency), which resulted in successive peaks attaining the same peak amplitude. Meanwhile, stimulation with 60 min or 100 min pulses (high frequency) resulted in damped oscillations, suggesting a need for a system reset between 100 and 200 min post-TNFα. However, Ashall et al found that shorter TNFα pulse intervals resulted in the most similar gene expression patterns to continuous TNFα stimulation.

Studies by Markus Covert's group furthered understanding of how TNFα dose affects RELA responsiveness, using live image analysis of RelA-/- mouse 3T3 fibroblasts expressing lentiviral RelA-dsRed under control of the endogenous promoter, simulating endogenous RelA expression, in the presence of a range of TNFα doses (0.01-10 ng/ml) (Tay et al., 2010). TNFα dose dramatically affected the proportion of cells responding with RelA nuclear translocation, with 3 % of cells responsive at 0.01 ng/ml TNFα and 50 % responsive at 0.1 ng/ml TNFα. Like Hoffman et al. (2002) and Werner et al. (2008), Tay et al. reported digital RelA activation, since total NF-κB activity on the single cell level, assayed by the area under the first peak, remained constant across TNFα concentrations. Furthermore, RelA activity could not be wholly due to pre-existing variation in TNFα sensitivity, since stimulating the same population of cells with two 20 min long TNFα pulses resulted in only 11 % of cells

responding to both pulses. TNFα dose also affected RelA response time, with the lowest TNFα doses resulting in a time to peak RelA activation of 50 min compared to 20 min at the highest TNFα doses, as well as higher variation in nuclear RelA localisation at lower TNFα doses. In terms of gene expression, Tay et al. identified distinct subsets of genes dependent on TNFα dose and duration: 'early genes' (e.g. IκBα and A20) are expressed rapidly (~1 hr) after TNFα stimulation and are dose and duration independent, while late genes (e.g. RANTES and CCL2) build up in expression over time and require persistent and high TNFα doses.

Kellogg and Tay also published a study in 2015, using MEFs and the same system as Tay et al. (2010), that discussed the effect of TNFα dose and oscillatory input specifically on 'entrainment' of NF-κB activity, which describes when activity becomes synchronised across cells and oscillation phase differences become constant. While persistent TNFα input at both high and low doses led to between-cell and within-cell variability with a natural period of around 90 min, oscillating TNFα signal with 120 min intervals entrained RelA nuclear translocation in MEFs, with higher amplitude of RelA nuclear oscillation and additionally higher transcription output. However, 60 min interval TNFα signals failed to evoke an entrained response and were associated with lower gene expression. Therefore, the authors propose that entrainment of NF-κB activity and maximisation of NF-κB transcriptional output requires careful matching of the input signal to the natural NF-κB frequencies present in the population. However, the range around the optimal period (90 min) appears non-normally distributed (Kellogg and Tay, 2015).

The effect of forced oscillatory signals on RELA oscillations has also been studied using endogenously tagged p65 by Zambrano et al., who used GFP knock-in MEFS cultured with a range of TNFα doses in a microfluidic device (Zambrano et al., 2016). Endogenous GFP-RelA in MEFs was identified as not naturally entrained, as constant 10 ng/ml TNFα stimulation resulted in asynchronous, heterogeneous, and damped oscillations. With 90 min TNFα pulsing, RelA dynamics became synchronous at higher doses. Nonetheless,

Zambrano et al. distinguish their results from Kellogg and Tay's 2005 study as they interpret the observed synchronisation in MEFS not to be entrainment. Based on live imaging and mathematical modelling, MEF's rapidly lost synchrony following TNFα stimulus removal, while entrained cells would have retained the memory of synchrony and gradually dephase once period forcing ceased.

In contrast with prior studies, Zhang et al. (2017) provided evidence that RELA nuclear translocation is not straightforwardly a switch-like or graded response but more likely a combination. Zhang et al. exposed the rhabdomyosarcoma cell line KYM1, stably expressing FP-RELA, to a single TNFα pulse for 30 seconds, 1 min or 5 min, with different TNFα concentrations. TNFα exposure conditions resulted in differences in RELA activation in terms of AUC and maximum fold-change. Notably, low concentrations and short pulses failed to evoke RELA nuclear translocation, while longer TNFα duration and higher doses have significantly lower non-responsive rates. For instance, a 30 second 0.01 ng/ml TNFα pulse induced a RELA response in 22 % of cells while a 30 second 50 ng/ml TNFα pulse activated 96 % of cells. Therefore, there appears to be a minimum TNFα threshold required for RELA activation, above which the RELA response is proportional to the TNFα input (Zhang et al., 2017b). Interestingly, Zhang et al. did not report oscillations in their data, with TNFα stimulation inducing a single RELA nuclear translocation pulse, based on average tracks, during the 300 min imaging session.

Altogether, whether TNFα dose and duration affect the peak amplitude or entrainment of RELA nuclear localisation is complex and requires further study. Generally, studies agree that a higher TNFα dose increases the fraction of responsive cells (Tay et al., 2010; Zhang et al., 2017b). However, early work suggests that unentrained total NF-κB activity is constant regardless of TNFα duration or concentration (Hoffmann et al., 2002; Werner et al., 2005), which is achieved on the single cell level by higher TNFα doses inducing a higher amplitude but shorter duration of RELA nuclear localisation compared to low TNFα doses (Tay et al., 2010). Meanwhile, later research suggests that TNFα dose and concentration affect more

parameters of RELA activation (Zhang et al., 2017b). Nonetheless, expression of early genes consistently appears to be TNFα concentration and duration independent, while expression of late genes is elevated by higher TNFα doses and persistent stimulation (Hoffmann et al., 2002; Ashall et al., 2009; Tay et al., 2010). Building evidence further indicates that RELA dynamics have inherent cell-to-cell and temporal variability within a cell resulting from intrinsic noise, such as from variation in IκBα/ε and A20 activity relative to NF-κB activity, in addition to extrinsic noise.

3.1.2 RELA dynamics and the cell cycle

In 2016, Mike's White group published pivotal work delineating heterogeneity in TNFα-mediated RELA translocation according to cell cycle progression, importantly providing temporal resolution. Ankers et al. assayed RELA nuclear-to-cytoplasmic intensity in SK-N-AS and HeLa cells stimulated with TNFα, after synchronising cells using double thymidine block and assessing cell cycle stage at the time of TNFα addition based on the Fluorescent Ubiquitination-based Cell Cycle Indicator (FUCCI) reporter. RELA translocated to the nucleus in cells at the G1/S boundary with a synchronous response while RELA nuclear translocation was delayed or repressed in S phase cells. Moreover, activation with TNFα at the G1/S boundary resulted in a statistically significant 10 % longer cell cycle length in HeLa cells. Ankers et al. looked into whether RELA is regulated by the E2F proteins, which are transcription factors involved in cell cycle regulation, with E2F1-3 functioning as transcriptional activators in the G1/S transition and repressed by hypophosphorylated RB (Chellappan et al., 1991; Wu et al., 2001). Previously, E2F1 was reported to induce apoptosis through NF-κB inhibition (Phillips et al., 1999). Ankers et al. reported that NF-κB induction of IκBα and IκBε are inhibited by E2F overexpression and demonstrated that NF-κB interacts physically with E2F1/2 by Co-IP. The authors hypothesised that E2F might control RELA nuclear occupancy through RELA-binding and inhibition of IκBα transcription,

which they supported by in silico modelling. Therefore, RELA activation appears to be suppressed during the S phase by E2F interaction.

Other studies have not reported the regulation of RELA live dynamics by the cell cycle but have described regulation by cell cycle factors on aspects of RELA activation. For instance, the tumour suppressor ADP-ribosylation factor (ARF) induces the DNA damage response kinases ATR- and Chk1-dependent phosphorylation of the RelA transactivation domain at threonine 505, leading to inhibition of RELA transcriptional activity and TNFα-induced cell death (Rocha et al., 2005). In addition, the CDK inhibitor p21 stimulates RELA transcriptional activity through modulation of the p300/CBP coactivator (Perkins et al., 1997) and the CDK inhibitor p16 binds to and inhibits the p65-p50 heterodimer with p16 overexpression reducing NF-κB transcriptional activity (Wolff and Naumann, 1999).

At the same time, RELA regulates cell proliferation in both cancer and non-malignant settings. In 1999, two studies showed that NF-κB signalling might promote cell cycle progression through Cyclin D induction. D-type cyclins interact with CDK4 and CDK6 during G1 and bind directly to pRB, mediating CDK-dependent phosphorylation of Rb. Consequently, D-type cyclins play a significant role in S-phase entry (Resnitzky et al., 1994; Xiong et al., 1991). Hinz et al. showed that NF-κB activates transcription from the cyclin D promoter through a proximal binding site and NF-κB binding is necessary for serum-stimulated Cyclin D transcription. Moreover, inhibiting NF-κB activity using a dominant-negative IκBα in several cell types, including mouse embryo fibroblasts and HeLa cells, resulted in reduced and delayed Cyclin D1 protein levels in G1, delay in pRB phosphorylation, and hindrance of S phase entry, which was overcome with ectopic cyclin D expression (Hinz et al., 1999). In line with these results, Guttridge et al. demonstrated that myoblast cells expressing IκB-SR have reduced proliferation rate and exit the cell cycle faster than control cells, and NF-κB activity is required for initiation of cyclin D, hyperphosphorylation of pRB and progression into S phase following FBS stimulation. The

authors also identified multiple NF-κB binding sites in the cyclin D promoter (Guttridge et al., 1999)

Studies have also shown that RELA can promote cell cycle arrest. For instance, overexpression of RELA, but not c-Rel, in pro-B cells induced G1 cell cycle arrest and apoptosis, which involved the DNA binding and transactivation domains of RELA. However, the same study also reported that RELA overexpression in an immature and mature B cell line did not induce cell cycle arrest or apoptosis, suggesting that the impact of RELA on the cell cycle changes with B cell development (Sheehy and Schlissel, 1999). Another study transduced fibroblasts and keratinocytes with p65 and p50 retrovectors which led to induction of p21 transcription in ketatinocytes but not fibroblasts, despite both cell types being susceptible to p21-induced growth inhibition (Hinata et al., 2003). Therefore, the studies above propose a role for RELA in G1 arrest. Meanwhile, a study using CEM T leukemic cells exposed to ionising radiation or the DNA topoisomerase II inhibitor etoposide identified that cells with activated NF-κB arrest in prolonged G2-M followed by cell cycle re-entry and survival. In contrast, cells without NF-κB activation underwent more transient G2-M arrest and cell death (Wuerzberger-Davis et al., 2005).

Thus, numerous studies have outlined a role for RELA, in addition to other NF-κB transcription factors (Bash et al., 1997; Schumm et al., 2006), in cell cycle progression and vice versa. However, the relationship between NF-κB signalling with the cell cycle is context-dependent and has not been assessed in PDAC cells. There are also insufficient studies assaying RELA dynamics and the cell cycle using timelapse information, leading to uncertainty over the specific parameters of RELA activation within the cell cycle framework.

3.1.3 Cell death and survival decisions downstream of TNFα

Following TNFα ligand binding to its cell surface receptor TNFRSF1A, either cell survival or cell death signalling can be activated, as reviewed thoroughly by Annibaldi and Meier, 2018 and Legrand et al., 2019. By default, the output of TNFα in most cells is survival via RELA

signalling, which is fundamentally activated to stimulate an inflammatory and anti-pathogen response, while cell death is actively repressed (Wang et al., 2006; Ting and Bertrand, 2016). In terms of death modes, TNFα can induce extrinsic apoptosis and, in some cases, necroptosis. During the TNFα response, the protein kinase RIPK1 acts as a crucial component of the switch between TNFα-induced life or death. RELA signalling requires RIPK1 to form part of a complex with TNFR1 (Complex I) (Ea et al., 2006) and also requires TAK1 phosphorylation of the IKK complex (Sakurai et al., 2003), which is blocked by certain pathogens (Orning et al., 2018). Switching to an apoptotic response to TNFα requires RIPK1 to leave Complex I and form Complex II with FADD, CASP9 and cFLIP (Kelliher et al., 1998; Wang et al., 2008; Dondelinger et al., 2013). cFLIP levels determine whether Complex II is degraded and apoptosis is blocked, or Complex II accumulates to activate caspase 8 (CASP8) and process the effector caspase 3 (Stennicke et al., 1998). CASP8 also cleaves BID enabling activation of BAX and BAK, which form pores within the mitochondrial outer membrane that enable release of cytochrome c and second mitochondria-derived activator of caspase (SMAC) - the latter targets inhibitor of apoptosis proteins (IAP) for degradation (Li et al., 1998; Du et al., 2000). The subsequent and defining moment for apoptosis is mitochondrial outer membrane permeabilisation, which commits the cell to death (Kerr et al., 1972; Amarante-Mendes et al., 1998).

Interestingly, although TNFα-associated cell death is typically apoptosis, TNF substances are eponymous for their initially identified role in necroptosis (Carswell et al., 1975). Necroptosis occurs when both NF-κB signalling and CASP8 activity are blocked and involves RIPK1 forming a complex (III) with RIPK3, which phosphorylates MLKL thus triggering mitochondrial pore formation (Lemaire et al., 1998; Cho et al., 2009; He et al., 2009; Sun et al., 2012). Necroptosis is contingent on highly cell-specific RIPK3 expression (Newton et al., 2004; Koo et al., 2015; Chen et al., 2018). A critical difference between TNFα-mediated apoptosis and necroptosis is immune activation: apoptosis is

immunologically silent while necroptosis promotes inflammation (Cho et al., 2009; Legrand et al., 2019).

Importantly, TNFα addition to a monoclonal population elicits heterogeneity in cell fate on the single cell level. However, it is unclear to what extent cell survival versus death is dependent on pre-existing factors in the cell, e.g. TRAIL, or the result of new processes and molecule expression. For example, Spencer et al. considered TNF-related apoptosis-inducing ligand (TRAIL) and showed that cell-to-cell variability in cell survival dependent on pre-determined differences in states or levels of proteins, with the rate of BID cleavage by CASP8/10 as one of the key determinants (Spencer et al., 2009). BID cleavage was found to be dependent on the expression of several proteins, including DR4/5 receptors, CASP8, and BID. Furthermore, Spencer et al. showed protein states are transiently inherited from mother to daughter cells, although sister cells diverge over time due to protein synthesis and consequently lose correlation in cell death probability. Thus, heterogeneity cell death in response to the TNF family member TRAIL appears to be regulated by predetermined factors.

TNFα dose also affects the distribution of cell death in a population, as demonstrated by Oyler-Yaniv et al. using fibroblasts co-cultured with naive or activated bone marrow-derived macrophages (BMDMs) and infected with Herpes Simplex Virus 1 (Oyler-Yaniv et al., 2020). Notably, Oyler-Yaniv et al. found that activated BMDMs, but not naive BMDMs, restrict viral spread and additionally produce high TNFα levels. Meanwhile, BMDMs lacking TNFα or WT BMDMs with TNFα-neutralising antibodies do not restrict viral spread. The authors provide evidence that restriction of viral spread via TNFα is dependent on TNFα-induced priming of cells for death and that TNFα shortens the time between viral infection and cell death. Increasing TNFα dose switches the death response from accurate, where only virus-infected cells die, to rapid cell death at the cost of accuracy, with both virus-infected and uninfected cells dying. The advantage of the latter scenario is that bystander cells are protected from

viral infection. Therefore, cell death decisions downstream of TNFα on the single cell level can optimise tissue level responses to pathogens.

3.1.4 Roles of RELA dynamics in cell survival

The role of RELA in TNFα-mediated cell fate decisions has been studied since the 1990s, with most work supporting a pro-survival role of RELA. Initial evidence came from RelA knockout mice, which are embryonic lethal due to hypersensitivity to TNFα and successive mass liver destruction by apoptosis (Beg et al., 1995a). Two studies in 1996 emphasised the protective roles of RELA from cell death (Beg and Baltimore, 1996; Wang et al., 1996). Beg and Baltimore's 1996 publication showed that RelA knockout mouse fibroblasts and macrophages treated with TNFα have significantly reduced viability compared to RelA wildtype cells, while Wang et al. showed that, in addition to TNFα, RelA protects cells exposed to ionising radiation or the chemotherapeutic daunorubicin from apoptosis. NF-κB activity is also implicated in multiple stages of T cell development as necessary for cell survival. For instance, haematopoietic stem cells deficient in RELA and NFKB1, as well as mice lacking IKKβ, do not generate lymphocytes as precursors undergo cell death by TNFα (Horwitz et al., 1997; Senftleben et al., 2001b). Moreover, all thymocytes have constitutive NF-κB activation (Körner et al., 1991) and spontaneous apoptosis is observed in thymocytes with NF-κB inhibition (Voll et al., 2000).

Mechanistically, RELA can inhibit cell death by inducing pro-survival genes such as cFLIP (Kreuz et al., 2001) and Bcl-2 (Tamatani et al., 1999). cFLIP forms a complex with and blocks caspase 8 which would prevent apoptosis and necroptosis (Chang et al., 2002; Yu et al., 2009), while Bcl-2 binds to Bax preventing Bax from forming pores in the mitochondrial outer membrane (Llambi et al., 2011). RELA also promotes the expression of the cellular inhibitor of apoptosis proteins 1 and 2 (cIAP1 and cIAP2) (Chu et al., 1997; Wang et al., 1998).

More recently, a study looked at how TNFα-induced RELA activation affected TNFα-induced necroptosis by live microscopy and mathematical modelling of death rate dynamics in L929 murine fibroblasts (Oliver Metzig et al., 2020). TNFα was found not to induce FLIP-L (long cFLIP) expression but did induce A20 expression in a RELA-dependent manner, which protected a subset of cells from transient TNFα exposure but not long-term TNFα. A20 was identified to inhibit the RIPK1-RIPK3 complex, therefore blocking necroptosis. Necroptosis is therefore dependent on TNFα duration and whether RELA dynamics are intact, as removing RelA by CRISPR led to earlier cell death. Thus, RELA may play an essential role in protecting cells from premature necroptosis.

On the other hand, an earlier study by Marie Oliver Metzig and supporting authors identified a potential role for RELA in promoting cell death (Oliver Metzig et al, 2016). In colon cancer cells in the presence of pan-caspase inhibitor Z-VAD, 5-fluorouracil (5-FU) induces necroptosis mediated by autocrine TNFα production via RELA. This was shown by 5-FU and Z-VAD combination increasing transcription of certain RELA target genes, including TNFα but not IκBα, compared to each treatment alone, and genetic silencing of RELA by siRNA blocking both autocrine TNFα production and necroptosis. Other studies have also provided evidence for pro-cell death roles of RELA in neurons. For example, the neurotoxic effects of the amino acid glutamate in rat primary neuronal cells are associated with NF-κB activation and blocking of NF-κB activation using aspirin or salicylate leads to a neuroprotective effect (Grilli et al., 1996).

Moreover, RELA may play a role in dying cells when activated in parallel. For instance, Yatim et al. identified that RIPK3-mediated necroptosis leads to RELA activation in a RIPK1 dependent-manner. Notably, RELA transcriptional activation of IL-6 in dying cells was necessary for CD8+ T cell activation through antigen cross-priming. Therefore, RELA activity may have an important role in cell-death initiated tumour immunity (Yatim et al., 2015)

In this chapter, I characterised single RELA translocation dynamics using live imaging and automated image analysis in two human PDAC cell lines - MIA PaCa2 and PANC1 - in response to the inflammatory cytokine TNFα. I then tested the effect of TNFα 'washout' on RELA nuclear localisation, which informs on the presence of mechanisms feeding back onto RELA activation in PDAC cells. Finally, I assessed whether TNFα-induced RELA dynamics are cell cycle dependent and how RELA translocation profiles relate to cell survival versus cell death on the single cell level.

3.2 Results

3.2.1 CRISPR-CAS9 FP-addition to RELA and PCNA

I used the frequently studied human PDAC lines MIA PaCa2 and PANC1 cells as models for studying PDAC biology as they harbour mutations common in PDAC, including KRAS and p53 mutations and homozygous deletions in CDKN2A/p16 (Deer et al., 2010). MIA PaCa2 and PANC1 cells are both epithelial in origin but have distinct cell morphology and are therefore also useful for analysis of cell shape interaction with RELA (Chapter 4). The MIA PaCa2 cell line is derived from the PDAC tumour of a 65 year old male, with the tumour involving the pancreas body and tail and the cancer spreading to the periaortic area (Yunis et al., 1977), while the PANC1 cell line is derived from a 56 year old male from a tumour arising from the pancreas head, with metastasis in one lymph node (Lieber et al., 1975). MIA PaCa2 cells have subpopulations of attached spindle-shaped cells and rounded detached cells, while PANC1 cells have more classical epithelial morphology and form sheets.

To study dynamic changes in RELA localisation over time, I used CRISPR-CAS9 gene editing to fluorescently tag endogenous RELA at the C-terminus with eGFP (abbreviated as RELA-GFP) (Figure 3.1A). The C-terminus was selected to avoid interference with the N-terminal Rel homology domain, which contains the transactivation domain and the DNA-binding domain. GFP+ clones were selected using FACS, single cell sorted and

expanded into monoclonal cell lines. The presence of edited alleles was checked by PCR and gel electrophoresis (Figure 3.1B), followed by extraction and DNA sequencing. Selected monoclonal lines were checked for responsiveness to 1 hr 10 ng/ml TNFα, which induced significant RELA nuclear localisation at all seeding densities (Figure 3.1C-C'). Furthermore, normal interaction with other NF-κB family members and IκB proteins was checked by Co-IP using GFP-Trap with MIA PaCa2 cells expressing endogenous RELA-GFP (Figure 3.1D-D').

Figure 3.1

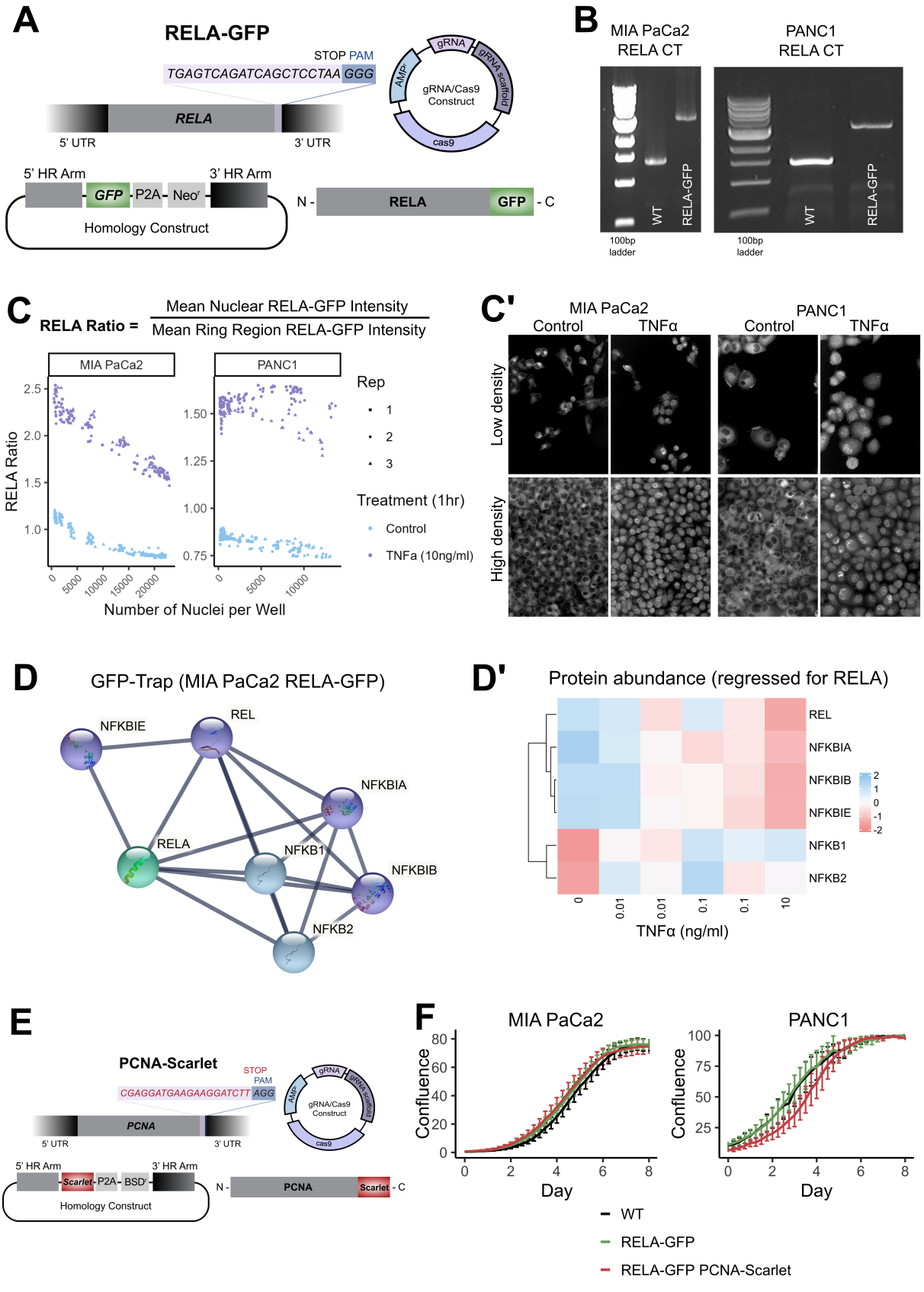
A
RELA-GFP
STOP PAM
TGAGTCAGATCAGCTCCTAA GGG
RELA
5' UTR
3' UTR
gRNA
gRNA scaffold
AMP
gRNA/Cas9 Construct
cas9
5' HR Arm
GFP
P2A
Neo
3' HR Arm
Homology Construct
N - RELA GFP - C
B
MIA PaCa2 RELA CT
PANC1 RELA CT
WT
RELA-GFP
100bp ladder
C
RELA Ratio = Mean Nuclear RELA-GFP Intensity / Mean Ring Region RELA-GFP Intensity
MIA PaCa2
PANC1
RELA Ratio
Number of Nuclei per Well
Rep
1
2
3
Treatment (1hr)
Control
TNFa (10ng/ml)
C'
MIA PaCa2
PANC1
Control
TNFα
Low density
High density
D
GFP-Trap (MIA PaCa2 RELA-GFP)
NFKBIE
REL
NFKBIA
RELA
NFKB1
NFKBIB
NFKB2
D'
Protein abundance (regressed for RELA)
REL
NFKBIA
NFKBIB
NFKBIE
NFKB1
NFKB2
TNFα (ng/ml)
E
PCNA-Scarlet
STOP PAM
CGAGGATGAAGAAGGATCTT AGG
PCNA
5' UTR
3' UTR
5' HR Arm
Scarlet
P2A
BSD
3' HR Arm
Homology Construct
N - PCNA Scarlet - C
F
MIA PaCa2
PANC1
Confluence
Day
WT
RELA-GFP
RELA-GFP PCNA-Scarlet

Figure 3.1 CRISPR-CAS9 tagging of RELA and PCNA

(A) Schematic of CRISPR gRNA and homology construct with neomycin (neo) resistance for tagging of the RELA C-terminus with GFP. (B) Agarose gel with gDNA extracted from the RELA C-terminus of WT and RELA-GFP tagged PDAC cells and amplified by PCR. (C) Well measurements RELA ratio (nuc/ring region RELA-GFP intensity) and (C') confocal microscopy images of cells seeded at varying densities and treated with 1 hr DMSO control or 10 ng/ml TNFα (n = 3 experimental repeats). (D-D') Summary of proteins detected by Co-IP and mass spectrometry using GFP-Trap in MIA PaCa2 RELA-GFP cells (see Results Chapter 5). Cells were treated with TNFα (0, 0.01, 0.1 or 10 ng/ml) for 1 hr. Pull-downs were analysed using mass spectrometry. n = 1 experimental repeats for 0 and 10 ng/ml TNFα and n = 2 experiments repeats for 0.01 and 0.1 ng/ml TNFα. (D) STRING network for pulled-down proteins in NF-κB signalling pathway. (D') Protein abundances at each TNFα dose adjusted to RELA abundance. (E) Schematic of CRISPR gRNA and homology construct with blasticidin (BSD) resistance for tagging of the RELA C-terminus with Scarlet. (F) Number of cells over time (Incucyte analysis) for PDAC cells +/- RELA-GFP +/- PCNA-Scarlet. Produced in Graphpad Prism.

I also introduced mScarlet-I to the C-terminus of PCNA (Proliferating Cell Nuclear Antigen; abbreviated as PCNA-Scarlet) – a processivity factor for DNA polymerase δ that functions during replication – which served as a nuclear marker for segmentation and as a cell cycle marker (Kurki et al., 1986; Barr et al., 2017) (Figure 3.1E). The proliferation rate of RELA-GFP tagged and double-tagged (addition of PCNA-Scarlet) cells was comparable to the wildtype counterparts, indicating that the PCNA alteration did not affect PCNA function (Figure 3.1F).

3.2.2 MIA PaCa2 cells respond to TNFα with sustained and non-oscillatory RELA nuclear translocation

To observe live RELA translocation dynamics in response to inflammatory stimuli, I used timelapse confocal microscopy with automated image analysis to track changes in RELA-GFP localisation on a single cell level in response to treatment with TNFα. 0.01 ng/ml TNFα is a physiological dose relevant to healthy and malignant tissue, while 0.1 ng/ml TNFα is found in highly inflammatory PDAC microenvironments (Zhao et al., 2016). 10 ng/ml TNFα was used in several studies assaying RELA translocation and is included for comparison, but is substantially above physiological levels (Zhao et al., 2016). RELA localisation was measured by segmenting nuclei and the ring region (the region around the nucleus in the cytoplasm) using the PCNA channel, then calculating the ratio between nuclear RELA-GFP intensity and mean ring region RELA-GFP intensity (Figure 3.2).

Figure 3.2

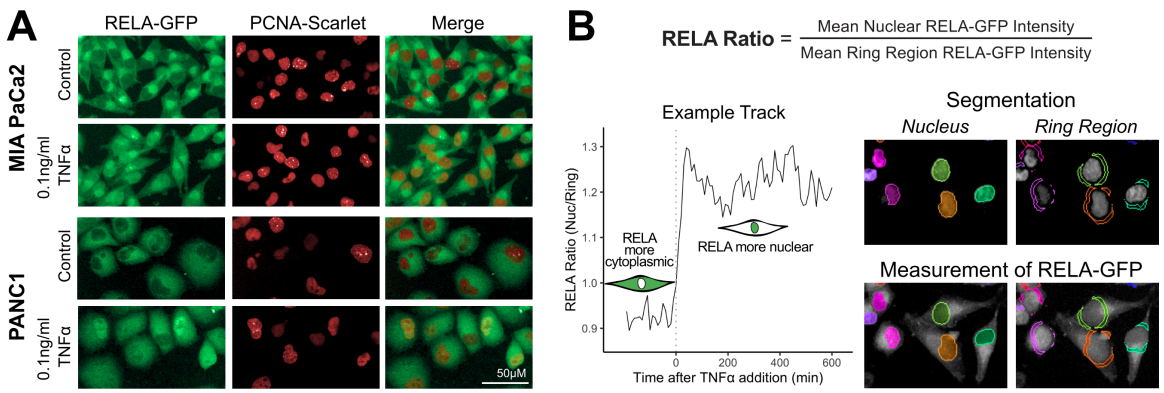
A
RELA-GFP
PCNA-Scarlet
Merge
MIA PaCa2
PANC1
Control
0.1ng/ml TNFα
50μM
B
RELA Ratio = Mean Nuclear RELA-GFP Intensity / Mean Ring Region RELA-GFP Intensity
Example Track
RELA Ratio (Nuc/Ring)
RELA more cytoplasmic
RELA more nuclear
Time after TNFα addition (min)
Segmentation
Nucleus
Ring Region
Measurement of RELA-GFP

Figure 3.2 Automated image-based quantification of RELA subcellular localisation

(A) Confocal microscopy of endogenous RELA-GFP and PCNA-Scarlet in MIA PaCa2 and PANC1 cells in control or 0.1 ng/ml TNFα conditions. (B) Example of automated segmentation of nuclear and ring regions using PCNA-Scarlet. RELA-GFP intensity is measured in both regions and a ratio is calculated to measure RELA localisation, with higher RELA ratios representing more nuclear RELA. RELA ratio is tracked over time on a single cell basis prior to and following TNFα treatment. Fixed cells are segmented and analysed using Columbus (PerkinElmer), StarDist (Fiji) or Nuclitrack for live imaging.

At the population level, varying TNFα levels in MIA PaCa2 led to largely monophasic RELA translocation responses (Figure 3.3A). However, I observed extensive cell-to-cell variability in RELA translocation dynamics. Therefore, I quantified RELA ratio on the single cell level for traces from all TNFα treatments from -120 min to +600 min relative to TNFα addition. I then used hierarchical clustering software to identify groups of RELA translocation responses (Dobrzyński et al., 2020). I identified four groups of RELA dynamics in MIA PaCa2 cells (Figure 3.3B and C).

Figure 3.3

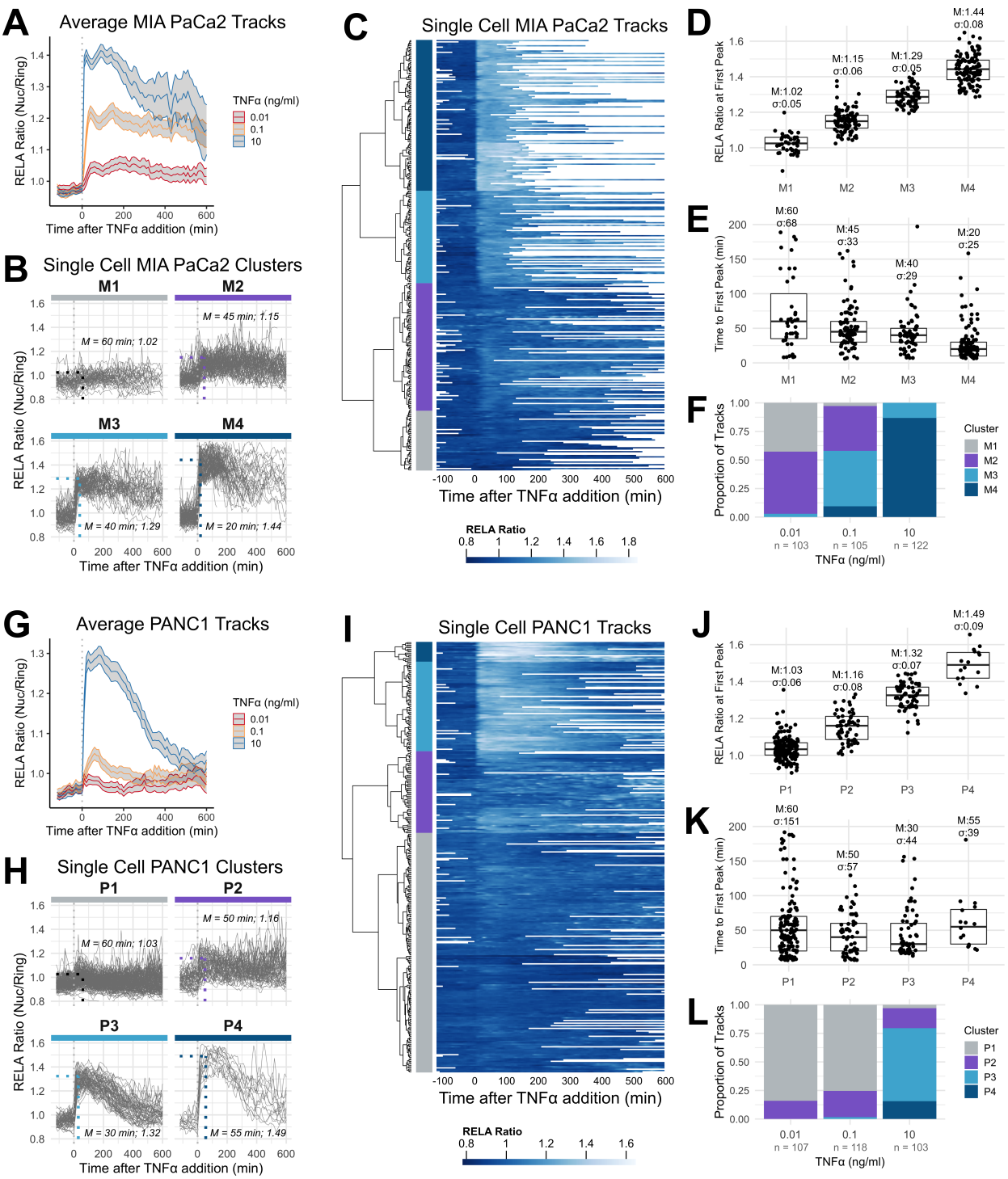
A
Average MIA PaCa2 Tracks
RELA Ratio (Nuc/Ring)
Time after TNFα addition (min)
TNFα (ng/ml)
0.01
0.1
10
B
Single Cell MIA PaCa2 Clusters
M1
M2
M3
M4
M = 60 min; 1.02
M = 45 min; 1.15
M = 40 min; 1.29
M = 20 min; 1.44
C
Single Cell MIA PaCa2 Tracks
Time after TNFα addition (min)
RELA Ratio
D
RELA Ratio at First Peak
M:1.02 σ:0.05
M:1.15 σ:0.06
M:1.29 σ:0.05
M:1.44 σ:0.08
E
Time to First Peak (min)
M:60 σ:68
M:45 σ:33
M:40 σ:29
M:20 σ:25
F
Proportion of Tracks
Cluster
0.01 n = 103
0.1 n = 105
10 n = 122
TNFα (ng/ml)
G
Average PANC1 Tracks
H
Single Cell PANC1 Clusters
P1
P2
P3
P4
M = 60 min; 1.03
M = 50 min; 1.16
M = 30 min; 1.32
M = 55 min; 1.49
I
Single Cell PANC1 Tracks
J
M:1.03 σ:0.06
M:1.16 σ:0.08
M:1.32 σ:0.07
M:1.49 σ:0.09
K
M:60 σ:151
M:50 σ:57
M:30 σ:44
M:55 σ:39
L
0.01 n = 107
0.1 n = 118
10 n = 103

Figure 3.3 Categories of RELA dynamics in PDAC cells in response to TNFα

(A-C) RELA-GFP translocation responses in MIA PaCa2 cells per TNFα dose (0.01 ng/ml, 0.1 ng/ml and 10 ng/ml) from -120 min to +600 min relative to TNFα addition. n = 50-60 tracked cells per TNFα dose for each of two experimental repeats. (A) Average RELA-GFP translocation responses. Lines denote the mean and grey ribbons represent the standard error of the mean (SEM). (B-C) Single cell RELA-GFP translocation responses. Hierarchical clustering of RELA ratio tracks of MIA PaCa2 collated from all TNFα treatments (0.01 ng/ml, 0.1 ng/ml and 10 ng/ml) into four groups using Time Course Inspector in R with the 'Ward D2' linkage method and 'Manhattan' dissimilarity measure. Heatmap is coloured according to the RELA ratio and each row represents an individual track/cell. Individual tracks per cluster are shown to the right. Clusters from MIA PaCa2 cells are prefixed with 'M'. (D) Amplitude and (E) time of first RELA-GFP ratio peak in individual cells for MIA PaCa2 cells for clusters M1-M4. Boxplots show median and interquartile range. M = median per cluster. σ = standard deviation per cluster. (F) Proportion of MIA PaCa2 tracks per TNFα treatment in each cluster M1-M4. (G) Average RELA-GFP translocation responses in PANC1 cells per TNFα dose. n = 50-60 tracked cells per TNFα dose. (H-I) Hierarchical clustering of RELA ratio tracks for PANC1 cells collated from all TNFα treatments (0.01 ng/ml, 0.1 ng/ml and 10 ng/ml). Clusters from PANC1 cells are prefixed with 'P'. (J) Amplitude and (K) time of first RELA-GFP ratio peak in individual cells for PANC1 cells per cluster P1-P4. Boxplots show median and interquartile range. M = median per cluster. σ = standard deviation per cluster. (L) The proportion of PANC1 tracks per TNFα treatment in each cluster P1-P4.

To profile clusters quantitatively, I detected peaks in RELA ratio tracks and calculated the amplitude and time after TNFα addition to reach the first peak. Clusters differed significantly in median first peak RELA ratios (amplitude), ranging from 1.02 (Cluster M1) to 1.44 (Cluster M4) (Figure 3.3D). Interestingly, 32 % of cells from Cluster M1, equivalent to 5 % of all tracked MIA PaCa2 cells, maintained predominantly cytoplasmic RELA (peak RELA ratio < 1) following TNFα addition.

Across TNFα doses, MIA PaCa2 cells had a median time to the first peak of 40 min, which is comparable to our findings in breast epithelial cells (Sero et al., 2015). However, I also observed heterogeneity in terms of the rate of RELA translocation, as clusters with higher peak RELA ratio peaked at a shorter time after TNFα addition (Figure 3.3E).

All TNFα doses evoked multiple RELA response classes with reproducible amounts of heterogeneity. There was a trend for increasing doses of TNFα to be associated with more rapid and more intense peak RELA ratios. M1 and M2 classes predominate at the TNFα low doses, while 10 ng/ml responses were enriched for M4 and M3 classes. All four classes were observed at physiological TNFα levels (0.1 ng/ml), leading to the highly heterogeneous responses (Figure 3.3F).

3.2.3 PANC1 cells respond to TNFα with damped and non-oscillatory RELA responses

I also assayed TNFα stimulated RELA dynamics in PANC1 cells. Overall, PANC1 cells had lower RELA nuclear translocation than the MIA PaCa2 cells. Moreover, 0.01 ng/ml and 0.1 ng/ml TNFα induced similar responses in PANC1 cells but not in MIA PaCa2 cells (Figure 3.3G), indicating a higher threshold before inflammation triggers a RELA response in PANC1 cells.

As with MIA PaCa2 cells, I identified four classes of TNFα-induced RELA responses in PANC1 cells: weakly responsive (Class P1); moderately responding with sustained peak

RELA ratio (Class P2), or strong response with damped nuclear RELA localisation (Clusters P3 and P4) (Figure 3.3H-K). 21 % of cells in Class P1, and 12 % of all PANC1 cells, maintained cytoplasmic localisation following TNFα stimulation (peak RELA ratio < 1) indicating around twice as many non-responsive PANC1 cells compared to MIA PaCa2 cells. PANC1 Clusters P3 and P4 represent a type of translocation response uncommon in MIA PaCa2 cells in which RELA nuclear localisation significantly drops after peaking. Thus, in contrast to MIA Paca2 cells where many cells sustain high nuclear RELA localisation, RELA activation declines following TNFα stimulation in PANC1 cells, typically resulting in re-localisation to the cytoplasm within 10 hours. As negative feedback signalling is a widely reported feature of RELA signalling (Hoffmann et al., 2002; Kearns et al., 2006), these data suggest that negative feedback regulation is intact in PANC1 cells but compromised in MIA PaCa2 cells.

Across TNFα doses, PANC1 cells had a median time to the first peak of 50 min, indicating moderately slower RELA nuclear translocation in PANC1 cells compared to MIA PaCa2 cells. PANC1 and MIA PaCa2 cells also differed in the proportion of cells falling into each RELA translocation class, especially at physiological TNFα doses. In MIA PaCa2 cells, RELA translocation dynamics exhibit continuity of responses at TNFα physiological levels (Figure 3.3F), as they can be grouped into all classes (M1-M4). Moreover, MIA Paca2 display incremental responses to increasing TNFα dose while RELA responses in PANC1 cells appear to be more ‘all-or-none’, whereby RELA either responds very little at physiological doses (class P1 and P2) or is ‘all in’ for hyperphysiological doses (class P3 and P4) (Figure 3.3L).

Strikingly, although MIA PaCa2 and PANC1 cells showed fluctuations in RELA ratio over time, neither demonstrated the amplitude or regularity of periodic oscillations on a single cell level observed in other cell lines (Nelson et al., 2004; Tay et al., 2010; Sero et al., 2015; Zambrano et al., 2016). As RELA oscillations are driven by negative feedback by IκBα (Hoffmann et al., 2002), lack of oscillations provides further evidence that IκBα function is

perturbed in MIA PaCa2 cells. Interestingly, although some form of negative feedback appears in PANC1 cells, the pathway parameters do not support oscillations.

3.2.4 RELA ratio at early timepoints correlates with RELA ratio at late timepoints and absolute nuclear abundance

To look for patterns in RELA responses, I measured the mean RELA ratio on a single basis in the whole tracked period (0-600 min), in the period immediately after TNFα addition (0-60 min), and in the period that most often succeeds peak nuclear RELA localisation (60-600 min) (Figure 3.4A and B). Absolute nuclear RELA intensity was also measured to identify whether nuclear occupancy (nuclear RELA) alone correlates with the fold-change in RELA localisation (RELA ratio). There were consistent and strong positive correlations between peak RELA ratio amplitude, mean RELA ratio in all periods, and nuclear abundance in all periods. Similar to previous reports in mouse fibroblasts and macrophages (Martin et al., 2020; Tay et al., 2010), I identified a negative non-linear correlation between time to peak RELA ratio and peak amplitude in human PDAC cells across TNFα doses, indicating that rapidly responding cells respond with higher nuclear localisation. However, within each TNFα treatment there was no clear relationship between the timing and amplitude of peak RELA ratio (Figure 3.4C). Interestingly, the RELA ratio at later timepoints scaled linearly with the RELA ratio at early timepoints across TNFα doses (MIA PaCa2 $R^2 = 0.85$; PANC1 $R^2 = 0.71$) as well as within TNFα doses (Figure 3.4D), as did the relationship between RELA ratio and nuclear abundance at early timepoints (Figure 3.4E). Therefore, the period immediately after TNFα addition is a good indicator of the prolonged RELA response in PDAC cells.

Figure 3.4

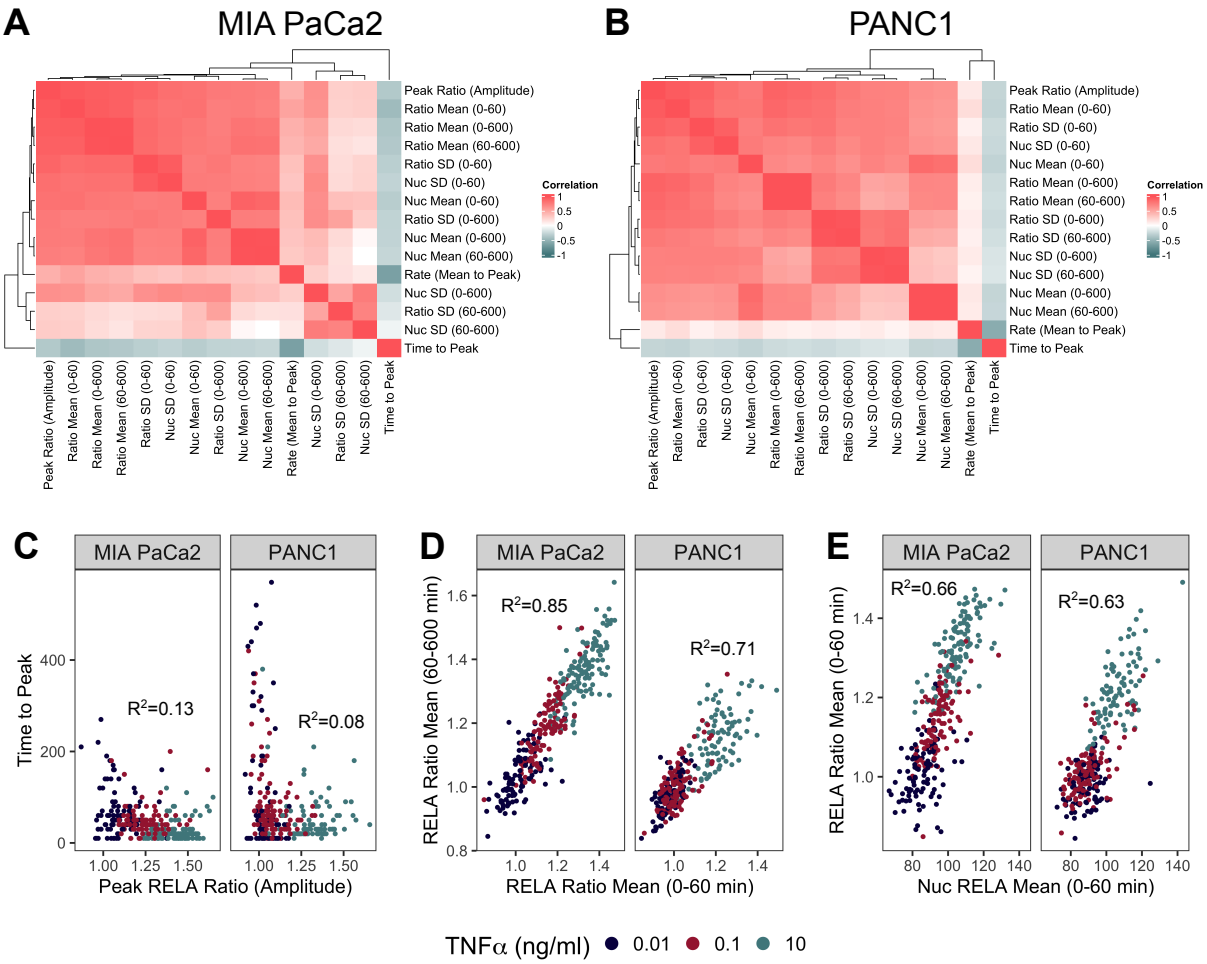
A
MIA PaCa2
B
PANC1
Peak Ratio (Amplitude)
Ratio Mean (0-60)
Ratio Mean (0-600)
Ratio Mean (60-600)
Ratio SD (0-60)
Nuc SD (0-60)
Nuc Mean (0-60)
Ratio SD (0-600)
Nuc Mean (0-600)
Nuc Mean (60-600)
Rate (Mean to Peak)
Nuc SD (0-600)
Ratio SD (60-600)
Nuc SD (60-600)
Time to Peak
Correlation
1
0.5
0
-0.5
-1
C
MIA PaCa2
PANC1
Time to Peak
Peak RELA Ratio (Amplitude)
R²=0.13
R²=0.08
D
RELA Ratio Mean (60-600 min)
RELA Ratio Mean (0-60 min)
R²=0.85
R²=0.71
E
RELA Ratio Mean (0-60 min)
Nuc RELA Mean (0-60 min)
R²=0.66
R²=0.63
TNFα (ng/ml) 0.01 0.1 10

Figure 3.4 Relationships between RELA dynamics features

(A-B) Correlations between single cell measurements of the mean and standard deviation for RELA ratio (nuc/ring region RELA intensity) or nuclear RELA, in addition to measurements for peak RELA ratio: amplitude, time to peak (minutes), and rate (amplitude/time). (C-E) Single cell RELA measurements. Point colours correspond to TNFα dose. (C) In MIA PaCa2 cells, peak RELA ratio amplitude and time to peak are not associated. In PANC1 cells, peak RELA ratio amplitude and time to peak (minutes) have a negative non-linear relationship across TNFα doses. (D) Within and across TNFα doses, RELA ratios at early timepoints (0-60 min) are positively correlated with RELA ratios at later timepoints (60-600 min) and also with (E) absolute nuclear RELA intensity at early timepoints following TNFα addition.

3.2.5 RELA translocation responses to TNFα are cell cycle independent

My data suggest that RELA translocation in some cells is unresponsive to TNFα-stimulation. As RELA nuclear translocation was identified as suppressed during S-phase of the cell cycle in HeLa cells (Ankers et al., 2016), I tested whether RELA translocation is cell cycle dependent in PDAC cells. To this end, I used changes in the appearance and intensity of endogenous PCNA-Scarlet to mark cell cycle transitions. Consistent with prior observations of PCNA appearance (Kurki et al., 1986), endogenous tagged PCNA-Scarlet appeared uniform in G1, punctate during S-phase, and uniform with high intensity in G2 (Figure 3.5A and B).

Figure 3.5

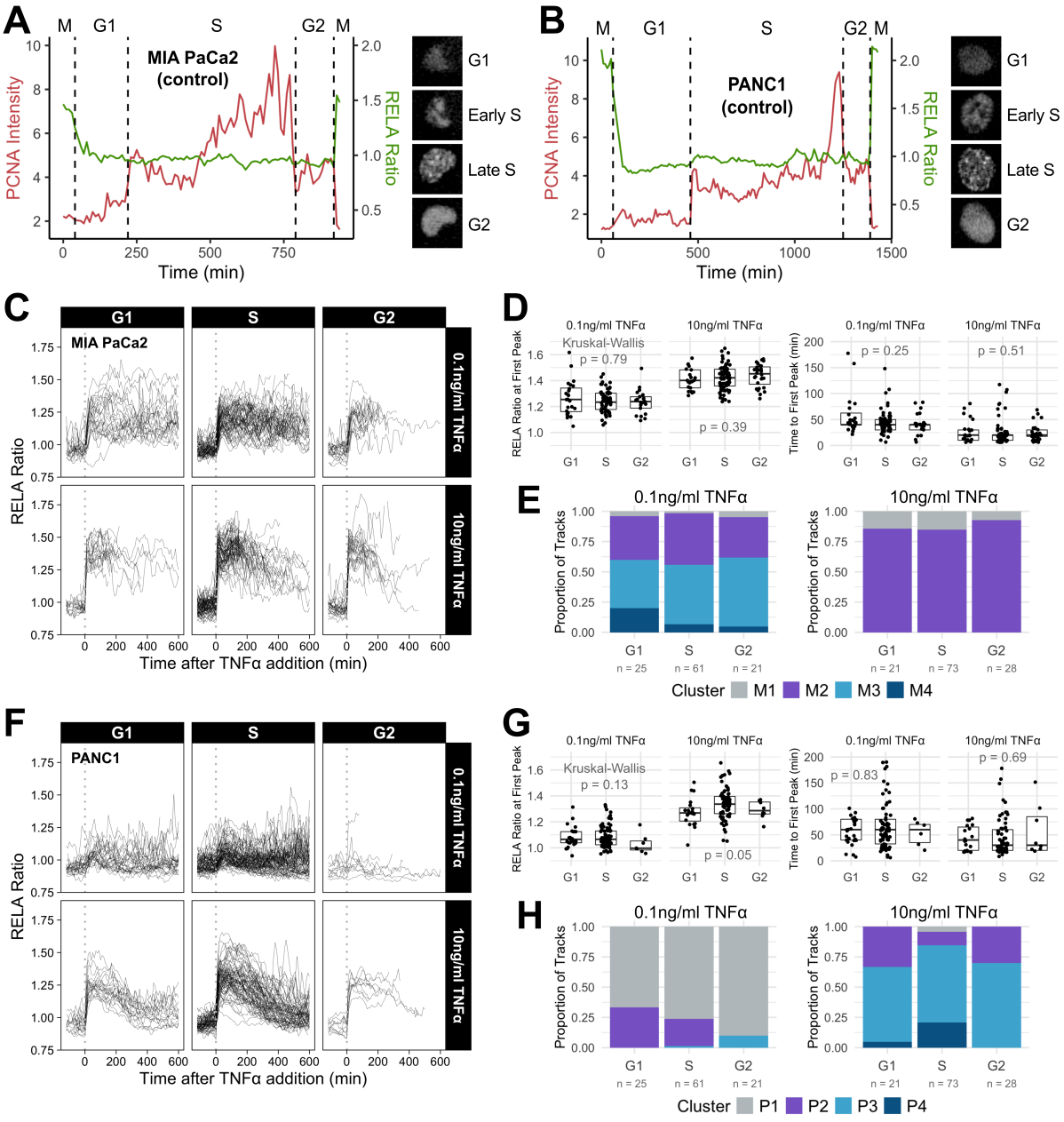
A
M G1 S G2 M
MIA PaCa2
(control)
PCNA Intensity
RELA Ratio
Time (min)
G1
Early S
Late S
G2
B
PANC1
(control)
C
MIA PaCa2
0.1ng/ml TNFα
10ng/ml TNFα
RELA Ratio
Time after TNFα addition (min)
D
Kruskal-Wallis
p = 0.79
p = 0.39
p = 0.25
p = 0.51
RELA Ratio at First Peak
Time to First Peak (min)
E
Proportion of Tracks
Cluster M1 M2 M3 M4
F
PANC1
G
p = 0.13
p = 0.05
p = 0.83
p = 0.69
H
Cluster P1 P2 P3 P4

Figure 3.5 Cell cycle independence of RELA nuclear translocation with TNFα

(A-B) Live imaging traces of endogenous PCNA-Scarlet and RELA ratio in single representative untreated (A) MIA PaCa2 cell (B) PANC1 cells. Measurements begin during cell birth, span across the cell cycle and conclude at the subsequent cell division. Images were taken at 10 min intervals. Nuclear PCNA-Scarlet (floored mean) and nuclear and ring region RELA-GFP measurements were calculated in Nuclitrack software. Transitions between cell cycle stages based on concomitant changes in PCNA intensity and appearance are marked with dashed lines. Images of PCNA-Scarlet corresponding to the tracked cell are shown to the right of each trace showing the cell in G1, an early timepoint during S phase, a late timepoint during S phase, and G2. (C) Single cell RELA ratio tracks for MIA PaCa2 cells categorised by cell cycle stage at the time of TNFα addition, based on the intensity and appearance of PCNA-Scarlet. (D) Single cell measurements for MIA PaCa2 cells of the RELA ratio at first peak (amplitude) and time to first peak per cell cycle stage and TNFα dose. Boxplots show median and interquartile range. (E) Proportion of RELA ratio tracks from MIA PaCa2 cells in each RELA translocation cluster grouped by cell cycle stage at the time of TNFα addition calculated separately for 0.1 ng/ml or 10 ng/ml TNFα treatment. (F) Cell cycle stage categorised single cells tracks for PANC1 cells. (G) Single cell measurements of RELA ratio at first peak (amplitude) and time to first peak per cell cycle stage and TNFα dose for PANC1 cells. (H) The proportion of RELA ratio tracks from PANC1 cells in each RELA translocation cluster grouped by cell cycle stage.

I categorised each tracked cell by cell cycle stage at the time of 0.1 ng/ml or 10 ng/ml TNFα addition and calculated the amplitude and timing of the first peak of RELA ratio, as well as the RELA translocation cluster distribution (Figure 3.5C-H). Broadly, I did not find differences in the time series profiles of RELA translocation responses between cells in different cell cycle stages (Figure 3.5C and F). I also did not find differences in the amplitude or time to RELA ratio peak (Figure 3.5D and G; Kruskal-Wallis Test, $p>0.05$), or enrichment of cell cycle stages in different RELA response clusters (Figure 3.5E and H) for MIA PaCa2 or PANC1 cells. Altogether, these data indicate that cell cycle progression does not underlie the observed heterogeneity in RELA translocation to TNFα in PDAC cells.

3.2.6 RELA nuclear translocation is required for survival with TNFα at the population level

As TNFα can induce cell death or survival (Hsu et al., 1995; Beg and Baltimore, 1996; Kelliher et al., 1998), I sought to assess whether PDAC cells can proliferate with prolonged TNFα treatment, given that TNFα is overexpressed with PDAC progression (Zhao et al., 2016). To assay the effect of physiologically low versus high TNFα on proliferation and cell survival, I detected the number of MIA PaCa2 cells over a 48 hr period with a range of TNFα concentrations (Figure 3.6A). MIA PaCa2 cells treated with 0.01 ng/ml or 0.1ng/ml TNFα increased in cell number over time with a mild delay compared to control cells. However, 10 ng/ml TNFα induced a net loss of cells. Therefore, on a population level, PDAC cells can proliferate in physiologically low and high concentrations of TNFα, but not in the presence of hyperphysiological TNFα.

Figure 3.6

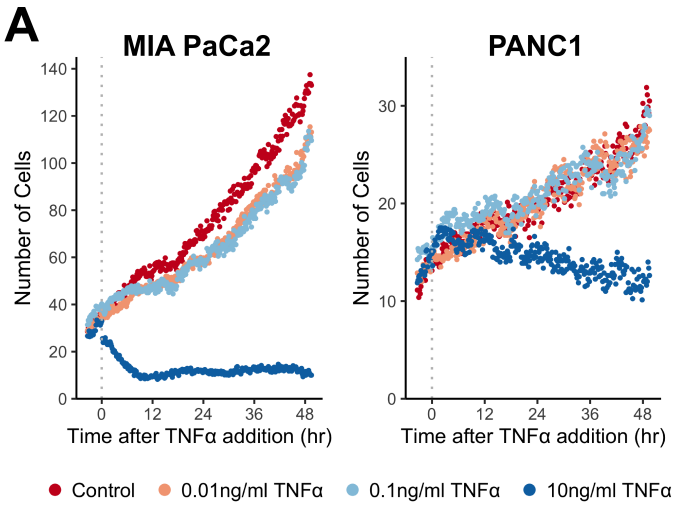

B Survival of tracked cells by treatment

MIAPaCa2

TNFα (ng/ml)	Dies		Survives	
	n	%	n	%
0.01	7	7	93	93
0.1	24	23	80	76
10	97	80	24	20

PANC1

TNFα (ng/ml)	Dies		Survives	
	n	%	n	%
0.01	18	19	75	81
0.1	41	36	73	64
10	54	61	35	39

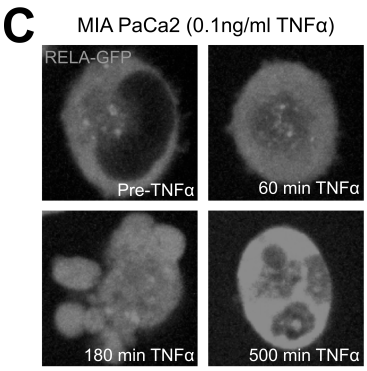

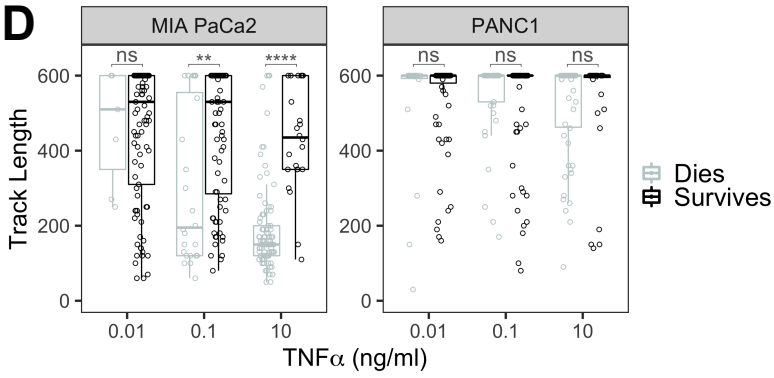

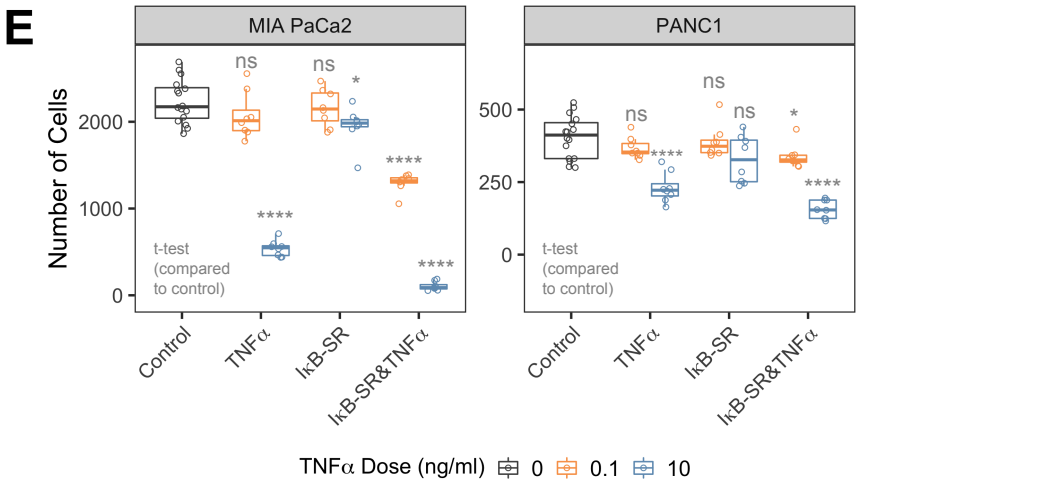

Figure 3.6 RELA is required for cell survival on the population level in the presence of TNFα

(A) Cell number over time (-3 hr to +48 hr) of MIA PaCa2 and PANC1 cells treated with TNFα, assessed by live imaging and automated image analysis. (B) Number and percentage of tracked cells dying or surviving during the 48 hr live imaging period. Percentages are calculated by cell line and TNFα dose. (C) Representative confocal microscopy images of RELA-GFP in an MIA PaCa2 cell undergoing cell death following 0.1 ng/ml TNFα. The cell displays blebbing and swelling before membrane breakdown. (D) Track length (minutes) prior to death or mitosis of MIA PaCa2 and PANC1 cells tracked for 10 hr following TNFα addition (0.01, 0.1 or 10 ng/ml). Boxplots show median and interquartile range. Statistical significance: t-test comparisons of dying versus surviving cells by cell line and TNFα dose, with Benjamini–Hochberg correction. ns (non-significant) = $p > 0.05$, * = $0 < 0.05$, ** = $p < 0.01$, *** = $p < 0.001$, **** = $p < 0.0001$. (E) Number of PDAC cells after 48 hr doxycycline induction of IκB-SR (1 μg/ml dox) and 10 hr treatment with TNFα (0.1 ng/ml or 10 ng/ml). Cell number was quantified using automated image analysis. Statistical significance obtained by comparisons of each treatment to cell line control with Benjamini–Hochberg correction. ns (non-significant) = $p > 0.05$, * = $0 < 0.05$, ** = $p < 0.01$, *** = $p < 0.001$, **** = $p < 0.0001$.

To assess whether cells subjected to TNFα undergo cell death and the effect of TNFα dose on the distribution of cell fate, I noted whether each tracked cell from Figure 3.3 dies or divides during the total 48 hr imaging period following TNFα treatment. As expected, I found that the percentage of dying cells increased with TNFα dose in both MIA PaCa2 and PANC1 cells (Figure 3.6B). Dying cells typically displayed blebbing followed by swelling then membrane breakdown (Figure 3.6C). The track lengths were shorter in dying compared to surviving MIA PaCa2 cells, with increasing TNFα also decreasing track length in dying cells with a median of 510, 195 and 150 min for 0.01, 0.1 and 10 ng/ml TNFα for MIA PaCa2 cells. Therefore, higher TNFα dose is associated with more rapid cell death in MIA PaCa2 cells. However, no difference in track length was observed between dying cells from each TNFα for PANC1 (median = 600 for all doses), perhaps due to the longer cell cycle length and slower response to TNFα in PANC1 cells (Figure 3.6D).

I investigated whether RELA nuclear translocation, which functions in pro-survival signalling downstream of TNFα (Beg and Baltimore, 1996), protects PDAC cells from TNFα regulated cell death. To test this, I introduced a doxycycline-inducible lentiviral construct encoding a non-degradable form of IκB, termed IκB-SR (Super Repressor), to the MIA PaCa2 cell line expressing RELA-GFP. I treated this cell line with TNFα (0.1 ng/ml or 10 ng/ml) for 10 hr with or without prior IκB-SR induction to test whether RELA nuclear translocation alters the effect of TNFα on cell survival. While IκB-SR induction or TNFα alone caused a minor reduction in cell number, IκB-SR in combination with TNFα at either dose caused a significant reduction in cell number (Figure 3.6E). Therefore, I concluded that RELA nuclear translocation promotes PDAC cell survival in physiologically high levels of TNFα.

3.2.7 Cell death is associated with high RELA nuclear localisation on the single cell level in MIA PaCa2 cells

In order to determine whether cell survival is associated with RELA dynamics on the single cell level, I considered whether there are differences in the mean and standard deviation of

RELA ratio or absolute nuclear abundance between surviving and dying cells at either early timepoints (0-60 min), later timepoints (60-600 min), or across the whole tracked period following TNFα addition (0-600 min) (Figure 3.7A and B). In response to 0.1 ng/ml TNFα, Both the RELA ratio and nuclear RELA were higher in MIA PaCa2 cells at later timepoints in dying cells compared to surviving cells while fluctuation in nuclear RELA (SD) was higher in surviving cells. At the same time, there were non-significant differences in RELA localisation by cell fate at early timepoints. In line with these findings, there were no differences in the rate, amplitude and timing of peak RELA ratio between dying and surviving MIA PaCa2 cells (Figure 3.7C). In terms of the distribution of RELA response clusters, dying cells have a higher proportion of M4 (strongly responding) cells, while surviving cells have a higher proportion of M2 (mildly responding) cells ($\chi^2 = 6.8$, $p = 0.08$) (Figure 3.7D).

Figure 3.7

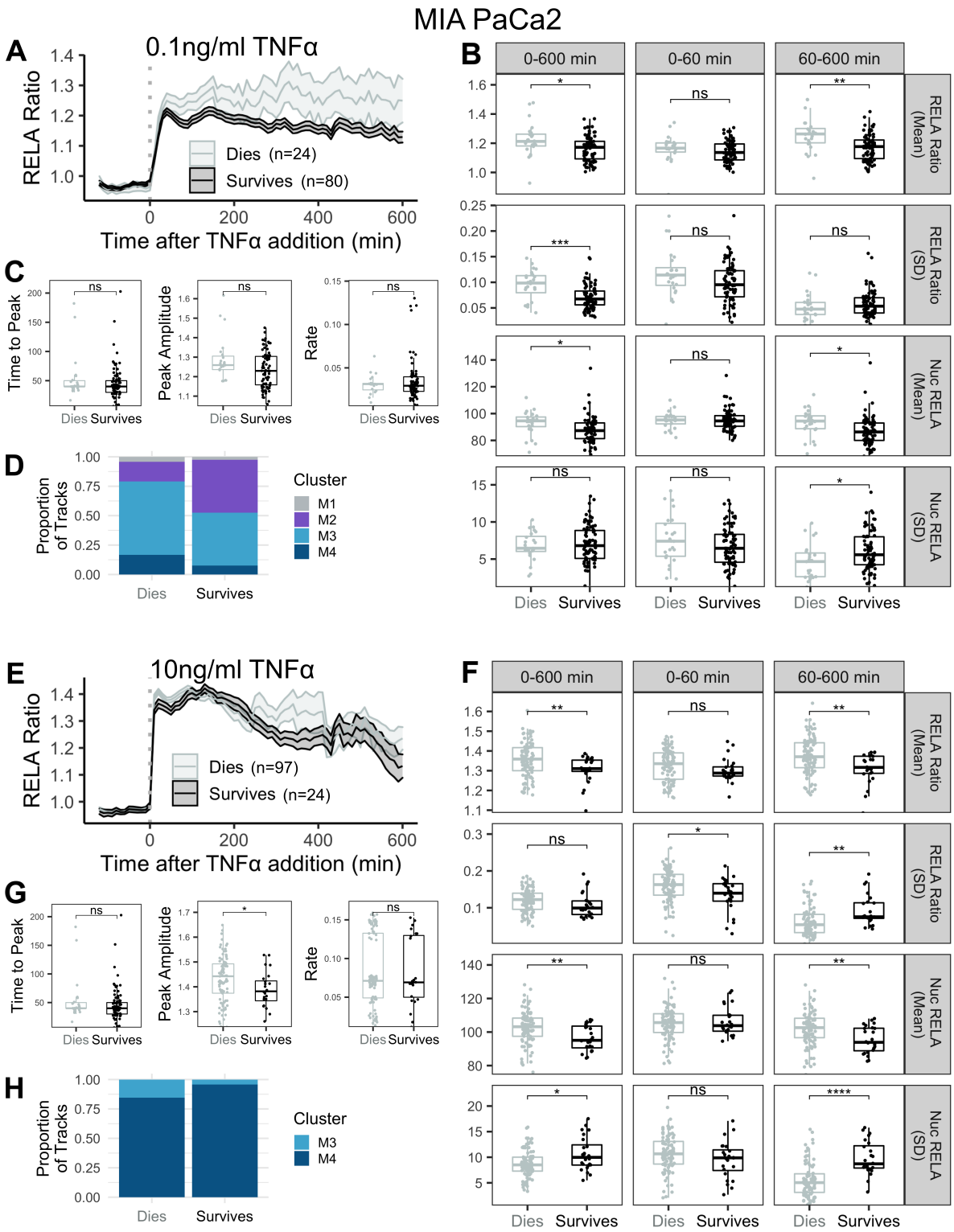
MIA PaCa2
A
0.1ng/ml TNFα
RELA Ratio
Dies (n=24)
Survives (n=80)
Time after TNFα addition (min)
B
0-600 min
0-60 min
60-600 min
RELA Ratio (Mean)
RELA Ratio (SD)
Nuc RELA (Mean)
Nuc RELA (SD)
Dies
Survives
C
Time to Peak
Peak Amplitude
Rate
ns
D
Proportion of Tracks
Cluster
M1
M2
M3
M4
E
10ng/ml TNFα
Dies (n=97)
Survives (n=24)
F
G
H
M3
M4

Figure 3.7 High RELA nuclear localisation is associated with cell death in MIA PaCa2 cells

MIA PaCa2 cells were treated with TNFα for 48 hr and single cells were categorised as dying or surviving during the imaging period. Data from two experimental repeats. (A-D) 0.1 ng/ml TNFα (n = 24 dying cells and 80 surviving cells). (E-H) 10 ng/ml TNFα (n = 97 dying cells and 24 surviving cells). (A and E) Tracks for mean RELA ratio and standard error by survival. (B and F) Single cell RELA statistics for tracked MIA PaCa2 cells by cell fate calculated for specified durations (0-60 min, 0-600 min or 60-600 min) following TNFα addition. Boxplots show median and interquartile range. Statistical significance (t-test with Benjamini-Hochberg correction): ns (non-significant) = $p > 0.05$, * = $0 < 0.05$, ** = $p < 0.01$, *** = $p < 0.001$, **** = $p < 0.0001$. (C and G) Single cell measurements for peak RELA amplitude, time to peak, and rate (amplitude/time to peak). Data for surviving and dying cells compared with student's t-test (two-tailed): ns (non-significant) = $p > 0.05$, * = $0 < 0.05$, ** = $p < 0.01$, *** = $p < 0.001$, **** = $p < 0.0001$. (D and H) The proportion of RELA ratio tracks in each RELA response cluster from Figure 3.3, grouped by cell fate.

With 10 ng/ml TNFα (Figure 3.7E and F), late timepoints (60-600 min) also showed higher nuclear RELA localisation in dying MIA PaCa2 cells compared to surviving MIA PaCa2 cells but more fluctuation in RELA localisation in surviving cells. Notably, the peak RELA ratio was higher in dying cells compared to surviving cells (Figure 3.7G). There were no statistically significant differences in cluster distribution by MIA PaCa2 cell survival responding to 10 ng/ml TNFα ($\chi^2 = 1.3$, $p = 0.26$) (Figure 3.7H).

With PANC1 cells, there was no association between RELA ratio dynamics or nuclear RELA abundance according to cell survival with 0.1 ng/ml TNFα (Figure 3.8A-D). However, surviving PANC1 cells in response to 10 ng/ml TNFα have higher nuclear RELA abundance, but not higher RELA ratio, at early timepoints following TNFα, though no differences in peak measurements or cluster distribution ($\chi^2 = 1.3$, $p = 0.26$) were observed (Figure 3.8E-H).

Overall, these data demonstrate that MIA PaCa2 cells with higher RELA nuclear localisation, particularly at post-peak timepoints, are more likely to die, while RELA dynamics in PANC1 cells are not significantly correlated with cell survival.

Figure 3.8

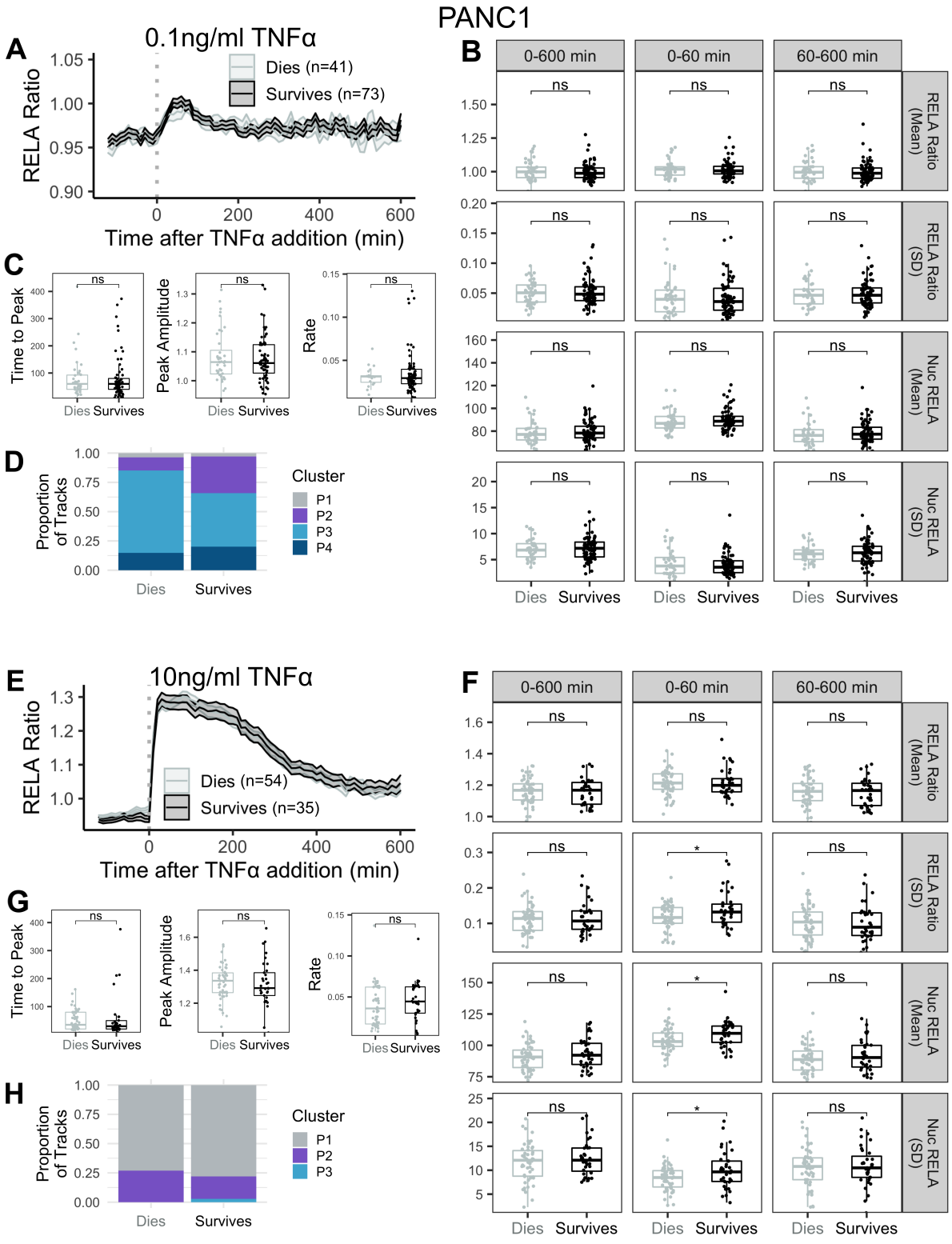
PANC1
A
0.1ng/ml TNFα
RELA Ratio
Dies (n=41)
Survives (n=73)
Time after TNFα addition (min)
B
0-600 min
0-60 min
60-600 min
RELA Ratio (Mean)
RELA Ratio (SD)
Nuc RELA (Mean)
Nuc RELA (SD)
C
Time to Peak
Peak Amplitude
Rate
D
Proportion of Tracks
Cluster
P1
P2
P3
P4
E
10ng/ml TNFα
Dies (n=54)
Survives (n=35)
F
G
H
ns
Dies
Survives

Figure 3.8 Cell death in PANC1 cells has a low association with RELA localisation

PANC1 cells were treated with TNFα for 48 hr and single cells were categorised as dying or surviving during the imaging period. Data from two experimental repeats. Statistics for significant results ($p<0.05$) are shown; all other results are non-significant. (A-D) 0.1 ng/ml TNFα (n = 41 dying cells and 73 surviving cells). (E-H) 10 ng/ml TNFα (n = 54 dying cells and 35 surviving cells). (A and E) Tracks for mean RELA ratio and standard error by survival. (B and F) Single cell RELA statistics for tracked PANC1 cells by cell fate calculated for specified durations (0-60 min, 0-600 min or 60-600 min) following TNFα addition. Boxplots show median and interquartile range. Statistical significance (t-test with Benjamini-Hochberg correction): ns (non-significant) = $p > 0.05$, * = $0 < 0.05$, ** = $p < 0.01$, *** = $p < 0.001$, **** = $p < 0.0001$. (C and G) Single cell measurements for peak RELA amplitude, time to peak, and rate (amplitude/time to peak). Data for surviving and dying cells compared with student's t-test (two-tailed): ns (non-significant) = $p > 0.05$, * = $0 < 0.05$, ** = $p < 0.01$, *** = $p < 0.001$, **** = $p < 0.0001$. (D and H) The proportion of RELA ratio tracks in each RELA response cluster from Figure 3.3, grouped by cell fate.

3.2.8 Removal of TNFα stimulation rapidly attenuates RELA nuclear localisation

I have shown that TNFα dose affects the timing and amplitude of peak RELA localisation in PDAC cells, but whether the duration of TNFα treatment and if continuous TNFα stimulation is required for the sustained RELA responses observed in PDAC cells remains unexplored. Therefore, I tested the effect of treating MIA PaCa2 cells with 0.1 ng/ml TNFα for 1 hr then replacing the cell culture medium with fresh DMEM and live imaged cells for a further 9 hr.

While continuous TNFα treatment resulted in a high and sustained RELA response in MIA PaCa2, 1 hr transient TNFα stimulation resulted in a pulse of RELA nuclear translocation peaking at a median 1.06 RELA ratio and lasting a median of 110 min (Figure 3.9A and A') (see Materials and Methods for peak, duration and rate detection). Similar to MIA cells exposed to continuous TNFα stimulation, 1 hr TNFα stimulation resulted in peaks around 50 min post-TNFα, with 40/50 (80 %) of cells peaking prior to the TNFα removal at 60 min, 7/50 cells (14 %) peaking at the time of TNFα removal, and 3/50 (6 %) of cells peaking after TNFα removal. Overall, the transient localisation of RELA in the nucleus with transient TNFα stimulation indicates that sustained RELA activation with continuous TNFα in MIA PaCa2 is not due to an autoregulatory positive feedback loop, but instead reliant on constant activation of the NF-κB pathway. Moreover, cell signalling for termination of RELA activity appears to be intact in PDAC cells.

Figure 3.9

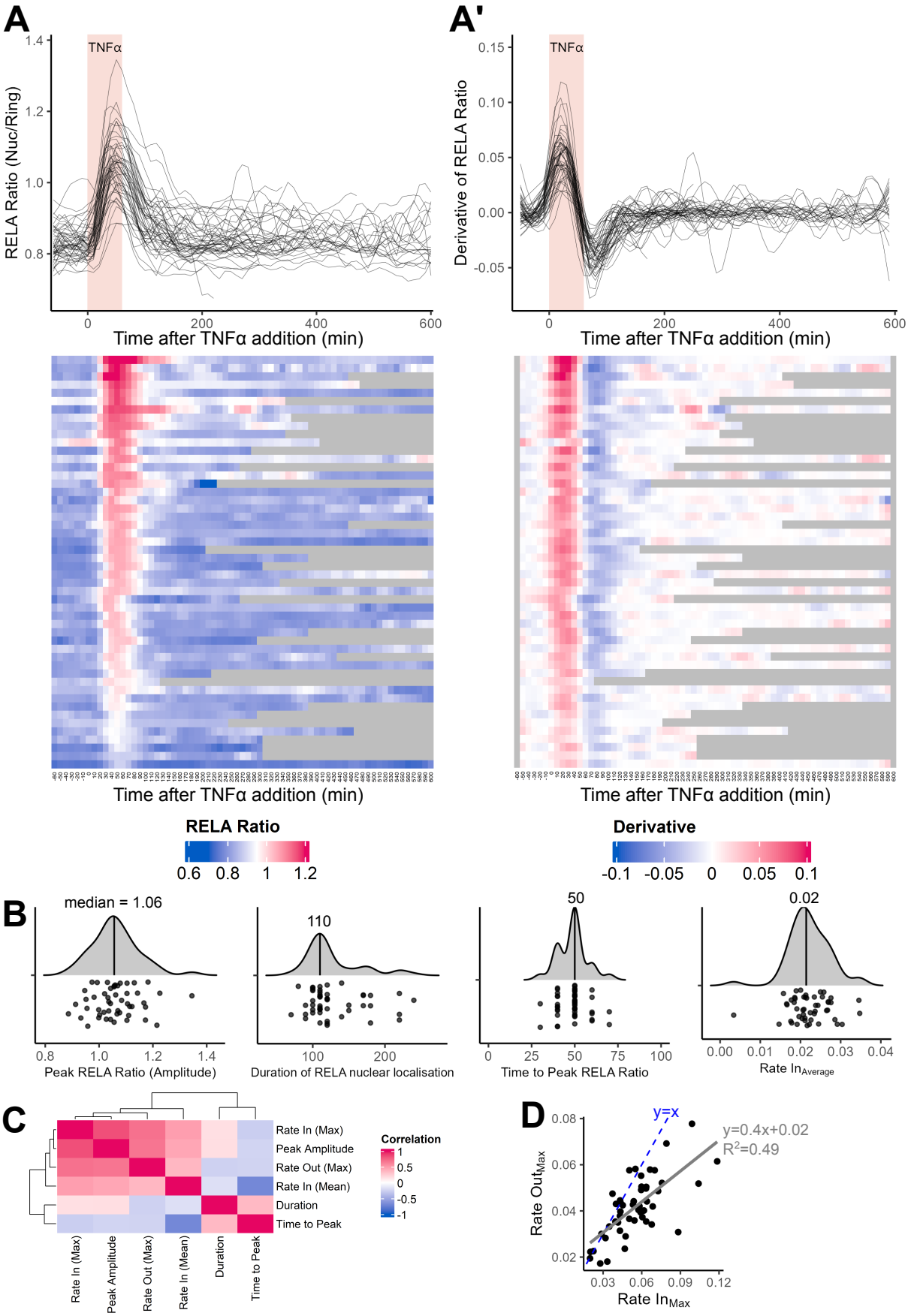
A
A'
TNFα
RELA Ratio (Nuc/Ring)
Derivative of RELA Ratio
Time after TNFα addition (min)
RELA Ratio
Derivative
B
median = 1.06
110
50
0.02
Peak RELA Ratio (Amplitude)
Duration of RELA nuclear localisation
Time to Peak RELA Ratio
Rate In_Average
C
Rate In (Max)
Peak Amplitude
Rate Out (Max)
Rate In (Mean)
Duration
Time to Peak
Correlation
D
y=x
y=0.4x+0.02
R²=0.49
Rate Out_Max
Rate In_Max

Figure 3.9 Removal of TNFα stimulation rapidly attenuates RELA nuclear localisation

(A and A') Single cell tracks for RELA ratio for MIA PaCa2 cells treated with TNF, which is then 'washed-out' and replaced with fresh medium after 1 hr. Cells were imaged for 1 hr prior to TNFα addition and for 9 hr after TNFα removal. (A) Heatmap colours correspond to RELA ratio. Tracks are ordered by peak RELA ratio, with decreasing peak RELA ratio amplitude from the top row downwards. (A') The first derivative (change in RELA ratio) for corresponding tracks in (A) by row. Heatmap colours correspond to the derivative value. (B) Single cell distributions for peak RELA ratio (amplitude), duration of nuclear localisation (minutes), time to peak RELA ratio (minutes), and average rate of RELA ratio change to peak RELA ratio for single cell tracks in (A). Lines and values above, show the median per measurement. (C) Correlations between single cell track features. (D) Scatter graph for single cell measurements of the maximum rate of RELA ratio change over time prior to peak RELA ratio (Rate In_{Max}) and the maximum rate of RELA ratio change over time after peak RELA ratio (Rate Out_{Max}). Rate In_{Max} is usually higher than Rate Out_{Max} and the two rates are positively correlated.

As the RELA ratio returns to basal levels following TNFα removal, unlike the sustained RELA responses observed with continuous TNFα stimulation, the presence of secondary pulses could be observed in a subset (8/40 cells). In Figure 3.9A and A', the tracks are ordered by peak RELA ratio, with the highest peak at the top-most row. Tracks with secondary pulses rank 5th, 6th, 8th, and 14th in peak RELA ratio amplitude, suggesting that secondary pulses are associated with high initial RELA activity.

MIA PaCa2 cell had a median peak amplitude of 1.06 achieved at a median of 50 min following TNFα addition (Figure 5.9B). The duration of nuclear localisation lasted between 25 and 75 min, with a median of 50 min across single cells. I also observed a normal distribution in the rate to peak nuclear localisation (right-most graph in Figure 5.9B), calculated on a single cell level as the peak amplitude / time to peak. Multiple features of the RELA dynamics tracks were strongly correlated, particularly the maximum rate of RELA ratio change to the peak and the peak amplitude (Figure 3.9C). This validates that cells responding more quickly to TNFα also respond with higher nuclear RELA localisation. In addition, the rate of RELA ratio change prior to the peak (nuclear translocation) was positively correlated with the rate of RELA ratio change after the peak, indicating that the rate of RELA deactivation is coupled to the rate of RELA activation. However, nuclear translocation appeared to occur more rapidly than cytoplasmic RELA re-localisation following TNFα washout (Figure 3.9D).

3.2.9 Summary

To characterise live single cell RELA dynamics in PDAC cells, I endogenously tagged RELA with GFP using CRISPR-CAS9 in two human PDAC cell lines and assayed RELA dynamics following TNFα addition from timelapse microscopy using automated image analysis. In both MIA PaCa2 and PANC1 PDAC cell lines, RELA nuclear translocation with TNFα is non-oscillatory and cell cycle independent. However, RELA is sustained in the nucleus in MIA PaCa2 while PANC1 cells gradually damp nuclear RELA localisation, with RELA

re-localisation to the cytoplasm within 10 hours. In terms of cell fate, I confirmed that RELA is required for cell survival with TNFα in the population level, but single dying cells have higher nuclear RELA compared to surviving cells.

3.3 Discussion

3.3.1 RELA dynamics are sustained and non-oscillatory in PDAC cells

RELA translocation dynamics in response to the potent cytokine TNFα have been characterised in several cell types, including a panel of human breast epithelial cells (Sero et al., 2015), SK-N-AS human neuroblastoma cells (Ashall et al., 2009), mouse fibroblasts (Tay et al., 2010), mouse macrophages (Martin et al., 2020), and HeLa human cervical cancer cells (Ankers et al., 2016; Lee et al., 2016). A commonly reported profile of TNFα-induced RELA translocation is periodic oscillation between the cytoplasm and nucleus. In PDAC cells, I did not identify the periodic oscillatory behaviour described in other cell types for the same imaging period at any TNFα doses. However, I did identify similarities in the timing of RELA translocation. For example, peak RELA nuclear localisation was achieved at a median of 40 min following TNFα treatment for MIA PaCa2 cells and 50 min for PANC1 cells, which are in a similar time frame to other cell types in the aforementioned studies.

Like other studies, I found that increasing TNFα dose increases the proportion of responsive cells, in a logarithmic manner in MIA PaCa2 cells and scaled with dose in PANC1 cells. While early studies into RELA responses to TNFα suggested that total RELA activity remains constant across TNFα doses of increasing magnitude (Hoffmann et al., 2002; Werner et al., 2005), my findings in PDAC cells support work by Zhang et al. (2017) in a panel of human cancer cell lines suggesting that the degree of RELA activation in responsive cells is enhanced by higher TNFα dose. Further insight into RELA dynamics could be gained from pulsing TNFα stimulation to mimic secretion by macrophages, in addition to testing the RELA response to other inflammatory stimuli like IL-1β and IL-6.

I also identified post-stimulation damped RELA translocation dynamics in PANC1 cells, which is a characteristic commonly observed in cell lines of other tissue origins (Nelson et al., 2004; Sero et al., 2015; Zambrano et al., 2016). Nonetheless, other studies reported much quicker cytoplasmic relocalisation of RELA (within 120 min of TNFα treatment) compared to PANC1 cells, for which RELA ratio falls < 1 at 400-500 min after TNFα treatment for clusters P3 and P4. Generally, I observed higher retention of RELA in the nucleus following the same TNFα doses in PDAC cells compared to other cell types, particularly in MIA PaCa2 cells, for which the majority of cells maintained predominantly nuclear RELA at the end of the 10 hr period following TNFα. Testing other PDAC cell lines, from different stages of malignancy would confirm how ubiquitous sustained RELA activation is among PDAC tumours and at which point during PDAC progression RELA upregulation occurs, although constitutive activation of RELA and upregulation of TNFα have been previously identified by static assays in PDAC models (Wang et al., 1999; Weichert et al., 2007; Zhao et al., 2016).

Differences between MIA PaCa2 and PANC1 cells in RELA dynamics, particularly the higher amplitude and more sustained response of MIA PaCa2 compared to PANC1, may result from differences in the abundance or distribution of TNFR, activity of TAK1 or IKKα, or expression of various IκB proteins. In addition, RIPK1 can contribute to RELA activation in a cell line specific manner. Therefore, further analysis into these signalling components' expression, activity or mutation could shed light on the mechanisms underlying RELA dynamics differences between MIA PaCa2 and PANC1 cells.

Crucially, I tagged RELA using CRISPR-CAS9 gene editing to characterise RELA in its natural genomic context and without overexpression. It would be useful to look at previously studied cell lines with fluorescent tagging at the endogenous locus, as other experiments have typically used exogenous RELA constructs with or without knockout of endogenous RELA. Additionally, I chose to tag the C-terminus of RELA to avoid perturbing the Rel homology domain present at the N-terminus, also because past exogenous overexpression

RELA fusion constructs used the C-terminus, which did not affect RELA function (Nelson et al., 2004; Tay et al., 2010; Sero et al., 2015). It would be interesting to test the effect of tagging the RELA N-terminus, mainly because the RELA C-Terminus contains the transactivation domain (Schmitz and Baeuerle, 1991), and assess whether this impacts RELA dynamics in PDAC cells.

Furthermore, I noted that the rate of nuclear 'import' is faster than the rate of 'export' following TNFα removal, based on the change in RELA ratio over time prior to and after peak RELA nuclear localisation (Figure 3.9D). Fluorescence recovery after photobleaching (FRAP) is a microscopy technique used to assess how quickly fluorescence returns after photobleaching, while the complementary technique fluorescence loss in photobleaching (FLIP) considers how the fluorescence loss advances across the cell. Both techniques could provide more precise rates of RELA shuttling between the nucleus and the cytoplasm. For example, a study published in 2009 assaying RELA with GFP knock-in (at the N-terminus) mouse embryonic fibroblasts combined FLIP with the nuclear export inhibitor leptomycin B or the protein synthesis inhibitor cycloheximide (Sung et al., 2009). Live imaging with these setups would provide further insight into the re-localisation of nuclear RELA back into the cytoplasm and the role of protein synthesis in RELA dynamics.

3.3.2 Perturbation of feedback in PDAC cells

IκBα is responsible for rapid relocalisation of RELA to cytoplasm and oscillations in RELA nuclear translocation. The sustained and non-oscillatory behaviour in MIA PaCa2 and PANC1 cells suggests a lack of IκBα activity in MIA PaCa2 and PANC1 cells. As damping of RELA nuclear localisation does occur but is much delayed to observations in other cell lines, this delayed negative feedback in PANC1 cells may be driven by IκBε or IκBβ, which have delayed NF-κB induced transcription compared to IκBα (Kearns et al., 2006). Indeed, the patterns of RELA dynamics observed in PDAC cells fit the profiles simulated by mathematical modelling and demonstrated by NF-κB DNA binding activity assayed by EMSA

of both 1) NFKBIA knockout cells (Hoffmann et al., 2002, Figure 2A and B), 2) cells with high IκBε and IκBβ synthesis (Hoffmann et al., 2002, Figure 2D).

Nonetheless, removing 0.1 ng/ml TNFα stimulation after 1 hr resulted in cytoplasmic relocalisation of RELA (Figure 3.9), indicating that the ability to terminate RELA activity is intact in MIA PaCa2 cells. Moreover, sustained RELA activation in MIA PaCa2 appears to rely on persistent stimulation of the NF-κB pathway by TNFα. It might be the case that transient NF-κB activity in MIA PaCa2 cells is sufficient to produce cytokines that could stimulate secondary RELA activity in an autocrine or paracrine manner. However, 8 % of cells (4/50) did display a second pulse of RELA nuclear translocation. The non-ubiquitous presence of secondary pulses may be because RELA nuclear abundance or the duration of RELA nuclear localisation is below a threshold for most cells, particularly because the cells displaying two pulses were at the higher end of the distribution of peak RELA ratios. Further work could test whether stimulation with 1 hr TNFα at 10 ng/ml or removal or 0.1 ng/ml TNFα after 5 hr stimulation expands the presence of secondary RELA activity pulses.

3.2.3 RELA dynamics are cell cycle independent in PDAC cells

RELA translocation responses to TNFα were also identified as dependent on the cell cycle phase at the time of TNFα addition in a study using double thymidine block to synchronise cells or Fluorescent Ubiquitination-based Cell Cycle Indicator (FUCCI) labelling to infer cell cycle phase (Ankers et al., 2016). HeLa cells treated with 10 ng/ml TNFα in late G1 displayed a stronger response than the population average, while S-phase cells showed a suppressed or delayed response. Furthermore, RELA was found to interact with E2F1, a transcription factor regulating the G1 to S transition, in late G1 when E2F1 levels are highest during the cell cycle. Additionally, E2F1 and RELA were found to negatively regulate each other, as E2F1 overexpression impairs the transcription of the gene encoding IκBα (a key target of RELA) while E2F1 transcription, as well as transcription of the E2F1 target Cyclin E, were impaired by RELA overexpression.

Conversely, I identified that MIA PaCa2 and PANC1 cells in all cell cycle stages are responsive to 10 ng/ml TNFα. At 0.1 ng/ml TNFα, I observed minimal dissimilarities in RELA translocation responses between cells in the different cell cycle stages in both PDAC lines. Conflicting reports of whether TNFα-induced RELA translocation is cell cycle regulated may be due to cancer cell type specific deregulation of cell cycle proteins (Cordon-Cardo, 1995; Otto and Sicinski, 2017) or RELA may not physically interact with E2F1 in PDAC cells in general or specifically in unsynchronised cells.

3.3.4 High RELA nuclear localisation is associated with cell death

TNFα has been shown to have higher expression in PDAC tissue and also in PanIN lesions, the precursor for PDAC, compared to healthy pancreatic tissue. Additionally, higher TNFα expression is associated with a poorer prognosis in PDAC patients (Zhao et al., 2016). TNFα may therefore aid oncogenesis and provide an advantage to PDAC tumours. However, a conundrum is that high TNFα levels can induce cell death via extrinsic apoptosis or necroptosis, which would be disadvantageous to cancer cells. In this study, I show that PDAC cells can still proliferate in the presence of physiologically high concentrations of TNFα (Figure 3.6A).

As cell number drastically decreases with combined IκB-SR expression and TNFα compared to each condition alone, I determined that survival of MIA PaCa2 and PANC1 cells is dependent on RELA nuclear translocation on the population level (Figure 3.6E). Therefore, I expected that individual surviving cells would upregulate nuclear RELA translocation compared to dying cells in response to TNFα. However, on the single cell level, I discovered that MIA PaCa2 cells with higher nuclear RELA translocation were more likely to die (Figure 3.7). Meanwhile, PANC1 cells that died or survived had similar RELA translocation dynamics (Figure 3.8). As the RELA ratio is higher in MIA PaCa2 cells compared to PANC1 cells at all TNFα doses, I hypothesise that there may be NF-κB target genes involved in cell death that require high and sustained RELA nuclear translocation for transcriptional activation.

Alternatively, high RELA activity in MIA PaCa2 cells in parallel with cell death could occur if RELA does not upregulate cFLIP or if RIPK3 is not expressed in MIA PaCa2 cells.

Having identified a correlation between high RELA activity and cell death, causation of cell death by RELA could be explored by moderately downregulating, but not completely inhibiting RELA as with IκB-SR, and assessing the effect on cell death frequency. In addition, the type of cell death mode observed in MIA PaCa2 and PANC1 cells in response to TNFα and whether cell death is causing RELA activation could be investigated using caspase inhibitors and SMAC mimetics.

Recently, a study by Oyler-Yaniv et al. showed that TNFα reduces the time between HSV1 infection and subsequent cell death. Moreover, TNFα increases the proportion of uninfected cells within the population that is exposed to HSV1 that die (false positives), which the authors describe as a 'speed accuracy trade-off' whereby TNFα increased cell death in both infected and uninfected cells to limit the viral spread in the whole population (Oyler-Yaniv et al., 2020). Given these findings, I expected to observe more similar RELA dynamics between dying and surviving PDAC cells at hyperphysiological TNFα levels (10 ng/ml) compared to 0.1 ng/ml TNFα. However, both TNFα doses were correlated with cell fate in PDAC cells. Therefore, I expect that if higher TNFα doses are tested, e.g. 50 ng/ml TNFα, the correlation between RELA dynamics features and cell survival would be disrupted due to a transition to faster but less selective cell death. Indeed, already in the 0.01-10 ng/ml range, I observed that raising the TNFα dose induces faster cell death in MIA PaCa2 cells, indicated by a shorter RELA track length (Figure 3.6D).

Chapter 4: Regulation of RELA by cell shape and the cytoskeleton

4.1 Introduction

4.1.1 Cell shape

Cell shape results from the culmination of external factors, including matrix stiffness (Yeung et al., 2005) and cell-cell adhesion (Wu et al., 2015), and internal factors like cortical tension (Chalut and Paluch, 2016), mutational status (Matthews et al., 2020), and metabolism (D'Anselmi et al., 2011). Cells need to have tightly controlled shape changes during multiple processes, including the cell cycle, during which an increase in cell area is required for dilution of the cell cycle inhibitor Rb (Zatulovskiy et al., 2020), and cell rounding during mitosis is important for correct spindle formation and faithful chromosome segregation (Lancaster et al., 2013). Moreover, cancer cells change shape during metastasis in order to migrate to and colonise other tissues. For example, melanoma cells can adopt a mesenchymal or amoeboid cell shape during collective cell migration, with mesenchymal cells using protrusions and adhesions (Hegerfeldt et al., 2002) and amoeboid cells using membrane blebbing to manoeuvre through gaps in the ECM (Sahai and Marshall, 2003; Cooper et al., 2015; Liu et al., 2015).

The epithelial to mesenchymal transition (EMT) is a reversible process pertinent to development and involves cell shape and signalling changes. Epithelial cells interact with the basement membrane and conversion to a mesenchymal cell type involves enhanced ability to migrate and invade, reorganisation of the cytoskeleton, and production of ECM-degrading enzymes. In general, there are three types of EMT: type 1 is associated with embryogenesis, type 2 with fibrosis and inflammation, and type 3 with malignant transformation (Kalluri and

Weinberg, 2009). The contribution of the epithelial to mesenchymal transition (EMT) to cancer has been extensively studied. Cancer-associated EMT is a multifaceted process but typically involves the acquisition of mesenchymal markers like the intermediate filament vimentin (Hendrix et al., 1997) and N-cadherin (Tomita et al., 2000). Importantly, EMT stimulates a cohort of transcription factors, including Snail and ZEB1, which cause large-scale transcriptional changes that contribute to cancer progression (Batlle et al., 2000; Cano et al., 2000; Aigner et al., 2007; Alves et al., 2009). EMT may also affect therapy resistance, as PDAC cell line morphology is associated with responsiveness to anticancer drugs. PDAC cells with high E-cadherin and low vimentin (epithelial) are more susceptible to the DNA synthesis inhibitor gemcitabine in terms of decreased cell viability, whereas PDAC cells with high vimentin and low E-cadherin expression (mesenchymal) are responsive to the tubulin-targeting drug abraxane (nab-paclitaxel) (Minami et al., 2021). On a related note, cell morphology is linked to metastatic ability, as shown in a study by Wu et al. that grew single cell derived breast cancer clones and determined their distinct morphological, genomic and gene expression profiles. Wu et al. demonstrated that gene expression and ability to metastasise to the lungs was correlated with single cell morphology (Wu et al., 2015).

On a broad scale, cell anatomy as a part of tissue organisation is used in histopathology to determine malignancy grade and delineate cancer from non-cancerous regions in patient samples (He et al., 2012). However, automated image analysis has accelerated the applications of cell shape analysis and cell shape is recognised as a readout of the cell's signalling state. For example, cell shape parameters can be used to predict the single cell localisation (nuclear versus cytoplasmic) of transcription factors (Sero et al., 2015) and coactivators (Sero and Bakal, 2017) involved in oncogenesis, observed by confocal microscopy. Furthermore, cell shape is effectively used as the readout for high throughput screens using systematic RNA interference to find gene knockdowns that skew the heterogeneity present in the wildtype population, presenting an alternative and innovative method for identifying genetic drivers of cancers (Bakal et al., 2007). This was implemented

in triple-negative breast cancer cells to identify RhoGEFs and RhoGAPs regulating YAP/TAZ subcellular localisation (Pascual-Vargas et al., 2017), in HeLa cervical cancer cells to identify interactors with microtubule-associated proteins required for mitotic spindle assembly (Barr and Bakal, 2015), and in *Drosophila* haemocytes to identify cell shape regulators conserved in mouse and human metastatic melanoma cells (Yin et al., 2013).

The cytoskeleton is a complex network of structural and regulatory components that collaborate to regulate cell shape. Crucial to the dynamic characteristic of cell shape, the cytoskeleton is also highly dynamic and is continuously remodelled. Two major networks of the cytoskeleton revolve around the components actin and tubulin, which crosstalk directly and through shared regulators during cell migration and in the regulation of cell shape and cell polarity (Dogterom and Koenderink, 2019).

4.1.2 Actin

Actin is an abundant 42 kDa globular protein essential in all eukaryotic cells (Stoddard et al., 2017). Actin was originally identified for its association with myosin and their role in muscle contraction as part of the classic sliding filament model (Hanson and Huxley, 1953). However, advancement in microscopy techniques has enabled a better understanding of actin as a cytoskeletal component that can act independently of myosin. Moreover, the visualisation of actin using phallotoxins conjugated to fluorescent markers, e.g. phalloidin, has accelerated research into the myriad of processes involving actin dynamics (Wulf et al., 1979; Vogl and Guttman, 2018).

Actin can exist in monomeric form (G-actin) or polymerise into actin filaments (F-actin). F-actin synthesis involves ATP binding to G-actin followed by the formation of actin dimers and trimers, from which actin filaments can elongate rapidly (Cooper et al., 1983; Tobacman and Korn, 1983; Goddette et al., 1986). Actin filaments have a barbed (+) end, to which the addition of monomers is rapid, and a slow-growing (-) pointed end at which ATP hydrolysis occurs (Woodrum et al., 1975). The actin cortex is a thin layer of actin under and attached to

the plasma membrane and is organised in a meshwork generated by actin branching proteins (Zigmond et al., 1979). In the cell, actin can be organised into stress fibres, which are one-dimensional actin bundles that are usually connected to focal adhesions - integrin-based macromolecular interfaces between the ECM and cytoskeleton (Machesky and Hall, 1997). Actin can also form protrusive structures on the cell edge that are involved in cell migration. These include lamellipodia, which are thin sheetlike protrusions consisting of branched and crosslinked networks, and filopodia, which have parallel actin bundles (Svitkina, 2018).

Actin binds to multiple proteins that are involved in actin capping, crosslinking, bundling, stabilisation, anchoring and mediation of signal transduction downstream of actin dynamics. Some of the key associated proteins and regulatory elements of actin are summarised in Table 4.1.

Table 4.1: Actin interactors

Component	Details
RhoGTPases	● Small (~21 kDa) signalling G proteins in the Ras superfamily ● Include RHOA, RAC1 and CDC42 ● Inactive when GDP-bound and activated by Guanine Nucleotide Exchange Factors (GEFs), which catalyse the exchange of GDP to GDP ● Inactivated by Guanine Activating Proteins (GAPs), which catalyse GTP hydrolysis to GDP ● Regulate cell shape and the cell cycle (Hart et al., 1991; Nobes and Hall, 1995; Hall, 1998)
ARP2/3	● Multi-subunit complex including ARP2, ARP3 and ARC proteins. ● Binds to pre-existing actin filaments to mediate the formation of branched actin networks. (Welch et al., 1997; Ma et al., 1998)
Formins	● e.g. DIAPH1 (mDia1), DAAM1/2, FMN1/2 ● Nucleates actin and mediates polymerisation into linear filaments ● RhoGTPase effector protein (Ishizaki et al., 2001; Pellegrin and Mellor, 2005; Aspenström et al., 2006)
Myosin	● Muscle and non-muscle myosin ● Motor proteins ● Use ATP hydrolysis to move along actin ● Involved in actin crosslinking

	● Involved in cell contractility (Hanson and Huxley, 1953; Rayment et al., 1993; Laevsky and Knecht, 2003)
ROCK	● Rho-associated kinases ● Effector of RhoA ● Involved in cell contractility by phosphorylating myosin light chain (MLC), increasing myosin II ATPase activity, and by inactivating MLC phosphatase (Kimura et al., 1996)
α-actinin	● Spectrin gene superfamily ● Has an N-terminal region with an actin binding domain (ABD), involved in cross linking actin filaments and anchoring actin to intracellular structures ● Localised to microfilaments and adherens junctions, where it binds actin to the plasma membrane (Beggs et al., 1992; Honda et al., 1998)
FAK	● Regulates focal adhesion turnover ● Mediates signal transduction downstream of focal adhesions including actin dynamics, regulating cell motility and proliferation (Burridge et al., 1988; Parsons et al., 2000).

Actin dynamics can regulate transcription by multiple mechanisms. Most directly, actin is actively transported into and out of the nucleus and nuclear G-actin interacts with RNA polymerases to initiate transcription (Hofmann et al., 2004). Actin also binds to MAL, a coactivator of the transcription factor serum response factor (SRF). Actin exports MAL from the nucleus and also blocks MAL binding to SRF target genes (Vartiainen et al., 2007). Actin is also a component of several nuclear chromatin-modifying complexes including INO80 and BAF (Zhao et al., 1998; Shen et al., 2000). Actin structures outside of the nucleus can regulate transcription, such as by positioning nuclei during actomyosin contractility (Huelsmann and Brown, 2014), or by stretching nuclear pores in response to forces on ECM adhesions, which has been shown to enable nuclear translocation of the Hippo pathway transcriptional coactivator YAP (Elosegui-Artola et al., 2017). Le et al. found that perinuclear actin can also indirectly regulate chromatin structure. Specifically, enrichment of the nuclear membrane protein Emerin enhances actin polymerisation around the nucleus in response to

stress, which reduces nuclear actin levels and causes transcription attenuation by enhancing polycomb-mediated gene silencing (Le et al., 2016).

4.1.3 Tubulin

Microtubules (MTs) are polymers of the protein tubulin and are present in all dividing and most differentiated eukaryotic cells (Desai and Mitchison, 1997). There are five known tubulin members: α, β, γ, δ, and ε. A subunit of MT is a heterodimer consisting of α and β tubulin monomers, which share 40 % homology at the amino acid level (Nogales et al., 1998) and each has a mass of ~50 kDa (Ohta et al., 1987). Tubulins are in the GTPase superfamily as they have a conserved GTP-binding domain in their N-terminal region. During MT polymerisation, GTP bound to β-Tubulin is hydrolysed and this is reversed by exchange of GDP on β-Tubulin for GTP during depolymerisation (Weisenberg et al., 1968; Spiegelman et al., 1977; Mitchison, 1993). Conversely, GTP bound to α-tubulin is more stable and is not hydrolysed during polymerisation, but is believed to affect tubulin stability (Menéndez et al., 1998).

Within an MT, α/β-tubulin heterodimers are arranged in linear protofilaments that interact laterally to form 25 nm diameter cylindrical structures that are hollow (Brinkley, 1997). MTs are predominantly composed of 13 protofilaments in vivo and 14 protofilaments in vitro (Evans et al., 1985). MT assembly requires nucleation and elongation phases. In vivo, spontaneous MT nucleation is prevented from the low cytosolic concentration of α/β-tubulin. Consequently, MT nucleation requires microtubule organising centers (MTOCs), of which the core subunit is γ-Tubulin (Wiese and Zheng, 2000). Similar to actin, MTs have a fast-growing plus end with a net gain and a slow growing minus end with a net loss, resulting in a ‘treadmilling’ effect (Margolis and Wilson, 1978, 1981).

One of the key functions for MTs occurs during cell division, during which MT arrays form the mitotic spindle during cell division, and function to orient the plane of cleavage and physically separate chromosomes (reviewed by Walczak and Heald, 2008). In non-dividing cells, MTs

position the nucleus and other organelles (Tran et al., 2001; Friedman et al., 2010) and form the motile structures flagella and cilia that propel cell movement (Porter and Sale, 2000). In some cancers, certain Tubulin isomers are overexpressed (Albahde et al., 2021). For instance, expression and nuclear localisation of Tubulin βIII are associated with lower life expectancy in colorectal cancer patients (Ruksha et al., 2019), while the Tubulin isoform βVI is highly expressed in PDAC cell lines, including MIA PaCa2, compared to HPDE cells and functions in anchorage-dependent growth (McCarroll et al., 2014).

4.1.4 Targeting the cytoskeleton to treat cancer

Targeting components of the cytoskeleton is a common strategy in cancer therapy, given the role of the cytoskeleton in cell division and cancer cell invasion, migration, and metastasis (reviewed by Hall, 2009). MT-targeting drugs generally work by inhibiting MT dynamics, which impacts spindle function and blocks cell cycle transition from metaphase to anaphase by inciting the mitotic checkpoint (Jordan et al., 1993; Li and Nicklas, 1995). Types of MT-targeting drugs include vinca alkaloids, colchicine, nocodazole, and taxanes. Colchicine binds to MTs at the junction of the α/β subunit, forming a stable complex that prevents primarily MT polymerisation and induces MT depolymerisation (Ravelli et al., 2004). Similarly, vinca alkaloids (e.g. vinblastine and vincristine) and nocodazole work by inducing MT depolymerisation and interfering with MT polymerisation (Lobert et al., 1996; Liu et al., 1998).

The taxane paclitaxel (taxol) is one of the most commonly used tubulin-targeting drugs in the clinic for cancer treatment and is an example of one of the many natural substances that target the cytoskeleton (Peterson and Mitchison, 2002). Paclitaxel was originally isolated by the Pacific yew tree, samples of which were collected in 1962 by the botanist Arthur Barclay and identified as toxic in living cells by the researchers Monroe E. Wall and Mansukh Wani in 1964 (Wani and Horwitz, 2014). Antagonistic to the effects of colchicine, nocodazole and

vinca alkaloids, taxanes act by stabilising MTs and promoting polymerisation (Schiff et al., 1979; Schiff and Horwitz, 1980).

For the treatment of PDAC, paclitaxel is provided as the standard of care in the form of nab-paclitaxel (nanoparticle albumin-bound) and combined with gemcitabine, a DNA synthesis inhibitor and precursor of a nucleotide analogue (Hertel et al., 1988; Ruiz van Haperen et al., 1993). The binding of paclitaxel to albumin increases paclitaxel uptake via transcytosis and reportedly increases tumour accumulation of paclitaxel, as due albumin-binding proteins are overexpressed in stromal fibroblasts surrounding tumours (Desai et al., 2006, 2009; Yardley, 2013). The synergy between nab-paclitaxel and gemcitabine has also been reported, for example, targeting of nab-paclitaxel to tumour stroma aids access of gemcitabine to the tumour. Moreover, nab-paclitaxel increases gemcitabine stabilisation by inactivating the gemcitabine catabolising enzyme cytidine deaminase, leading to an increase in intratumoral gemcitabine concentrations (Frese et al., 2012). The gemcitabine/nab-paclitaxel combination was approved as a treatment for PDAC in 2013, following a Phase III clinical trial (MPACT) with 861 patients randomised to receive gemcitabine monotherapy or gemcitabine/nab-paclitaxel. The MPACT trial reported a median overall survival of 8.5 and 6.7 months and progression-free survival of 3.7 months and 5.5 months for the Gemcitabine monotherapy and Gemcitabine/nab-paclitaxel treatment arms respectively (Von Hoff et al., 2013). Paclitaxel is also commonly used as the standard of care in combination with other chemotherapy for the treatment of breast cancer (Gradishar et al., 2005), non-small cell lung cancer (Socinski et al., 2012), and ovarian cancer (du Bois et al., 2003).

Targeting specific tubulin isoforms associated with cancer is another approach being explored (Albahde et al., 2021). The novel therapeutic VERU-111 - an inhibitor of the tubulin isoforms βI, βIII and βVI - was reported in a 2019 study assaying its efficacy and mechanism in pancreatic cancer cells (Kashyap et al., 2019). The authors found that VERU-111 causes in vitro G2/M cell cycle arrest and induces apoptosis through regulation of the mitochondrial

proteins Bcl-xL, Bcl-2, Bax, and Bad. In xenograft mouse models, VERU-111 suppresses tumour growth.

Actin-targeting drugs have been studied extensively for anti-tumour effects (Małecki et al., 2010; Huang et al., 2012a, 2012b). One type of actin-targeting drug are cytochalasins, which are toxins originating from several fungi species and have over 60 different subtypes, though only cytochalasin B and D have been studied in detail (Trendowski, 2015). Cytochalasins have a high affinity to F-actin (Flanagan and Lin, 1980) and bind exclusively to the barbed end of actin filaments with a stoichiometry of one cytochalasin per actin filament (Goddette and Frieden, 1986), capping the end and preventing actin subunit addition or removal (Brown and Spudich, 1981). This results in stabilisation of actin filaments and reduction in actin filament mass (Jordan and Wilson, 1998), consequently disrupting actin network organisation and causing the formation of filamentous actin aggregates (Schliwa, 1982) Other actin-binding drugs include latrunculin and jasplakinolide, which are derived from marine sponges (Kashman et al., 1980; Inman and Crews, 1989). In general, actin-binding drugs have failed to translate clinically due to toxicity, however, modulating actin dynamics indirectly by targeting FAK or integrins may be a promising therapeutic approach (Murphy et al., 2020; Li et al., 2021), particularly since integrin and FAK inhibition appears to impact cancer cell proliferation, survival, invasion and migration (O'Brien et al., 2014; Reader et al., 2019), as well as make tumours amenable to immunotherapy by reducing fibrosis in the microenvironment (Jiang et al., 2016).

4.1.5 Regulation of RELA by actin and tubulin polymerisation

In addition to modulation of RELA by various mechanical properties (Section 1.2.6), decades-old work has shown that chemically inhibiting actin or tubulin dynamics can directly increase RELA binding to DNA, assayed by EMSA, and RELA-dependent gene expression based on reporter activity. The first study in this series was carried out in 1995 by Rosette & Karin, who used nocodazole or warming to 37 °C to depolymerise MTs and showed that

these activate NF-κB DNA binding and NF-κB target gene expression, with the timecourse of NF-κB activation lagging behind changes in MT depolymerisation by 15 min (Rosette and Karin, 1995). In 1999, pre-treatment of cells with taxol was shown to reduce IκBα phosphorylation and degradation and prevent NF-κB activation by Phorbol 12-myristate 13-acetate (PMA), a modulator of focal adhesion formation and actin polymerisation. However, taxol did not affect TNFα induced IκBα phosphorylation or NF-κB activation (Spencer et al., 1999). Finally, MT disassembly by vinblastine increases translocation of NF-κB complexes mostly containing p65 with p50 (Bourgarel-Rey et al., 2001).

Similar research was carried out to test the effect of chemical inhibition of actin on NF-κB activity. Nemeth et al. treated two colorectal cancer cell lines with cytochalasin D and latrunculin B and both increased RELA DNA binding and RELA-dependent transcriptional activity. Cytochalasin D and latrunculin B also increased gene expression and release of chemokines IL-8 and CXCL1 in a RELA-dependent manner (Németh et al., 2004) Another study identified that a range of antioxidants block activation of NF-κB complexes predominantly p50-p65 heterodimers, suggesting that RELA is dependent on cell redox status. Additionally, RELA activation could be induced with H_2O_2 treatment (Kustermans et al., 2005). Studies have also shown that RELA co-operates with the actin-binding protein α-actinin 4 (described in Table 4.1). In epidermoid carcinoma cells, RELA and α-actinin 4 colocalise across actin stress fibres and membrane lamellae and RELA Co-IP pulls down α-actinin 4 in cell and nuclear extracts. Moreover, TNFα stimulates nuclear localisation of both α-actinin 4 and RELA (Babakov et al., 2008). However, overexpression of full-length ACTN4 (ACTN4F1) does not affect nuclear accumulation of RELA, but ACTN4F1 and RELA co-expression does enhance luciferase activity downstream of the *c-fos* promoter compared to expression of each gene alone, suggesting that ACTN4F1 is a coactivator for RELA (Aksenova et al., 2013).

Cytoskeletal components are predicted to regulate RELA gene expression in a study that identified modulators of RELA regulated transcription using combined liquid

chromatography-mass spectrometry and ChIP-Seq, in addition to analysing gene expression using data from 2158 tumour samples published by Expression Project (Li et al., 2014). Li et al. found 297 proteins previously reported to interact with RELA and 365 new ones, with several cytoskeletal proteins included in the subset of modulators that affect the greatest number of RELA target genes. These modulators include one of three isoforms of actin (ACTG1); the MT and actin connecting factor MACF1 which is involved in cytoskeleton dynamics homeostasis; and radixin, a component of the ezrin-radixin-moesin (ERM) complex that acts as a linker between the actin cytoskeleton and plasma membrane.

4.1.6 RELA regulation of cell shape and the cytoskeleton

Although the regulation of RELA by cytoskeletal (Section 4.1.5) and mechanical components (Section 1.2.6) has been widely studied, there is limited evidence for the inverse relationship. The most commonly explored route of RELA regulation of cell shape considers RELA regulation of the EMT process (reviewed by Min et al., 2008). For example, RELA was identified as a key mediator of EMT in a mouse model of breast cancer progression (Huber et al., 2004). One experiment included in this study involved seeding Ras-transformed breast epithelial cells on a porous support. Cells in basal conditions have an epithelial phenotype but TGF-β treatment for 5 days resulted in strand-shaped vimentin-positive cells with weakly expressing E-cadherin. However, in the presence of non-degradable IκB, NF-κB activity is blocked resulting in cell death and failure of cells to undergo EMT, shown by retention of high levels of E-cadherin and failure to upregulate vimentin. Additionally, cells with constitutive activation of IKK-2 have increased NF-κB activity and undergo EMT even in the absence of TGF-β, with spindle-shaped, vimentin-positive, and E-cadherin negative cells. Another study showed that induction of the vimentin gene following expression of the Tax transactivator protein encoded by the human T-cell leukaemia virus type 1 is likely to involve NF-κB, as systematic deletion of different sections of the vimentin promoter narrowed down the

involvement of a 30 bp region, within which an 11 bp sequence with homology to the NF-κB binding sequence is present (Lilienbaum et al., 1990).

In addition to enhancement of mesenchymal markers, RELA reportedly promotes suppression of epithelial morphology via Snail and ZEB1/ZEB2 regulation (Min et al., 2008). The Snail family of transcriptional repressors promote EMT during development and in cancer progression, partially through E-cadherin repression (Batlle et al., 2000; Cano et al., 2000; Carver et al., 2001). There are multiple studies that provide evidence that Snail transcription is regulated by NF-κB activity. Examples of this include that GSK3 inhibition stimulates *SNAI1* (gene encoding Snail) via NF-κB signalling (Zhou et al., 2004), induction of *SNAIL1* mRNA during EMT is reversed by NF-κB inhibition (Kim et al., 2007), and *Snail1* transcription in *Drosophila* is directly activated by the NF-κB homologue Dorsal (Ip et al., 1992). Similarly, the ZEB1 and ZEB2 transcription factors are involved in several tumour types (Larsen et al., 2016; Maturi et al., 2018; Slowicka et al., 2020) and are regarded as EMT modulators, as ZEB2 represses the transcription of epithelial cell junctional genes (Vandewalle et al., 2005) and ZEB1 ectopic expression induces downregulation of E-cadherin and disbandment of cell-cell junctions (Eger et al., 2005). Chua et al. showed that stably overexpressing constitutively active RELA in MCF10A cells elevates expression of ZEB1 and ZEB2 and transient RELA overexpression increases ZEB1 promoter activity and an EMT phenotype (Chua et al., 2007).

Furthermore, studies by Sero et al. (2015) and Georgouli et al. (2019) propose RELA involvement in a feedback loop with cell shape or myosin activity. Sero et al. showed that MCF10A cells with epithelial morphology have low RELA nuclear localisation and cells with mesenchymal morphology have high RELA nuclear localisation. Since RELA has been shown to promote EMT, the authors suggest that RELA may enforce mesenchymal morphology. This hypothesis is supported by their findings that manipulating cells into a mesenchymal shape, using the ROCK inhibitor Y27 or with high substrate stiffness, leads to higher RELA activation. Moreover, RELA expression was associated with the expression of

the EMT marker N-cadherin. Oppositely, the promotion of an epithelial cell shape or depletion of N-cadherin reduced RELA expression (Sero et al., 2015). At the same time, myosin II activity in melanoma cells is shown to promote the secretion of IL-1 which leads to RELA nuclear translocation. In turn, A375 cells depleted in NFKB1 or with inhibition of IKKβ activity have reduced pMLC2 cortical levels and loss of cell roundness. Thus, IKKβ and RELA appear to drive myosin II activity in a positive feedback loop in amoeboid melanoma cells (Georgouli et al., 2019).

Some studies have assessed the effect of TNFα on the cytoskeleton and cell morphology but the extent of dependence on RELA activity is unclear. For example, Lim et al. showed that treatment of monocytes with very low TNFα concentrations (1-100 pmol/L) for 30 min causes cytosolic RhoA to rapidly translocate to the plasma membrane via the ezrin/radixin/moesin complex. This was shown to involve actin polymerisation dependent on RELA activation, as treatment with the NF-κB inhibitor Pyrrolidine dithiocarbamate blocks actin polymerisation with TNFα (Lim et al., 2009; Liu et al., 1999). Meanwhile, Mitra et al. show that F-actin intensity in fibroblasts rapidly decreases with a much higher TNFα concentration (20 ng/mL) but the same duration (30 min), identifying a more substantial fold-change decrease in cells with enforced rectangular shape compared to circular morphology (Mitra et al., 2017). However, Mitra et al. do not speculate on the involvement of RELA, but it may be implied that the short treatment time is insufficient to involve RELA activity. Nonetheless, it is possible that RELA may be altering the basal state of the cell and thus affecting the response when TNFα stimulation occurs, rather than TNFα activation of RELA inducing transcription of genes involved in cell shape regulation.

In this chapter, I used a combination of quantitative single cell imaging and Bayesian analysis to analyse how the heterogeneity in RELA nuclear translocation between and within PDAC cell lines relates to differences in cell morphology cytoskeletal organisation, in particular actin and tubulin abundance and distribution. I also test how chemical modulation of the cytoskeleton by a range of small molecules affects RELA localisation, in order to

understand the cell signalling mechanisms underlying dependency of RELA activity on cytoskeletal dynamics. Finally, I test the effect of TNFα on PDAC cell morphology and cytoskeletal organisation, while assessing the dependence on and interaction with RELA nuclear translocation using an inducible non-degradable form of IκB.

4.2 Results

4.2.1 Measurement and selection of morphological and cytoskeletal features

Because the same TNFα concentration can lead to variable responses, I proposed that there are cell-intrinsic mechanisms that dictate the extent of RELA translocation in PDAC cells. Having previously identified relationships between cell shape and RELA localisation in breast cells (Sero et al., 2015), I hypothesised that differences in actin and tubulin organisation, which lead to cell shape differences, may explain differences in RELA dynamics. To test this, I expanded the dataset to include images of the human immortalised PDAC cell lines MIA PaCa2, PANC1, Capan1, SW1990 and PANC05.04, as well as the non-malignant retinal epithelial line RPE1. I treated these cell lines with TNFα (1 hr) and stained cells for DNA, RELA, F-actin and α-tubulin (Figure 4.1A).

Figure 4.1

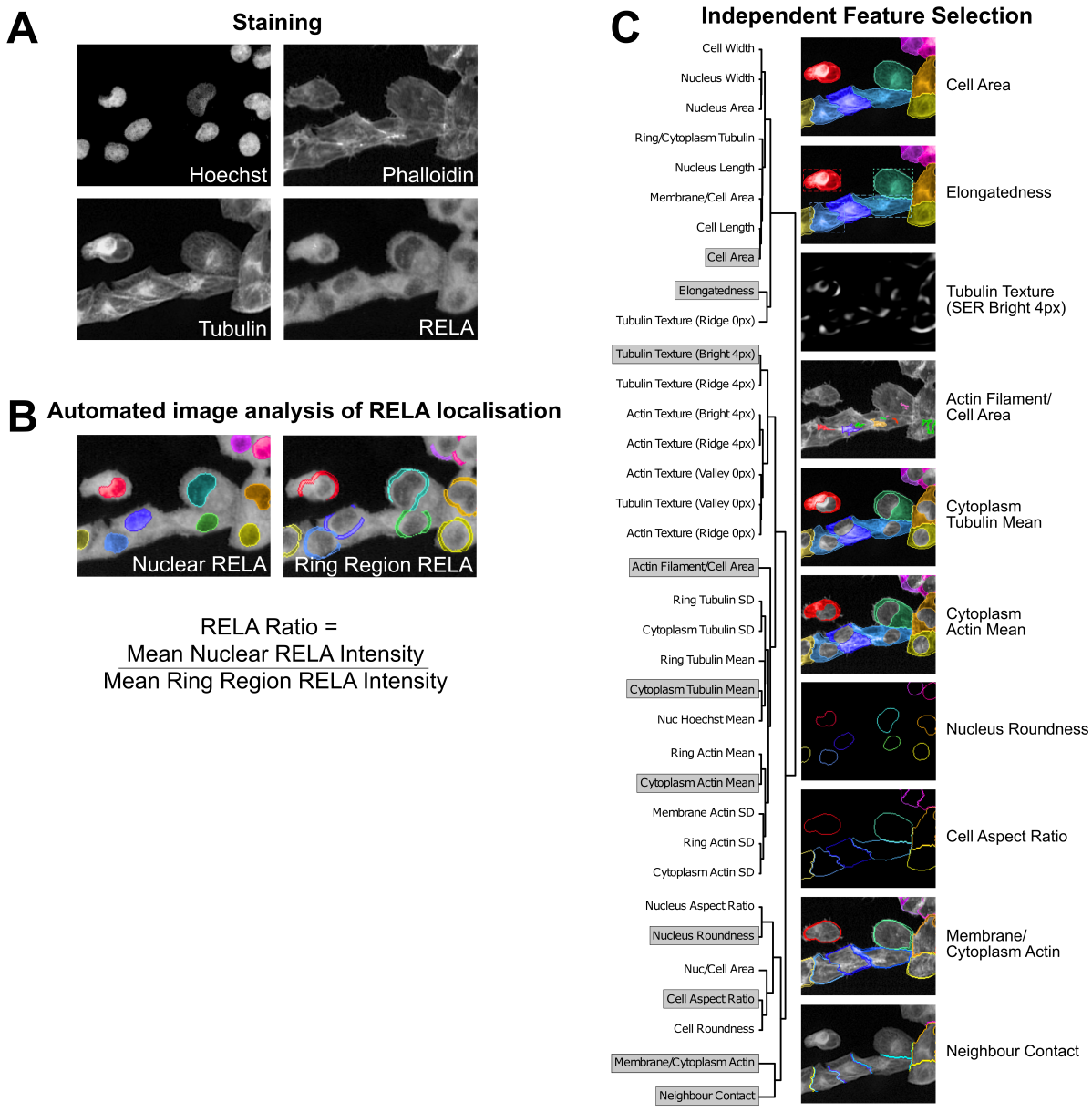
A
Staining
Hoechst
Phalloidin
Tubulin
RELA
B
Automated image analysis of RELA localisation
Nuclear RELA
Ring Region RELA
RELA Ratio =
Mean Nuclear RELA Intensity
Mean Ring Region RELA Intensity
C
Independent Feature Selection
Cell Width
Nucleus Width
Nucleus Area
Ring/Cytoplasm Tubulin
Nucleus Length
Membrane/Cell Area
Cell Length
Cell Area
Elongatedness
Tubulin Texture (Ridge 0px)
Tubulin Texture (Bright 4px)
Tubulin Texture (Ridge 4px)
Actin Texture (Bright 4px)
Actin Texture (Ridge 4px)
Actin Texture (Valley 0px)
Tubulin Texture (Valley 0px)
Actin Texture (Ridge 0px)
Actin Filament/Cell Area
Ring Tubulin SD
Cytoplasm Tubulin SD
Ring Tubulin Mean
Cytoplasm Tubulin Mean
Nuc Hoechst Mean
Ring Actin Mean
Cytoplasm Actin Mean
Membrane Actin SD
Ring Actin SD
Cytoplasm Actin SD
Nucleus Aspect Ratio
Nucleus Roundness
Nuc/Cell Area
Cell Aspect Ratio
Cell Roundness
Membrane/Cytoplasm Actin
Neighbour Contact
Cell Area
Elongatedness
Tubulin Texture (SER Bright 4px)
Actin Filament/ Cell Area
Cytoplasm Tubulin Mean
Cytoplasm Actin Mean
Nucleus Roundness
Cell Aspect Ratio
Membrane/ Cytoplasm Actin
Neighbour Contact

Figure 4.1 Independent cell feature selection

(A-C) Automated image analysis of RELA localisation, cell shape, and the cytoskeleton. (A) Staining by immunofluorescence (α-tubulin and RELA) and dyes marking DNA (Hoechst) and F-actin (phalloidin). Cell regions were segmented using Hoechst and α-Tubulin stains and features were measured in these regions using the four stains. (B) RELA ratio is calculated by dividing RELA intensity in the nucleus by RELA intensity in the ring region (the cytoplasmic region immediately surrounding the nucleus). (C) Hierarchical clustering of 35 normalised cell features (excluding RELA measurements) measured in five PDAC cell lines and RPE1 cells. Independent features selected (one per cluster) are highlighted in the dendrogram and displayed in the images beside.

I used automated image analysis to segment cell regions and measure 35 geometric, cytoskeletal and Hoechst features, as well as RELA ratio (Figure 4.1B) in approximately 160,000 cells. I used hierarchical clustering to reduce the 35 cell features to ten independent features (Figure 4.1C). Selected features include classical measurements of cell shape (‘Cell Area’, ‘Cell Aspect Ratio’ and ‘Nucleus Roundness’), mean measurements of actin and tubulin intensity in the cytoplasm, ‘Tubulin texture’ which identifies dense clusters of Tubulin, and the ratio of ‘Actin filament area’ to ’Cell area’ which assays actin stress fibre abundance.

4.2.2 PDAC cell lines are morphologically diverse

I used principal component analysis (PCA) to assess the morphological diversity of the six cell lines using normalised data for the nine reduced features from the technical replicates (three experiments in total) for cells under control conditions (Figure 4.2). PCA largely clustered data by cell line, indicating distinct cell morphology and cytoskeletal organisation between cell lines. PCA also validated that the reduced cell features were sufficient to capture the morphological heterogeneity in the PDAC lines. Notably, MIA PaCa2 cells scored low on several cell features due to particularly small area, distorted nuclei (low nucleus roundness) and low abundance of actin that was localised in areas of the cytoplasm away from the membrane. In contrast, PANC1 cells have a notably high cell aspect ratio (ratio of width to length), with less elongation and neighbour contact compared to the other cell lines.

Figure 4.2

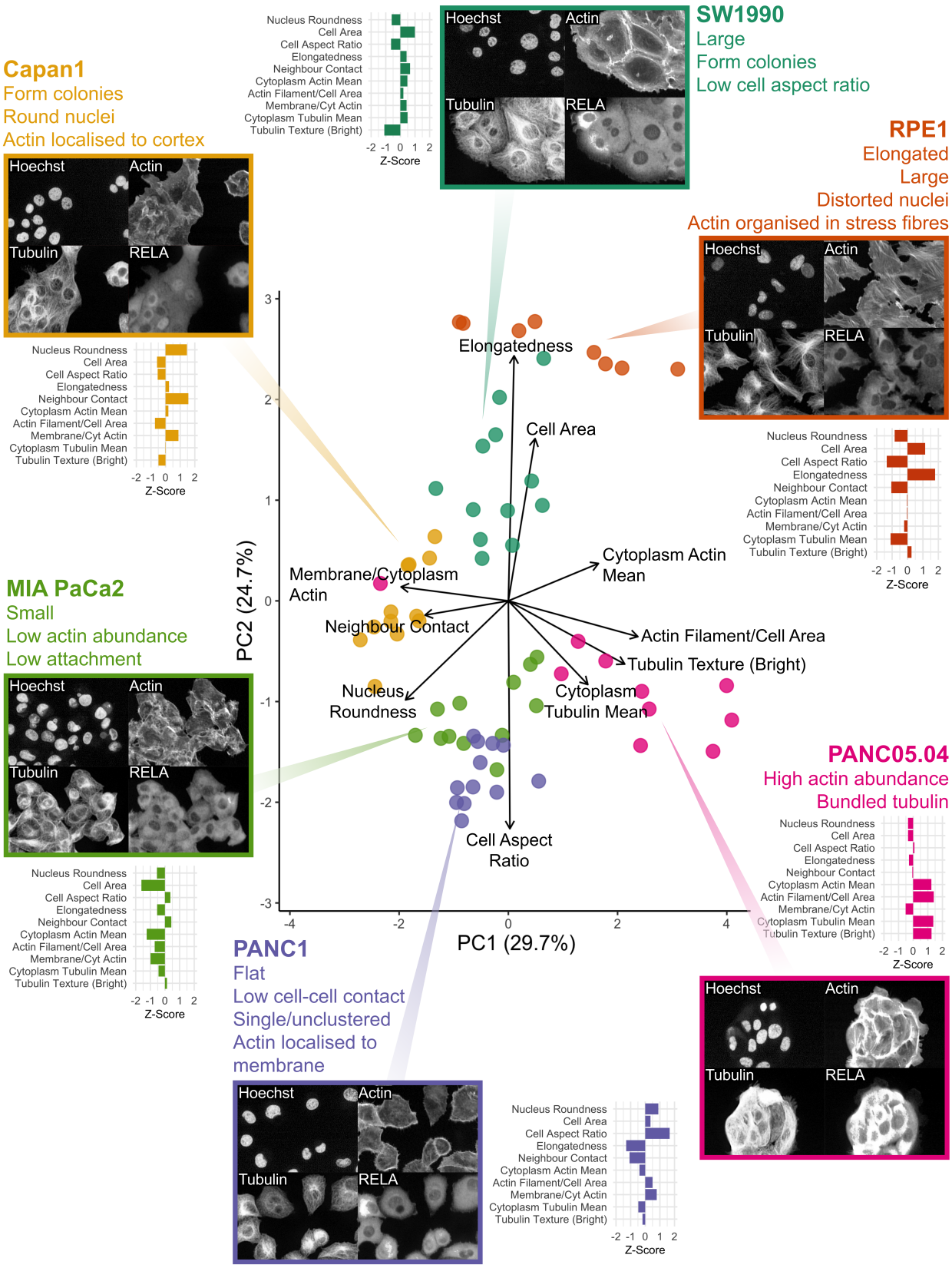
Capan1
Form colonies
Round nuclei
Actin localised to cortex
Hoechst
Actin
Tubulin
RELA
Nucleus Roundness
Cell Area
Cell Aspect Ratio
Elongatedness
Neighbour Contact
Cytoplasm Actin Mean
Actin Filament/Cell Area
Membrane/Cyt Actin
Cytoplasm Tubulin Mean
Tubulin Texture (Bright)
-2 -1 0 1 2
Z-Score
SW1990
Large
Form colonies
Low cell aspect ratio
RPE1
Elongated
Large
Distorted nuclei
Actin organised in stress fibres
MIA PaCa2
Small
Low actin abundance
Low attachment
PANC1
Flat
Low cell-cell contact
Single/unclustered
Actin localised to membrane
PANC05.04
High actin abundance
Bundled tubulin
PC2 (24.7%)
PC1 (29.7%)
Elongatedness
Cell Area
Cytoplasm Actin Mean
Membrane/Cytoplasm Actin
Neighbour Contact
Actin Filament/Cell Area
Tubulin Texture (Bright)
Nucleus Roundness
Cytoplasm Tubulin Mean
Cell Aspect Ratio

Figure 4.2 Morphological diversity of PDAC cell lines

Principal Component Analysis (PCA) of the ten reduced features used in Bayesian analysis for five PDAC cell lines and RPE1 using two principal components (PC1 and PC2). Overlayed is a biplot (arrows) as an indication of the contribution of each cell feature to the two PCs. Circles represent technical replicates. n = four biological repeats. Horizontal bar graphs for individual cell lines show mean z-scores for each feature, calculated across the six cell lines to compare differences in each feature between the cell lines. Z-scores were calculated using the mean and standard deviation for control measurements across all lines for each biological repeat. Displayed is the mean Z score across all biological repeats (n = 4). Images for each cell line show Hoechst, phalloidin marking F-actin (Actin), α-tubulin (Tubulin) and RELA staining by immunofluorescence.

4.2.3 PDAC cell lines have variable RELA responses to TNFα

To assess heterogeneity in RELA responses to TNFα, I measured the RELA ratio (nuc/ring region RELA intensity) in the five PDAC cell lines by immunofluorescence. Across the five PDAC cell lines, the variance of RELA ratios generally increased with TNFα concentration. Cell lines also had varied sensitivity to TNFα in RELA localisation (Figure 4.3A). Similar to the observations with live imaging, immunofluorescence showed that while MIA PaCa2 cells display a substantial increase in nuclear RELA localisation to increasing TNFα treatment, PANC1 cells only have slightly higher nuclear localisation in physiologically high (0.1 ng/ml) compared to physiologically low (0.01 ng/ml) doses of TNFα. Moreover, many cells in 0.01 ng/ml TNFα have RELA ratios overlapping with those in the control treatment, which is in line with the findings from live imaging that most PANC1 cells are unresponsive to 0.01 ng/ml TNFα. I found that the PDAC cell lines SW1990 and PANC05.04 were similar to PANC1 in that high RELA nuclear localisation was only induced in the hyperphysiological dose of TNFα (10 ng/ml). The most similar cell line to MIA PaCa2 was the non-malignant line RPE1, which showed significantly more nuclear localisation of RELA and also higher variation in RELA localisation within each population at increasing TNFα doses.

Figure 4.3

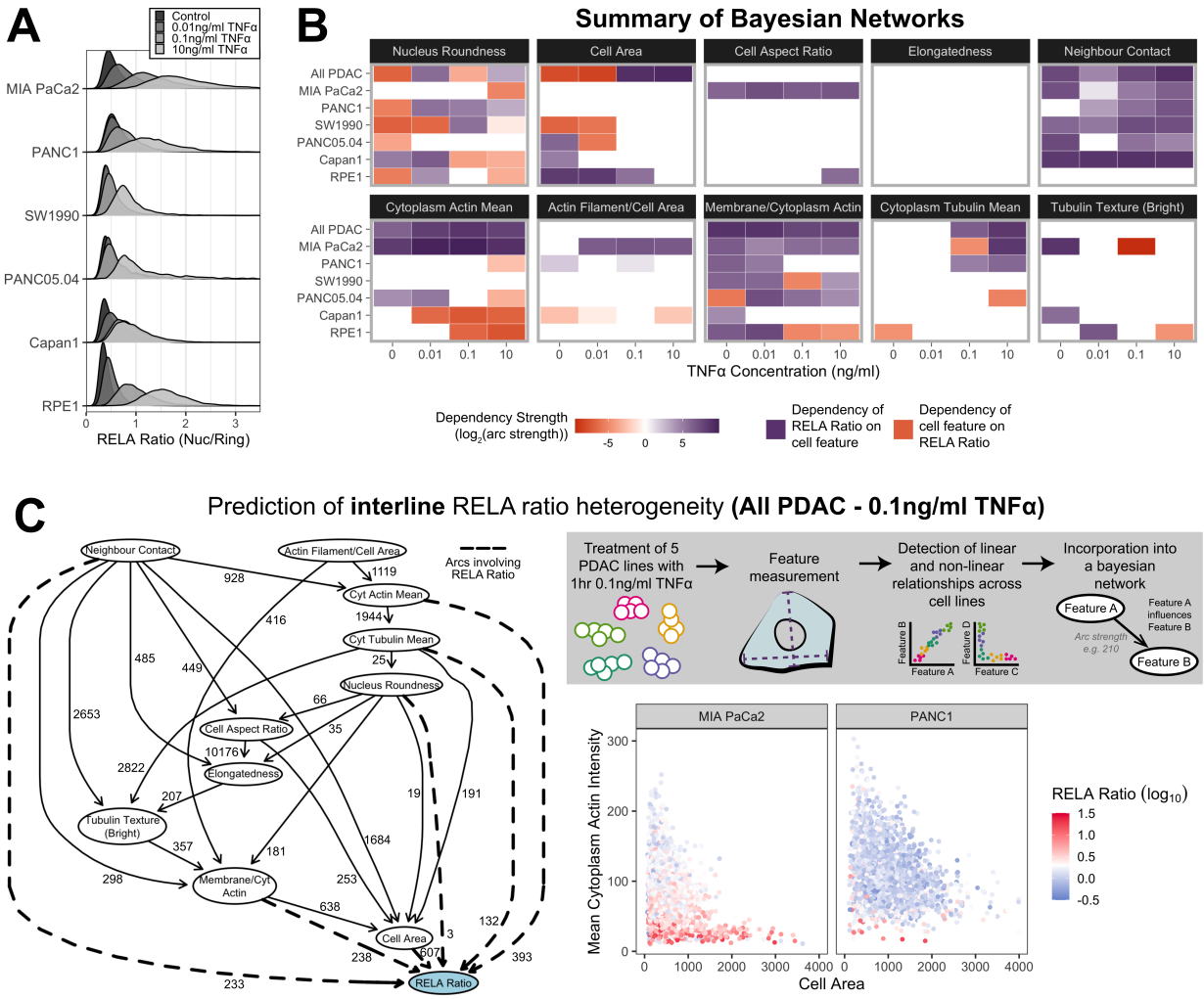
A
Control
0.01ng/ml TNFα
0.1ng/ml TNFα
10ng/ml TNFα
MIA PaCa2
PANC1
SW1990
PANC05.04
Capan1
RPE1
RELA Ratio (Nuc/Ring)
B
Summary of Bayesian Networks
Nucleus Roundness
Cell Area
Cell Aspect Ratio
Elongatedness
Neighbour Contact
Cytoplasm Actin Mean
Actin Filament/Cell Area
Membrane/Cytoplasm Actin
Cytoplasm Tubulin Mean
Tubulin Texture (Bright)
All PDAC
TNFα Concentration (ng/ml)
Dependency Strength
(log2(arc strength))
Dependency of RELA Ratio on cell feature
Dependency of cell feature on RELA Ratio
C
Prediction of interline RELA ratio heterogeneity (All PDAC - 0.1ng/ml TNFα)
Neighbour Contact
Actin Filament/Cell Area
Arcs involving RELA Ratio
Cyt Actin Mean
Cyt Tubulin Mean
Nucleus Roundness
Cell Aspect Ratio
Elongatedness
Tubulin Texture (Bright)
Membrane/Cyt Actin
Cell Area
RELA Ratio
Treatment of 5 PDAC lines with 1hr 0.1ng/ml TNFα
Feature measurement
Detection of linear and non-linear relationships across cell lines
Incorporation into a bayesian network
Feature A influences Feature B
Arc strength e.g. 210
MIA PaCa2
PANC1
Mean Cytoplasm Actin Intensity
Cell Area
RELA Ratio (log10)

Figure 4.3 Heterogeneity between PDAC cell lines in single cell RELA responses to TNFα and dependence on cytoskeletal and geometric features

(A) Single cell RELA ratio distributions by immunofluorescence and automated image analysis. (B) Dependencies involving RELA ratio in Bayesian network models generated with single cell data for individual treatments or cell lines, or for all cell lines collated (top row per cell feature section). Purple indicates that RELA ratio depends on the cell feature in the Bayesian network model. Orange represents that a cell feature depends on RELA ratio. Dependency strengths are calculated as $\log_2(|\text{arc strength}|)$, multiplied by -1 for dependencies of cell features on RELA ratio. (C) Bayesian networks models incorporating data from all PDAC lines (RPE1 excluded) treated for 1 hr with 0.1 ng/ml TNFα. Values next to arcs represent the strength of the probabilistic relationship expressed by the arc (arc strength). Arcs leading to or away from RELA Ratio are dashed. The grey box (C) depicts a schematic of the Bayesian modelling. The scatterplot shows the relationship between two cell features that are predicted to cause changes in RELA ratio.

4.2.4 Actin organisation differences are predictive of heterogeneity in TNFα-mediated RELA localisation between and within PDAC cell lines

To identify features that underlie differences in RELA localisation, I normalised single cell measurements across all PDAC cell lines and TNFα treatments then collated and incorporated them into Bayesian networks. Bayesian network models use statistical inference that can be applied to heterogeneous experimental data to predict the conditional dependence of components/features on each other. Bayesian network models appear as influence diagrams consisting of nodes, each representing a measured feature, and arcs between the nodes that depict predicted dependencies between the nodes. Bayesian network models are powerful tools as they can represent linear and non-linear relationships, direct and indirect interactions, and illustrate multiple interacting nodes simultaneously (Sachs et al., 2005). I employed a hybrid class of Bayesian algorithm ('rsmax2') that generates models using a combination of constraint-based and score-based approaches (Scutari et al., 2018). This algorithm only allows unidirectional arcs in the Bayesian network, therefore it is possible that a reverse relationship may also exist but is not as statistically likely as the relationship indicated.

To establish patterns in RELA dependencies across PDAC lines, I generated Bayesian network models for each cell line for varying TNFα concentrations and summarised dependencies involving RELA ratio in Figure 4.3B. RELA ratio had a strong and consistent relationship with neighbour contact across all PDAC lines but not in the non-malignant line RPE1. RELA ratio was frequently dependent on cytoplasm actin intensity, cytoplasm tubulin intensity and membrane/cytoplasm actin, suggesting that TNFα mediated RELA nuclear translocation is dependent on cytoskeletal dynamics in PDAC cells. Conversely, nucleus roundness was predicted to be dependent on RELA ratio in several contexts. Some dependencies between RELA ratio and a cell feature changed with TNFα, including the

dependency of RELA ratio on cytoplasm tubulin mean which was more probable with TNFα, while correlations between RELA ratio and cell area were more probable in basal conditions.

To identify cell features that likely explain RELA localisation differences between cell lines at high levels of inflammation, I focused on the Bayesian model for 1 hr 0.1ng/ml TNFα that incorporated data from all five PDAC lines (Figure 4.3C). The features with the strongest statistical likelihood of influencing RELA localisation differences between cell lines were cell area and cytoplasm actin mean, which both negatively correlated with RELA ratio. These data suggest that the smaller cell area and lower actin abundance of MIA PaCa2 cells compared to PANC1 cells contribute to increased RELA nuclear translocation in MIA PaCa2 cells in response to TNFα.

I assessed which features may underlie heterogeneity in RELA localisation within PDAC cell lines (Figure 4.4A). RELA ratio differences within both the MIA PaCa2 (Figure 4.4B) and PANC1 (Figure 4.4C) cell lines were predicted to depend on actin stress fibre abundance. MIA PaCa2 cells showed additional dependencies on actin cytoplasm intensity and actin membrane/cytoplasm intensity, which I interpret as the amount of cortical actin and could reflect membrane tension, while PANC1 cells showed unique dependencies of RELA localisation on tubulin abundance (mean cytoplasm tubulin intensity) and nuclear roundness. Overall, these data show that the relationship between RELA localisation and the cytoskeleton, in particular actin networks, is cell-line specific.

Figure 4.4

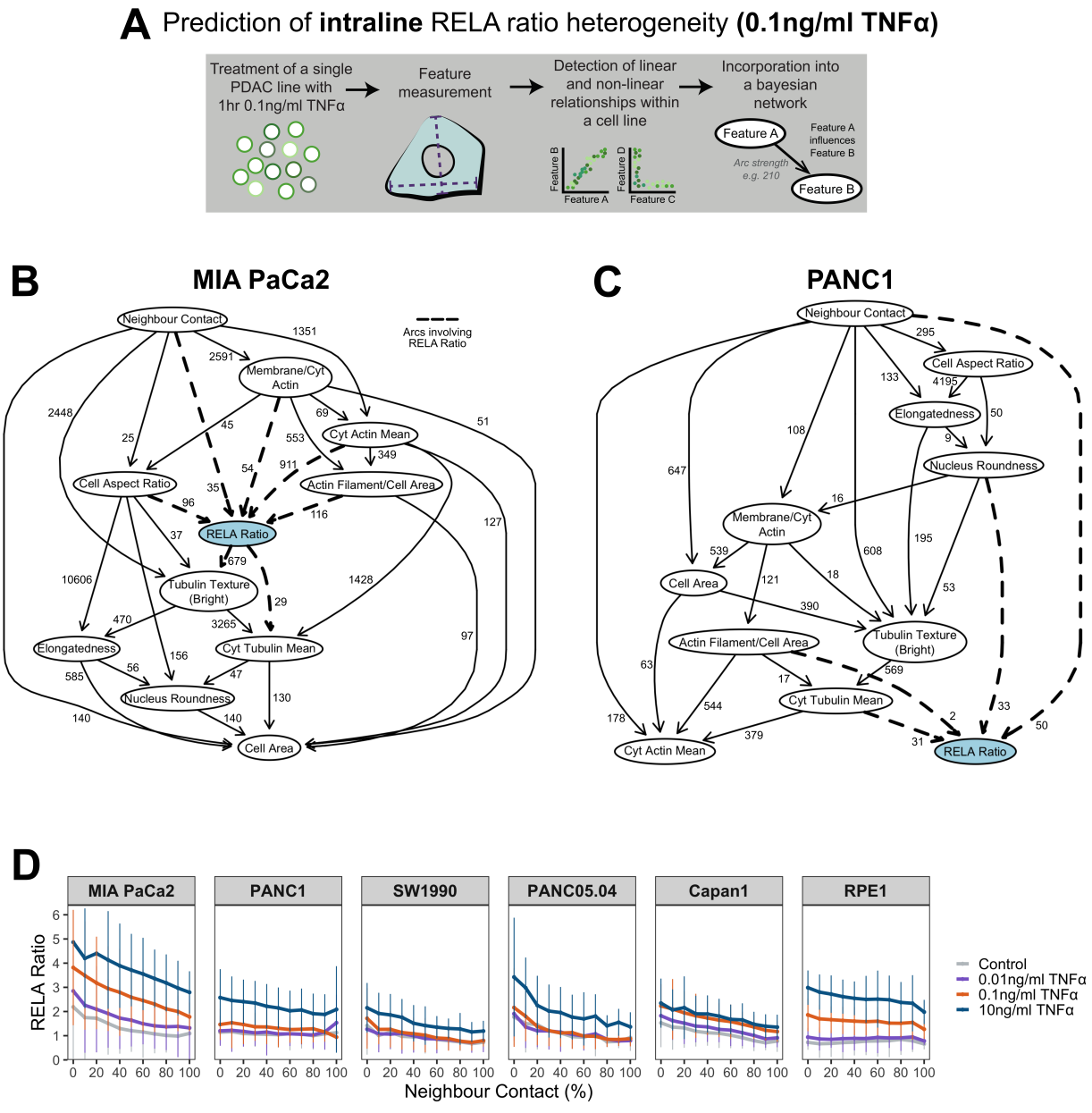
A Prediction of intraline RELA ratio heterogeneity (0.1ng/ml TNFα)
Treatment of a single PDAC line with 1hr 0.1ng/ml TNFα
Feature measurement
Detection of linear and non-linear relationships within a cell line
Incorporation into a bayesian network
Feature A
Feature A influences Feature B
Arc strength e.g. 210
Feature B
Feature B
Feature A
Feature D
Feature C
B MIA PaCa2
C PANC1
Arcs involving RELA Ratio
Neighbour Contact
Membrane/Cyt Actin
Cyt Actin Mean
Cell Aspect Ratio
Actin Filament/Cell Area
RELA Ratio
Tubulin Texture (Bright)
Elongatedness
Cyt Tubulin Mean
Nucleus Roundness
Cell Area
D
MIA PaCa2
PANC1
SW1990
PANC05.04
Capan1
RPE1
RELA Ratio
Neighbour Contact (%)
Control
0.01ng/ml TNFα
0.1ng/ml TNFα
10ng/ml TNFα

Figure 4.4 Bayesian analysis of cell feature differences influencing the heterogeneity of RELA ratio within PDAC cell lines

(A) Schematic of Bayesian networks modelling features in a single cell line treated with 0.1 ng/ml TNFα. (B-C) Bayesian networks models incorporating data from (A) MIA PaCa2 or (B) PANC1 cells only. (D) Mean RELA ratio +/- standard deviation against (rounded) neighbour contact by treatment.

Interestingly, neighbour contact was predicted by Bayesian modelling to influence several cytoskeletal features in both MIA PaCa2 and PANC1 cells. Having previously identified a negative correlation between RELA ratio and breast epithelial cells (Sero et al., 2015), I tested whether this relationship also existed in PDAC cells by calculating the RELA ratio at each TNFα dose for cells grouped by neighbour contact (Figure 4.4D). I found that in most TNFα doses and PDAC lines, RELA ratio was lower in cells with higher neighbour contacts, suggesting that RELA nuclear translocation is contact inhibited in PDAC cells.

4.2.5 Cytoskeletal and cell shape features correlate with RELA translocation classes

To test whether relationships exist between cell features and TNFα-induced live RELA translocation response profiles for PDAC cells, I used RELA-GFP-expressing MIA PaCa2 and PANC1 cells fixed at 60 min following 0.1 ng/ml TNFα treatment and stained for F-actin, α-Tubulin and DNA. I allocated cells to RELA translocation response clusters based on RELA ratio, using the mean and standard deviation for live tracked cells at 60 min to define RELA ratio limits for each cluster (Figure 4.5A). Cluster prediction accuracy was tested by re-clustering tracked cells based and optimised by varying the number of standard deviations from the mean to set cluster limits. Generally, increasing limits with a higher number of standard deviations enabled more cells to be clustered but reduced prediction accuracy. RELA translocation clusters were predicted with high accuracy (> 80 %) as early as 20 min after TNFα addition for MIA PaCa2 cells, while PANC1 cells were only accurately predicted 50 min after TNFα addition. Clusters were generated using the mean +/- 0.6 SD for both cell lines, yielding 89 % accuracy with 53 % of cells clustered at 60 min for MIA PaCa2 cells and 82 % accuracy with 57 % of cells clustered for 60 min for PANC1 cells.

Figure 4.5

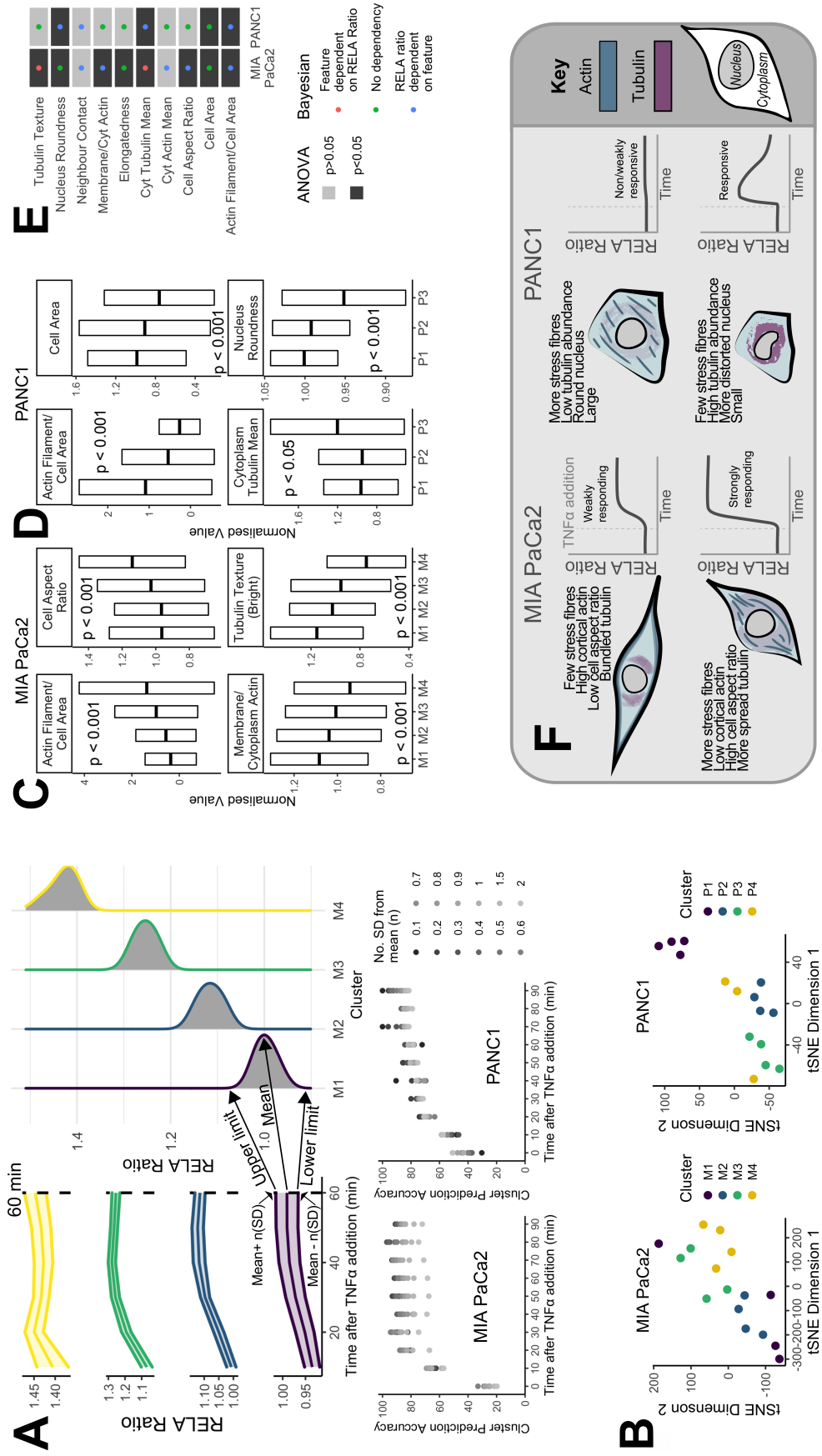
A
60 min
RELA Ratio
Mean+ n(SD)
Upper limit
Mean
Mean - n(SD)
Lower limit
Time after TNFα addition (min)
Cluster
M1
M2
M3
M4
MIA PaCa2
PANC1
Cluster Prediction Accuracy
No. SD from mean (n)
B
tSNE Dimension 1
tSNE Dimension 2
P1
P2
P3
P4
C
MIA PaCa2
Actin Filament/ Cell Area
Membrane/ Cytoplasm Actin
Cell Aspect Ratio
Tubulin Texture (Bright)
Normalised Value
p < 0.001
D
PANC1
Cell Area
Nucleus Roundness
Actin Filament/ Cell Area
Cytoplasm Tubulin Mean
p < 0.05
E
Tubulin Texture
Nucleus Roundness
Neighbour Contact
Membrane/Cyt Actin
Elongatedness
Cyt Tubulin Mean
Cyt Actin Mean
Cell Aspect Ratio
Cell Area
Actin Filament/Cell Area
MIA PaCa2
PANC1
ANOVA
p>0.05
p<0.05
Bayesian
Feature dependent on RELA Ratio
No dependency
RELA ratio dependent on feature
F
MIA PaCa2
PANC1
Few stress fibres
High cortical actin
Low cell aspect ratio
Bundled tubulin
TNFα addition
Weakly responding
Strongly responding
Non/weakly responsive
Responsive
Time
More stress fibres
Low tubulin abundance
Round nucleus
Large
Few stress fibres
High tubulin abundance
More distorted nucleus
Small
More stress fibres
Low cortical actin
High cell aspect ratio
More spread tubulin
Key
Actin
Tubulin
Nucleus
Cytoplasm

Figure 4.5 Cytoskeletal and cell shape features correlate with RELA translocation response profiles

(A) Schematic illustrating method for RELA translocation response cluster classification. RELA ratio limits per cluster are defined by the mean and a number (n) of standard deviations from the mean, calculated from live imaged cells tracked and categorised by hierarchical clustering at a defined timepoint after 0.1 ng/ml TNFα addition. Cells are independently sorted into clusters based on RELA ratio at the same timepoint after 0.1 ng/ml TNFα addition. Below are cluster prediction accuracies at 10 min intervals following TNFα addition. Prediction accuracy is calculated as the percentage of clustered cells tracked through live imaging with the correct cluster identified using the limits set by the model. (B) Predictions of RELA dynamics clusters for fixed MIA Paca2 and PANC1 cells overlaid onto t-SNE analysis by well averages of the cell shape and cytoskeletal features used for Bayesian analysis, excluding Neighbour Contact. (C-D) Data from fixed cells for the same experiment as (B), showing single cell data for four measured cell features with high statistical significance by ANOVA between RELA translocation clusters. Bars show mean +/- SD. (E) Summary of identified relationships between RELA ratio and cell features by cross-referencing cell shape and RELA translocation clusters (tested by ANOVA) and independently by Bayesian analysis. (F) Schematic summarising identified relationships between cell shape and cytoskeletal features with RELA translocation response to TNFα. MIA PaCa2 cells with more actin stress fibres (actin filament/cell area), low cortical actin (membrane/cytoplasm actin), low cell aspect ratio (width to length) and more spread tubulin are more likely to have high nuclear RELA translocation in response to 0.1 ng/ml TNFα. PANC1 cells can be unresponsive or responsive to 0.1 ng/ml TNFα, with responsiveness correlated to actin stress fibre and tubulin abundance, as well as nucleus roundness and cell area.

t-distributed stochastic neighbour embedding (tSNE) analysis of ten independent cell shape and cytoskeletal features showed that cells with the same RELA translocation response profile cluster together and therefore have similar cell shape and cytoskeletal organisation (Figure 4.5B). Features different between RELA translocation clusters were identified by ANOVA, using all clusters (M1-M4) for MIA PaCa2 cells and clusters P1-P3 for PANC1 cells due to a lack of P4-type responding cells to 0.1 ng/ml TNFα. MIA PaCa2 cells with a high number of actin filaments, less cortical actin (membrane/cytoplasm actin), higher cell aspect ratio (width to length) and less bundled tubulin (Tubulin Texture Bright) were more likely to fit a high nuclear RELA translocation response to 0.1 ng/ml TNFα (Figure 4.5C). Conversely, PANC1 cells with more actin filaments were more likely to be unresponsive (Cluster P1) to 0.1 ng/ml TNFα, while cells with smaller cell area, higher tubulin abundance and low nucleus roundness were more likely to induce RELA nuclear translocation following 0.1 ng/ml TNFα (Clusters P2 and P3) (Figure 4.5D).

In Figure 4.5E and Figure 4.5F, I summarised the identified relationships between RELA ratio and cell features by the two statistical methods: 1) cross-referencing cell shape and RELA translocation response assayed by ANOVA, 2) Bayesian analysis. In MIA Paca2 cells, decreased cortical actin, but increased stress fibre assembly, increased roundness, and expansion of tubulin networks predicted high levels of chronic RELA translocation. These changes are characteristic of increased contractility and decreased cell-ECM adhesion. In PANC1 cells, contractility also appears to predict increased RELA activation as evidenced by decreased cell area, and PANC1 cells with distorted nuclei also have higher RELA ratios. However, in contrast to MIA PACA2 cells, RELA activation occurs acutely and is suppressed over time in PANC1 cells. Overall, these analyses show that heterogeneity in RELA translocation dynamics is linked to heterogeneity in cell shape and cytoskeletal organisation in PDAC cells in a cell-line dependent manner.

4.2.6 Biochemical perturbation of the cytoskeleton modulates the effect of TNFα on RELA translocation

As cytoskeletal organisation and cell shape were identified as predictors of TNFα induced RELA translocation, I tested the effect of interfering with cytoskeletal and cell shape dynamics on RELA localisation by employing drugs targeting tubulin, actin, myosin, or focal adhesion (FA) dynamics. I ascertained optimal doses by treating MIA PaCa2 cells with concentration ranges for 24 hr, or 3 hr for SMIFH2 (Figure 4.6). Interestingly, both myosin targeting drugs caused minimal effects on actin abundance and higher doses were required to affect cell spreading in MIA PaCa2 cells compared to previous observations in breast cells (Sero et al., 2015).

Figure 4.6

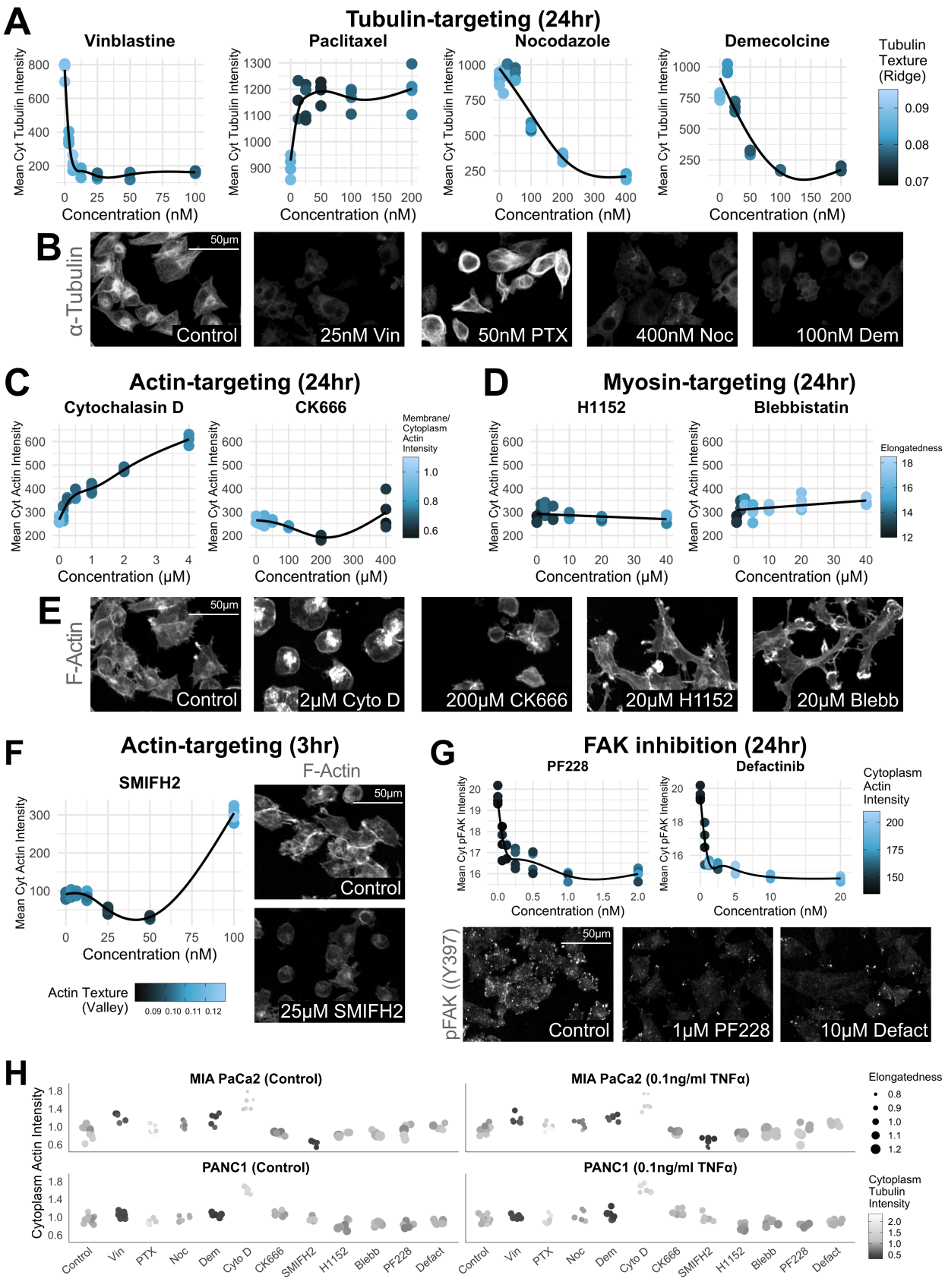
A
Tubulin-targeting (24hr)
Vinblastine
Paclitaxel
Nocodazole
Demecolcine
Mean Cyt Tubulin Intensity
Concentration (nM)
Tubulin Texture (Ridge)
B
α-Tubulin
50μm
Control
25nM Vin
50nM PTX
400nM Noc
100nM Dem
C
Actin-targeting (24hr)
Cytochalasin D
CK666
Mean Cyt Actin Intensity
Concentration (μM)
Membrane/ Cytoplasm Actin Intensity
D
Myosin-targeting (24hr)
H1152
Blebbistatin
Elongatedness
E
F-Actin
Control
2μM Cyto D
200μM CK666
20μM H1152
20μM Blebb
F
Actin-targeting (3hr)
SMIFH2
F-Actin
Actin Texture (Valley)
25μM SMIFH2
G
FAK inhibition (24hr)
PF228
Defactinib
Mean Cyt pFAK Intensity
Cytoplasm Actin Intensity
pFAK ((Y397)
1μM PF228
10μM Defact
H
MIA PaCa2 (Control)
MIA PaCa2 (0.1ng/ml TNFα)
PANC1 (Control)
PANC1 (0.1ng/ml TNFα)
Cytoplasm Actin Intensity
Cytoplasm Tubulin Intensity
Control
Vin
PTX
Noc
Dem
Cyto D
CK666
SMIFH2
H1152
Blebb
PF228
Defact

Figure 4.6 Dose responses of MIA PaCa2 cells to drugs targeting the cytoskeleton

(A-G) Dose responses of cytoskeleton-targeting drugs and representative images of MIA PaCa2 cells (absence of TNFα). n = four technical replicates per drug dose. (H) Cytoplasm actin intensity (y-axis), Elongatedness (point size) and cytoplasm tubulin intensity (point colour) of cells treated with selected concentrations of each cytoskeletal drug in the presence or absence of 1 hr 0.1 ng/ml TNFα. All measurements are normalised to the control for each cell line and TNFα dose (0 or 0.1 ng/ml). Points show two technical (well) replicates for three biological repeats per treatment combination.

To assay the effect of cytoskeleton interference on TNFα-stimulated RELA translocation, I treated MIA PaCa2 and PANC1 cells with selected drug doses for 2 hr then simultaneously with 10 ng/ml TNFα for 1 hr. Broadly, I found that inhibitors with similar mechanisms induce analogous effects on RELA translocation. In MIA PaCa2 cells, targeting actin had inhibitor-specific effects on RELA localisation (Figure 4.7A). Actin nucleation is the formation of a complex of actin monomers from which actin filaments can form. CK666 inhibits the ARP2/3 complex – a key mediator of actin filament nucleation and branching (Mullins et al., 1998), while SMIFH2 inhibits formins (Rizvi et al., 2009), which promote actin nucleation and elongation of pre-existing filaments to produce long straight filaments (Pruyne et al., 2002). SMIFH2, and to a lesser extent CK666, significantly downregulated nuclear RELA localisation in MIA PaCa2, indicating that nucleation of both branched actin and actin stress fibres function in TNFα-mediated RELA nuclear translocation. Cytochalasin D, which binds to the growing end of actin filaments and inhibits polymerisation (Schliwa, 1982), caused no effect on RELA ratio, indicating that actin organisation, rather than actin polymerisation itself, contributes to RELA nuclear translocation.

Figure 4.7

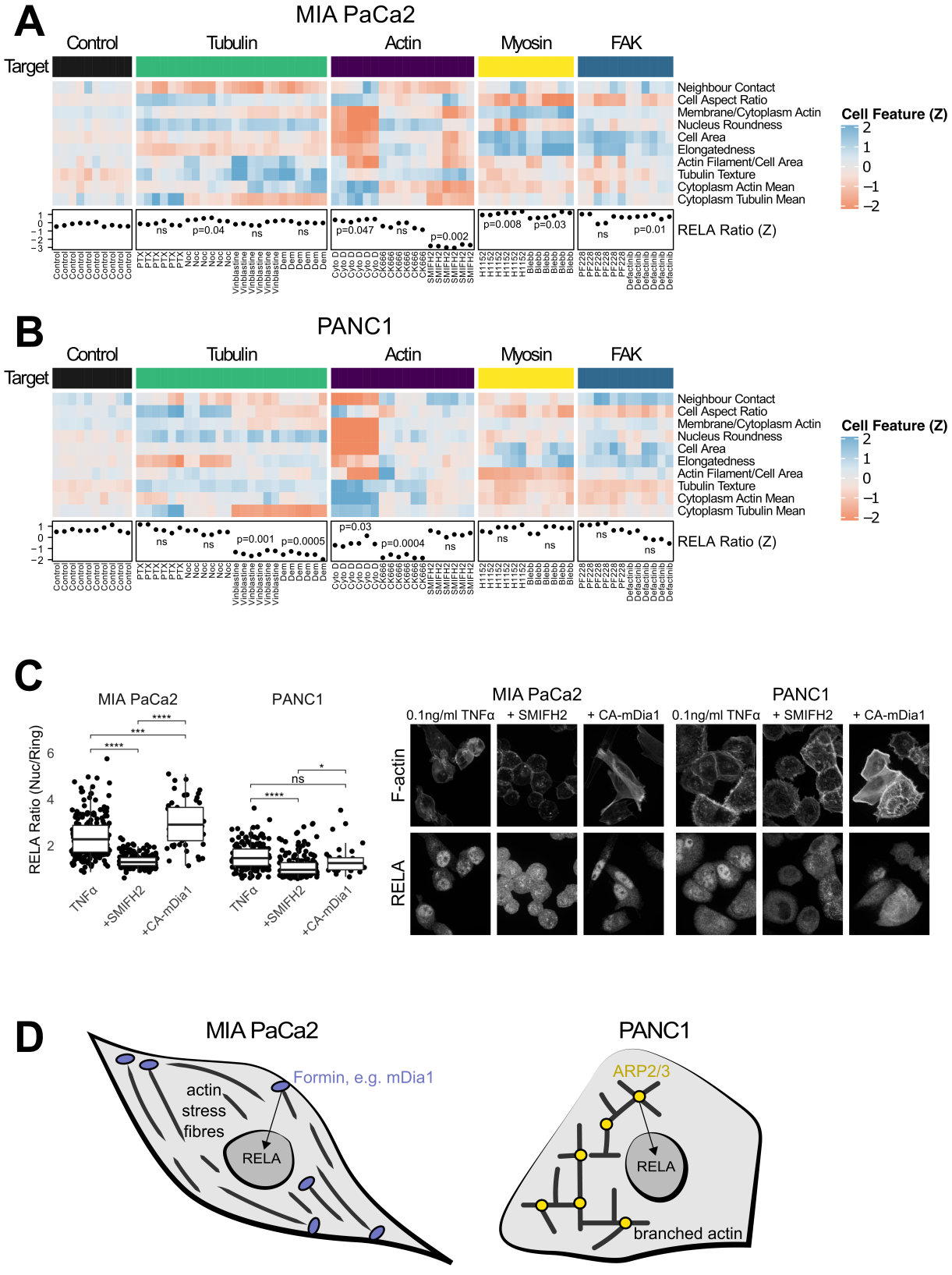
A
MIA PaCa2
Control
Tubulin
Actin
Myosin
FAK
Target
Neighbour Contact
Cell Aspect Ratio
Membrane/Cytoplasm Actin
Nucleus Roundness
Cell Area
Elongatedness
Actin Filament/Cell Area
Tubulin Texture
Cytoplasm Actin Mean
Cytoplasm Tubulin Mean
Cell Feature (Z)
2
1
0
−1
−2
RELA Ratio (Z)
ns
p=0.04
ns
ns
p=0.047
ns
p=0.002
p=0.008
p=0.03
ns
p=0.01
B
PANC1
Control
Tubulin
Actin
Myosin
FAK
Target
Neighbour Contact
Cell Aspect Ratio
Membrane/Cytoplasm Actin
Nucleus Roundness
Cell Area
Elongatedness
Actin Filament/Cell Area
Tubulin Texture
Cytoplasm Actin Mean
Cytoplasm Tubulin Mean
Cell Feature (Z)
RELA Ratio (Z)
ns
ns
p=0.001
p=0.0005
p=0.03
p=0.0004
ns
ns
ns
ns
ns
C
MIA PaCa2
PANC1
RELA (Nuc/Ring)
TNFα
+SMIFH2
+CA-mDia1
MIA PaCa2
PANC1
0.1ng/ml TNFα
+ SMIFH2
+ CA-mDia1
F-actin
RELA
D
MIA PaCa2
actin
stress
fibres
Formin, e.g. mDia1
RELA
PANC1
ARP2/3
RELA
branched actin

Figure 4.7 Modulation of TNFα-mediated RELA translocation by cytoskeletal perturbation using small molecule inhibitors

(A-B) Fold-changes for cell shape and cytoskeletal measurements following 3 hr drug treatment and normalised to the drug control (no cytoskeletal drug). Below are the corresponding fold-changes for RELA ratio (1 hr 10 ng/ml TNFα/control) normalised to the drug control. Data are shown for technical replicates/well averages (two technical replicates per three biological repeats). PTX = paclitaxel; Noc = nocodazole; Dem = Demecolcine; Cyto D = Cytochalasin D; Blebb = Blebbistatin; PF228 = PF573228. Statistics shown for multiple t-tests with Benjamini-Hochberg correction comparing each treatment to the control RELA ratio. ns (non-significant) = $p > 0.05$. The p-values for all results where $p < 0.05$ are shown and rounded to 1 significant figure, aside from Cyto D (MIA PaCa2) which is rounded to 2 significant figures for clarity of the significant test result. (C) Single cell RELA ratios in MIA PaCa2 and PANC1 cells treated with 0.1 ng/ml TNFα, with additional treatment with the formin inhibitor SMIFH2 or 24 hr transfection with CA-mDia1-GFP (constitutively active mDia1). Representative images per cell line and condition are shown. Statistical significance (multiple t-tests with Benjamini-Hochberg correction): ns (non-significant) = $p > 0.05$, * = $0 < 0.05$, ** = $p < 0.01$, *** = $p < 0.001$, **** = $p < 0.0001$. (D) RELA nuclear translocation is dependent on actin structure in PDAC cells, with a higher dependency on the nucleation of stress fibres in MIA PaCa2 cells and on the nucleation of branched actin in PANC1.

H1152 targets Rho-kinase (ROCK), preventing ROCK phosphorylation of myosin light chain that normally promotes actin-binding and consequently contractility, while blebbistatin blocks myosin II ATPase and subsequently interferes with actin contractility (Sasaki et al., 2002; Kovács et al., 2004). In MIA PaCa2 cells, myosin/ROCK inhibition and defactinib/PF228 inhibition of FAK increased cell area and elongation as expected but had minimal effects on actin and tubulin abundance and distribution, and all increased RELA nuclear translocation. These data suggest that cell contractility or focal adhesion dynamics may suppress TNFα-induced RELA nuclear translocation independently of actin and tubulin dynamics.

Similar to MIA PaCa2 cells, actin perturbations caused reductions in RELA ratio in PANC1 cells (Figure 4.7B), however, PANC1 cells were more sensitive to CK666 and cytochalasin D compared with MIA PACa2. Myosin and FAK inhibition caused milder effects on cell shape in PANC1 cells compared to MIA PaCa2, which may be related to the flat/less contractile morphology of PANC1 cells observed in Figure 4.2, and these drug groups caused non-significant changes in RELA ratio in PANC1 cells.

Tubulin-targeting drugs are commonly used in cancer chemotherapy and either prevent MT assembly (vinblastine and nocodazole), limit MT formation and cause MT depolymerisation (demecolcine) or stabilise MTs and prevent disassembly (paclitaxel) (Spencer and Faulds, 1994; Vasquez et al., 1997; Gigant et al., 2005; Tangutur et al., 2017). While targeting tubulin had no effect on RELA localisation in MIA PaCa2 cells, PANC1 cells were sensitive to tubulin inhibition, particularly tubulin depolymerisation by vinblastine and demecolcine caused reductions in RELA ratio. This supports the predictions using Bayesian modelling that RELA is dependent on tubulin dynamics in PANC1 cells but not in MIA PaCa2 cells.

Having screened for drugs targeting the cytoskeleton that perturb RELA nuclear translocation and identified SMIFH2 as a significant hit, I investigated the relationship between formin dynamics and RELA activity. On the single cell level, MIA PaCa2 and PANC1 cells had more cytoplasmic RELA localisation with SMIFH2 and TNFα combination

compared to TNFα alone, with a more significant change in MIA PaCa2 cells (Figure 4.7C). Formin overactivation via constitutively active mDia1 (CA-mDia-GFP) (Rao et al., 2013) resulted in an increase in RELA ratio with TNFα in MIA PaCa2 cells, but no difference in PANC1 cells, compared to TNFα alone.

Altogether, these data identify that actin structure and dynamics in PDAC cells modulate RELA subcellular localisation, however, the precise apparatus for this is different between MIA PaCa2 and PANC1 cells, as predicted by differing influences by actin features on RELA ratio assessed by Bayesian analysis. RELA nuclear translocation is highly dependent on nucleation of actin stress fibres in MIA PaCa2 cells, whereas RELA nuclear translocation is dependent more on nucleation of branched actin in PANC1 cells (Figure 4.7D).

4.2.7 RELA translocates to the cytoplasm with cell spreading and attachment

Having observed the effects of chemically induced spreading by H1152 and blebbistatin on RELA nuclear translocation, I tested whether physiological initiation of spreading affects TNFα-mediated RELA nuclear translocation. To this end, I seeded MIA PaCa2 and PANC1 cells co-expressing RELA-GFP and PCNA-Scarlet incubated with SiR-Actin on a plastic matrix and immediately imaged to capture changes in RELA localisation as cells attach and spread. Cells were treated before imaging with 0.1 ng/ml TNFα (or a BSA/PBS control) to assay whether any relationships observed are sustained with TNFα. I also treated adhered cells with 0.1 ng/ml TNFα and imaged with the same parameters for comparison (Figure 4.8A and B).

Figure 4.8

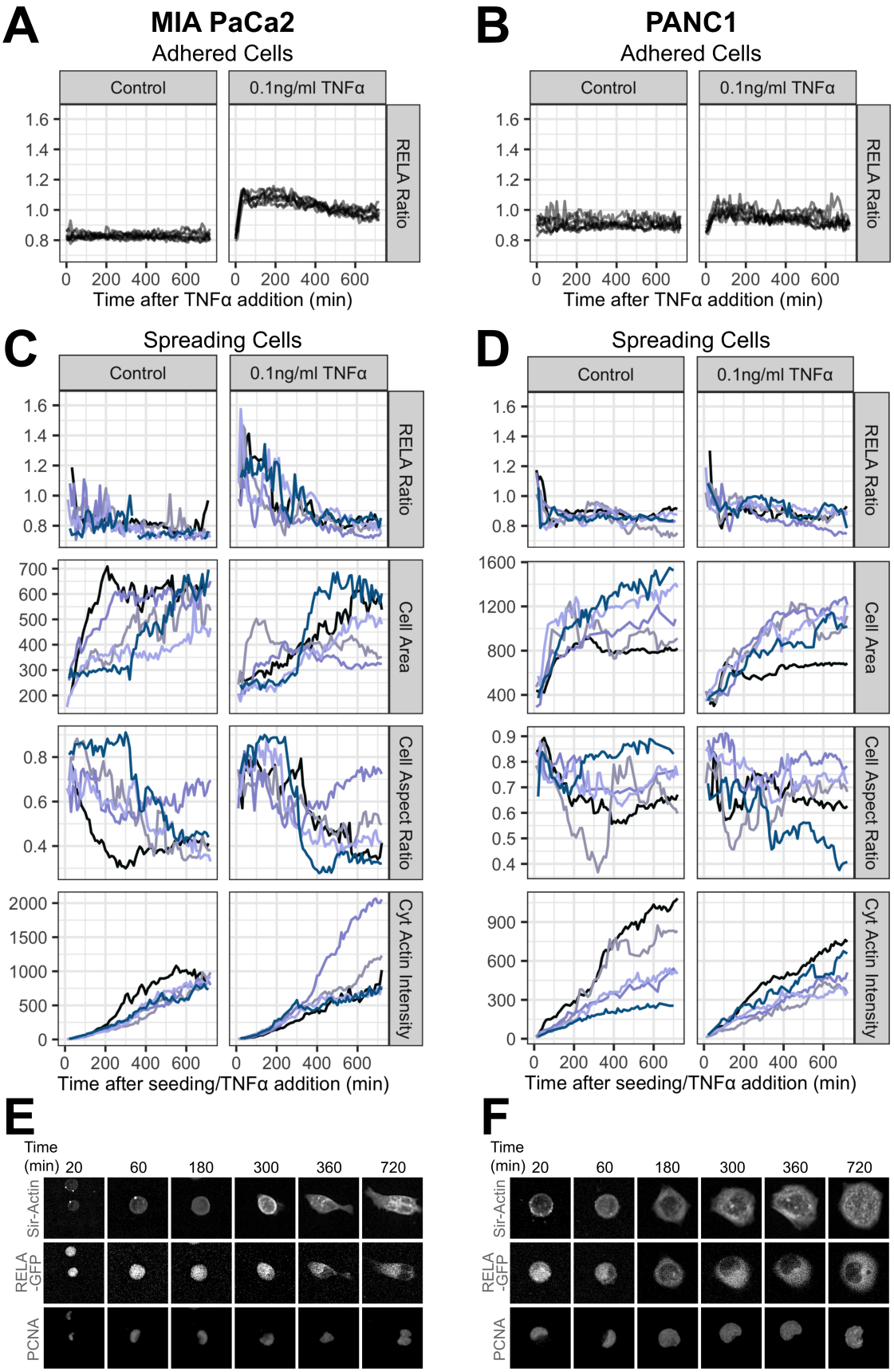
A
MIA PaCa2
Adhered Cells
Control
0.1ng/ml TNFα
RELA Ratio
Time after TNFα addition (min)
B
PANC1
Adhered Cells
C
Spreading Cells
Cell Area
Cell Aspect Ratio
Cyt Actin Intensity
Time after seeding/TNFα addition (min)
D
E
Time (min)
20
60
180
300
360
720
Sir-Actin
RELA -GFP
PCNA
F

Figure 4.8 Cell spreading antagonises nuclear RELA localisation

(A-B) Well averages for RELA ratio (calculated from endogenous RELA-GFP) over time, following 0.1 ng/ml TNFα or BSA/PBS (control) addition, in (A) MIA PaCa2 and (B) PANC1 cells seeded one day prior and adhered to the plate. (C-D) Single cell traces of cell area (each line colour represents an individual cell), cell aspect ratio (ratio of width to length), mean cytoplasm actin intensity and RELA ratio in MIA PaCa2 and PANC1 cells imaged immediately after seeding and treatment with BSA/PBS (control) or 0.1 ng/ml TNFα. All cells were imaged at 10 min intervals for 12 hr. Cells seeded immediately prior to imaging were incubated with SiR-Actin before seeding and measurements were calculated for five cells per treatment and cell line. Measurements were calculated by automated image analysis using Columbus software (PerkinElmer). Line colours correspond to cell identities. Below are representative images of SiR-Actin, RELA-GFP and PCNA-Scarlet in the corresponding cell lines at indicated times after seeding and treatment.

In spreading cells, I measured sharp increases in cell area as cells attached to the underlying matrix followed by a gradual increase in cell area as cells spread (Figure 4.8C and D). Cell aspect ratio generally reduced over time and significant drops in cell aspect ratio occurred at the same timepoints of significant increases in cell area on a single cell basis. After decreasing, cell aspect ratio typically remained minimal in MIA PaCa2 cells but often increased again in PANC1 cells in the latter half of the assay, finalising with higher cell aspect ratios compared to MIA PaCa2. These observations suggest that PANC1 cells may require a certain level of attachment and spreading before undergoing morphogenesis to attain roundness again. Moreover, PANC1 cells appeared to spread more quickly than MIA PaCa2 cells, since they required a shorter amount of time to reach maximum cell area, and PANC1 cells were 2-3 times larger in cell area compared to MIA PaCa2 cells.

In all cells in the presence and absence of TNFα, RELA ratio sharply decreased with attachment to the underlying matrix then gradually RELA ratio decreased with cell spreading, demonstrating a negative correlation between RELA ratio with cell area and a positive correlation between RELA ratio with cell aspect ratio. These patterns are in line with the predictions from fixed MIA PaCa2 and PANC1 cells using immunofluorescence (Figure 4.5C and D) and collectively show that nuclear localisation of RELA is negatively correlated with cell spreading.

When comparing RELA localisation following TNFα treatment in spreading cells (Figure 4.8A and B) versus in adhered cells (Figure 4.8C and D), I observed that TNFα-induced RELA nuclear localisation is not sustained as well in spreading cells compared to adhered cells. In MIA PaCa2 cells, RELA becomes predominantly cytoplasmic within approximately 400 min after TNFα addition in spreading cells, while all responsive adhered MIA PaCa2 cells retain nuclear localisation of RELA even 600 min following TNFα addition. In PANC1 cells, both spreading and adhered cells can lose RELA nuclear localisation following TNFα addition, but cytoplasmic re-localisation of RELA is attained quicker in actively spreading cells, approximately 200 min after TNFα treatment, versus > 400 min in adhered cells.

Interestingly, cell suspension at the beginning of the imaging period did not hinder TNFα-induced RELA nuclear translocation, as cells with TNFα treatment started with higher RELA ratios compared to cells with control treatment.

On the whole, these data suggest that pre-attachment and spreading of cells prior to TNFα treatment is not required for TNFα-mediated activation of RELA but is required for maintaining long term nuclear localisation of RELA in PDAC cells.

4.2.8 RELA regulate cytoskeletal architecture and cell shape

RELA has been identified as a regulator of EMT in transformed breast epithelial cells, as RELA inhibition (Huber et al., 2004) and reduction of RELA transcript and protein levels (Pires et al., 2017) cause loss of mesenchymal markers identified as NF-κB target genes. To test whether TNFα and RELA regulate cell shape and cytoskeletal dynamics in PDAC cells, I measured 35 cytoskeletal, cell shape and Hoechst features in MIA PaCa2 RELA-GFP cells expressing IκB-SR (non-degradable IκB) in the absence or presence of 10 hr 0.1 ng/ml TNFα.

I used PCA (Figure 4.9A) to test whether RELA activation and inhibition are associated with morphological and cytoskeletal changes in MIA PaCa2 cells. PCA revealed that IκB-SR induction in combination with TNFα causes a significant change in cell morphology/cytoskeletal organisation from basal conditions or compared with IκB-SR induction or TNFα alone. The PCA biplot indicates that cytoskeletal features contribute to PC1 and PC2 in the direction of the shift with the combination treatment, suggesting that concomitant TNFα treatment and RELA inactivation are required for perturbation of the cytoskeleton. Meanwhile, most cell shape feature contributions match the shift in TNFα treatment compared to both control and combination treatments, suggesting that alteration of cell shape by TNFα treatment is dependent on RELA nuclear translocation.

Figure 4.9

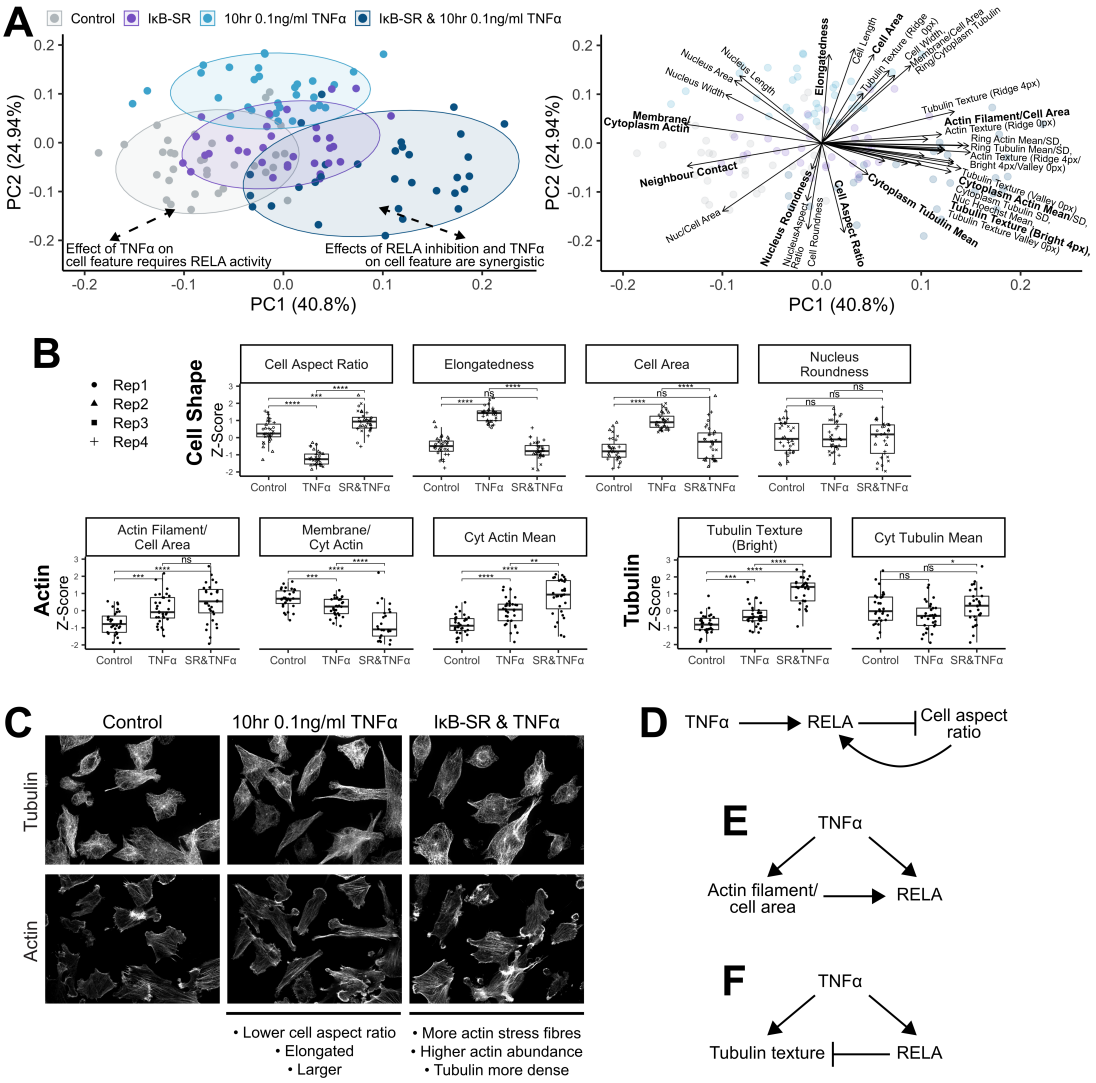
A
Control
IκB-SR
10hr 0.1ng/ml TNFα
IκB-SR & 10hr 0.1ng/ml TNFα
PC2 (24.94%)
PC1 (40.8%)
Effect of TNFα on cell feature requires RELA activity
Effects of RELA inhibition and TNFα on cell feature are synergistic
Membrane/ Cytoplasm Actin
Neighbour Contact
Nuc/Cell Area
Nucleus Roundness
Cell Aspect Ratio
Cytoplasm Tubulin Mean
Elongatedness
Cell Area
Actin Filament/Cell Area
Cytoplasm Actin Mean
Tubulin Texture (Bright 4px)
B
Rep1
Rep2
Rep3
Rep4
Cell Shape
Z-Score
Cell Aspect Ratio
Elongatedness
Cell Area
Nucleus Roundness
Actin
Actin Filament/ Cell Area
Membrane/ Cyt Actin
Cyt Actin Mean
Tubulin
Tubulin Texture (Bright)
Cyt Tubulin Mean
Control
TNFα
SR&TNFα
C
Control
10hr 0.1ng/ml TNFα
IκB-SR & TNFα
Tubulin
Actin
• Lower cell aspect ratio
• Elongated
• Larger
• More actin stress fibres
• Higher actin abundance
• Tubulin more dense
D
TNFα
RELA
Cell aspect ratio
E
TNFα
Actin filament/ cell area
RELA
F
TNFα
Tubulin texture
RELA

Figure 4.9 Effect of TNFα and RELA nuclear translocation on cell shape and the cytoskeleton

(A-C) Effect of 10 hr 0.1 ng/ml TNFα on cytoskeletal/cell shape features in MIA PaCa2 RELA-GFP cells using a doxycycline-inducible lentiviral construct expressing IκB-SR (a non-degradable form of IκB). n = four experimental repeats. (A) Principal Component Analysis (PCA) separating cells using 35 cell shape, cytoskeletal and Hoechst features under the treatment conditions. Analysed using technical replicates (wells) normalised per experimental repeat (z-scores), with each circle representing a technical replicate. Frames in the left graph represent the 90 % confidence region (probability ellipse) for each treatment. The right graph shows a biplot determined by the contribution of each feature to the two principal components. (B) Z-Scores for technical replicates per treatment (eight technical replicates per biological repeat for each treatment) for each selected cell feature, normalised per biological repeat (n = four biological repeats). Statistical annotations above boxplots show results from two-tailed t-tests with Benjamini-Hochberg correction for multiple comparisons. Statistical significance: ns (non-significant) = $p > 0.05$, * = $0 < 0.05$, ** = $p < 0.01$, *** = $p < 0.001$. **** = $p<0.0001$. (C) Representative images MIA PaCa2 RELA-GFP IκB-SR cells with control treatment, 10 hr 0.1 ng/ml TNFα, IκB-SR induction (48 hr treatment with dox), or 10 hr 0.1ng/ml TNFα with IκB-SR induction. Stained with Hoechst, phalloidin and α-tubulin antibody. (D-F) Illustrations of the interactions between TNFα and RELA localisation with either cell shape or cytoskeletal organisation. (D) TNFα inhibits cell aspect ratio (width to length) in a manner dependent on RELA nuclear translocation. Conversely, cell aspect ratio upregulates RELA nuclear translocation. (E) TNFα upregulates RELA directly and TNFα also increases actin stress fibre abundance, which further upregulates RELA. (F) TNFα upregulates RELA nuclear translocation and tubulin clustering. RELA inhibits tubulin clustering, as tubulin is most dense in the presence of TNFα with RELA inactivation.

8/9 independent features (neighbour contact excluded) were modulated by TNFα and/or RELA inhibition (Figure 4.9B and C). Cell area, elongatedness and cell aspect ratio were regulated by TNFα in a RELA dependent manner, as cell area and elongatedness both increase with TNFα treatment only in the absence of IκB-SR, while cell aspect ratio decreases with TNFα only without IκB-SR.

Overall, TNFα and RELA generally co-operate in the regulation of cell shape but are antagonistic in the regulation of cytoskeletal organisation. TNFα in combination with IκB-SR caused a significant change in cytoplasm actin mean, membrane/cytoplasm actin and bright tubulin texture, compared with IκB-SR or TNFα alone. This indicates opposing effects of TNFα and RELA nuclear translocation on these cytoskeletal features and that RELA nuclear translocation is required for basal (control) cytoskeletal organisation in the presence of high TNFα levels. Notably, Bayesian analysis had predicted a strong dependency of tubulin texture on RELA activity in MIA PaCa2 cells (Figure 4.4B), which was found to have a negative correlation in Figure 4.5C. IκB-SR analysis confirmed this negative relationship experimentally, as tubulin texture increases significantly with RELA inactivation.

Collective analysis of cytoskeletal and cell shape regulation of RELA and the opposing relationship using IκB-SR induction suggest that TNFα-mediated RELA activation is involved in complex networks with actin, tubulin and cell shape. Identified relationships include: (1) TNFα inhibits cell aspect ratio via RELA causing cell elongation, while cell aspect ratio (reduction in elongation) positively upregulates RELA nuclear translocation (Figure 4.9D); (2) TNFα upregulates RELA both directly and through upregulation of actin stress fibres (Figure 4.9E); (3) TNFα upregulation of tubulin compaction is countered by TNFα-mediated RELA activation that inhibits clustering of tubulin (Figure 4.9F).

4.2.9 Summary

To predict whether cell shape and the cytoskeleton regulate RELA dynamics in PDAC cells, I incorporated single cell measurements of RELA, actin, tubulin and cell shape into Bayesian

network modelling to identify conditional dependencies of RELA on cell features. The Bayesian networks predicted that differences in TNFα-induced RELA responses between PDAC cells are related to differences in actin organisation. To test this, I used small molecule perturbation of actin, tubulin and cell shape dynamics, which suppressed or enhanced RELA nuclear localisation in a cell line-specific manner. Finally, I assessed morphological and cytoskeletal changes in MIA PaCa2 with TNFα in the presence or absence of non-degradable IκBα, which revealed that RELA nuclear translocation required for basal (control) cytoskeletal organisation in the presence of high TNFα levels.

4.3 Discussion

4.3.1 Association between RELA nuclear translocation and actin organisation by predictive modelling

I used Bayesian modelling of five PDAC lines as an unbiased and high dimensional approach to determine whether descriptors of cell shape and the cytoskeleton correlate with RELA localisation. The Bakal lab previously used Bayesian modelling to show that RELA localisation in a panel of breast cells is strongly dependent on neighbour contact, cell area, and protrusiveness in the presence and absence of TNFα (Sero et al., 2015). In the present study, I extended the analysis to include measurements of actin and tubulin organisation and found that differences in cytoplasmic actin intensity, as well as measures of actin localisation (cortical versus cytoplasmic actin), correlated with differences in RELA ratio within and between PDAC cell lines.

4.3.2 Potential mechanisms for actin regulation of RELA

I tested the effect of modulating the cytoskeleton and cell shape, using small molecule inhibitors, on RELA subcellular localisation in PDAC cells in the presence of TNFα. Perturbing actin dynamics significantly downregulated RELA nuclear localisation in both

PDAC cell lines. However, RELA nuclear localisation was more perturbed by inhibition of formin activity in MIA PaCa2 cells and by inhibition of ARP2/3 activity in PANC1 cells, suggesting differing contributions of actin stress fibres and branching to the overall organisation of actin and subsequently cell shape in these two cell lines, in addition to different influences of the nucleation of actin branches and stress fibres on RELA nuclear translocation. Given the similar RELA ratio distributions of MIA PaCa2 with RPE1 cells, and between PANC1 with SW1990 and PANC05.04, it is predicted that these subsets of PDAC cell lines have similar regulation of RELA by actin dynamics. This analysis should be extended by treating a panel of PDAC cell lines with ARP2/3 and formin inhibitors and assaying RELA localisation. In addition, further analysis of the different ARP2/3 complex components expressed in each PDAC cell line could be carried out. Each ARP2/3 complex member has a different contribution to pancreatic cancer cell migration (Rauhala et al., 2013) and the ARP1CA subunit has elevated expression in pancreatic cancer cell lines and is associated with pancreatic cancer invasiveness (Laurila et al., 2009). Further study could look into whether ARP2/3 regulation of RELA functions in the metastatic process.

The higher impact of inhibition of actin polymerisation by cytochalasin D on RELA translocation in PANC1 cells compared to MIA PaCa2 cells also suggests that actin structures are more dynamic in PANC1 cells. As the serum response factor coactivator MAL is sequestered in the cytoplasm by monomeric actin and then released when actin is incorporated into F-actin filaments (Miralles et al., 2003), I hypothesised that actin may regulate RELA in a similar manner. However, the insufficiency of cytochalasin D to affect RELA nuclear translocation in MIA PaCa2 cells suggests that actin polymerisation alone is insufficient to regulate RELA localisation.

Furthermore, the relationship between neighbour contact, actin remodelling, and RELA translocation remains a source for further study. As I observed a negative correlation between neighbour contact and RELA, as well as several dependencies of actin features on neighbour contact predicted by Bayesian modelling, I suggest that neighbour contact may

regulate RELA by altering actin structure. For example, lamellipodia are structures formed and maintained by actin branches that assemble at the leading edge of cells and the periphery of wounds (Jacinto et al., 2001). This may represent a mechanism used by PDAC cells to sense the environment – and whether in contact with extracellular matrix or other cells – to modulate RELA activity accordingly. This could be looked into by testing the effect of actin inhibition on RELA localisation of cells with different proportions of neighbour contact. Mechanistically, one route which may be mediating the transduction of contact information is through β-catenin or p120 (δ) catenin proteins. p120 catenin regulates the stability of adherens junctions, which are cell-cell adhesions composed of cadherins and catenins as well as cytoskeletal adaptor proteins. p120 inhibits RELA activity as p120 null epidermal cells have activated nuclear RELA and p120 null mice have chronic inflammation (Perez-Moreno et al., 2006). Genetic silencing of p120 in PDAC cells could therefore provide insight into whether neighbour contact inhibits RELA via adherens junctions and actin structure.

I hypothesise that the cell signalling between actin dynamics and RELA likely involves RhoGTPases, which are central regulators of actin that have been previously linked to the NF-κB pathway (Tong and Tergaonkar, 2014). For instance, NIH-T3 cells with dominant-negative mutant CDC42 or RhoA, but not Rac-1, have significantly lower NF-κB transcriptional activity in response to TNFα compared to their wildtype counterparts (Perona et al., 1997). Conversely, NF-κB transcriptional activity was found to be dependent on Ras-related C3 botulinum toxin substrate 1 (RAC1) in lung cancer cells (Gastonguay et al., 2012). I have also shown that RELA regulation by cell shape and neighbour contact is regulated in breast cells by RhoA (Sero et al., 2015), a RhoGTPase involved in actin stress fibre regulation (Nobes and Hall, 1995). Moreover, RhoA is inhibited in vitro and in vivo by p120-catenin (Anastasiadis et al., 2000). It would therefore be interesting to determine whether RhoA plays a role in regulating RELA and also screen for other RhoGTPases regulating actin nucleation and branching and RELA translocation in PDAC.

Potential mechanisms for actin regulation of RELA may also be hypothesised from research on the mechanosensitive transcriptional regulator YAP. For example, YAP nuclear translocation is upregulated when forces are applied to ECM adhesions, which leads to nuclear flattening and stretching of nuclear pores via the actin cytoskeleton (Elosegui-Artola et al., 2017). Actin remodelling may therefore affect RELA localisation by reshaping nuclear pores, which could impact RELA nuclear import or export.

4.3.3 Cell spreading can promote and suppress RELA nuclear translocation

I identified opposing relationships between cell spreading and RELA nuclear translocation in PDAC cells depending on the mechanism in which cell spreading is induced. Chemically induced spreading using the ROCK inhibitor H1552 or the myosin inhibitor Blebbistatin increased nuclear RELA localisation, indicating a positive relationship between RELA nuclear translocation and spreading. Conversely, RELA localisation becomes more cytoplasmic as PDAC cells spread following matrix attachment (Figure 4.8), indicating a negative correlation between RELA nuclear translocation and cell spreading. The relationship between RELA activation and spreading may depend on whether spreading is a temporary and transitory state, which I observed in the present study through live imaging or a long-term state due to chemical inactivation. The state of spreading in individual PDAC cells in basal conditions could be a temporary or permanent state, which would need further study.

I predict that spreading does not directly alter RELA localisation but acts through another factor such as mechanical tension or actomyosin contractility. This hypothesis is supported by a study in 3T3 fibroblasts considering the effects of cell shape and mechanical tension on RELA localisation using micropatterns to stabilise cells into a rectangular or circular shape (Mitra et al., 2017). Cells in the circular morphology, which were classified as relaxed and less spread with low contractility, showed higher nuclear localisation of RELA and a higher fold-change in RELA localisation following 30 min TNFα than cells with rectangular

morphology, which were described as stretched and well-spread with a high degree of myosin contractility. Conversely, the spread rectangular cells had higher RELA nuclear localisation after 60 min TNFα compared to the relaxed circular cells. Mitre et al's (2017) findings support the proposition that relaxed cells are more responsive in RELA nuclear translocation with shorter TNFα treatment, but stretched cells can retain RELA nuclear localisation for longer periods.

4.3.4 Feedback loops between RELA activation and cytoskeletal remodelling

These data collectively suggest that there are feedback loops between inflammation, RELA activation and the cytoskeleton in PDAC. For example, I have shown that the effect of TNFα treatment on nuclear localisation of RELA is dependent on actin abundance, which is itself enhanced by TNFα and RELA inhibition. Moreover, relationships between RELA localisation and cytoskeletal or cell shape features can be enhanced (e.g. cytoplasm tubulin mean) or suppressed (e.g. nucleus roundness) with TNFα treatment (Figure 4.3B). I also identified that TNFα can alter cell shape in a RELA-dependent manner, but that RELA activation typically enforces normal cytoskeletal dynamics by countering the effects of TNFα (Figure 4.9). In particular, I found that acute (1 hr) and sustained (10 hr) TNFα treatment increased cytoplasmic actin intensity in MIA PaCa2 cells that was enhanced with RELA inactivation, which contrasts findings that acute TNFα treatment (up to 20 min) decreased actin intensity in 3T3 fibroblasts (Mitra et al., 2017). Moreover, TNFα promoted elongatedness in a RELA-dependent manner. The effects of TNFα and RELA on both actin and cell elongation suggest that RELA may inhibit RhoA, ROCK or MLC in PDAC cells, which also counters a previous report that NF-κB signalling supports myosin II activity in amoeboid melanoma cells (Georgouli et al., 2019).

4.3.5 Modulating RELA activity therapeutically through actin inhibition

Targeting RELA nuclear translocation is an attractive therapeutic strategy, as RELA activity may promote a high-inflammatory PDAC tumour microenvironment through regulation of cytokine production (Ling et al., 2012; Steele et al., 2013), in addition to regulating cell processes that underlie PDAC oncogenesis (Melisi et al., 2009) and therapeutic resistance (Arlt et al., 2003). My data suggest that RELA activation may be fine-tuned in PDAC by targeting both the cytoskeleton and inflammation. For instance, anti-TNFα therapy previously determined ineffective in advanced pancreatic patients (Wu et al., 2013) may be effective when combined with therapy targeting the cytoskeleton. Moreover, tissue specific and patient specific actin or tubulin dynamics may present a therapeutic opportunity.

Although compounds directly targeting actin are toxic and unusable in the clinic, there is potential to target actin-regulating proteins (Bryce et al., 2019). The ability to target actin in cancer cells selectively may be enabled by tissue specificity and isoform diversity of ARP2/3 complex components (Abella et al., 2016; Jay et al., 2000), upregulation of the Tpm3.1 isoform of the actin-binding protein Tropomyosin in cancer cells (Stehn et al., 2013), or tumour-specific upregulation of the prosurvival kinase protein kinase C-ε which accumulates at actin bundles (Foerster et al., 2014).

Chapter 5: Multiomics identification of interactors and effectors of TNFα-mediated RELA nuclear translocation in PDAC cells

5.1 Introduction

5.1.1 RELA is a pleiotropic transcription factor

RELA responds to a myriad of environmental stresses, including inflammation (Osborn et al., 1989), oxidative stress (Zhou et al., 2001), and mechanical stress (Sero et al., 2015). Moreover, RELA has hundreds of transcriptional targets and can regulate diverse processes, including inflammation (Collart et al., 1990; Hiscott et al., 1993), cell survival (Antwerp et al., 1996; Barkett and Gilmore, 1999), cell proliferation (Hinata et al., 2003), and EMT (Zhou et al., 2004). In addition to responding to a variety of upstream inputs, RELA signalling is 'pleiotropic', meaning that pathway activation produces many distinct outputs. The pleiotropic nature of RELA requires specificity in the transcriptional target expression that is induced by RELA so that the appropriate stress response is initiated according to the context.

5.1.2 Cells with different RELA dynamics have distinct transcriptional output

The transcriptional specificity of RELA is controlled at multiple levels. These include post-translational modifications to RELA (Zhong et al., 1997, 1998), interaction with different co-transcriptional activators and repressors (Berghe et al., 1999; Ashburner et al., 2001), and interaction with other transcription factors (Webster and Perkins, 1999; Tong et al., 2016). Critically, a further layer of specificity in RELA output is believed to be encoded by RELA translocation dynamics. Cells with different RELA dynamics have distinct transcriptional output. An early demonstration of this was a live imaging study that

manipulated RELA dynamics by exposing SK-N-AS neuroblastoma cells to a single TNFα pulse, repeated TNFα pulses, or chronic TNFα stimulation (Ashall et al., 2009). The different TNFα treatments induced distinct live RELA translocation dynamics, in particular differences in the amplitude of RELA nuclear localisation. These distinct dynamics were also linked to different RELA target gene expression, quantified by RT-PCR. More recently, live imaging coupled with single cell RNA-seq of the same cells confirmed that cells with different profiles of RELA translocation dynamics, induced by the bacterial membrane component LPS, have distinct target gene expression patterns (Lane et al., 2017). Therefore, even a single stimulus type (e.g. TNFα or LPS) can result in single cell heterogeneity in RELA activation and target gene expression.

5.1.3 Target gene specificity of different NF-κB stimuli

Independent NF-κB pathway stimuli also have functionally discrete gene expression. Pathogen associated molecular pattern (PAMP) molecules are microbial molecules that are detected by pattern recognition receptors (PRRs) (Medzhitov and Janeway, 1997). LPS is an example of a PAMP that is a ligand for Toll-like receptor (TLR) 4, within the TLR family of PRRs (Shimazu et al., 1999). Although LPS and the cytokine TNFα both induce RELA activation by IKK activity and IκBα degradation, LPS and TNFα induce distinct transcriptional programs that are linked to different IKK activity profiles. Werner et al. showed that LPS induced IKK activity is delayed compared to TNFα induced IKK activity while controlling for IKK abundance (Werner et al., 2005). Gene microarrays showed that genes with a high fold-change highly overlapped between LPS and TNFα at 1 hr after stimulation, with only 38 % of genes being stimulus-specific, while 79 % of genes were stimulus-specific at 8 hours post-stimulation.

Ligand-specific RelA dynamics and gene activation were also reported in mouse cells exposed to a panel of TLR family ligands, using both an immune cell type (RAW264.7 mouse macrophages) and a non-immune cell type (NIH3T3 mouse fibroblasts) (Martin et al.,

2020). Ligand and cell-specific correlations between features of RelA dynamics and nascent-level gene expression were identified, with over half of induced genes linked to RelA dynamics. Notably, nascent gene expression strongly correlated with the duration of RELA nuclear occupancy.

5.1.4 Temporal patterns of RELA target gene expression

Studies have shown that transcripts upregulated by RELA fall into discrete categories based on the timing of mRNA expression. Tian et al. used microarray analysis in HeLa cells assayed at 1 hr, 3 hr or 6 hr stimulation with 25 ng/ml TNFα (Tian et al., 2005). To narrow down genes likely to depend on RELA, they used the Tet-On system for dox-repression of IκB-SR (non-degradable IκBα) and followed-up genes differentially expressed between the presence and absence of dox. Focusing on 74 genes with a 3-fold change at any timepoint between TNFα with dox and TNFα alone, they confirmed targets using ChIP and identified 'early', 'middle' and 'late' response groups based on their peak expression relative to the time of TNFα stimulation. Notably, the different groups corresponded with distinct biological functions. The 'early' genes, which had peak expression 1 hr after TNFα addition, included cytokines (*IL6* and *IL8*) and *TNFAIP3* (encoding the protein TNFAIP3 also known as A20): a deubiquitinating enzyme previously shown to inhibit NF-κB activation (Song et al., 1996). Tian et al. found that late genes, which peaked 6 hr after TNFα addition, included those encoding cell surface receptors, adhesion molecules and signal adaptors. In addition, there were a small proportion of genes with biphasic expression and another group with higher induction with RELA inhibition (Tian et al., 2005).

Further studies have shown that transcripts with different temporal regulation require different minimum TNFα concentrations and associated RELA translocation dynamics. Tay et al. (2010) carried out live imaging using 3T3 mouse fibroblasts with a range of TNFα doses from 0.01-10 ng/ml and showed that higher TNFα doses induce more persistent oscillations and faster RELA activation. Subsequent analysis of 23 RELA target genes by

qPCR also identified ‘early’, ’intermediate’ and ‘late’ genes. In this case, ‘early’ genes also included the negative feedback gene A20 as well as *NFKBIA*, the gene encoding IκBα - a RELA target known to be induced rapidly after RELA activation (discussed further in section 5.1.5). Interestingly, Tay et al. found that early genes are induced by all TNFα doses and only require a short burst of RELA localisation for expression, even at the lowest doses. Meanwhile, ‘late’ genes encoded several proteins involved in cell death, including *Ccl2*, *Trail*, *Casp4*, and *Ripk2*. ‘Late’ genes were only induced at high TNFα doses and expression increased with persistent RELA oscillations, suggesting that these genes require constant TNFα stimulation.

Therefore, on the system level, temporally distinct gene expression allows RELA to upregulate different processes based on the persistence and intensity of the cell stress. However, whether genes can also be categorised into temporal clusters when there is a lack of oscillations and sustained RELA activation is not known. I have identified that endogenous RELA does not oscillate in PDAC cells, and this provides a useful system to understand the contribution of oscillations to temporal patterns of RELA target gene expression.

5.1.5 Negative feedback by IκB proteins

In 1993, several studies concurrently published pivotal work demonstrating that RELA functions in an autoregulatory negative feedback loop with IκB proteins (Brown et al., 1993; Scott et al., 1993; Sun et al., 1993). These studies showed that TNFα-mediated IκBα degradation and NF-κB activation is followed by an increase in IκBα mRNA and IκBα protein synthesis, which is in turn followed by NF-κB inhibition by IκBα. Meanwhile, in vivo experiments highlighted the importance of the IκBα member of the IκB protein family as a potent suppressor of NF-κB activation, since IκBα deficient mice die within 7-8 days after birth, with abnormal haematopoiesis and constitutive RELA activation (Beg et al., 1995b). Conversely, IκBε knockout mice are healthy, fertile, and without constitutive RELA activation (Mémet et al., 1999).

In vitro time course studies pioneered by Alexander Hoffmann shed light on how different IκB proteins coordinate to produce the final NF-κB activation pattern (Hoffmann et al., 2002). These experiments used mice engineered for deletion of IκBα, β or ε, and assayed NF-κB activity using electrophoretic mobility shift assays (EMSA) following TNFα stimulation. Cells which have WT IκBα with combined IκBβ and IκBε deletion were highly oscillatory. In contrast, cells with IκBα deletion in combination with IκBε or IκBβ deletion have continually increasing RELA activity that plateaus at high activity compared to basal levels. Hoffman et al. used computational modelling to show that IκBα mediates strong negative feedback with NF-κB, resulting in rapid inactivation following RELA activation and an oscillatory NF-κB activation profile. IκBβ and IκBε respond more slowly to NF-κB activation and act to damp the long-term oscillations of the NF-κB response, as well as stabilise NF-κB activation during chronic stimulation. A follow-up study, also using computational modelling and EMSA for experimental validation, elucidated that IκBε expression is out of phase and delayed compared to IκBα (Kearns et al., 2006). Therefore, IκBε is believed to function in fine tuning RELA oscillations. Moreover, while only IκBα is necessary for complete repression of RELA activity following transient (15 min) TNFα stimulation, both IκBα and IκBε are involved in mediating termination of RELA activity, as IκBα-/- IκBε-/- double knockout cells have more sustained RELA activity compared to IκB-/- alone. Given that I observed sustained RELA activity and a lack of oscillations in PDAC cells (Chapter 3), I hypothesise that negative feedback by IκB proteins is misregulated in PDAC cells.

In this chapter, I use a systems biology approach combining RNA-seq and Co-IP with protein mass spectrometry to identify the target genes and interactors of RELA in PDAC cells, then assess how their expression changes temporally and with TNFα dose. I also explore how the TNFα signalling pathway is configured in MIA PaCa2 and PANC1 cells, given the sustained TNFα-induced RELA nuclear translocation characterised in Chapter 3.

5.2 Results

5.2.1 TNFα-regulated genes cluster by TNFα dose and RELA dependence

To identify genes regulated by TNFα at early (1 hr) versus late (5 hr) timepoints in PDAC cells, RNA-seq analysis was carried out at these times using MIA PaCa2 and PANC1 cells treated with 0.01, 0.1 or 10 ng/ml TNFα. TNFα treatments were in the presence or absence of dox-induction of IκB super repressor (IκB-SR) to determine which genes require RELA nuclear translocation. 236 genes were differentially expressed in high TNFα (0.1 or 10 ng/ml) versus basal conditions, with the majority of genes (186) upregulated by TNFα (Figure 5.1A and B). To identify patterns of gene expression, the 236 genes were organised by hierarchical clustering into seven clusters, each with distinct dynamics or dependence on RELA (Figure 5.1C and D; list of genes and clusters in Appendix Table A1).

Figure 5.1

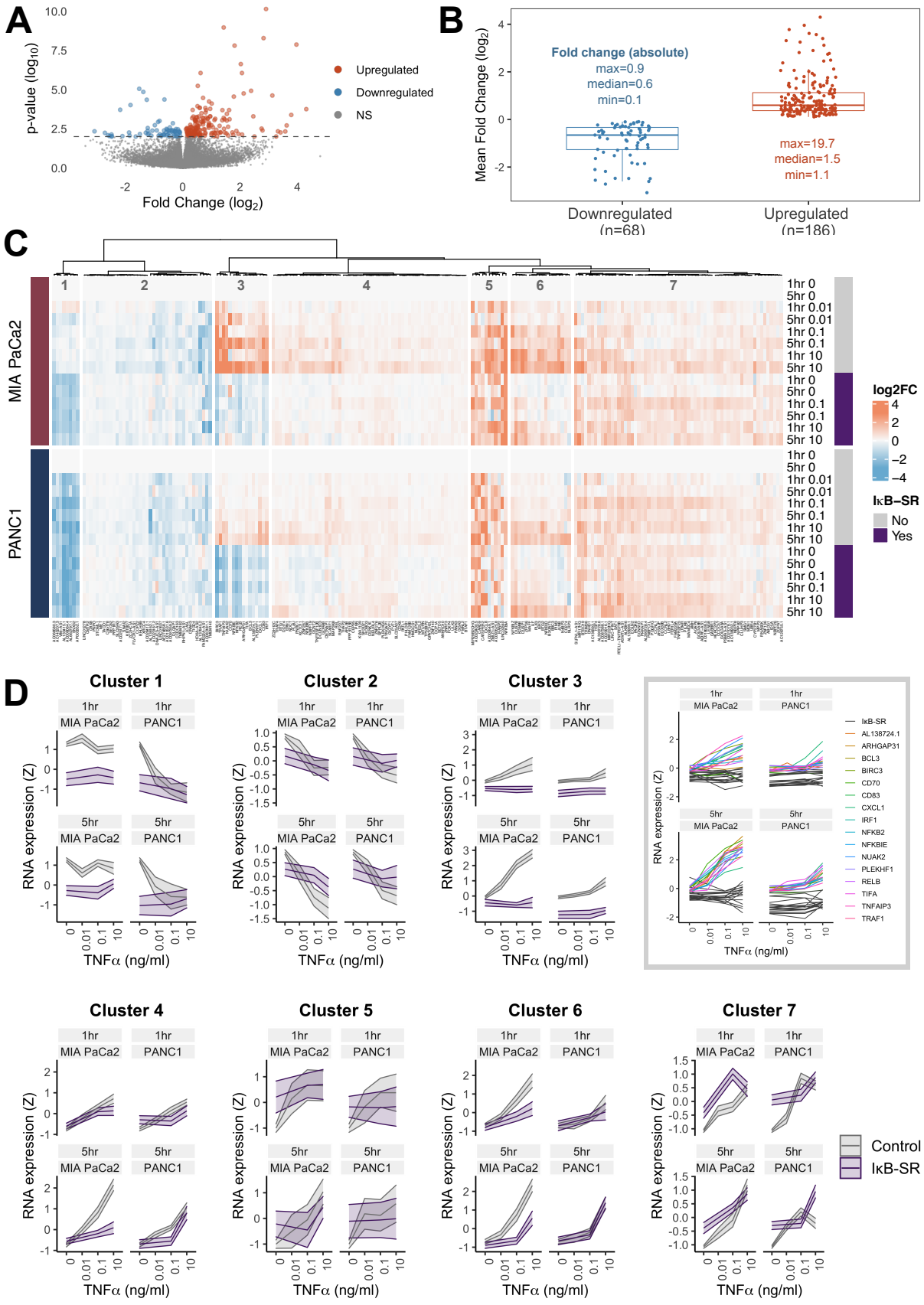
A
p-value (log10)
Fold Change (log2)
Upregulated
Downregulated
NS
B
Mean Fold Change (log2)
Fold change (absolute)
max=0.9
median=0.6
min=0.1
max=19.7
median=1.5
min=1.1
Downregulated (n=68)
Upregulated (n=186)
C
MIA PaCa2
PANC1
log2FC
IκB–SR
No
Yes
D
Cluster 1
Cluster 2
Cluster 3
Cluster 4
Cluster 5
Cluster 6
Cluster 7
RNA expression (Z)
TNFα (ng/ml)
Control
IκB-SR

Figure 5.1 Genes regulated by TNFα and RELA in human PDAC cells

(A) Volcano plot of p-value against mean fold-change (log_2) per gene comparing RNA expression with high TNFα (0.1 ng/ml or 10 ng/ml) to control conditions (no TNFα) across MIA PaCa2 and PANC1 cells. Counts were normalised and log_2 fold-changes were calculated using DESeq2. (B) Mean fold-change (log_2) across in MIA PaCa2 and PANC1 cells for genes significantly downregulated (n = 68) or upregulated (n = 186) by TNFα ($p < 0.01$) from (A). Also displayed are the maximum, median and minimum absolute fold changes for downregulated and upregulated genes. (C) Clustered heatmap of TNFα regulated genes. Normalised counts from DESeq2 were log_2 transformed and relative to the respective control (no TNFα or IκB-SR) per timepoint (1 hr or 5 hr) and cell line (MIA PaCa2 or PANC1), then z-scored across all samples independent per gene. Columns are annotated by gene and rows are annotated by cell line, TNFα dose and time, and presence of IκB-SR. (D) Z-scores for all genes per cluster, faceted by cell line and treatment time (1 hr or 5 hr). Ribbons show the 95 % confidence interval and the middle line depicts the mean. Colour corresponds to presence of IκB-SR. Individual data for Cluster 3 are shown, coloured by gene for control (no IκB-SR) data and grey for all data with IκB-SR (all genes).

Cluster 3 shows genes with clear dependence on RELA activation in both MIA PaCa2 and PANC1 cells (Figure 5.1C and D). Moreover, Cluster 3 has genes significantly upregulated by TNFα in a dose-dependent manner and these genes are more highly upregulated by TNFα in MIA PaCa2 compared to PANC1 cells. This is consistent with the RELA dynamics observed by live imaging whereby 0.1 ng/ml is sufficient to dramatically increase RELA nuclear localisation in MIA PaCa2 cells while 10 ng/ml TNFα is required for PANC1. Cluster 3 genes also have higher RELA expression at 5 hr TNFα compared to 1 hr TNFα in both cell lines, indicating that they are associated with prolonged RELA activation. As expected from the RELA and TNFα dose dependent properties of this cluster, known RELA targets such as *RELB*, *NFKB2* and *BIRC3* are present (Lombardi et al., 1995; Bren et al., 2001; Frasor et al., 2009). Cluster 3 also has the immune ligands CD70 and CD83. Interestingly, Cluster 3 contains Rho GTPase activating protein 31 (*ARHGAP31*) and NUAK family kinase 2 (*NUAK2*), which are involved in the regulation of actin (Tcherkezian et al., 2006; Vallenius et al., 2011).

Two clusters of TNFα-regulated genes in PDAC cells are downregulated by TNFα (Figure 5.1C and D) in a dose-independent manner: Cluster 1 and Cluster 2. Cluster 1 consists of long non-coding RNAs (lncRNAs) and are further downregulated by IκB-SR in the MIA PaCa2 cell line only. Cluster 2 (Figure 5.1C and D) genes are entirely independent of RELA.

The remaining clusters (Figure 5.1C and D) contain genes upregulated by TNFα. Cluster 4 genes are similar to Cluster 3 in that their expression is higher at 5 hr versus 1 hr, but Cluster 4 genes have more moderate upregulation by TNFα. Moreover, Cluster 4 genes appear only to be RELA-dependent with 5 hr TNFα (Figure 5.1D Cluster 4). Clusters 5 and 7 (Figure 5.1C and D) are upregulated by TNFα in a dose independent manner. Finally, genes in Cluster 6 (Figure 5.1C and D) are dose dependent but time-independent TNFα treatment.

Notably, 20 % (46/236) of genes regulated by TNFα are in the TNFα or NF-κB signalling pathways according to the GSEA gene sets (Subramanian et al., 2005) and 24 % (11/46) of

these are strongly TNFα dose and RELA dependent (Cluster 3), while all are upregulated by TNFα (Clusters 3-7). This suggests that TNFα and RELA may stimulate positive feedback in PDAC cells that contribute to sustained RELA nuclear translocation.

5.2.2 TNFα upregulates *NFKBIB* and *NFKBIE* in a RELA dependent manner in PDAC cells

As the gene encoding IκBα (*NFKBIA*) is upregulated by RELA (Brown et al., 1993; Scott et al., 1993; Sun et al., 1993), negative feedback with IκBα is believed to lead to the oscillatory RELA dynamics in other cell types responding to TNFα (Hoffmann et al., 2002). Since RELA oscillations are absent in PDAC cells, I hypothesised that negative feedback with IκBα may be perturbed in PDAC cells. Indeed, The Human Protein Atlas reports that pancreatic tissue has among the lowest *NFKBIA* RNA expression of human tissues (Figure 5.2A).

Figure 5.2

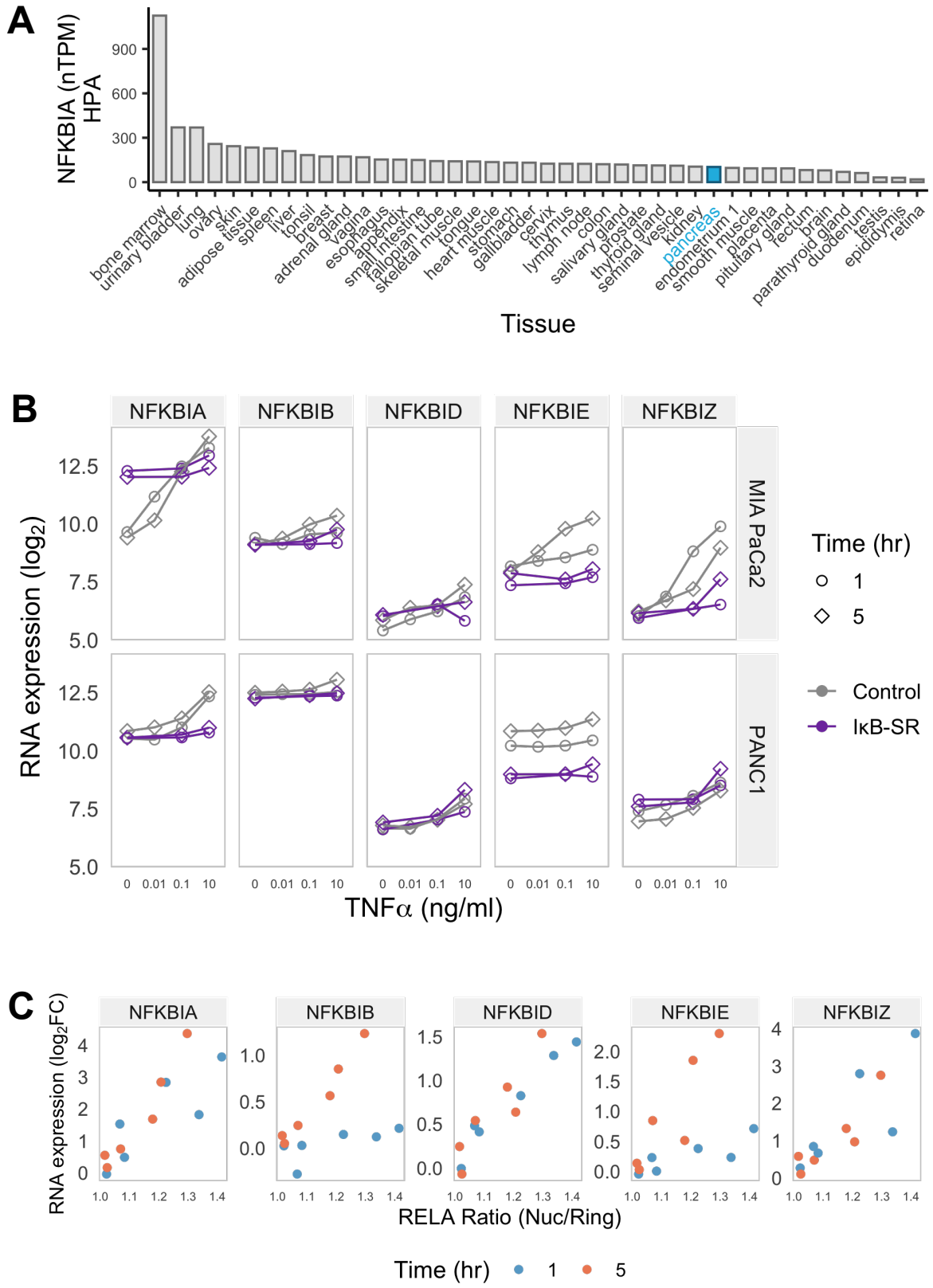
A
NFKBIA (nTPM)
HPA
900
600
300
0
bone marrow
urinary bladder
lung
ovary
skin
adipose tissue
spleen
liver
tonsil
breast
adrenal gland
vagina
esophagus
appendix
small intestine
fallopian tube
skeletal muscle
heart muscle
tongue
stomach
gallbladder
cervix
thymus
lymph node
colon
salivary gland
prostate
thyroid gland
seminal vesicle
kidney
pancreas
endometrium 1
smooth muscle
pituitary gland
placenta
rectum
brain
parathyroid gland
duodenum
testis
epididymis
retina
Tissue
B
NFKBIA
NFKBIB
NFKBID
NFKBIE
NFKBIZ
MIA PaCa2
PANC1
RNA expression (log2)
12.5
10.0
7.5
5.0
0
0.01
0.1
10
TNFα (ng/ml)
Time (hr)
1
5
Control
IκB-SR
C
NFKBIA
NFKBIB
NFKBID
NFKBIE
NFKBIZ
RNA expression (log2FC)
RELA Ratio (Nuc/Ring)
Time (hr)
1
5

Figure 5.2 Expression of genes encoding IκB proteins in PDAC cells

(A) RNA expression (normalised - nTPM) from the Human Protein Atlas (Consensus dataset) (Karlsson et al., 2021). (B) RNA-seq expression of IκB protein-encoding genes in MIA PaCa2 and PANC1 cells treated with TNFα for 1 or 5 hr, in the presence of IκB-SR or a DMSO control. Normalised counts were generated by DESeq2 and $\log_2$ transformed. (C) RNA expression calculated as the fold-change to the respective control (no TNFα) per timepoint (1 hr or 5 hr) and cell line (MIA PaCa2 or PANC1), against corresponding RELA ratio (nuc/ring region RELA-GFP intensity) mean measurements from timelapse imaging, matched by TNFα dose, cell line, and treatment time. All treatments are in the absence of IκB-SR expression.

RNA-seq in MIA PaCa2 and PANC1 cells revealed that TNFα upregulates several IκB protein-encoding genes: *NFKBIA* (Cluster 5), *NFKBIB* (Cluster 4), *NFKBIE* (Cluster 3), *NFKBID* (Cluster 6) and *NFKBIZ* (Cluster 6) (Figure 5.2B). Of these, *NFKBIA* has the highest absolute RNA expression in MIA PaCa2 cells and *NFKBIB* has the highest abundance in PANC1 cells, while *NFKBID* and *NFKBIZ* have the lowest RNA expression in both cell lines. The categorisation of the IκB-encoding genes into different clusters (from Figure 5.1C) reveals that they each have distinct dynamics in PDAC cells. *NFKBIE* and, to a lesser extent, *NFKBIB* are upregulated by TNFα in a dose-dependent manner and are highly dependent on RELA nuclear translocation. *NFKBID* and *NFKBIZ* expression also increase with TNFα dose but are only RELA dependent in MIA PaCa2 cells.

NFKBIA encodes IκBα, the core repressor of RELA nuclear translocation (Baeuerle and Baltimore, 1988b), and *NFKBIA* expression is strongly induced by increasing TNFα doses and is more responsive in MIA PaCa2 cells compared to PANC1. While the dependence of *NFKBIA* expression on TNFα dose is clear, the interpretation of the RELA dependence of *NFKBIA* is made more complicated by the expression of the IκB-SR transgene, which encodes murine *Nfkbia.* Mouse *Nfkbia* has an approximately 90 % sequence conservation with human *NFKBIA* (Ensembl), which means it is possible that expression of IκB-SR itself, which contains an *NFKBIA* sequence, is being detected in the transcript levels. If this is the case, IκB-SR appears to be more highly expressed following dox-induction in MIA PaCa2 than PANC1 cells.

Setting aside these potential artifacts of transgene expression, it appears that suppressing RELA expression in MIA PaCa2 cells paradoxically induces strong *NFKBIA* expression that is unaffected by increasing doses of TNFα. In contrast, in PANC1 cells, *NFKBIA* RNA expression alters more conventionally with TNFα (increases) or RELA inactivation (no change).

When comparing RELA expression of IκB-encoding genes to RELA nuclear localisation based on live imaging for the corresponding TNFα dose and duration, upregulation of all transcript levels was proportional to RELA nuclear localisation (Figure 5.2C). *NFKBIA*, *NFKBID* and *NFKBIZ* fit the profile of 'early' genes as they are highly expressed from 1 hr TNFα treatment and do not significantly differ in expression depending on TNFα duration. *NFKBIB* and *NFKBIE* show a clear distinction in RNA expression between 1 hr and 5 hr TNFα treatment and therefore class as 'late' genes associated with sustained RELA activation.

5.2.3 TNFα regulates the transcription of efficiently translated genes involved in the TNFα pathway

To determine how well TNFα and RELA-regulated changes in the transcriptome translate to proteomic changes, protein mass spectrometry was carried out in MIA PaCa2 and PANC1 samples matched to the RNA-seq data. Of the 236 RNA transcripts significantly regulated by TNFα, 79 genes were sufficiently detected by mass spectrometry and analysed further. Genes varied in their 'translation efficiency', with the majority of genes having a positive correlation between RNA and protein expression (Figure 5.3A).

Figure 5.3

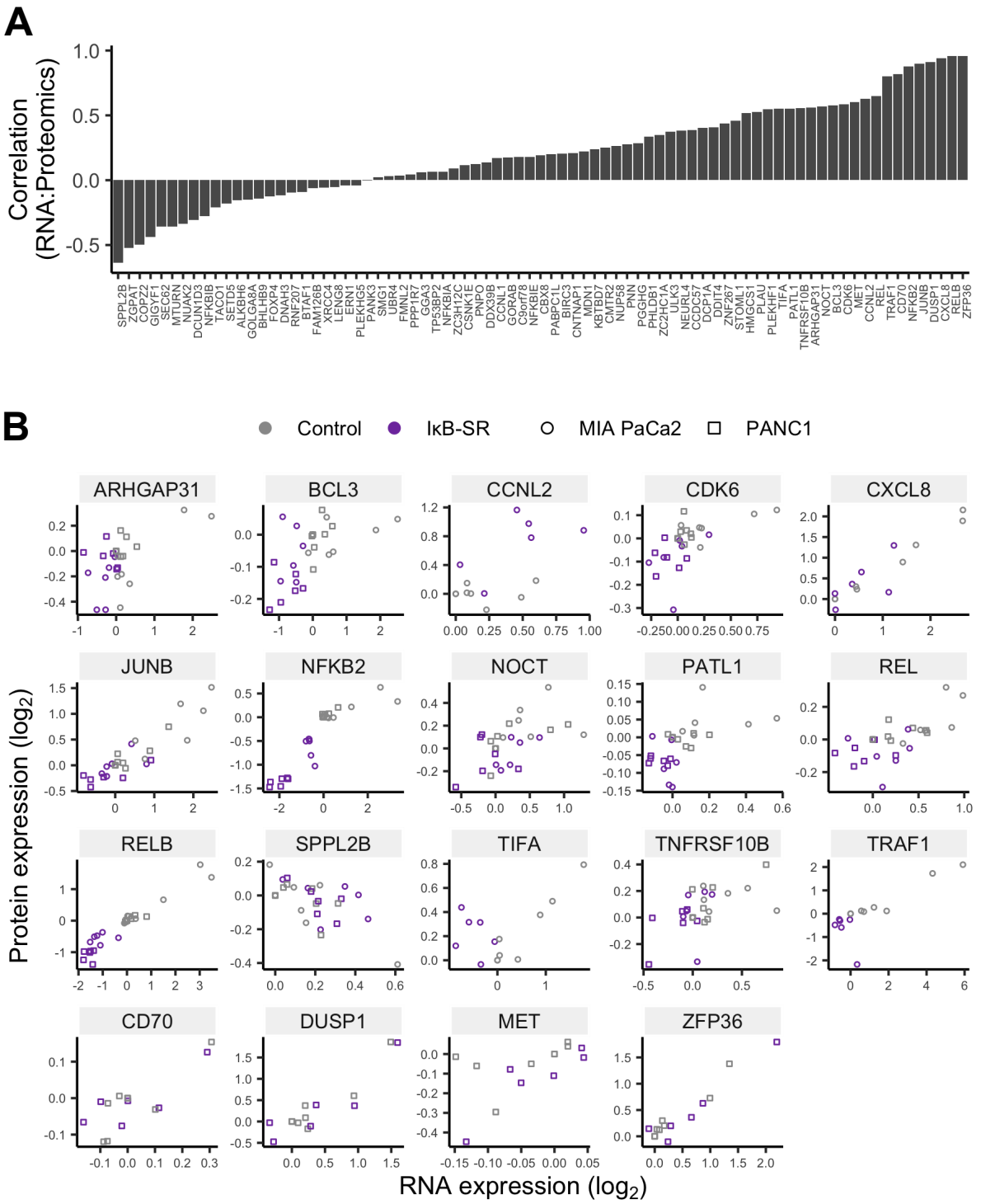
A
Correlation (RNA:Proteomics)
1.0
0.5
0.0
-0.5
SPPL2B ZGPAT COPZ2 GIGYF1 SEC62 MTURN NUAK2 DCUN1D3 NFKBIB TACO1 SETD5 ALKBH6 GOLGA8A BHLHB9 FOXP4 DNAH3 RNF207 BTAF1 FAM126B XRCC4 LENG8 ERN1 PLEKHG5 PANK3 SMG1 UBR4 FMNL2 PPP1R7 GGA3 TPST2 NFKBIA ZC3H12C CSNK1E PNPO DDX39B CCNL1 GORAB C9orf78 NFKBIE CBX8 PABPC1L BIRC3 CNTNAP1 MDN1 KBTBD7 CMTR2 NUP58 PNN PGGHG PHLDB1 ZC2HC1A ULK3 NEURL4 CCDC57 DCP1A DDIT4 ZNF267 STOML1 HMGCS1 PLAU PLEKHF1 TIFA PATL1 TNFRSF10B ARHGAP31 NOCT BCL3 CDK6 MET CCNL2 REL TRAF1 CD70 NFKB2 JUNB DUSP1 CXCL8 RELB ZFP36
B
Control
IκB-SR
MIA PaCa2
PANC1
ARHGAP31
BCL3
CCNL2
CDK6
CXCL8
JUNB
NFKB2
NOCT
PATL1
REL
RELB
SPPL2B
TIFA
TNFRSF10B
TRAF1
CD70
DUSP1
MET
ZFP36
Protein expression (log2)
RNA expression (log2)

Figure 5.3 Translation efficiency of TNFα-regulated genes in PDAC cells

(A) Pearson's correlation coefficients for TNFα regulated genes (from Figure 5.1B or C with low MS detection omitted) for proteomics abundance (MS) against RNA expression (RNA-seq) across samples from MIA PaCa2 and PANC1 cells with dox-inducible IκB-SR +/- TNFα (0.01, 0.1 or 10 ng/ml). Data is $\log_2$ transformed and calculated as the fold-change to the respective control (no TNFα or IκB-SR) per timepoint (1 hr or 5 hr) and cell line (MIA PaCa2 or PANC1). (B) Proteomics and RNA expression ($\log_2$ fold-change to control) for genes in (A) with an absolute Pearson's correlation coefficient > 0.55.

The detected IκB genes *NFKBIA* (r = 0.06), *NFKBIB* (r = -0.28), *NFKBIE* (r = 0.18) have low correlations to their protein abundance. This is expected as these proteins rapidly degrade following TNFα-induced phosphorylation of IκB proteins by the IKK complex (Chen et al., 1995; Shirane et al., 1999).

Genes with high translation efficiency (|Pearson's correlation| > 0.55) are in Figure 5.3B. Several of these are in the TNFα signalling pathway: the canonical NF-κB factors RELB (r = 0.96) and NFKB2 (r = 0.88), the TNFα receptor signalling adaptor TRAF1 (r = 0.80), the chemokine CXCL8 (IL-8; r = 0.94), and the transcription factor JUNB (r = 0.90). TRAF1 and CXCL8 are involved in the activation of the canonical NF-κB signalling pathway (Manna and Ramesh, 2005). Other TNFα-activated genes with highly correlated RNA to protein expression include CD70 (r = 0.82), which is the ligand for the T cell co-stimulatory molecule CD27 (Tesselaar et al., 2003); the ZFP36 Ring Finger Protein (r = 0.96); and Dual Specificity Phosphatase 1 (DUSP1; r = 0.91), which dephosphorylates MAP kinases (Shah et al., 2014). ZFP36 suppresses TNFα production by promoting *TNF* mRNA decay (Carballo et al., 1998), while DUSP1 reportedly counteracts ZFP36 in the regulation of TNFα (Shah et al., 2016). The gene with the strongest negative correlation with protein abundance is Signal Peptide Peptidase Like 2B (SPPL2B ; r = -0.63), which is known to cleave TNFα to release the intracellular domain (Friedmann et al., 2006). The negative correlation between *SPPL2B* RNA and protein expression suggests that the protein is degraded by TNFα. Overall, TNFα induces the transcription of several genes in PDAC cells that translate into proteins functioning in both limiting or enhancing TNFα signalling.

5.2.4 TNFα-regulated transcripts in PDAC cells encode proteins that physically or functionally interact with RELA

To look for TNFα-mediated RELA regulated genes that may in turn regulate RELA activity, I pulled down proteins binding to RELA using GFP-Trap (Co-IP) in MIA PaCa2 cells expressing endogenously tagged RELA-GFP (Figure 5.4A) treated with TNFα at 0, 0.01, 0.1

or 10 ng/ml for 1 hr. 60 proteins were pulled down consistently across treatments. 53/60 proteins pulled down by GFP-Trap have confirmed interactions with RELA, while seven novel RELA-interacting proteins were identified: FHL2, GREB1, RAB11B, RAB3GAP2, RRBP1, SPTCL, TUBB3. Interestingly, GFP-Trap pulled down a number of mitochondria-associated proteins irrespective of TNFα dose: TIMMDC1, TOMM40, TIMM23B, NDUFA4, TUFM, and three members of the SLC25 family (for full protein names see Abbreviations list). These may be related to RELA's role in regulating cell death.

5/60 proteins from the pull-down have significantly different binding to RELA (t-test $p < 0.1$) in high (0.1 and 10 ng/ml) versus low (0 and 0.01 ng/ml) TNFα conditions (Figure 5.4B). Eukaryotic translation initiation factor 3 subunit B (EIF3B) and Prolyl 4-Hydroxylase Subunit α1 (P4HA1) increase binding to RELA at higher TNFα doses, while IκBα (*NFKBIA*), IκBβ (*NFKBIB*), IκBε (*NFKBIE*) and the cytochrome C oxidase subunit NDUFA4 have reduced binding to RELA with TNFα in MIA PaCa2 cells.

To identify whether TNFα-regulated genes interact with RELA, I assessed which of the proteins encoded by TNFα-regulated genes are directly pulled down by GFP-Trap (blue ellipse in Figure 5.4C and grey/purple nodes in Figure 5.5), or interacts with RELA indirectly by physically or functionally interacting with a protein pulled down by GFP-Trap (referred to as 'secondary interactors'), as assessed by STRING analysis (green ellipse in Figure 5.4C and orange nodes in Figure 5.5).

Figure 5.4

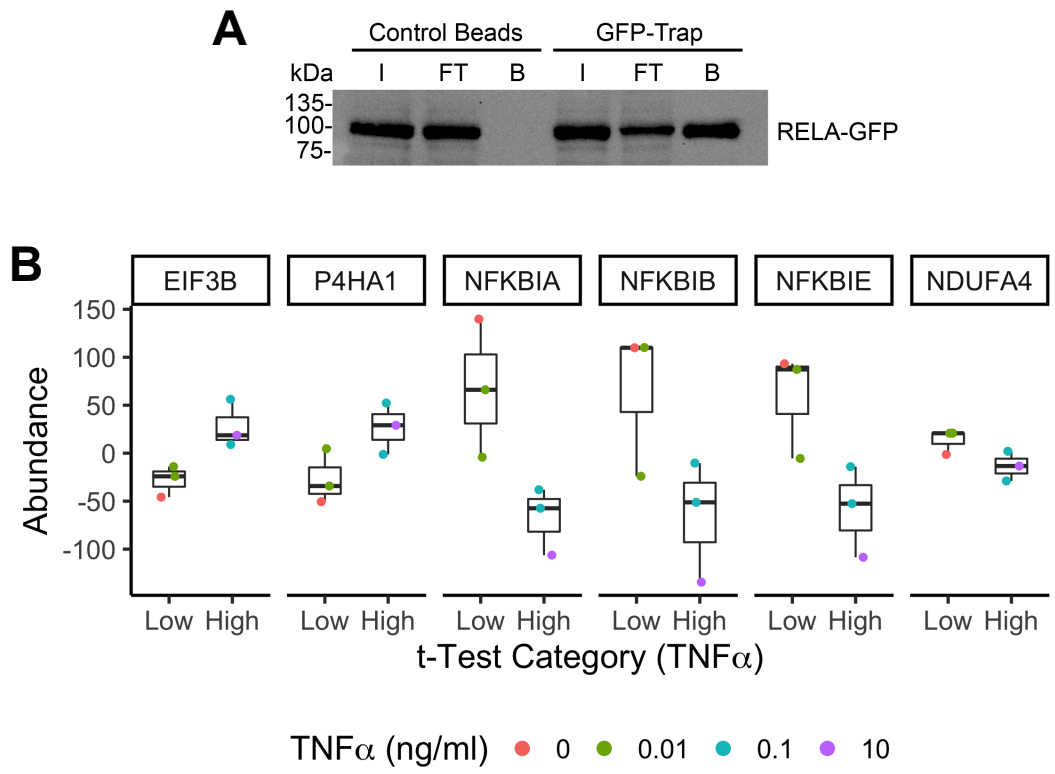
A
Control Beads
GFP-Trap
kDa
I
FT
B
I
FT
B
135-
100-
75-
RELA-GFP
B
EIF3B
P4HA1
NFKBIA
NFKBIB
NFKBIE
NDUFA4
Abundance
150
100
50
0
-50
-100
Low High
t-Test Category (TNFα)
TNFα (ng/ml)
0
0.01
0.1
10

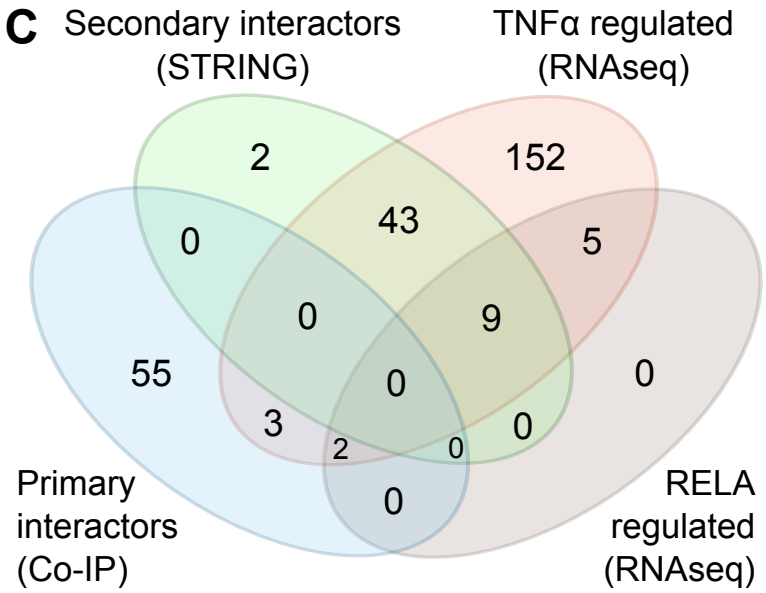
C
Secondary interactors (STRING)
TNFα regulated (RNAseq)
2
152
43
0
5
0
9
55
0
0
3
0
2
0
0
Primary interactors (Co-IP)
RELA regulated (RNAseq)

Figure 5.4 GFP-Trap identification of direct RELA interactors in MIA PaCa2 cells and overlap with TNFα-regulated genes

(A) Western blotting of input (I), flow-through (FT) and elution from beads (B) for control agarose and GFP-Trap agarose beads with MIA PaCa2 cells expressing RELA-GFP in basal conditions. Stained using an anti-RELA antibody (Abcam; 16502). (B) Genes encoding proteins pulled down by GFP-Trap with significantly different (t-test $p < 0.05$) binding to RELA under low TNFα (0 or 0.1 ng/ml) compared to high TNFα (0.1 or 10 ng/ml) treatment. (C) Number of genes TNFα and/or RELA regulated by RNA-seq in MIA PaCa2 and PANC1 cells (Figure 5.1B or C) directly pulled down by GFP-Trap in MIA PaCa2 cells or indirectly interacting with RELA via a pulled down protein (secondary interaction) as determined by STRING protein association analysis.

57 proteins were identified as TNFα targets (RNA-seq) with primary (Co-IP) or secondary (STRING) interactions with RELA (intersections of red ellipse with blue and green ellipses in Figure 5.4C). Genes were determined as highly dependent on RELA nuclear translocation if included in Cluster 3 of the TNFα-regulated genes in PDAC (Figure 5.1C). Of the 57 TNFα targets interacting with RELA, 11 are additionally dependent on RELA nuclear translocation (intersections of grey ellipse with blue and green ellipses in Figure 5.4C and yellow-bordered nodes in Figure 5.5). Only 5 proteins that were induced by TNFα physically interact with RELA (intersection of red and blue ellipses in Figure 5.4C and purple nodes in Figure 5.5). However, many proteins regulated by TNFα were secondary interactors, meaning that they functionally or physically interact with proteins that are direct interactors with RELA.

Figure 5.5

Edge Key (STRING)

- Experimental
- Database
- Neighbour
- Fusion
- Co-occurrence
- Textmining
- Co-expression
- Homology

Node Key

- Direct RELA interactor only (Co-IP)
- Direct RELA interactor (Co-IP) and TNFα target (RNASeq)
- Secondary RELA interactor (STRING) and TNFα target (RNASeq)
- TNFα target only (RNASeq)
- RELA target (RNASeq Cluster 3)

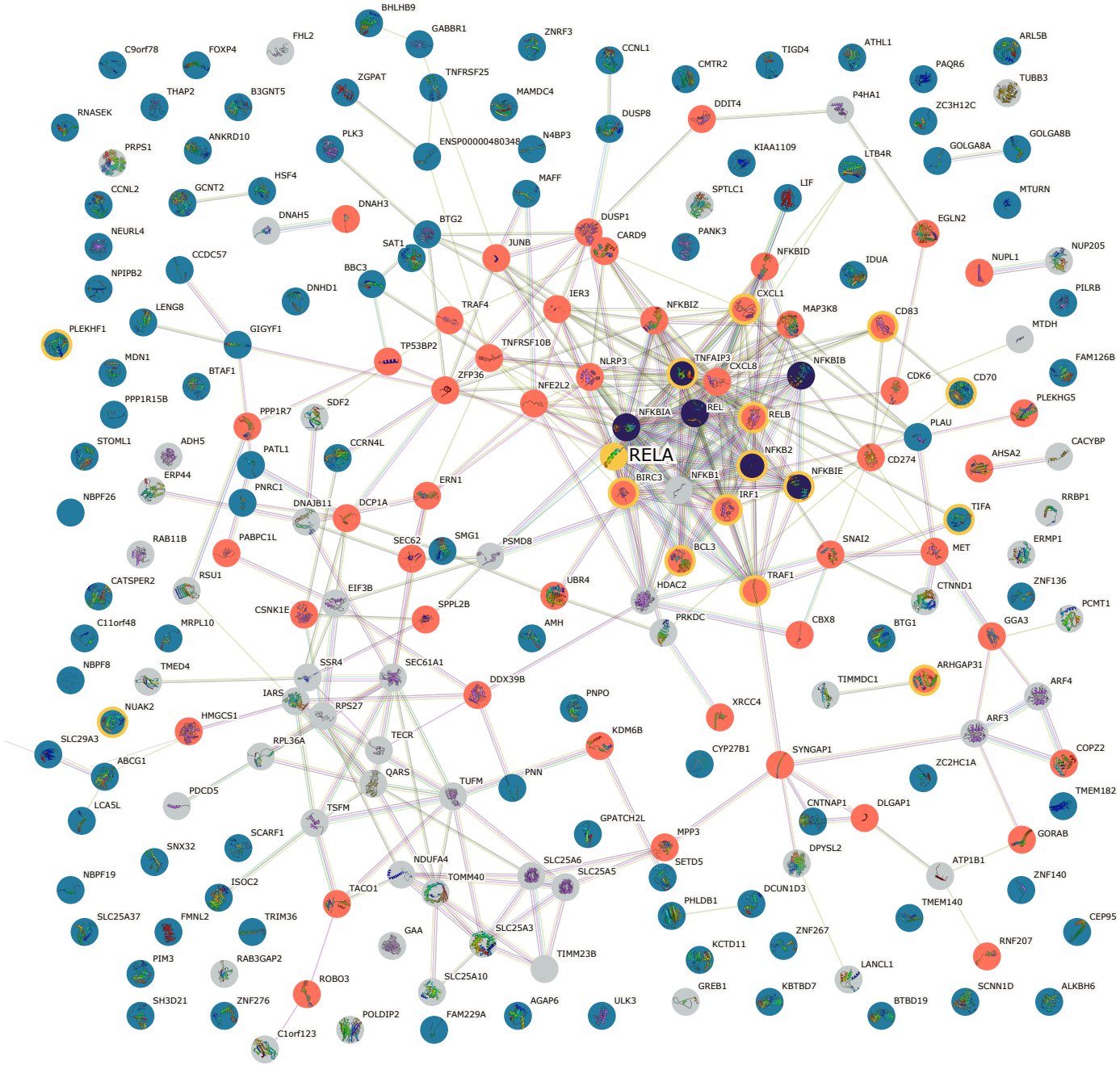

Figure 5.5 Protein-protein interactions between TNFα regulated genes and RELA

STRING protein interaction analysis of genes predicted to be TNFα or RELA regulated by RNA-seq in MIA PaCa2 and PANC1 cells, in addition to genes encoding proteins pulled down by GFP-Trap in MIA PaCa2 cells expressing endogenous RELA-GFP, as indicated by the node colour. Edges were generated in STRING and coloured by identification method (experimentally or through curated databases) and whether interacting proteins are physically or functionally interacting.

Some secondary interactors are of interest because they are regulators of the cytoskeleton. These include ARHGAP31, Snail Family Transcriptional Repressor 2 (SNAI2), and Ubiquitin protein ligase e3 component n-recognin 4 (UBR4). ARHGAP31 is upregulated by TNFα via RELA (Cluster 3) and interacts indirectly with RELA through TIMMDC1. ARHGAP31 regulates the GTPases RAC1 and CDC42, subsequently controlling lamellipodia and filopodia formation (Lamarche-Vane and Hall, 1998), as well as membrane blebbing (Tcherkezian et al., 2006). Meanwhile, TNFα downregulates the expression of *SNAI2* (encoding the protein SNAI2/SLUG; Cluster 2) in a dose and RELA independent manner. This is counter-intuitive as SNAI2 is a transcriptional repressor of the epithelial marker E-cadherin (Batlle et al., 2000) and is upregulated by TNFα in other cell types, including colorectal cancer cells (Wang et al., 2013). Lastly, TNFα upregulates *UBR4* (p600; Cluster 7), an E3 ubiquitin-protein ligase that functions in the cytoplasm as a mediator of integrin-mediated cell survival and membrane ruffling, while in the nucleus UBR4 acts as a part of the chromatin scaffold (Nakatani et al., 2005).

5.2.5 MIA PaCa2 and PANC1 cells upregulate distinct biochemical pathways

To identify which signalling pathways are differentially upregulated between MIA PaCa2 and PANC1 cells, I analysed RNA-seq data for cells treated with varying TNFα levels for 1 hr and 5 hr. Differential expression between the cell lines was analysed using DESeq2, which identified 915 genes with $\log_2$ fold-change (mean across samples) > 2.5 and adjusted $p < 10^{-20}$. 308 genes are upregulated in the MIA PaCa2 cell line and 607 are upregulated in the PANC1 cell line (Figure 5.6A and Appendix Table A2).

Figure 5.6

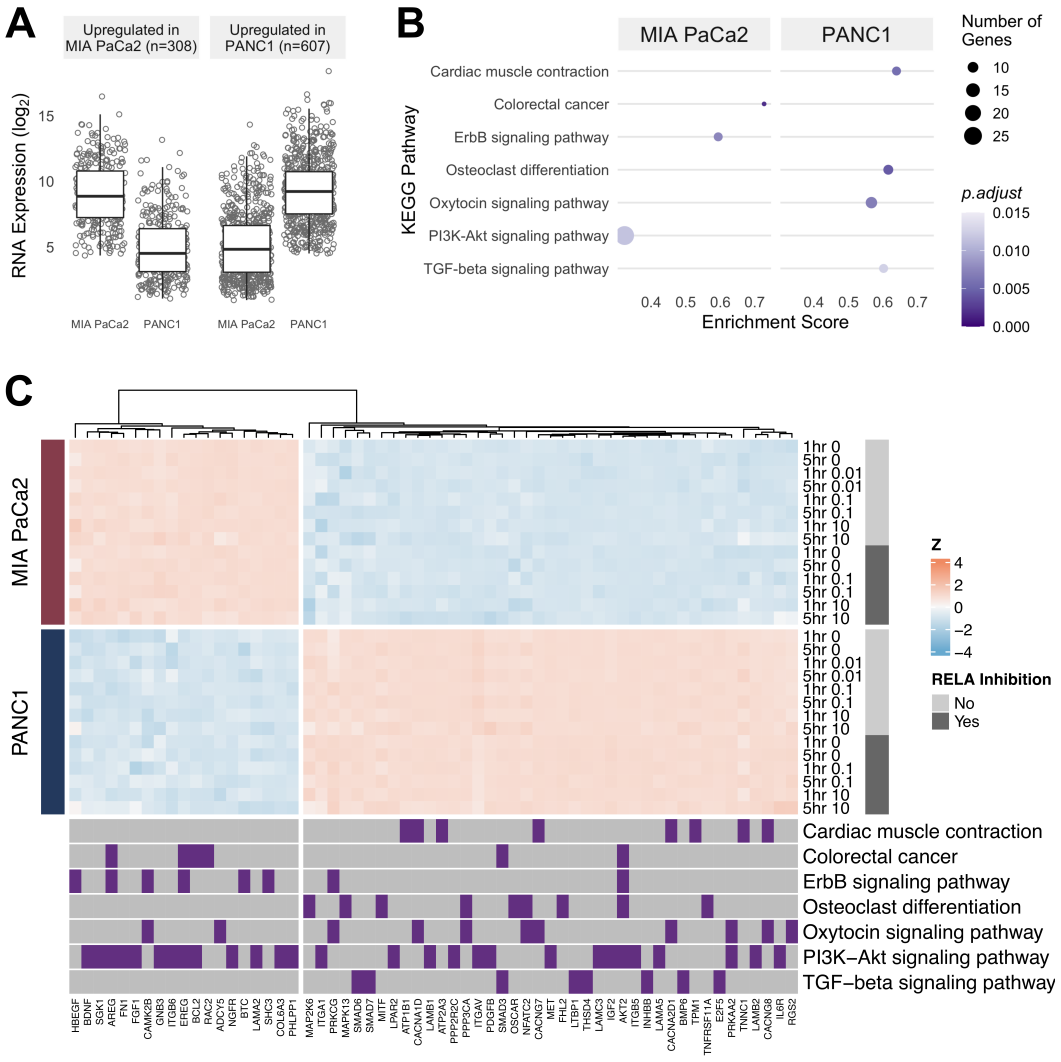
A
Upregulated in MIA PaCa2 (n=308)
Upregulated in PANC1 (n=607)
RNA Expression (log2)
15
10
5
MIA PaCa2
PANC1
MIA PaCa2
PANC1
B
MIA PaCa2
PANC1
KEGG Pathway
Cardiac muscle contraction
Colorectal cancer
ErbB signaling pathway
Osteoclast differentiation
Oxytocin signaling pathway
PI3K-Akt signaling pathway
TGF-beta signaling pathway
0.4 0.5 0.6 0.7
0.4 0.5 0.6 0.7
Enrichment Score
Number of Genes
10
15
20
25
p.adjust
0.015
0.010
0.005
0.000
C
MIA PaCa2
PANC1
1hr 0
5hr 0
1hr 0.01
5hr 0.01
1hr 0.1
5hr 0.1
1hr 10
5hr 10
Z
4
2
0
−2
−4
RELA Inhibition
No
Yes
Cardiac muscle contraction
Colorectal cancer
ErbB signaling pathway
Osteoclast differentiation
Oxytocin signaling pathway
PI3K−Akt signaling pathway
TGF−beta signaling pathway

Figure 5.6 Distinct RNA expression and KEGG pathways between MIA PaCa2 and PANC1 cells

(A) RNA expression of genes differentially expressed between MIA PaCa2 and PANC1 cells determined using DEseq2 and filtered for a $\log_2$ fold change > 2.5 and adjusted $p < 10^{-20}$. Of 915 hits, 308 are upregulated in MIA PaCa2 and 607 are upregulated in PANC1. (B) KEGG pathways enriched in the 915 differentially expressed genes between MIA PaCa2 and PANC1 cells. Analysis was carried out using the clusterProfiler R package (Yu et al., 2012) with a p-value cutoff of 0.02 and minimum gene set size of 10. (C) Clustered heatmap of RNA expression (Z scored by gene) of the 60 genes differentially regulated between MIA PaCa2 and PANC1 cells and present in the KEGG pathways enriched by cell line.

Using the 915 differentially expressed genes, I carried out gene set enrichment analysis (GSEA) using the clusterProfiler library in R to identify KEGG biological pathways upregulated in MIA PaCa2 or PANC1 cells (Figure 5.6B and Figure 5.6C). Genes showed significantly different RNA expression between MIA PaCa2 and PANC1 cells regardless of TNFα treatment or RELA activation (Figure 5.6C). MIA PaCa2 cells are enriched for pathways associated with cancer - including PI3K-Akt signalling, which is upregulated in PDAC (Ruggeri et al., 1998; Waddell et al., 2015), in addition to ErbB signalling pathway, and genes associated with colorectal cancer. PANC1 cell lines upregulated pathways associated with differentiated states, in particular cardiac muscle contraction, osteoclast differentiation and oxytocin signalling. These pathways upregulated in PANC1 appear exclusive to PANC1 cells, unlike the pathways upregulated in MIA PaCa2 which contain genes upregulated in both cell lines, as shown in the annotations at the bottom of Figure 5.6C. Overall, GSEA suggests that MIA PaCa2 adopt a more stem-like shape while PANC1 cells are more differentiated. These data are in line with the spindle-shaped morphology of MIA PaCa2 versus the more characteristically epithelial morphology of PANC1 cell (Figure 4.2).

Interestingly, PANC1 cells significantly upregulated the TGFβ pathway, which is commonly dysregulated in PDAC tumours through mutation or deletion of the transcription factor SMAD4 (Hahn et al., 1996), although both MIA PaCa2 and PANC1 cells express wildtype SMAD4 (Deer et al., 2010). PANC1 cells have upregulated RNA expression of the *SMAD3*, *SMAD6* and *SMAD7* transcription factors, suggesting that the TGFβ pathway may play a significant role in PANC1 cells.

5.2.6 Summary

In order to identify the target genes and interactors of RELA in PDAC cells, I treated MIA PaCa2 and PANC1 cells treated with TNFα in the presence or absence of IκB-SR and carried out RNA-seq. I identified genes that are upregulated by TNFα in a RELA dependent

manner, including two genes (NUAK2 and ARHGAP31) involved in actin regulation and multiple genes involved in the TNFα response. Notably, the expression of the genes encoding the IκB proteins IκBβ and IκBε are dependent on TNFα dose, TNFα duration, and RELA nuclear translocation. Using Co-IP, I identified that RELA also binds to IκBβ and IκBε, in addition to IκBα. These data suggest that IκBβ and IκBε, which are previously implicated in the suppression of RELA oscillations (Hoffmann et al., 2002), may function in feedback loops with RELA in PDAC.

5.3 Discussion

5.3.1 Clusters of TNFα-regulated genes in PDAC cells

In this chapter, I identified that TNFα significantly regulates 236 genes in the human PDAC cell lines MIA PaCa2 and PANC1, with the majority of genes upregulated by TNFα. Interestingly, most genes were not dependent on RELA nuclear translocation, suggesting that they are upregulated by alternative pathways downstream of TNFα, such as JNK (Reinhard et al., 1997) or the non-canonical NF-κB signalling pathways (Malinin et al., 1997). A subset of genes (Clusters 3, 4 and 6) was found to be regulated in a TNFα dose dependent manner, while other genes (Clusters 1, 5 and 7) displayed a binary response to TNFα. The 16 genes identified as highly dependent on RELA in Cluster 3 are TNFα dose dependent and have higher upregulation in MIA PaCa2 cells compared to PANC1 cells. This indicates that the transcription of these genes is proportional to the continuous degrees of RELA nuclear localisation observed on the single cell level by image-based analysis in MIA PaCa2 and PANC1 cells (Chapter 3). Most TNFα-regulated genes were found to be altered by 1 hr TNFα treatment, while Cluster 3 and Cluster 4 genes clearly displayed higher expression at 5 hr TNFα versus 1 hr TNFα. Therefore, TNFα regulates a combination of early and late genes in PDAC cells, while RELA-regulated genes tend to be late genes.

5.3.2 TNFα and RELA regulate the expression of genes at multiple stages of the TNFα response

RNA-seq, Co-IP and STRING analysis revealed that TNFα and RELA regulate multiple stages of the TNFα response in PDAC cells, from receptor activation through to regulation of RELA activity and chemokine production. The TNFα receptor-related genes included TNFRSF10B (TNFα target and secondary RELA interactor), TNFRSF25 (TNFα target only), TRAF1 (RELA target and secondary RELA interactor), and TRAF4 (TNFα target and secondary RELA interactor).

Furthermore, TNFα upregulates CD70 via RELA. CD70 is a transmembrane protein and member of the TNF superfamily that interacts with the receptor CD27, with CD70-CD27 interactions involved in the maintenance of T cell immunity and B cell activation (Goodwin et al., 1993; Agematsu et al., 1998). CD70 expression is typically restricted to antigen-activated T and B lymphocytes (Wachsmann et al., 2012), but CD70 expression is reported in selected cancers (Hishima et al., 2000; Meulenaere et al., 2016) including 25 % of pancreatic cancer cases (Ryan et al., 2010). Interestingly, CD27 expression in HEK-293 cells moderately upregulates activation of p65:p50 heterodimers, while CD70 binding to CD27 significantly augments NF-κB activation (Yamamoto et al., 1998). Therefore, CD70 could drive sustained RELA activation in a positive feedback loop.

In addition to IκB proteins (discussed in Section 5.3.3), TNFα and RELA upregulate TNFAIP3/A20 and Sequestosome 1 (SQSTM1), which are reported to regulate RELA activity. TNFAIP3/A20 negatively regulates RELA through the regulation of RIP proteins (Wertz et al., 2004). Meanwhile, SQSTM1 activation by IL-1α was found to induce a feedforward loop sustaining RELA activity through upregulation of p62 transcription in a *Kras*^{G12D} PDAC mouse model (Ling et al., 2012). However, another study found that IKK promotes pancreatic homeostasis by suppressing p62, while p62 promotes oxidative and ER stress that induce pancreatitis, suggesting that RELA and p62 are in antagonistic pathways

(Li et al., 2013). These latter findings are supported by a recent study showing that p62 trafficks RELA to nucleolar aggresomes to trigger apoptosis following cell stress (Lobb et al., 2021). Therefore, RELA feedback loops with A20 and SQSTM1 is an intriguing source for further study.

In addition, TNFα upregulates the chemokine CXCL1 via RELA (Cluster 3) and the chemokine CXCL8 (IL-8; Cluster 5) independently of RELA. High CXCL1 levels are typically associated with tumour progression and CXCL1 has been shown to promote NF-κB activity, which in turn increases invasiveness and EMT of cancer cells (Cao et al., 2014; Wang et al., 2018). In contrast, a study using a PDAC mouse model found that murine RelA upregulation of CXCL1 promotes oncogene-induced senescence, indicating a tumour suppressor role for the TNFα-RELA-CXCL1 axis in PDAC (Lesina et al., 2016). It would be interesting to identify whether TNFα and RELA stimulation of chemokines contributes to the sustained RELA nuclear translocation observed in PDAC cells in an autocrine or paracrine manner.

TNFα-induced RELA activation also elevated *BIRC3* expression, with *BIRC3* first identified as a RELA target in 1997. BIRC3, also known as CIAP2, is a member of the Inhibitor of Apoptosis family of proteins. In particular, the BIRC3 C-terminal RING domain is involved in suppressing TNFα cytotoxicity and BIRC3 appears to promote cell survival through a signal amplification loop with RELA (Chu et al., 1997).

Interestingly, the RNA expression of TNFα-regulated genes variably correlated with corresponding protein expression, though genes involved in the TNFα signalling pathway tended to highly correlate with protein abundance. Differences in RNA and protein levels can arise from mRNA degradation, splicing, post-translational modifications, or protein degradation (Shyu et al., 2008). A subset of TNFα-regulated genes (7/8 genes in Cluster 1) are lncRNAs and therefore do not translate to proteins. Several lncRNAs are associated with pancreatic cancer with diverse biological functions, including regulation of proliferation, metastasis and cell survival (Cheng et al., 2015; Yoshimura et al., 2018). In addition, certain

lncRNAs modulate RELA activation and target gene expression (Rapicavoli et al., 2013), including modification of RELA-induced TNFα expression by the lncRNA *HOTAIR* (Wu et al., 2016). Consequently, further studies should test the functions of the identified TNFα downregulated lncRNAs in Cluster 1, as well as study whether they are differentially expressed in healthy pancreatic tissue compared to PDAC tissue or harbour tumour suppressive roles.

Finally, RNA-seq identified that RELB and NFKB2 are upregulated by TNFα via RELA, while Co-IP showed that NFKB2 binds directly to RELA. Importantly, RELA upregulation of RELB and NFKB2 is elevated after 5 hr TNFα treatment compared to 1 hr. Therefore, sustained RELA activation in PDAC cells drives higher RNA and protein levels of the non-canonical NF-κB factors. My results also indicate that activation of the canonical NF-κB pathway is the primary outcome of TNFα induction, while the non-canonical pathway is activated as a secondary effect. Sequential activation of the NF-κB pathways may provide a mechanism for temporal control over the induction of NF-κB targets, as RELA targets are induced rapidly after TNFα induction while non-canonical targets are only expressed with sustained inflammation. This may function particularly in the regulation of immune cells. For example, non-canonical NF-κB is required for B cell maturation (Morrison et al., 2005) and osteoclastogenesis during persistent inflammation (Vaira et al., 2008).

5.3.3 Genes encoding IκB proteins have distinct expression dynamics in PDAC cells

IκB proteins play a major role in regulating RELA dynamics, with IκBα implicated in promoting RELA oscillations and rapid attenuation of RELA following stimulus removal, while IκBβ and IκBε are associated with delayed modulation of RELA activity (Hoffmann et al., 2002; Kearns et al., 2006). Binding to and inducing expression of IκB proteins, as well as expression of several previously reported NF-κB targets including those in the TNFα pathway, validates the functionality of RELA endogenously tagged with GFP at the

C-terminus, which could have impacted the transactivation domain of RELA (Schmitz and Baeuerle, 1991). These data also suggest that negative feedback mechanisms are intact in PDAC cells, but may be configured differently to other cell types.

In MIA PaCa2 cells, *NFKBIA* basal levels are high and *NFKBIA* is markedly elevated by TNFα treatment. Interestingly, when IκB-SR is induced and RELA is retained in the cytoplasm, MIA PaCa2 cells maintain high and TNFα-dose independent *NFKBIA* levels. These results are incongruous with the expected levels of NFKBIA in each condition, whereby *NFKBIA* induction is suppressed by IκB-SR induction, which is observed in PANC1 cells. This is because NF-κB is widely accepted as the core transcription factor regulating *NFKBIA* induction (Sun et al., 1993). A trivial explanation for this is that the high *NFKBIA* levels in IκB-SR-induced MIA PaCa2 cells are an artifact of reads from the mouse IκB-SR transcript being attributed to the human *NFKBIA* gene.

Assuming that the increase in *NFKBIA* is not an artifact, one explanation for these results is that MIA PaCa2 cells are configured such that *NFKBIA* levels are high in the basal state (or absence of RELA) and that RELA can bind to the *NFKBIA* promoter in a repressive state, e.g. with acetylation at lysine 310 on RELA and subsequent binding to the repressive histone marker HDAC2 (Ashburner et al., 2001). This is supported by capture of HDAC2 by GFP-Trap in MIA PaCa2 RELA-GFP cells. In this scenario, high basal *NFKBIA* is revealed in the presence of IκB-SR due to displacement of repressive RELA, while in the absence of IκB-SR, TNFα shifts RELA to a more activatory state by promoting acetylation of RELA on lysine 310. This hypothesis could be tested by analysing the post-translational modifications of RELA in various TNFα conditions and the presence/absence of IκB-SR. In addition, the sequences for endogenous *NFKBIA* and the *NFKBIA* sequence present in the IκB-SR construct could also be compared and the *NFKBIA* reads quantified by RNA-seq could be reanalysed to differentiate between the two sources of *NFKBIA*. This idea could also be tested by depleting cells of RELA by means other than the expression of the IκB-SR transgene, for example via siRNA or degron tags targeting RELA.

In PDAC cells, I found that TNFα stimulates induction of the genes encoding the atypical IκB proteins IκBδ (NFKBID) and IκBζ (NFKBIZ). IκBδ, also known as $IκB_{NS}$, has been identified to impair IL-6 production downstream of LPS, but not TNFα, and promote constitutive and potent DNA binding of p50:p50 homodimers (Hirotani et al., 2005). Overall, IκBδ regulates T regulatory cell development in the thymus (Schuster et al., 2012). Similar to IκBδ, IκBζ is activated by LPS, as well as IL-1β signalling, and not by TNFα (Muta et al., 2003; Yamamoto et al., 2004). IκBζ is believed to impact RELA activity without affecting RELA nuclear translocation, by associating with RELA in the nucleus and positively or negatively modulating target gene expression (Totzke et al., 2006). Moreover, IκBζ has negligible detection in basal conditions and IκBζ expression is dependent on activation of the innate immune system (Willems et al., 2016). In line with this, I found that the absolute RNA levels of *NFKBID* and *NFKBIZ* are low in both MIA PaCa2 and PANC1 in resting conditions (Figure 5.2B). However, in contrast to other studies, NFKBID and NFKBIZ are TNFα-responsive in both PDAC cell lines and additionally RELA dependent in the MIA PaCa2 line, indicating distinct IκBδ and κBζ signalling in PDAC to other cell types. Furthermore, *NFKBID* and NFKBIZ are upregulated by 1 hr TNFα treatment and class as 'early' genes (Figure 5.2C), similar to *NFKBIA*, which is a good indicator that they function in the negative regulation of RELA activation (Tay et al., 2010). However, the mechanism underlying this is unclear as neither IκBδ or IκBζ physically interact with RELA based on Co-IP.

Finally, IκBβ and IκBε were found to directly bind to RELA and *NFKBIB* RNA expression is higher compared to *NFKBIA* RNA expression in PANC1 cells, suggesting that IκBβ and IκBε likely play a key role in regulating RELA activity in PDAC cells. As TNFα upregulates *NFKBIB* and *NFKBIE* in a dose and RELA dependent manner, these data provide evidence for a negative feedback loop between RELA and IκBβ/ε in PDAC cells. Support for this hypothesis stems from the non-oscillatory RELA dynamics observed with TNFα in both PDAC cell lines (Section 3.2.2 and Section 3.2.3), which match the previously determined

profiles of non-oscillatory RELA dynamics in mouse fibroblasts specifically in the presence of high IκBβ and IκBε levels, or in the absence of IκBα (Hoffmann et al., 2002)

Altogether, these results should be explored further using systematic depletion or ablation of each IκB gene to validate their functions in PDAC cells, in addition to repetition of the RELA Co-IP using PANC1 cells. The differences in RELA dynamics between MIA PaCa2 and PANC1 cells, in particular the long term damped RELA nuclear localisation present in PANC1 cells, may be due to the higher expression of *NFKBIB* in PANC1 cells or the potential repression of *NFKBIA* by RELA in MIA PaCa2 cells. Interestingly, the Depmap (Cancer Dependency Map) project by the Broad Institute reports no mutations in IκB-encoding genes or NF-κB factors in either MIA PaCa2 or PANC1 cells.

5.3.4 TNFα and RELA regulate genes involved in cytoskeletal dynamics

Here, we present the first evidence that ARHGAP31 is a target of TNFα or RELA. Moreover, ARHGAP31 is not previously associated with pancreatic cancer. ARHGAP31 is the human orthologue for the mouse protein cdGAP (mCdc42 GTPase-activating protein) and ARHGAP31 inactivates the GTPases CDC42 and RAC1 (Lamarche-Vane and Hall, 1998; Tcherkezian et al., 2006). CDC42 is involved in the formation of premigratory filopodia in PDAC cells and promotes invasiveness (Razidlo et al., 2018). RAC1 expression is required for the development of PDAC tumours, in addition to the formation of the ADM and PanN precursors in $KRAS^{G12D}$ mouse models (Heid et al., 2011), indicating that RAC1 may play a role in actin remodelling during PDAC initiation. Interestingly, gain-of-function truncating mutations in ARHGAP31 cause Adams-Oliver syndrome, a condition characterised by patches of missing skin (Southgate et al., 2011). The finding that TNFα upregulates ARHGAP31 in PDAC cells via RELA prompts several vital questions: 1) how does RELA upregulation of ARHGAP31 affect actin structures and actin-related processes (migration and invasion) in PDAC cells? 2) Does ARHGAP31 play a tumour suppressor or oncogenic

role in PDAC? 3) Does ARHGAP31 regulate RELA activity? 4) How does ARHGAP31 modulate the PDAC microenvironment?

My results also demonstrate that TNFα upregulates RNA expression of the kinase *NUAK2* (SNARK), while *NUAK2* expression is abrogated in the presence of IκB-SR. NUAK2 is highly expressed in several tumour types and NUAK2 inactivation sensitises cells to FAS-induced apoptosis, while NUAK2 overexpression promotes apoptotic resistance, indicating that NUAK2 functions in promoting cell survival (Legembre et al., 2004). A key substrate for NUAK2 is myosin phosphatase target subunit 1 (MYPT1) (Yamamoto et al., 2008) and NUAK2 is reported to maintain actin stress fibres in growing cells by inhibiting MYPT (Vallenius et al., 2011). In MIA PaCa2, I found that RELA nuclear localisation is downregulated by stress fibre inhibition using a formin inhibitor and RELA is upregulated by constitutive activity of the formin mDia1. Together, these results suggest that NUAK2 promotes RELA nuclear translocation in a positive feedforward loop. This hypothesis is plausible as NUAK2 increases the activity of the mechanosensitive transcriptional coactivator YAP through stimulation of actin polymerisation and myosin activity (Yuan et al., 2018). Notably, NUAK2 is a prognostic marker for PDAC and is associated with a favourable prognosis according to The Human Protein Atlas (Appendix 3), which proposes a potential tumour suppressor role for NUAK2 in PDAC.

In addition to regulating *ARHGAP31* and *NUAK2* RNA expression in PDAC cells, TNFα causes moderate downregulation of the EMT factor *SNAI2* and TNFα upregulates the cytoskeleton regulator *UBR4*. Additional analysis could look into whether depletion of each cytoskeleton-associated gene affects the relationship between RELA and actin organisation, in particular, the nucleation of stress fibres and branched actin. Moreover, these cytoskeletal signalling axes may be pertinent to sustained RELA activation in PDAC and may contribute to the highly inflammatory and fibrotic PDAC tumour microenvironment, which warrants further investigation using 3D models and co-culture with fibroblasts and immune cells.

5.3.5 Cell line specific biochemical pathway activation in MIA PaCa2 and PANC1 cells

MIA PaCa2 and PANC1 cells have a similar genotype in terms of the main drivers of PDAC, with both harbouring mutant KRAS, mutant p53, homozygous deletions in p16, and wildtype SMAD4 (Deer et al., 2010). Here, GSEA identified that PANC1 cells upregulate genes involved in cardiac muscle contraction, oxytocin signalling and osteoclast differentiation, compared with MIA PaCa2 cells, therefore attributing pathways associated with differentiated states to PANC1 cells. Upregulation of osteoclast differentiation may be of particular interest for further investigation as this pathway is tightly linked to NF-κB signalling. Osteoclasts are multinucleated cells that form from precursors attracted to sites on bone surfaces and stimulated with certain cytokines (Boyce et al., 2015). Bone is continuously remodelled to eliminate damaged bone and there are more than one million remodelling sites in the adult skeleton (Manolagas, 2000). The number of sites increases in the presence of TNFα or RANKL, which both activate NF-κB signalling, which can both promote or suppress osteoclast formation (Franzoso et al., 1997; Li et al., 2000; Boyce et al., 2015). It is intriguing that genes associated with osteoclasts are upregulated in PDAC cells. Potentially of note is that there is a variant of PDAC tumours which contain osteoclast-like large cells (Luchini et al., 2017), while the PANC1 cell line harbours a small proportion of aberrantly large cells.

Meanwhile, the ErbB pathway and genes associated with colorectal cancer are upregulated in MIA PaCa2, which may indicate overlap in signalling between colorectal cancer and a subset of PDAC cancers. This may be expected as both solid tumours are highly inflammatory (Steele et al., 2013; Neagu et al., 2019). The ERBB protein family consists of four receptor tyrosine kinases including the epidermal growth factor receptor (EGFR/ERBB1/HER1), which stimulates the MAP kinase signalling pathway, and the other ERBB receptors ERBB2 (HER2/neu), ERBB3 (HER3) and ERBB4 (HER4). All four ERB receptors can be overexpressed in PDAC, for instance, *Kras*^{G12D} mouse models with

inhibition or genetic ablation of EGFR fail to form PDAC tumours (Ardito et al., 2012). Similarly, ERBB2 activating mutations in PDAC cells promotes tumour growth and removes dependency on KRAS (Li et al., 2020). My data suggest that a subset of PDAC tumours may be particularly amenable to treatment with ERBB2 inhibitors, which have been extensively developed for the treatment of aggressive breast cancer (Schroeder et al., 2014).

Interestingly the TGF-β signalling pathway is also upregulated in PANC1 cells, despite the presence of wildtype SMAD4 in this cell line (Deer et al., 2010). SMAD4 is mutated or deleted in around 50 % of PDAC tumours (Tascilar et al., 2001), while deregulation of all four major PDAC drivers - KRAS, p53, p16 and SMAD4 - only occurs in 38 % of all PDAC tumours (Rozenblum et al., 1997). Upregulation in PANC1 cells of SMAD3, SMAD6 and SMAD7 may present an alternative route for interfering with TGF-β signalling in a PDAC tumour that already harbours deregulation of the other three drivers, albeit the TGF-β pathway is activated in PANC1 cells in contrast to the typical suppression of this pathway in PDAC. Nonetheless, pro-tumourogenesis roles of SMAD proteins have been reported for PDAC. For example, a study found that SMAD3 accumulates in the nuclei of tumour cells and is absent in healthy epithelial cells of the pancreas, with SMAD3 upregulation associated with higher tumour grade (Yamazaki et al., 2014). Yamazaki et al. also found that SMAD3 knockdown upregulates E-cadherin and reduces expression of the mesenchymal marker vimentin, suggesting that SMAD3 promotes EMT. Similarly, an independent study found that depletion of SMAD3 in PANC1 cells reduces TGF-β1-induced cell motility (Ungefroren et al., 2011). Finally, the IKK activator TAK1 is named for its upregulation by the TGF-β pathway (Yamaguchi et al., 1995), providing a mechanism by which RELA activity may be hyperactivated in PANC1 cells.

The identification of distinct signalling pathways in MIA PaCa2 and PANC1 cells may aid molecular stratification of PDAC patients and potentially link these strata to RELA signalling. For example, PDAC tumours with hyperactive PI3K and ErbB signalling, and therefore similarity to MIA PaCa2 cells, may be more likely to have sustained RELA activation. Further

research could investigate the dependence of RELA signalling, as well as PDAC development or progression, on the identified pathways and highlighted genes.

Chapter 6: Single cell RELA responses to reovirus infection

6.1 Introduction

6.1.1 Immunotherapy and oncolytic viruses

Harnessing the immune system to target cancer cells, termed ‘immunotherapy’, gained considerable momentum during the 21st century for multiple tumour types, in particular melanoma and non-small cell lung cancer (Doroshow et al., 2019; Weiss et al., 2019). Notably, researchers James Allison and Tasuku Honjo were awarded the 2018 Nobel Prize in Medicine or Physiology for their development of immune checkpoint inhibitors, which increase immune activation by targeting the CTLA4 and PD1 pathways that are co-opted by many tumour types (Leach et al., 1996; Freeman et al., 2000).

There are now many approaches that aim to leverage the immune system to treat tumours. Prominent among these are oncolytic viruses (OVs), which work in part by recruiting the immune system to eliminate cancerous cells. OVs selectively replicate in and kill cancer cells, either intrinsically (Hashiro et al., 1977) or due to laboratory modification (Harrington et al., 2015). OVs vary in replication strategies and also in genome structure, as they can be single stranded or double stranded and RNA or DNA-based (Harrington et al., 2019). Several types of OVs are in preclinical or clinical development, including reoviruses, herpes viruses, adenoviruses, and echoviruses (Doniņa et al., 2015; Harrington et al., 2020; Liang, 2018; Mahalingam et al., 2018). Although OV mechanisms vary by virus type and are not fully elucidated, they broadly evoke an anti-tumour effect by 1) causing direct cell lysis, 2) initiating the innate and adaptive immune responses (Hemminki et al., 2020). Currently, the only OV in Europe and the US with regulatory approval is the dsDNA herpes simplex virus

(HSV)-based therapy talimogene laherparepvec (T-VEC), which was approved in 2015 for advanced melanoma (Andtbacka et al., 2019).

6.1.2 Reoviruses

Reoviruses are non-enveloped dsRNA oncolytic viruses in the *Reoviridea* family that are in late-stage clinical development (list of clinical trials in Gong et al., 2016). Natural reovirus infections in humans are common, with up to 100 % of adults showing seropositivity in some populations (Minuk et al., 1985), but infection is often asymptomatic or characterised by mild symptoms affecting the respiratory system or gastrointestinal tract (Sabin, 1959). There are several identified reovirus serotypes that infect mammals: Type 1 Lang, Type 2 Jones, Type 3 Abney, and Type 3 Dearing (T3D) (Norman and Lee, 2000). The reovirus strain T3D (also termed 'RT3D') has been implemented in clinical trials (Müller et al., 2020)

Reoviruses infect cells via interaction of the σ attachment protein with the junctional adhesion molecule A (JAM-A) (Barton et al., 2001) and α-linked sialic acid (Paul et al., 1989), followed by endocytosis into the host cell mediated by β1 integrins (Maginnis et al., 2006). The virus enters the cytoplasm after partial uncoating by endolysosomes, resulting in transcriptionally active cores that have the machinery required to initiate viral replication (Odegard et al., 2004; Schulz et al., 2012). Transcription within these cores releases positive-sense single-stranded RNAs (ssRNAs) transcripts into the cytoplasm (Li et al., 1980), which are translated to form new viral proteins and also used as templates for negative-sense ssRNA synthesis (Tenorio et al., 2019). Outer-capsid proteins are added to progeny cores (Chandran et al., 1999) and the reovirus is released from the host cell by a mechanism that is not well understood (Phillips et al., 2018).

In the 1970s, it was discovered that cancer cells are more susceptible to reovirus infection compared to normal cells (Hashiro et al., 1977; Duncan et al., 1978). The reovirus subtype T3D entered into clinical trials as an unmodified agent in the early 2000s, initially trademarked as Reolysin and currently manufactured as Pelareorep. Since, results have

indicated that T3D may have limited efficacy as monotherapy, but reovirus may be promising in combination with radiation (Twigger et al., 2008), immune checkpoint blockade (Rajani et al., 2016; Samson et al., 2018), or classic chemotherapy. For instance, cisplatin-paclitaxel has a synergistic effect with reovirus to increase cancer cell death, via apoptosis, in vitro and in vivo with head and neck cancer models (Roulstone et al., 2013). Combinations with targeted approaches are also being explored preclinically, for example, reovirus in combination with BRAF or MEK inhibition in BRAF mutant melanoma cell lines enhances apoptosis associated with ER stress (Roulstone et al., 2015).

6.1.3 Virus detection in human cells and deregulation in cancer

In humans, pathogens are detected by pattern recognition receptors (PRRs), including Toll-like receptors (TLRs), which are extracellular PPRs, and retinoic acid-inducible gene I (RIGI) like receptors (RLRs) and Protein Kinase R (PKR), which are intracellular PRRs. There are two types of RLR that function as signalling molecules: RIGI and melanoma differentiation associated gene 5 (MDA5) (Loo et al., 2008). Viral RNA recognition by PRRs activates transcription factors including Interferon Regulatory Factor 3 (IRF3) and RELA, which induce expression of type 1 interferons (IFNs) (Sato et al., 2000; Alexopoulou et al., 2001). Secreted IFNs then stimulate the production of genes that block various stages of the virus life cycle (Schneider et al., 2014).

Studies have identified an association between reovirus permissiveness and EGFR-RAS-MAPK signalling, which may explain selective replication of reovirus in cancer cells, as components of the EGFR-RAS-MAPK signalling axis are commonly mutated in cancer. Initially, it was shown that cell lines previously resistant to reovirus infection become susceptible when transfected with the gene encoding epidermal growth factor receptor (EGFR) (Strong et al., 1993), or the structurally related protein v-erbB (Strong and Lee, 1996). Moreover, reovirus can bind directly to an N-terminal domain of EGFR (Tang et al., 1993). Involvement of RAS signalling was identified when transfection of cells with activated

Ras prevented phosphorylation of the serine/threonine protein kinase PKR, maintaining PKR in an inactive state (Strong et al., 1998). In healthy cells, PKR binding to viral dsRNA binding results in PKR dimerisation, autophosphorylation and activation. Activated PKR phosphorylates and inactivates eIF2, a protein essential for mRNA translation, therefore preventing the translation of virus transcripts (Bischoff and Samuel, 1989). However, the role of RAS in reovirus infection is uncertain since the cytotoxic effects of reovirus in head and neck cancer and melanoma cell lines occur independently of RAS and EGFR (Song et al., 2009; Twigger et al., 2012).

6.1.4 Reovirus-induced cell death

Apoptosis was recognised early on in research considering cell death following reovirus infection, with binding of the TNF-related apoptosis inducing ligand (TRAIL) to its receptors and activation of caspases, including caspase 3 and caspase 8, shown to be upregulated with reovirus infection (Clarke et al., 2000; Kominsky et al., 2002). Nonetheless, reovirus induced cell death can occur independently of caspases, suggesting that reoviruses can elicit cell death by other mechanisms (Berger and Danthi, 2013). One suggested mode is autophagy, which is upregulated by reovirus following ER stress in multiple myeloma by 24 hr after reovirus treatment (Thirukkumaran et al., 2013). More recently, reovirus has been shown to induce necroptosis, which requires IFN-β production following sensing of genomic RNA of incoming virus particles in early-stage of reovirus infection, and then requiring efficient dsRNA synthesis in the late-stage reovirus infection (Berger et al., 2017)

6.1.5 Roles for NF-κB signalling in reovirus infection

NF-κB signalling plays a critical role in activating anti-tumour immunity following reovirus infection. This was initially identified through the use of the synthetic dsRNA analogue polyinosine:polycytidylic acid (poly(I:C)), which leads to a TLR3-dependent increase in

NF-κB luciferase reporter activity, as well as production of type 1 interferons and TNFα (Alexopoulou et al., 2001).

Dendritic cells (DC) are antigen-presenting cells that link the innate and adaptive immune responses. In 2008, it was shown by Alan Melcher's group that treatment of human myeloid DC with reovirus results in DC maturation and production of pro-inflammatory cytokines. Production of pro-inflammatory cytokines was abrogated with inhibition of NF-κB activity using caffeic acid phenethyl ester (CAPE) (Errington et al., 2008). A follow-up study by the Melcher lab in 2011 demonstrated that when reovirus-infected human melanoma cells die, they secrete cytokines associated with NF-κB activity. These cytokines elicit a chemotactic response in DC, natural killer, and anti-melanoma cytotoxic T cells. Therefore, NF-κB induction of pro-inflammatory cytokines can recruit immune effector cells, which may contribute to the removal of reovirus-infected cells separately from direct oncolysis (Steele et al., 2011).

In addition to key roles in activating the immune system, accumulating evidence suggests that RELA is involved in reovirus-induced cell death itself. Infection of HeLa cells with high levels of reovirus (100 MOI for 48 hr) results in nuclear translocation of p65 and p50, shown by EMSA, accompanied by NF-κB directed transcription. Of note, reovirus induced apoptosis is abrogated in the presence of a proteasome inhibitor, which prevents NF-κB activation. Connolly et al. provided further evidence for NF-κB involvement in apoptosis by showing that apoptosis is repressed in p65 or p50 knockout cells, as well as repressed in cells expressing IκB-SR (non-degradable IκBα) that causes constitutive NF-κB repression (Connolly et al., 2000). The mechanism underlying the involvement of NF-κB signalling in cell death is still not well understood. However, a study treating MEFs with reovirus (MOI 10) showed that IFN synthesis and signalling are not required for subsequent apoptosis, but that apoptosis can be mediated by NF-κB and pIRF3 upregulation of NOXA, a member of the pro-apoptotic Bcl-2 protein family (Knowlton et al., 2012). In addition to affecting NF-κB activity and nuclear translocation, the mRNA levels of NF-κB genes are upregulated by reovirus

infection. Thirukkumaran et al. reported a 4-fold increase in RELA and a 2.5-fold increase in p105 (p50 precursor) mRNA levels, following 24 hr reovirus infection (40 MOI) of two breast cancer cell lines. Using the pharmacological compounds CAPE and N-Acetyl-Leu-Leu-Norleu-al, they further showed that reovirus-induced apoptosis is dependent on NF-κB upregulation of p53 upregulated modulator of apoptosis (PUMA) (Thirukkumaran et al., 2017). Therefore, in contrast to the body of research supporting pro-survival roles of RELA downstream of TNFα signalling, multiple lines of research suggest that RELA promotes cell death following reovirus infection.

In this chapter, I characterised live single cell RELA translocation dynamics in response to reovirus infection in the PDAC cell lines PANC1 and MIA PaCa2, in addition to the melanoma cell line A375. I also tested the effect on RELA dynamics and cell death of combining reovirus with the PARP inhibitor talazoparib, based on a screen carried out by Joan Kyula, Victoria Roulstone and Kevin Harrington, in collaboration with Chris Lord (ICR).

6.2 Results

6.2.1 PANC1, but not MIA PaCa2, cells respond to reovirus with RELA nuclear localisation and cell death

Although it is generally accepted that reovirus infection leads to increased RELA activation, previous studies have not looked into the heterogeneity of RELA activation on the single cell level, or the time resolution of RELA nuclear translocation relative to OV exposure. Therefore, I sought to characterise the effect of reovirus (T3D) infection on live single cell RELA dynamics in the PDAC cell lines PANC1 and MIA PaCa2.

For 96 hr, I live-imaged RELA-GFP expressing PDAC cells infected with T3D with a range of multiplicity of infection (MOI; 1.25-40) - the ratio of virus particles to the number of host cells - or treated with 0.1 ng/ml TNFα. Average RELA ratios per treatment and time point showed that MIA PaCa2 cells are resistant to RT3D, with minimal RELA ratio changes, while highly

responsive to TNFα (Figure 6.1A). In contrast, PANC1 cells, which respond with a lower RELA ratio to TNFα compared to MIA PaCa2 cells, were sensitive to RT3D at all MOI, with RELA ratio generally increasing with MOI and reaching a maximum by 20 MOI. In PANC1 cells, RT3D induced significantly higher RELA ratios compared to TNFα, for example, the maximum RELA ratio for MOI 20 is 1.66 and for 0.1 ng/ml TNFα is 1.15. Moreover, while RELA ratio peaked early after stimulation by TNF, OV exposure caused a more gradual increase in RELA nuclear localisation. This delay in RELA ratio rate of change with RT3D may reflect time for viral replication, slower signal transduction in RT3D response signalling compared to TNFα signalling or dependency of RELA activation on secreted factors following RT3D infection. Quantification of cell number over time showed resistance in MIA PaCa2 in terms of cell death, while PANC1 cells reduced in cell number with increasing MOI (Figure 6.1B). Interestingly, the lowest MOI (1.25) only caused a reduction in cell number from 48 hr after infection.

Figure 6.1

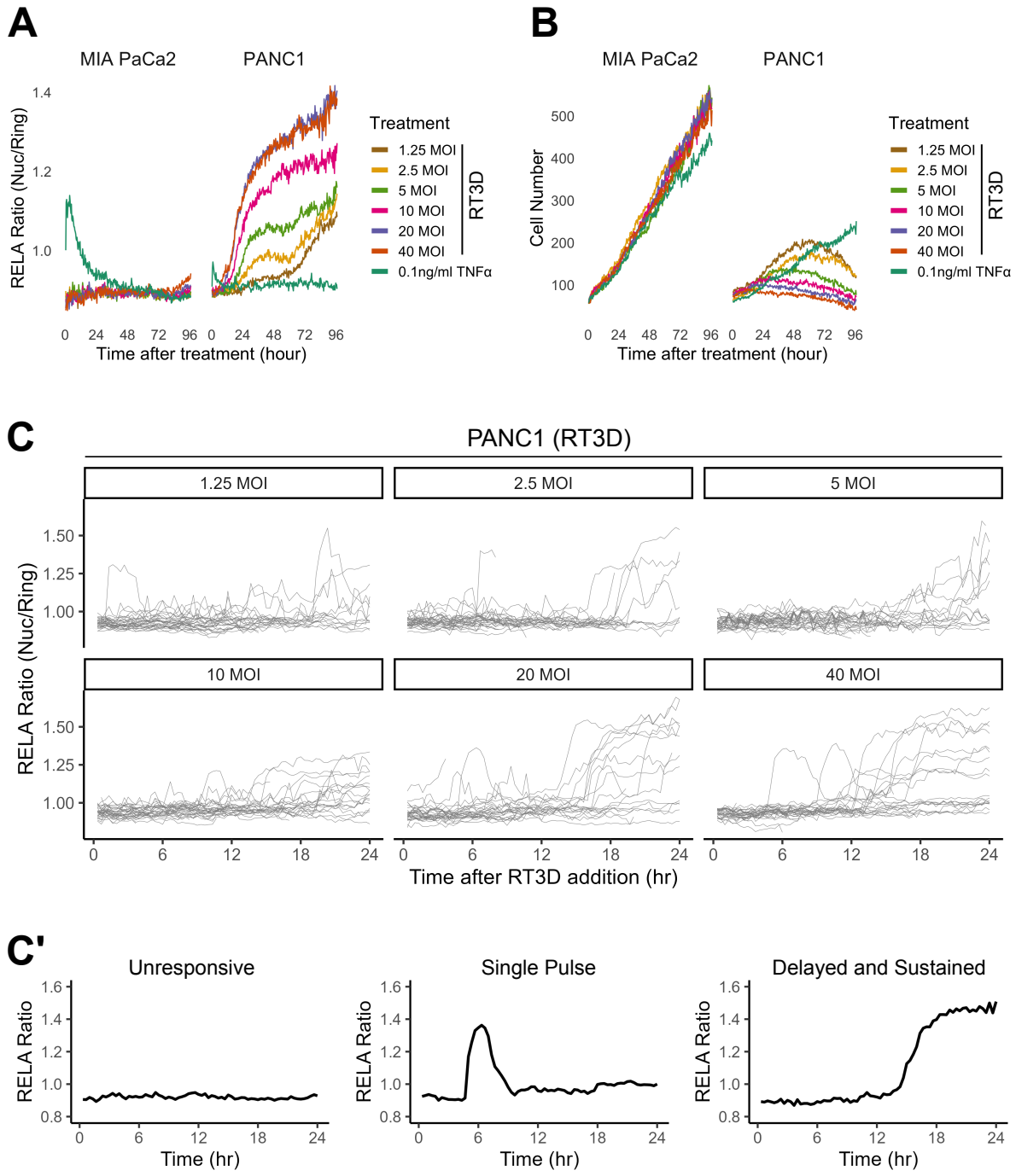
A
MIA PaCa2
PANC1
RELA Ratio (Nuc/Ring)
Time after treatment (hour)
Treatment
1.25 MOI
2.5 MOI
5 MOI
10 MOI
20 MOI
40 MOI
0.1ng/ml TNFα
RT3D
B
Cell Number
C
PANC1 (RT3D)
Time after RT3D addition (hr)
C'
Unresponsive
Single Pulse
Delayed and Sustained
Time (hr)

Figure 6.1 PANC1, but not MIA PaCa2, cells responds to reovirus with RELA nuclear localisation and cell death

(A) Average RELA ratio and (B) Cell Number for MIA PaCa2 and PANC1 cells imaged at 20 min intervals for 96 hr following reovirus T3D infection (MOI 1.25-40) or 0.1 ng/ml TNFα treatment. (C) Single cell RELA ratio measurements for PANC1 cells infected with RT3D for 96 hr. n = 30 tracked cells per RT3D MOI. (C') Example tracks for categories of RT3D-induced RELA dynamics observed in (C). Cells either had minimal RELA ratio changes (unresponsive), a single pulse of RELA nuclear localisation, or sustained RELA nuclear localisation starting after 12 hr from RT3D infection.

I tracked individual PANC1 cells for 24 hr following RT3D infection to identify different categories of reovirus-induced RELA dynamics (Figure 6.1C). Single cell tracks revealed that PANC1 cells can be unresponsive, have a single pulse of RELA nuclear translocation lasting 2.5-4.5 hours, or have sustained RELA nuclear localisation from ~12 hours after RT3D infection (Figure 6.1C').

6.2.2 Talazoparib enhances reovirus-induced cell death in A375 melanoma cells

The Harrington lab (ICR) have previously carried out a screen to identify drugs that increase reovirus killing efficacy in A375 melanoma cells. This screen used 80 drugs and treatment with a range of RT3D MOI (Figure 6.2A). The Poly (ADP-ribose) polymerase (PARP) inhibitor talazoparib (BMN-673) was identified as having a synthetic lethal interaction with reovirus infection (Figure 6.2B). The PARP family of enzymes catalyse the transfer of ADP-ribose to itself or other target proteins and function in DNA repair, apoptosis, and chromatin remodelling. The most well-characterised PARP protein is PARP1, which acts in multiple DNA repair pathways including the repair of single-stranded breaks. After detecting and binding to a single-stranded break, PARP1 synthesis of ADP-ribose polymers facilitates recruitment of proteins to repair the break (D'Amours et al., 1999; Ray Chaudhuri and Nussenzweig, 2017). Currently, PARP inhibition in the clinic is primarily used for the treatment of BRCA1/2 mutated breast and ovarian cancers (Farmer et al., 2005; Mateo et al., 2019).

Figure 6.2

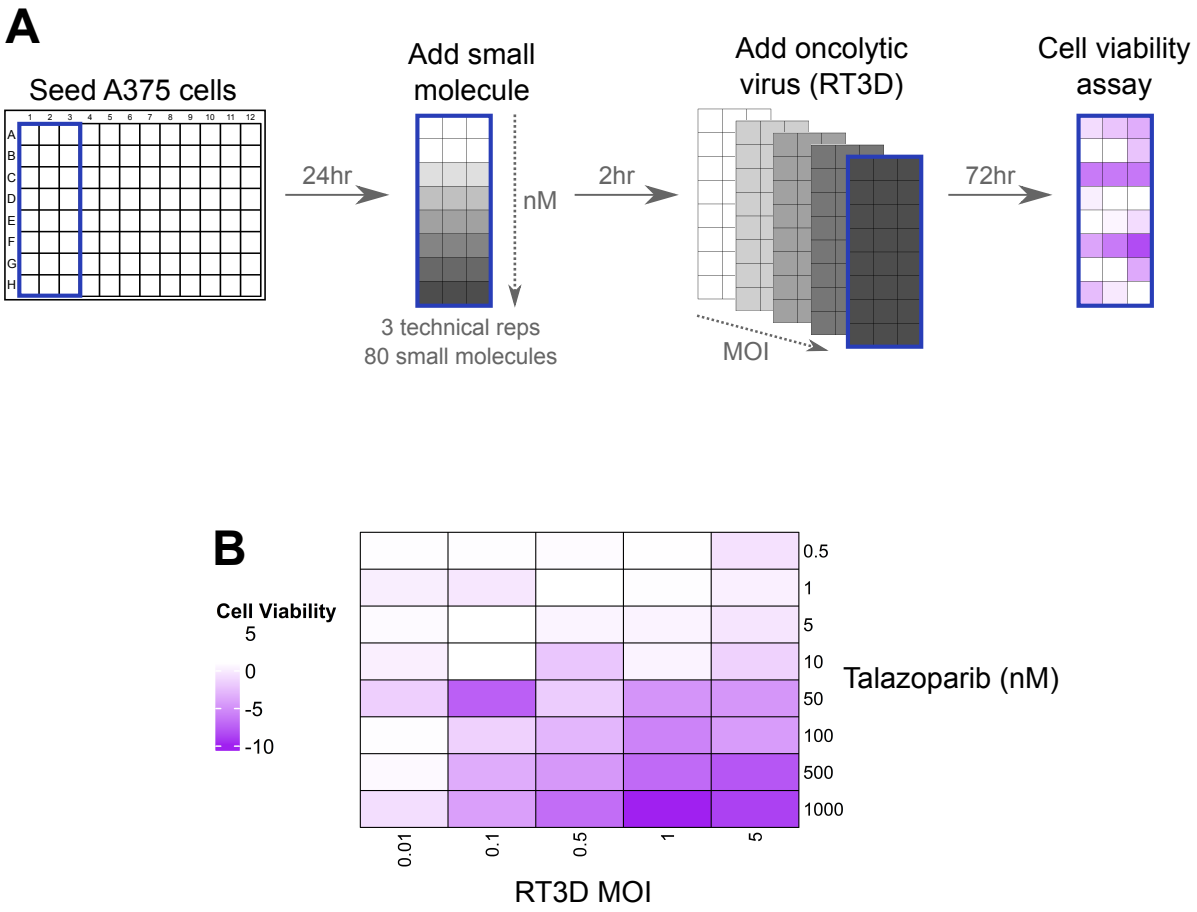
A
Seed A375 cells
1 2 3 4 5 6 7 8 9 10 11 12
A
B
C
D
E
F
G
H
24hr
Add small molecule
nM
3 technical reps
80 small molecules
2hr
Add oncolytic virus (RT3D)
MOI
72hr
Cell viability assay
B
Cell Viability
5
0
-5
-10
0.5
1
5
10
50
100
500
1000
Talazoparib (nM)
0.01
0.1
0.5
1
5
RT3D MOI

Figure 6.2 Drug screen for synthetic lethal interactions with reovirus

(A) In preliminary assays conducted by the Harrington and Lord labs (ICR), 80 drugs were screened to identify synthetic lethal combinations with reovirus. A375 cells were pre-treated with DMSO or eight concentrations of each drug for 2 hr prior to 72 hr RT3D infection (MOI 0.01-5). Cell viability was assessed using the CellTiter Glo Luminescent Cell Viability Assay. (B) Cell viability z-scores for A375 cells treated with talazoparib and RT3D. Measurements were normalised to the DMSO control and pseudo viral dose, then z-scored against other drugs on the same plate.

To assay the effects of reovirus and PARP inhibition on RELA dynamics on the single cell level, I generated an A375 cell line with endogenously tagged RELA using the same CRISPR-CAS9 method for tagging the PDAC cell lines (Figure 3.1). Functional RELA dynamics were validated by confirming cytoplasmic RELA localisation in basal conditions and nuclear translocation with 1 hr 10 ng/ml TNFα treatment (Figure 6.3A and B). From the A375 RELA-GFP cell line, I generated a subclone with endogenous PCNA-Scarlet for use in timelapse microscopy (Figure 6.3C).

Figure 6.3

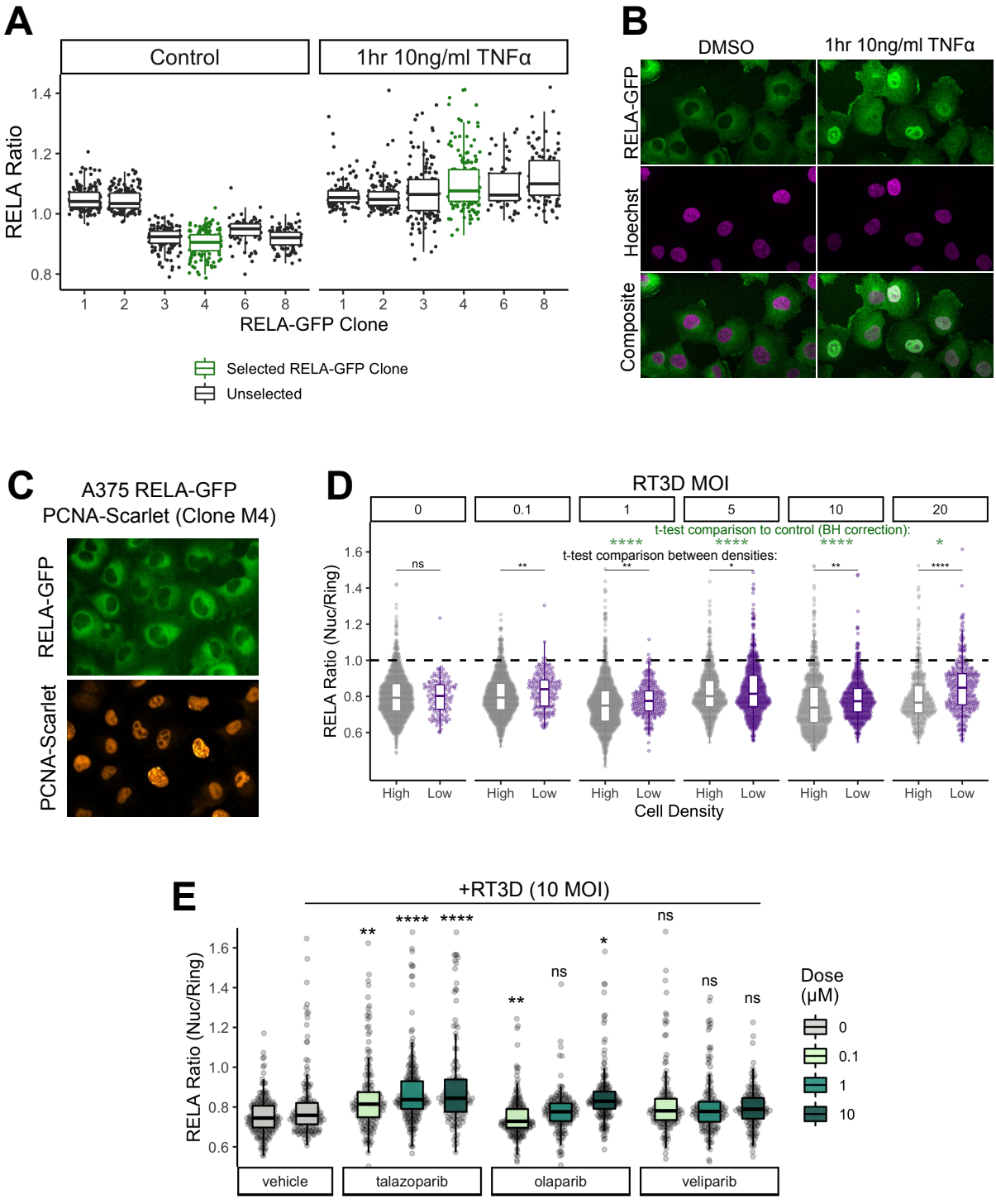
A
Control
1hr 10ng/ml TNFα
RELA Ratio
RELA-GFP Clone
Selected RELA-GFP Clone
Unselected
B
DMSO
1hr 10ng/ml TNFα
RELA-GFP
Hoechst
Composite
C
A375 RELA-GFP
PCNA-Scarlet (Clone M4)
RELA-GFP
PCNA-Scarlet
D
RT3D MOI
t-test comparison to control (BH correction):
t-test comparison between densities:
RELA Ratio (Nuc/Ring)
Cell Density
E
+RT3D (10 MOI)
RELA Ratio (Nuc/Ring)
vehicle
talazoparib
olaparib
veliparib
Dose (μM)

Figure 6.3 A375 cell line generation and reovirus combination with PARP inhibition

(A) Response of A375 clones, with endogenously tagged RELA-GFP by CRISPR-CAS9, to 1 hr 10 ng/ml TNFα treatment. The selected clone (Clone 4) has cytoplasmic RELA (ratio of nuclear/cytoplasmic RELA intensity < 1) with the BSA/PBS control treatment and nuclear RELA localisation (RELA ratio > 1) with TNFα. (B) Confocal microscopy images of A375 RELA-GFP Clone 4 in 1 hr BSA/PBS control or 10 ng/ml TNFα treatment. (C) Images of monoclonal cell line (termed Clone M4) generated from A375 RELA-GFP Clone 4 with additional endogenous tagging of PCNA with Scarlet by CRISPR-CAS9. (D) Single cell measurements of RELA ratio (nuc/ring region RELA-GFP intensity) of A375 RELA-GFP cells seeded at a low or high confluence and infected with RT3D MOI 0-20 for 48 hr. Statistics in green represent two-tailed t-test comparisons (both densities collated) for each RT3D MOI compared to the control (MOI 0), with Benjamini-Hochberg correction. Statistics in black show results for two-tailed t-test comparisons between low and high cell seeding density, carried out independently per MOI. ns (non-significant) = $p > 0.05$, * = $0 < 0.05$, ** = $p < 0.01$, *** = $p < 0.001$, **** = $p < 0.0001$. (E) Single cell RELA ratio measurements of A375 RELA-GFP cells pre-treated with a PARP inhibitor (talazoparib, olaparib or veliparib) at 0, 0.1, 1 or 10 μM for 2 hr followed by 48 hr RT3D infection (MOI 10). RT3D data were compared using multiple two-tailed t-test comparisons for each treatment compared to RT3D alone with Benjamini-Hochberg correction for multiple testing. ns (non-significant) = $p > 0.05$, * = $0 < 0.05$, ** = $p < 0.01$, *** = $p < 0.001$, **** = $p < 0.0001$.

To test the minimum MOI required to induce RELA nuclear translocation in A375 cells, I infected A375 RELA-GFP cells with RT3D MOI 0-20 (Figure 6.3D). Since seeding density is known to affect TNFα-mediated RELA nuclear translocation (Sero et al., 2015), A375 cells were seeded at a low or high confluence to test whether cell density affects RT3D induction of RELA. Multiple t-test comparisons to the control with Benjamini-Hochberg correction, with data collated from both densities per MOI, showed that RT3D induced significant RELA nuclear translocation with all MOI tested (0.1, 1, 5, 10 and 20; green statistics in Figure 6.3D). RELA ratio was also significantly higher with low density cell seeding compared to high density (black statistics in Figure 6.3D; t-test) with all MOI but not in the absence of RT3D (MOI 0). For this reason, I seeded cells hereafter at a low density to prevent potential contact inhibition of RELA.

To validate whether small molecule inhibition of PARP affects RT3D-induced RELA nuclear translocation, I pre-treated A375 RELA-GFP cells with talazoparib, olaparib or veliparib for 2 hr followed by 48 hr RT3D infection (10 MOI) (Figure 6.3E). Talazoparib, olaparib and veliparib differ in potency in PARP trapping and were all included in the original drug screen. Talazoparib and olaparib increased RELA nuclear localisation following reovirus infection, while veliparib caused no detectable changes in RELA ratio. As expected from the screen, talazoparib had the most significant effect on RELA nuclear translocation. Overall, PARP inhibition was confirmed to increase the effects of RT3D on RELA nuclear translocation.

6.2.3 Talazoparib and reovirus induce heterogeneous single cell RELA responses

To assay the effects of talazoparib on live RELA translocation dynamics, I tracked A375 and PANC1 cells expressing RELA-GFP and PCNA-Scarlet following RT3D 10 MOI addition with 2 hr 1 μM talazoparib pre-treatment, calculating the RELA ratio for each cell and time point. An MOI of 10 was used as this induces a high proportion of both A375 and PANC1 cells with

nuclear RELA without reaching the maximum RELA ratio, allowing scope for RELA ratio changes.

In both cell lines, average tracks showed a higher RELA ratio over time with combination treatment compared to talazoparib or T3D alone (Figure 6.4A and B). Individual RELA ratio tracks showed heterogeneity on the single cell level, with only a subset of cells with a ‘high’ RELA ratio (maximum > 1.2). A375 cells have a binary RELA response, with A375 cells either having high or no nuclear RELA localisation, while PANC1 cells displayed continuous levels of nuclear RELA (Figure 6.4C).

Figure 6.4

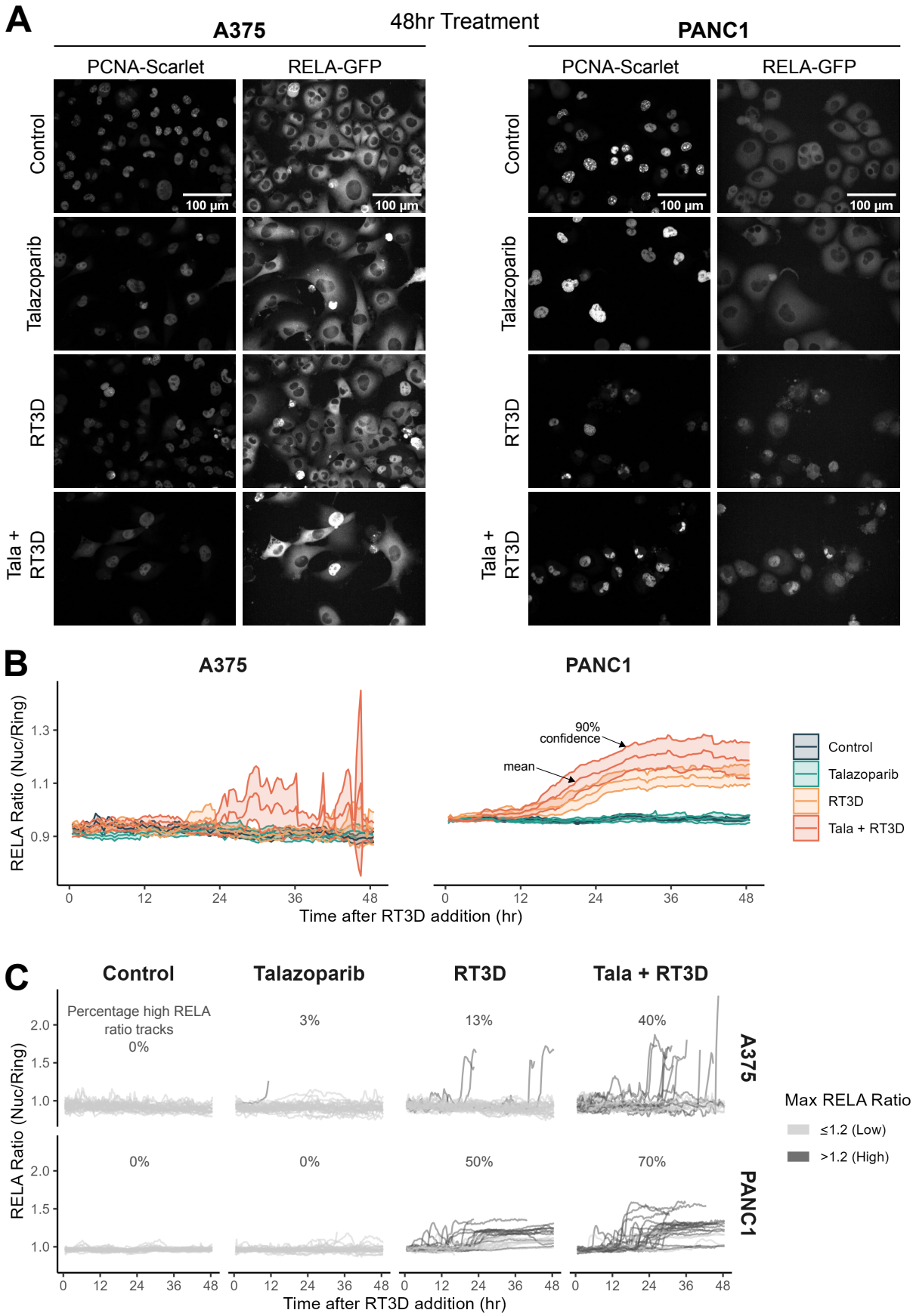
A
A375
48hr Treatment
PANC1
PCNA-Scarlet
RELA-GFP
Control
Talazoparib
RT3D
Tala + RT3D
100 µm
B
A375
PANC1
RELA Ratio (Nuc/Ring)
90% confidence
mean
Control
Talazoparib
RT3D
Tala + RT3D
Time after RT3D addition (hr)
C
Control
Talazoparib
RT3D
Tala + RT3D
Percentage high RELA ratio tracks
0%
3%
13%
40%
0%
0%
50%
70%
A375
PANC1
Max RELA Ratio
≤1.2 (Low)
>1.2 (High)
Time after RT3D addition (hr)

Figure 6.4 Talazoparib and reovirus induce heterogeneous RELA responses on the single cell level

(A-C) A375 and PANC1 cells treated with 2 hr DMSO control or 1 μM talazoparib, followed by additional 48 hr RT3D MOI 10 infection or PBS control. (A) Confocal microscopy images of endogenous RELA-GFP and PCNA-Scarlet at 48 hr after RT3D treatment. (B-C) RELA ratio (nuc/ring region RELA-GFP intensity) tracks per cell line and treatment. n = 50-60 per condition. (B) Mean tracks (lines) and ribbons representing the 90% confidence interval. (C) Single cell tracks coloured by maximum RELA ratio per track (≤ 1.2 light grey; > 1.2 dark grey). Percentages of tracks per condition with a maximum RELA ratio > 1.2 per condition are shown.

6.2.4 Reovirus-induced cell death is associated with high RELA nuclear localisation

To determine the effect of combined talazoparib and reovirus on cell death in A375 and PANC1 cells, I noted whether each tracked cell, or daughter cell (in cases where the tracks include divisions), died or survived by the end of the imaging period. In both cell lines, a higher percentage of tracked cells died during the 48 hr imaging period with combination treatment compared with talazoparib or T3D alone (Figure 6.5A).

Figure 6.5

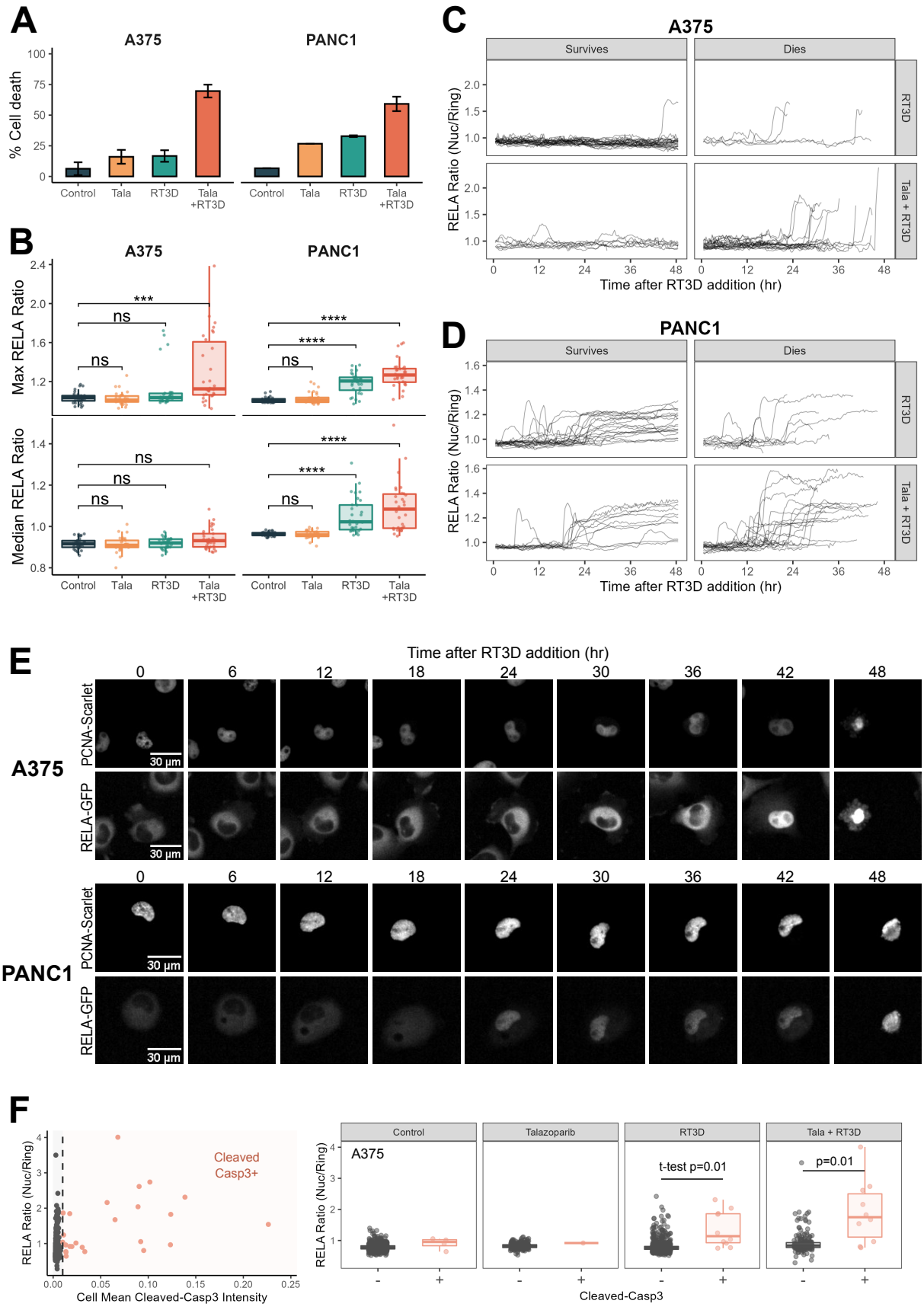
A
A375
PANC1
% Cell death
Control
Tala
RT3D
Tala +RT3D
B
Max RELA Ratio
Median RELA Ratio
ns
***
****
C
A375
Survives
Dies
RT3D
Tala + RT3D
RELA Ratio (Nuc/Ring)
Time after RT3D addition (hr)
D
PANC1
E
Time after RT3D addition (hr)
PCNA-Scarlet
RELA-GFP
30 µm
F
Cleaved Casp3+
Cell Mean Cleaved-Casp3 Intensity
Control
Talazoparib
t-test p=0.01
p=0.01
Cleaved-Casp3

Figure 6.5 Reovirus-induced cell death is associated with high RELA nuclear localisation

(A) Percentage of A375 or PANC1 cells dying in the 48 hr imaging period with control, 1 μM talazoparib, 48 hr RT3D MOI 10, or combination treatment. Two biological repeats for all A375 treatments and PANC1 combination treatment. One biological repeat for remaining PANC1 treatments. (B) Maximum and median RELA ratios by single cell tracks for A375 and PANC1 cells infected with RT3D MOI 10 with or without 2 hr 1 μM talazoparib pre-treatment. n = 30 tracked cells per treatment and cell line. Statistical significance shown for comparisons of each treatment to cell line control with Benjamini–Hochberg correction. ns (non-significant) = $p > 0.05$, * = $0 < 0.05$, ** = $p < 0.01$, *** = $p < 0.001$, **** = $p < 0.0001$. (C) Single cell tracks corresponding to (B). (D) Images of an A375 and a PANC1 cell relative to the timing of RT3D MOI 10 infection, with 2 hr 1 μM talazoparib pre-treatment. A375 cell: RELA nuclear translocation occurs rapidly ~42 hr after RT3D infection and cell death is rapid. PANC1 cell: RELA nuclear translocation occurs gradually from ~18 hr following RT3D infection and cell death is slow. (E) Left: categorisation of cells as cleaved casp3+ or cleaved casp3- based on mean cell cleaved casp3 intensity by IF. Right: Single cell RELA ratio measurements for cleaved casp3+ and cleaved casp3- cells by treatment. Statistics shown with ‘RT3D’ and ‘Tala + RT3D’ treatments depict t-test comparisons between RELA ratios in the cleaved casp3+ and cleaved casp3- populations. There are insufficient numbers of cleaved casp3- cells in ‘Control’ and ‘Talazoparib’ treatments for statistical comparison.

To determine whether there is an association between RELA activity and cell death on the single cell level, I considered whether cells dying or surviving with RT3D infection had different RELA dynamics (Figure 6.5B-D). A375 cells have a significantly higher maximum RELA ratio with combination talazoparib and RT3D treatment compared to each treatment alone or control treatment but no significant change in the median RELA ratio, as expected from the binary RELA activity observed in A375 cells. In PANC1 cells, differences in both maximum and median RELA ratios were observed by treatment and reovirus infection alone was sufficient to increase RELA ratio compared to the control. Therefore, PARP inhibition appears to increase reovirus induced cell death in both PANC1 and A375 cells, but has a more substantial effect on enhancing reovirus induced RELA activity in A375 cells compared to PANC1 cells. Single cell tracks also revealed that PANC1 cells maintained high RELA nuclear localisation for long periods (> 24 hr), while A375 cells died quickly following high RELA activity (~8 hr), as shown in Figure 6.5E.

To discern whether the cell death associated with high RELA nuclear translocation involves caspase activation, A375 cells treated with talazoparib, reovirus or combination treatment were stained for cleaved casp3 by IF and cells were assigned as cleaved-Casp3 ‘positive’ or ‘negative’ based on mean cell cleaved-Casp3 intensity (Figure 6.5F). Single cell measurements showed that few A375 cells in control or talazoparib treatment were cleaved-Casp3+ and there was no difference in RELA ratio based on cleaved-Casp3 staining. However, cells treated with reovirus have higher RELA ratios for cleaved-Casp3+ cells compared to cleaved-Casp3- cells, indicating that A375 cells undergoing cell death involving Caspase 3 cleavage have higher RELA activity compared to surviving cells following RT3D infection. Moreover, PARP inhibition increased the frequency of cells with RT3D-induced Caspase 3 cleavage and was associated with high RELA activity.

6.2.5 RELA colocalises to the nucleus with the transcription factor pIRF3 in response to reovirus infection

Since pIRF3 has been shown to co-regulate cytokine production with NF-κB signalling following reovirus infection, I was interested in whether RELA and pIRF3 are upregulated in the same cells following reovirus infection on the single cell level. To test this, I stained for pIRF3 by IF in A375 and PANC1 RELA-GFP cells treated with RT3D MOI 10 with or without talazoparib pre-treatment (Figure 6.6A and B). In all treatments, RELA and pIRF3 nuc/ring region intensities had a positive correlation indicating colocalisation and possible shared upstream signalling. In both A375 and PANC1 cells, pIRF3 and RELA have higher nuclear localisation with reovirus infection compared to control or talazoparib alone. In A375 cells, talazoparib and reovirus combination further increased nuclear pIRF3 and RELA localisation compared to reovirus alone. Linear models fit to pIRF3 plot against RELA were limited to R^2 from 0.26 to 0.53 depending on the cell line and treatment, with the best fit achieved in control conditions in either line. In general, I observed that cells with high nuclear pIRF3 localisation generally also have high RELA nuclear localisation, while cells with high RELA nuclear localisation did not always have high nuclear pIRF3, as exemplified by the indicated cells in Figure 6.6A' and B' (orange arrows: high nuclear RELA and pIRF3; blue arrows: high nuclear RELA and low nuclear pIRF3).

Figure 6.6

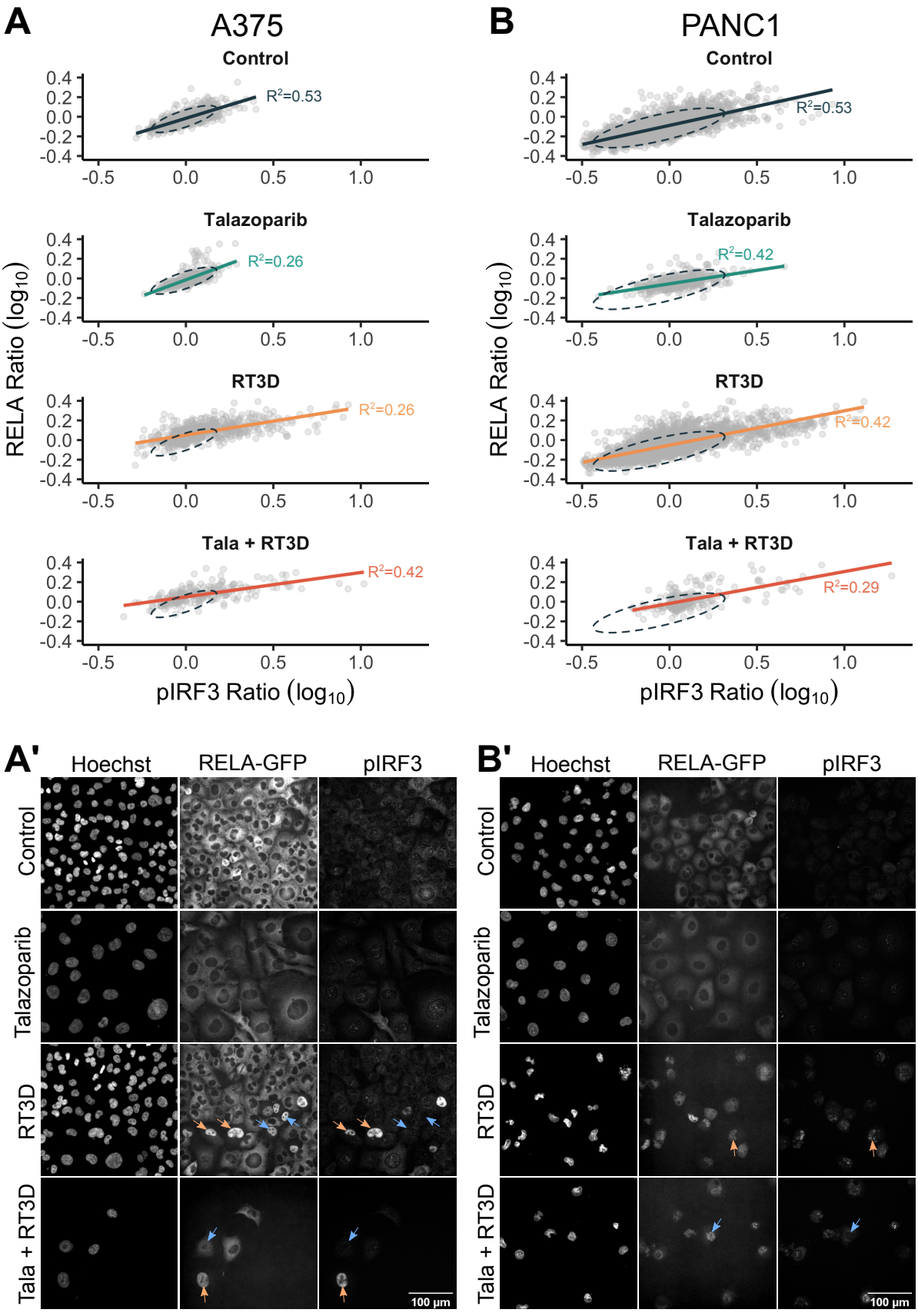
A
A375
Control
R²=0.53
Talazoparib
R²=0.26
RT3D
R²=0.26
Tala + RT3D
R²=0.42
RELA Ratio (log10)
pIRF3 Ratio (log10)
B
PANC1
Control
R²=0.53
Talazoparib
R²=0.42
RT3D
R²=0.42
Tala + RT3D
R²=0.29
RELA Ratio (log10)
pIRF3 Ratio (log10)
A'
Hoechst
RELA-GFP
pIRF3
Control
Talazoparib
RT3D
Tala + RT3D
100 µm
B'
Hoechst
RELA-GFP
pIRF3
Control
Talazoparib
RT3D
Tala + RT3D
100 µm

Figure 6.6 RELA-GFP and pIRF3 colocalisation

(A-B) Single cell measurements of nuc/ring region RELA-GFP intensity (log10) against nuc/ring pIRF3 intensity (log_{10}). Cells treated with control 1 hr DMSO or 1 μM talazoparib and additional 48 hr RT3D MOI 10 or PBS control. Linear models fitted using geom_smooth function in ggplot by treatment and cell line. Black dashed lines represent straight-line models and solid lines fitted to a quadratic formula (A'-B') Corresponding confocal microscopy images of hoechst, endogenous RELA-GFP and pIRF3 IF staining in PANC1 and A375 cells for quantification in (A-B). Orange arrows indicate examples of cells with high RELA and pIRF3 nuclear localisation. Blue arrows indicate examples of cells with high RELA but low pIRF3 nuclear localisation.

6.2.6 Summary

To quantify single cell RELA dynamics, I infected MIA PaCa2 and PANC1 PDAC cells with reovirus and assayed endogenous RELA-GFP cellular localisation changes and cell death. MIA PaCa2 cells are resistant to reovirus infection in terms of cell death and RELA nuclear translocation, while PANC1 cells respond to reovirus with cell death preceded by sustained and varied cell-to-cell levels of RELA nuclear localisation. I additionally assayed endogenous RELA-GFP changes in the melanoma cell line A375 with reovirus infection. Dying A375 cells have transient and binary RELA nuclear translocation, while surviving A375 cells lack nuclear RELA. Further, I confirmed a cell viability screen result that PARP inhibition enhances reovirus-induced cell death, while additionally finding that PARP inhibition increases the proportion of cells with RELA nuclear localisation. Overall, RELA nuclear localisation following reovirus infection is associated with reovirus-induced cell death and is a useful readout for reovirus efficacy.

6.3 Discussion

6.3.1 Single cell RELA responses to reovirus are diverse and distinct from TNFα-mediated RELA dynamics

This thesis chapter has provided the first characterisation of the dynamics of RELA responses to reoviruses at the single cell level. In contrast to a study assaying sensitivity of PDAC cell lines to reovirus based on cell viability (Etoh et al., 2003), I identified that MIA PaCa2 cells are resistant to reovirus infection in terms of cell death and I additionally showed that MIA PaCa2 cells maintain cytoplasmic RELA localisation with reovirus infection. Meanwhile, PANC1 cells can be unresponsive to reovirus infection or, when responsive, can have a pulse of RELA nuclear translocation or delayed and sustained RELA nuclear localisation. Therefore, MIA PaCa2 cells are more sensitive to TNFα than PANC1 cells but less sensitive to reovirus in terms of RELA nuclear translocation. The specificity of reovirus

infection by PDAC cell line may stem from the ability to uptake reoviruses, which is dependent on the interaction between the reovirus σ attachment protein and JAM-A, which functions as a receptor (Barton et al., 2001). Strikingly, the gene encoding JAM-A (*F11R*) is in the list of genes differentially expressed between MIA PaCa2 and PANC1 cells identified by RNA-seq (Appendix Table A2), with *F11R* RNA expressed 54 times higher in PANC1 cells compared to MIA PaCa2 cells. Therefore, differences in JAM-A expression between MIA PaCa2 and PANC1 cells should be looked into further on the protein level. Moreover, *FLLR* should be depleted in PANC1 cells to validate whether reovirus infection is dependent on JAM-A.

It is also interesting that the patterns of RELA nuclear translocation induced by reovirus versus TNFα treatment in PANC1 cells are distinct. Reovirus infection results in more delayed RELA nuclear translocation compared to TNFα, which induces instant RELA nuclear translocation. Moreover, RELA nuclear localisation is damped over time with TNFα but builds up over time with reovirus infection in the majority of PANC1 cells. It is therefore expected that the positive and negative feedback loops governing RELA dynamics differ between TNFα and reovirus treatment, and these pathways are likely to be configured differently between A375 and PANC1 cells. For instance, the higher RELA activity and quicker cell death observed in A375 cells compared to PANC1 cells may be due to stronger positive feedback with cytokine signalling. Particularly given the delay in RELA activation after reovirus addition, it would be interesting to resolve whether RELA activation is a secondary response to cytokine production following reovirus infection, which could be investigated using a TNFα neutralising antibody or by refreshing the medium to remove secreted cytokines, e.g. 10 hr after reovirus addition.

Unlike A375 cells which die quickly after high RELA activation, PANC1 cells can have a single pulse of RELA activity followed by near to basal levels of RELA activation, or otherwise sustained RELA activity that typically plateaus. These dynamics patterns suggest that negative feedback plays a critical role in directing RELA dynamics in PANC1 cells.

Follow-up experiments could include assessing the roles of the different IκB proteins and A20 in determining whether PANC1 cells are non-responsive, have a single pulse of RELA activation, or display sustained RELA activation. Furthermore, it would be interesting to test the sensitivity of PDAC cells to other OVs, e.g. the dsDNA viruses T-VEC and RP1, and whether alternative categories of RELA dynamics are induced.

As RELA dynamics determine transcriptional output, I predict that the discrete RELA dynamics induced by TNFα and reovirus in PANC1 cells lead to differential RELA-regulated gene expression and phenotypic outcomes, particularly since reovirus infection led to significantly higher RELA ratios than TNFα. Moreover, reovirus infection may upregulate different RELA targets, or time-dependent expression changes in the same targets, between PANC1 and A375 cells. This may explain the contrasting cell death dynamics induced by reovirus in PANC1 and A375 cells. For instance, the sustained RELA activity in PANC1 cells may upregulate genes involved in a distinct cell death mode to the genes upregulated by the short burst of high RELA activity in A375 cells. Single cell RNA-seq analysis of transcripts correlated with RELA activity could be useful in elucidating the tumour-specific roles of RELA in reovirus infection.

6.3.2 Oncolytic viruses as a potential therapeutic strategy for targeting PDAC

A number of phase I/II clinical trials have investigated the tolerability and efficacy of OVs in pancreatic cancer patients. The clinical trials completed are reviewed extensively by Haller, Monaco & Essani (2020). Many OVs explored in pancreatic cancer have focused on the adenovirus-based therapy ONYX-015, which appears to selectively replicate in cells with p53 mutations (Bischoff et al., 1996), a genetic event common in PDAC tumours (Waddell et al., 2015). However, ONYX-015 has limited efficacy as monotherapy and has issues with low viral replication (Hecht et al., 2003). Current research seeks to use genetic engineering to increase the efficacy of adenovirus vectors for PDAC treatment. One strategy is to remodel the tumour microenvironment to make PDAC tumours more accessible to OVs,

chemotherapy, and immune system infiltration. One example is VCN-01, an oncolytic adenovirus with insertion of PH20 hyaluronidase that breaks down the ECM component hyaluronan, and has been shown to decrease tumour stiffness in patients and exert an anti-tumour effect in PDAC models (Bazan-Peregrino et al., 2021).

Reovirus efficacy for pancreatic cancer treatment has been assessed as monotherapy and in combination with chemotherapy or immune checkpoint blockade. This included a phase II clinical study in 2016 with 37 patients and was revealed to have no effect on progression-free survival, as monotherapy or combined with paclitaxel and carboplatin (Noonan et al., 2016). Similarly, an independent phase II clinical trial with 34 chemotherapy-naive patients combined reovirus with gemcitabine and identified efficient viral replication in tumour cells and low toxicity, with no clinical benefit compared to gemcitabine alone (Mahalingam et al., 2018). An associated study examined primary tumour biopsies from a single patient before and after 25 cycles of combined gemcitabine and reovirus treatment over 23 months. Analysis showed reovirus protein accumulation, ER stress and caspase 3 processing and NOXA expression, indicating induction of cell death by the combined treatment by expected mechanisms (Mahalingam et al., 2015). The trial published by Mahalingam et al., 2018 indicated PDL1 upregulation and encouraged investigation into combining reovirus treatment with anti-PDL1 inhibitors, which is currently being investigated for pancreatic cancer (Mahalingam et al., 2020).

One of the reasons why PDAC tumours have been considered for reovirus treatment is the ubiquitous overactivation of KRAS observed in PDAC patients (Rozenblum et al., 1997), suggesting that pancreatic cancer cells may be highly susceptible to reovirus infection. This hypothesis was supported by in vitro analysis of five pancreatic cancer cell lines, including PANC1 and MIA PaCa2 (Etoh et al., 2003). The results showed cell death following reovirus infection (MOI 10) and suppression of pancreatic tumour growth in murine xenograft models using PANC1 and BxPC3 cell lines, with no notable side effects suggesting potential specificity in impacting cancer over non-cancerous cells. My results show that RAS

activation is insufficient to provide susceptibility to reovirus infection, demonstrated by the resistant MIA PaCa2 cell line, which have an activating KRAS G12C mutation (Suwa et al., 1994). Consequently, the relevance of KRAS mutations in pancreatic cancer susceptibility to reovirus remains unknown, particularly as the clinical trial published by Noonen et al. (2016) noted that the KRAS status in pancreatic cancer patients did not impact progression-free survival with reovirus treatment. RAS signalling is believed to be important in reovirus killing of cancer cells (Strong et al., 1998), while reovirus efficacy is independent of EGFR and RAS signalling in melanoma and head and neck cancer respectively (Song et al., 2009; Twigger et al., 2012). Therefore, it would be interesting to test whether reovirus infection in PANC1 cells is dependent on the MAPK pathway. Furthermore, the response of PDAC mouse models to reovirus infection could be tested with and without induction of *Kras*^{G12D} (Ying et al., 2012).

6.3.3 RELA activity can be used as a predictor of reovirus efficacy

My results indicate that assaying RELA is an attractive strategy for identifying combination treatments, as RELA nuclear translocation correlates with reovirus-induced cell death on both the population and single cell level. Furthermore, assaying RELA localisation using image analysis presents a method to screen for treatments that synergise with reovirus infection in a high throughput manner that is more informative than cell viability alone. As previous studies identified that RELA plays a crucial role in cytokine production and activating immune cells following reovirus infection (Steele et al., 2011), whether and how single cell RELA nuclear translocation correlates with immunogenicity should be investigated. This is particularly important because patient immunophenotype is associated with reovirus response in pancreatic cancer patients (Noonan et al., 2016).

Here, PARP inhibition using talazoparib is presented as a potential strategy for overcoming limited reovirus potency in PDAC and there is incentive to test whether PARP inhibition and reovirus have an anti-tumour effect in PDAC mouse models. We (J. Kyula, V. Roulstone, F.

Butera et al.) are currently looking into how PARP inhibition mediates reovirus infection in melanoma cells, focusing on the relationship between talazoparib, PARylation and DISC-mediated apoptosis, as well as the effect of PARP inhibition on the reovirus-induced immune response.

6.3.4 Crosstalk between RELA and pIRF3 on the single cell level

Quantification of RELA and pIRF3 localisation identified a positive correlation between these transcription factors in terms of reovirus-induced nuclear translocation on the single cell level. Our findings support reported shared upstream signalling by NF-κB factors and pIRF3 in two studies from 2003. Specifically, the IκB kinase homologs from the non-canonical NF-κB signalling pathway, IκB kinase-ε (IKKε) and TANK-binding kinase-1 (TBK1), were identified as essential for activating IRF3 after viral infection and dsRNA stimulation of TLR3 (Fitzgerald et al., 2003; Sharma et al., 2003). Moreover, Fitzgerald et al. demonstrated that IKKε and TBK1 mediate activation of IFNβ and RANTES, both genes previously found to be co-regulated by NF-κB and IRF3 (Wathelet et al., 1998; Génin et al., 2000).

Multiple studies have carried out systems-level identification of transcripts co-regulated by IRF3 and RELA. For example, nascent transcripts in lipid A-stimulated mouse macrophages analysed using RNA-seq, ChIP-seq, and binding motif analysis identified five genes dependent on IRF3 expression with strong NF-κB ChIP seq peaks and NF-κB promoter motifs (*Ccl5*, *Ifnb1*, *Cxcl10*, *Gbp5*, and *Irg1*). Tong et al. also identified that IRF3 and RELA differ temporally in their contribution to target gene expression. For instance, RELA binding to the promoters of *Cxcl10*, *Gbp5*, and *Irg1* occurs by 15 min post lipid A treatment, but expression at this timepoint is unaltered by *Irf3* knockout. However, the expression of the three target genes at later timepoints is affected by Irf3 expression. Moreover, the five IRF3 target genes with NF-κB binding motifs have considerably higher average induction (643-fold) compared to four targets without NF-κB motifs (40-fold), suggesting possible enhancement of IRF3 target gene expression by NF-κB activity (Tong et al., 2016).

Interestingly, in silico analysis of gene promoter sequences found multiple genomic regions with both pIRF3 and NF-κB binding sites, confirmed with publicly available ChIP-seq, and identified that IRF1 and IRF7 (but not IRF3) are upregulated by RELA, while IRF3 binding sites are not present on promoters of genes for any of the NF-κB family members (Iwanaszko and Kimmel, 2015). Further research following from my results could consider the signalling basis behind the frequent occurrence of high nuclear RELA localisation in cells with high pIRF3 nuclear localisation but an absence of the inverse relationship. Given that RELA and pIRF3 are unlikely to upregulate each other's transcription, one possibility is that reovirus infection initially activates pIRF3, which then stimulates cytokine production that triggers RELA nuclear translocation in the same cell or nearby cells. Alternatively, RELA and IRF3 may be upregulated at the same time in single cells but IRF3 is displaced to the cytoplasm quicker than RELA. Insight into these hypotheses could be gained from live imaging of both RELA and IRF3 translocation following reovirus infection to decipher the temporal sequence of their upregulation.

Chapter 7: General Discussion and Future Directions

7.1 Heterogeneity and configuration of single cell RELA responses in PDAC cells

7.1.1 TNFα

To characterise previously unknown single cell RELA dynamics in PDAC cells, I used CRISPR-CAS9 genome editing to tag RELA at the endogenous locus with GFP in the human PDAC cell lines MIA PaCa2 and PANC1. Using live imaging and automated image segmentation, tracking and analysis, I characterised RELA dynamics in response to the cytokine TNFα (Sections 3.2.2 and 3.2.3), which is upregulated with PDAC progression (Zhao et al., 2016). Strikingly, PDAC cells show atypical RELA responses compared to reports in other cell types (Ashall et al., 2009; Tay et al., 2010; Sero et al., 2015), as PDAC cells maintain prolonged nuclear RELA localisation and RELA responses are cell cycle independent. Single cell RELA responses are also highly heterogeneous, as cells displayed continuous degrees of RELA nuclear localisation and a subset of non-responsive cells. The key differences between the two PDAC cell lines are that MIA PaCa2 cells respond with higher, more rapid, and sustained RELA nuclear localisation compared to PANC1 cells, while PANC1 cells have a damped RELA response over time. Similar to other cell lines (Ashall et al., 2009; Tay et al., 2010; Sero et al., 2015), RELA nuclear translocation occurs immediately following TNFα addition and peak nuclear RELA localisation occurs around 1 hr post-TNFα, with the median time to peak of 40 min for MIA PaCa2 and 50 min in PANC1.

The distinction in RELA dynamics between PDAC with other cell types may be attributed to the use of knock-in RELA-GFP in this study, since most studies that have assayed RELA localisation used exogenous RELA fusion constructs. As RELA upregulates several genes involved in positive and negative feedback, as corroborated in the present study using

RNA-seq, RELA overexpression could interfere with its intrinsic dynamics. Nonetheless, other studies that have tagged RELA endogenously did detect oscillations, such as in MEFs (Sung et al., 2009; Zambrano et al., 2016) and MCF7 breast cancer cells (Stewart-Ornstein and Lahav, 2016).

One of the considerations for use of exogenous RELA is that RELA dynamics should function as normal provided that the ratio of RELA and its inhibitor IκBα is maintained (Nelson et al., 2002; Lee et al., 2014; Patel et al., 2021). The high sensitivity of PDAC cells to TNFα and lack of oscillations suggest that PDAC cells suppress negative feedback imposed by IκBα. In 2002, Hoffman et al. demonstrated that oscillations in NF-κB DNA binding are due to negative feedback with IκBα, which is encoded by a gene (*NFKBIA*) upregulated by NF-κB factors. Hoffman et al. also identified that IκBβ and IκBε, encoded by *NFKBIB* and *NFKBIE* respectively, have delayed suppression of NF-κB DNA binding compared to IκBα. Cells with high IκBβ and IκBε, or absence of IκBα, lose oscillations stimulated by TNFα. These findings motivated inspection into RELA interaction with IκB proteins and upregulation of IκB genes by TNFα in PDAC cells. Using Co-IP with MIA PaCa2 cells, I found that RELA binds to IκBα, IκBβ and IκBε and binding to each is suppressed in high TNFα concentrations. Furthermore, RNA-seq with varying TNFα doses in the presence/absence of IκB-SR showed that TNFα significantly upregulates *NFKBIB* and *NFKBIE* expression in a TNFα dose and RELA-dependent manner. Although TNFα also stimulates transcription of the *NFKBIA* gene in both MIA PaCa2 and PANC1 cells, the absolute RNA levels of *NFKBIB* are higher than those for *NFKBIA* in PANC1 cells, indicating that IκBβ may play a prominent role in regulating RELA dynamics in PDAC cells. To fully elucidate the mechanism for RELA hyperactivation in PDAC, the roles of IκBα, IκBβ and IκBε need to be unravelled through systemic depletion and overexpression.

An alternative interpretation for sustained RELA activation in PDAC is the presence of positive feedback loops. Using RNA-seq in PDAC cells, TNFα was found to upregulate the chemokine CXCL8/IL8, which is known to promote RELA activity (Manna and Ramesh,

2005). In addition, TNFα upregulates expression of the TNF receptor superfamily protein TNFRSF10B and two of the seven TNFR adaptor proteins: TRAF1 and TRAF4. TRAF1 and TRAF4 are associated with oncogenic functions and their expressions are elevated in multiple cancers, including pancreatic cancer (Witkiewicz et al., 2015) and bladder cancer (Robertson et al., 2017). Furthermore, RNA-seq revealed that genes in the TNFα pathway are expressed early (1 hr versus 5 hr) following TNFα treatment, while RNA expression of TNFα pathway genes correlated highly with corresponding protein abundance. Consequently, TNFα rapid upregulation of inputs into the TNFα pathway in PDAC cells could ostensibly sustain high RELA activity. However, TNFα removal after 1 hr stimulation caused rapid cytoplasmic relocalisation of RELA (Section 3.2.8), suggesting that 1 hr TNFα treatment and RELA nuclear localisation does not stimulate sufficient positive feedback to maintain RELA activation. This experiment also revealed that the mechanism for rapid removal of RELA from the nucleus, which is likely mediated by IκBα, is intact in PDAC cells.

In terms of the cell cycle independence of RELA nuclear translocation in PDAC cells (Figure 3.5), this may be explained by the lack of binding to E2F1 or E2F4 based on Co-IP, while binding to E2F1 causes the suppression of RELA activation following the G1/S transition in HeLa and SK-N-AS cells (Ankers et al., 2016). Interestingly, I did find that RELA binds to EIF3 and this interaction is enhanced by TNFα treatment, while prior reports indicate that EIF3 upregulates E2F1 expression (Ma et al., 2019).

7.1.2 Reovirus

This thesis contains the first single cell analysis of RELA responses to infection by the dsRNA oncolytic virus reovirus and achieved this with temporal resolution using timelapse imaging (Chapter 6). In terms of RELA nuclear translocation and cell death, MIA PaCa2 are highly sensitive to TNFα but resistant to reovirus. In contrast, PANC1 cells respond to reovirus with RELA nuclear translocation and cell death rates proportional to MOI. In individual PANC1 cells, RELA either translocates to the nucleus as a single transient pulse,

or gradually increases and plateaus with high RELA nuclear localisation. Notably, RELA responses are delayed (~12hr) but more intense with reovirus infection compared to TNFα. For example, the maximum RELA ratio in PANC1 cells for 0.1 ng/ml TNFα is 1.15 and for reovirus at MOI 20 is 1.66. Therefore, single cell RELA responses to reovirus in PDAC cells are entirely divergent to those observed with TNFα.

Work by Barton et al. (2001) identified the requirement for binding of the viral attachment protein σ1 to junction adhesion molecule A (JAM-A) for reovirus infection in human neuronal-precursor cells. Moreover, Barton et al. showed that reovirus-induced NF-κB activation is dependent on JAM-A. Therefore, differences in JAM-A expression may explain the susceptibility of PANC1 cells and resistance of MIA PaCa2 cells to reovirus infection. Indeed, the gene encoding JAM-A, *F11R*, is present in the list of genes identified by RNA-seq to be differentially expressed between MIA PaCa2 and PANC1 cells (Appendix Table A2). Notably, the RNA expression of *F11R* is approximately 54 times higher in PANC1 cells compared to MIA PaCa2 cells, which would explain the observed reovirus-induced RELA nuclear translocation and cell death exclusively in the PANC1 cell line. Subsequently, inhibition or depletion of JAM-A in PANC1 cells, or re-expression of JAM-A in MIA PaCa2 cells, should be tested to validate this hypothesis.

PANC1 cells also respond to reovirus infection distinctly to A375 cells, as A375 cells have switch-like RELA activation rapidly followed by cell death. Better insight into the signalling molecules contributing to the disparate RELA dynamics could be efficiently gained by phosphoproteomics analysis at various timepoints (e.g. 0, 12, 24, 36, 48 hours) after reovirus infection. This would also aid in establishing the relationship between RELA and the transcription factor IRF3, which correlated in subcellular localisation on the single cell level (Figure 6.6). RNA-seq analysis revealed that IRF3 is unlikely to be upregulated by NF-κB activation by TNFα, or TNFα itself, in PDAC cells. However, TNFα did upregulate the related transcription factor IRF1 via RELA in both MIA PaCa2 and PANC1 cells. Since ectopic expression of IRF1 protects cells from infection of a diverse range of RNA viruses

(Schoggins et al., 2011), IRF1 expression may present another mechanism for protection by MIA PaCa2 cells against reovirus infection.

Future work into single cell RELA responses in PDAC cells could consider responses to alternative inputs. For instance, RELA responses to LPS or immune molecules relevant to PDAC, including IL-6 (Okada et al., 1998) and IL-1α (Tjomsland et al., 2011), as well as the chemokines identified by RNA-seq as upregulated by TNFα in PDAC cells: CXCL1 and CXCL8. Furthermore, RELA responses should be tested with other oncolytic viruses implemented in the clinic, such as the dsDNA virus RP1 (Emamekhoo et al., 2022). In particular, it would be interesting to test whether RELA activation in PDAC cells affects chemotaxis of immune cells, which is the case for reovirus-infected melanoma cells with dendritic cells (Steele et al., 2011). Ultimately, analysis of RELA responses could be carried out in mice using orthotopic PDAC tumours, in order to determine whether the dynamics observed in 2D culture translate in vivo (Sparks et al., 2018). This would be best carried out with endogenous tagging of RELA in mouse cells to enable the use of mice with intact immune systems.

7.2 Roles for RELA in PDAC cells

The distinct RELA dynamics displayed by PDAC cells in response to TNFα suggest that RELA may have unique biological functions in PDAC cells, since RELA target gene expression is dependent on the parameters (frequency, period, amplitude) of RELA oscillations (Nelson et al., 2004). This thesis provides a mechanistic basis for RELA regulation of the cytoskeleton (discussed in Section 7.3), cell survival, and immune components in PDAC.

For all RELA targets, target gene expression could be linked to single cell RELA dynamics by performing live imaging of RELA-GFP followed by single cell RNA-seq, while conserving cell identity. Lane et al. (2017) achieved this by live imaging mouse macrophages expressing murine RelA fused to a GFP variant, in combination with RNA-seq carried out at three

timepoints. Another approach would be to use live imaging followed by endpoint immunofluorescence with iterative staining (Gut et al., 2018). This method would be more straightforward to keep track of cells but is dependent on antibody availability. Due to the demand of these workflows, it would be generally beneficial to initially validate the identified RELA targets using Ch-IP.

7.2.1 Cell survival

TNFα can upregulate both pro-survival and pro-cell death signalling (Kelliher et al., 1998). In PDAC cells, live imaging revealed that PDAC cells continue to proliferate at high TNFα levels (Figure 3.6A), although a subset of cells undergo cell death at rates proportional to TNFα dose. Experiments with IκB-SR revealed that RELA is needed for cell survival of MIA PaCa2 and PANC1 cells on the population level (Figure 3.6E). However, on the single cell level, MIA PaCa2 cells with higher RELA ratio and higher nuclear RELA abundance die in response to 0.1 ng/ml or 10 ng/ml TNFα (Figure 3.7), though no relationship between RELA dynamics and cell death was identified in PANC1 cells (Figure 3.8). The cell line discrepancy may be related to the significantly higher upregulation of TNFα-regulated genes by MIA PaCa2 compared to PANC1, as shown by RNA-seq.

In addition to proteins directly in the TNFα pathway, like those related to the TNFα receptor, RELA activation in PDAC cells upregulates genes that encode proteins that may control cell survival. One example is NUAK2, which inhibits cell death induced by diverse mechanisms, as reviewed thoroughly by van de Vis et al., 2021. Key instances include NUAK2 protection against Fas-induced apoptosis in MCF7 cells (Legembre et al., 2004) and promotion of ROCK-mediated cell survival in myoblasts (Lessard et al., 2016). TNFα-induced RELA activation is also associated with elevated *BIRC3* expression. BIRC3 is reported to suppress TNFα cytotoxicity by upregulating the pro-survival functions of RELA (Chu et al., 1997).

Furthermore, Co-IP revealed that RELA directly binds to several mitochondrial-associated proteins: TIMMDC1, TOMM40, TIMM25B, NDUFA4, TUFM, and three SLC25 family

members (full names in Abbreviations list). The interactions between RELA and these mitochondrial proteins could be investigated to better understand RELA regulation of apoptosis. The type of cell death initiated by TNFα in PDAC cells could also be narrowed down through the use of caspase inhibitors and by checking the expression of RIPK1 and RIPK3 (Annibaldi and Meier, 2018; Legrand et al., 2019). With reovirus infection, it would be interesting to test whether IκB-SR expression or IKK inhibition increase or decrease cell death in PDAC and melanoma cells, given the body of literature associating RELA with the promotion of cell death in this context (Knowlton et al., 2012; Thirukkumaran et al., 2017).

7.2.2 Immune system

RELA plays a major role in hematopoiesis, in particular DC and granulocyte development, lymphocyte survival maturation, and the development of secondary lymphoid tissues (Beg et al., 1995a; Alcamo et al., 2002; Wang et al., 2007). RELA also functions in the activation of macrophages in the innate immune response through cytokine and chemokine upregulation (Collart et al., 1990). These functions can contribute to anti-tumour immunity (He et al., 2010) but may also promote oncogenesis (Ling et al., 2012), as supported by the frequent mutations in NF-κB signalling leading to constitutive RELA activity in lymphoid malignancies (Bargou et al., 1997; Nagel et al., 2014). RELA is also hyperactive in several inflammation-associated solid tumours, including pancreatic cancer (Wang et al., 1999; Qian et al., 2020).

Using RNA-seq, I identified that TNFα-driven RELA activation significantly upregulates the non-canonical NF-κB transcription factors RELB and NFKB2. Unlike the wide-reaching canonical NF-κB pathway, the non-canonical pathway is primarily responsible for immune cell development (Morrison et al., 2005). My data suggest that sustained RELA activation leads to *RELB* and *NFKB2* expression, as *RELB* and *NFKB2* have higher RNA expression at 5 hr than 1 hr following TNFα treatment. *RELB* and *NFKB2* expressions are also dependent on RELA nuclear translocation. The temporal expression of RELB and NFKB2 is in line with

the consensus that, compared to the canonical pathway, non-canonical NF-κB activity builds more slowly and relies on de novo protein synthesis (Sun, 2011). Interestingly, I found that TNFα upregulates the expression of *BIRC3* (encoding Baculoviral IAP repeat-containing protein 3) via RELA with similar dynamics to RELB and NFKB2. As BIRC3 is implicated in suppressing alternative NF-κB signalling (Zarnegar et al., 2008), the effects of TNFα and RELA on non-canonical NF-κB signalling are complex. Overall, it would be worthwhile to fluorescently tag RELB in RELA-GFP-expressing PDAC cells and quantify the connections between their dynamics. A good line of enquiry would be to relate RELA and RELB dynamics to the development of immune cell subtypes co-cultured with PDAC cells.

RNA-seq also showed that RELA upregulates the chemokine *CXCL1*. CXCL1 binds to the receptor CXCR2 (Ravindran et al., 2013) and studies have associated CXCL1-CXCR2 to PDAC using mouse models with varied results. In one study, *Cxcr2* knockout in *Kras*^{G12D} mice had prolonged survival associated with inhibition of PDAC angiogenesis and invasion. This study also provided evidence that the CXCL1-CXCL2 axis controls the proportion of M1 versus M2-like tumour-associated macrophages infiltrating the tumour (Sano et al., 2019). Conversely, another study found that CXCR2 promotes senescence, with pancreas-specific *Cxcr2* ablation in *Kras*^{G12D} mice increasing cell proliferation and reducing mouse survival (Lesina et al., 2016). Therefore, the role of RELA upregulation of CXCL1 and its effect on PDAC initiation and progression remains an intriguing source for further study.

7.3 Crosstalk between RELA nuclear translocation and actin dynamics in PDAC cells

In this thesis, I have extended the understanding of cytoskeletal and cell shape regulation of RELA in PDAC cells. Using high throughput and high content image analysis combined with Bayesian analysis, I discovered that heterogeneity in RELA localisation in MIA PaCa2 and PANC1 cells is linked to actin organisation and cell shape.

I tested the effects of small molecule inhibitors targeting various aspects of cytoskeletal dynamics and found that formin inhibition in MIA PaCa2 cells and ARP2/3 inhibition in PANC1 cells downregulates nuclear RELA localisation. These results provide evidence that the nucleation of actin stress fibres and branched actin function in regulating RELA activation with TNFα. Across a panel of PDAC lines, MIA PaCa2 cells have notably small cell area, low nucleus roundness, and actin more localised to stress fibres, while PANC1 have high cell aspect ratio and actin more localised to the cortex (Figure 4.2). These contrasting morphologies likely contribute to the disparate contributions of actin components to RELA activation. Moreover, a number of genes involved in cytoskeletal dynamics, including several integrins, are differentially expressed between MIA PaCa2 and PANC1 cells (Appendix Table A2).

Using conditional IκB-SR expression and immunofluorescence, I additionally found that TNFα and RELA regulate the cytoskeleton (Figure 4.9). In particular, TNFα causes elongation and moderate enlargement of MIA PaCa2 cells, while TNFα in combination with IκB-SR induction enhances actin stress fibre formation. In support of this, RNA-seq identified that RELA significantly upregulates expression of *ARHGAP31* and *NUAK2*, which are previously implicated in actin regulation (Lamarche-Vane and Hall, 1998; Vallenius et al., 2011). Given that NUAK2 is implicated in cell survival (Legembre et al., 2004; Lessard et al., 2016), NUAK2 may be a central link between RELA signalling, actin dynamics, and cell fate. Follow-up should focus on whether NUAK2 and ARHGAP31 promote RELA activation in positive feedforward loops, in addition to considering the effect of *ARHGAP31* and *NUAK2* depletion on actin stress fibres and branched actin. Alternatively, analysis of RELA, actin and cell survival could consider the interaction between RELA and the mitochondrial protein TIMMDC1 pulled down by GFP-Trap, as *TIMMDC1* is present at the same genomic locus as *ARHGAP31* (Chromosome 3q13.33).

The data in this thesis could be explored further by testing how the PDAC stroma affects the relationship between RELA, actin and cell shape. Moreover, research could look into

whether actin and cell shape affect the susceptibility of PDAC cells to oncolytic viruses or whether oncolytic viruses promote EMT associated with RELA upregulation. Initial proof of this concept comes from NF-κB regulation of the T cell leukaemia virus type I protein Tax in the promotion of vimentin expression (Lilienbaum et al., 1990), as well as RELA-dependent enhanced expression of vimentin, fibronectin and Snail family zinc finger 1 following stimulation with the synthetic dsRNA analogue poly(I:C) (Tian et al., 2017).

7.4 Targeting RELA signalling as a therapeutic route for PDAC treatment

In non-resected PDAC patients, the 5-year survival has remained unchanged from 1975 to 2011 (Bengtsson et al., 2020), warranting the need for identification of new therapeutic routes to target PDAC. RELA is hyperactive in 50-70 % of PDAC tumours (Wang et al., 1999; Vimalachandran et al., 2005; Weichert et al., 2007) and contributes to both cancer progression (Fujioka et al., 2003a; Melisi et al., 2009) and resistance to chemotherapy (Bold et al., 2001; Kunnumakkara et al., 2007).

Using a systems biology approach, I identified 57 proteins (Figure 5.4C - central sections of the Venn diagram) which can be viewed as prime candidates for targeting RELA signalling in PDAC. These candidates could be used in RNAi or CRISPRi high-throughput screens assaying cell survival and RELA activation, or narrowed down based on which are currently druggable. NUAK2 may be a promising target as kinases contain an ATP-binding cleft that is a druggable pocket and can contain additional druggable sites distal to the ATP or substrate binding pockets conferring inhibitor specificity (Lamba and Ghosh, 2012). Meanwhile, there are readily available rescue constructs for ARHGAP31 that provide a practical benefit for testing ARHGAP31 domain contributions to desired phenotypes (He et al., 2011). Alternatively, research may choose to focus on one of the novel RELA interactors identified by Co-IP in MIA PaCa2 cells: FHL2, GREB1, RAB11B, RAB3GAP2, RRBP1, SPTCL, and TUBB3; since these may provide PDAC-specific vulnerabilities for targeting RELA. Finally, a route for enhancing RELA activity could be to target DUSP1, for which the RNA and protein

levels are upregulated by TNFα (Figure 5.1C and Figure 5.3B). DUSP1 elevates TNFα (Shah et al., 2016) and also targets ERK activity (Camps et al., 2000), which could potentially offset the KRAS overactivation characteristic of PDAC.

Nonetheless, targeting of RELA in PDAC cells requires careful consideration of the pleiotropic nature of RELA activity. It is important to modulate RELA activity in a way that enhances tumour suppressive effects, such as cell death and activation of immune cells, without encouraging oncogenic processes like EMT, proliferation, or survival of tumour cells. The promotion of inflammation harmful to the patient also needs to be avoided. Issues with the diverse activities of RELA have led to toxic effects that have limited the progression of therapies targeting NF-κB signalling in the clinic (Ramadass et al., 2020). In addition to focusing on targets with PDAC-specific expression, inflated RELA activity in PDAC cells could be exploited for therapeutic gain. For instance, it may be the case that moderate RELA activity promotes cell survival, while sustained and elevated RELA activation leads to cell death. This is indicated by the association of cell death with high RELA ratios on the single cell level in MIA PaCa2 cells treated with TNFα and in PANC1 and A375 cells infected with reovirus. Therefore, systemic upregulation of RELA activity may be more likely to induce cell death in PDAC than tissues with lower basal levels of RELA activity.

A promising aim for targeting RELA dynamics would be to improve the efficacy of oncolytic viruses and other immunotherapies, as RELA is a master regulator of the immune system (Hayden et al., 2006) and oncolytic viruses are inherently cancer-specific (Hashiro et al., 1977; Duncan et al., 1978). Furthermore, dsDNA viruses can be genetically engineered to target other aspects of PDAC biology, such as the incorporation of hyaluronidase enzymes to target the PDAC stroma (Rodríguez-García et al., 2015). This thesis provides compelling evidence that RELA can be used as a readout to assess oncolytic virus efficacy in high throughput screens.

7.5 Limitations

In addition to the limitations outlined in sections 7.1-7.4, I identified other limitations of this thesis that function as sources for further study.

The majority of experiments in this thesis assaying RELA dynamics in PDAC were limited to two pancreatic cancer cell lines (MIA PaCa2 and PANC1), both of which are immortalised non-primary human models. Whether the conclusions identified in this thesis, in particular the sustained activation and lack of oscillations in RELA signalling with TNFα, are general to all pancreatic cancer cell lines or specific to the two that were studied are unclear. Furthermore, the aspects of pancreatic cell lines that make them highly sensitive to TNFα remain unknown. This thesis provides a clue that differences in IκB factors may distinguish pancreatic cells from cells of other tissue origin, however, how differences in IκB proteins arise - e.g. by genetic, biochemical or extracellular means - need to be studied further. A direct comparison between cell lines of pancreatic and alternative origins also needs to be carried out.

A general limitation of the experiments used throughout this thesis is that they are performed in 2D adhered models. While 2D models are cost-effective and simple models that are useful for hypothesis generation, they lack important aspects of in vivo tumours (as reviewed by Kapałczyńska et al., 2018). Protocols for developing pancreatic organoids derived from patient samples or from stem cells have vastly improved in recent years (Huang et al., 2015; Driehuis et al., 2019) and are generally accepted to recapitulate the morphology of patient tumours on both the micro (single cell) and macro (pancreatic structures) scale (Jensen and Teng, 2020). Moreover, organoids and other complex 3D models can incorporate components of the PDAC tumour microenvironment that are predicted to affect RELA signalling, including fibrosis/stiffness (Sero et al., 2015), CAFs themselves (Huang et al., 2021), and immune cells (Baeuerle and Henkel, 1994).

In Chapter 4, I described mechanosensitivity of RELA in terms of disruption of RELA nuclear translocation by drugs targeting cell shape and the actin and tubulin cytoskeletons. In addition, I identified correlations between TNFα-induced RELA nuclear localisation and measurements of actin abundance and organisation. Nonetheless, this thesis does not test whether these phenomena are RELA-specific or general mechanisms of transcription factor regulation. To determine this, the same experimental conditions should be repeated with assay of other transcription factors, such as p53, AP1 and IRF proteins, as well as the other NF-κB proteins and the mechanosensitive co-activator YAP. Furthermore, the result that actin nucleation and branching impacts RELA nuclear translocation is reliant on the use of a small molecule drug (SMIFH2) with identified non-specific targets (Isogai et al., 2015). A role of formin activity in the regulation of RELA should be confirmed by other means, e.g. siRNA of a range of formins and associated rescue experiments (Copeland et al., 2007; Young and Copeland, 2010).

In Chapter 5, I identified TNFα-regulated genes with use of a non-degradable form of IκB to determine which of these genes rely on RELA nuclear translocation. While this approach identifies genes reliant on RELA, it does not identify whether the genes are direct or indirect RELA targets. This could be checked using promoter analysis for presence of the NF-κB motif for each gene or confirmed directly using ChIP-Seq (examples in Borghini et al., 2018 and Ngo et al., 2020).

Lastly, in Chapter 6, I observed cell-to-cell variability in responsiveness to reovirus in terms of RELA nuclear translocation, with A375 melanoma cells shown to have binary RELA nuclear translocation with reovirus infection. However, this thesis does not identify which factors determine whether a cell is RELA-responsive. Ideally, the responsive and non-responsive cells could be isolated and sequenced on the DNA and RNA/protein level, in order to determine if there are genetic differences or differences in cell states that correlate with RELA responsiveness to reovirus. A difficulty in this is that A375 cells that have reovirus-induced RELA nuclear translocation die quickly after this translocation event, which

could be overcome by using an apoptosis inhibitor. Alternatively, RELA-responsive and non-responsive cells could be assessed using single cell RNA-seq, with cells expressing high levels of *NFKBIA* and other TNFα signalling pathway genes as those that are likely to have high RELA nuclear localisation.

7.6 Summary

This thesis used high content and high throughput automated image analysis to characterise endogenous RELA dynamics in human PDAC cells in response to two immune-related inputs: TNFα and reoviruses. Critically, this work was carried out in a tumour type in which there is a pressing need for novel therapeutics and additionally in which TNFα and RELA activity are clinically relevant (Wang et al., 1999; Zhao et al., 2016).

Strikingly, live imaging analysis revealed that PDAC cells respond atypically to TNFα with sustained, non-oscillatory and cell cycle independent responses. I also found that the PDAC cell line more sensitive to TNFα, MIA PaCa2, is resistant to reovirus infection, while PANC1 cells respond to reovirus infection with intense and sustained RELA nuclear translocation followed by gradual cell death. Remarkably, high RELA nuclear translocation was associated with cell death with both TNFα and reovirus exposure.

Using immunofluorescence, Bayesian analysis and small molecule inhibition, I identified that actin abundance and organisation correlate with heterogeneity in RELA nuclear translocation on the single cell level. In particular, MIA PaCa2 cells with actin high stress fibre abundance and PANC1 cells with more branched actin have higher RELA nuclear translocation with TNFα. Combining RNA-seq, Co-IP and proteomics, I identified that TNFα and RELA regulate multiple genes encoding proteins involved in cytoskeletal dynamics, including ARHGAP31 and NUAK2. TNFα and RELA also modulate several stages in the TNFα signalling pathway. Notably, sustained RELA activation upregulates the *NFKBIB* and *NFKBIE* genes encoding the RELA inhibitors IκBβ and IκBε, as well as the non-canonical NF-κB factors RELB and NFKB2.

Future work should use the identified feedback loops involving RELA and actin as a strong basis for modulating RELA activity in PDAC and/or enhancing responses to oncolytic viruses, particularly focusing on the candidates identified by multiomics. Targeting RELA may also exploit the sustained RELA activation observed in PDAC cells for therapeutic gain. Finally, the relationship between RELA and various IκB proteins warrants further investigation to understand the control of RELA activity in PDAC cells.

7.7 Conclusions

To characterise RELA dynamics in PDAC cells, I tagged RELA endogenously with GFP using CRISPR-CAS9 in the PDAC cell lines MIA PaCa2 and PANC1. I exposed PDAC cells to the cytokine TNFα or to the oncolytic virus reovirus and quantified live RELA-GFP dynamics using automated image analysis. TNFα stimulated rapid RELA nuclear translocation in both PDAC cell lines, with MIA PaCa2 cells maintaining high nuclear RELA localisation for a prolonged (10 hr imaging) period and PANC1 cells displaying gradual re-localisation of RELA to the cytoplasm. Reovirus infection caused cell death and RELA nuclear translocation with delayed dynamics compared to TNFα and exclusively in the PANC1 cell line. Notably, TNFα and reovirus generated extensive heterogeneity between and within cell lines in RELA nuclear localisation. Using Bayesian network analysis, I predicted that differences in RELA localisation with TNFα are conditionally dependent on differences in actin organisation. To test this, I treated PDAC cells with small molecule inhibitors targeting cell shape and cytoskeletal dynamics, which could suppress or enhance TNFα-induced RELA nuclear translocation in a cell line-specific manner. Finally, I identified a number of genes dependent on TNFα and RELA nuclear translocation, including the actin regulators *NUAK2* and *ARHGAP31*, which may be important for RELA dynamics in PDAC cells. These prospective RELA targets may also be used as candidates for targeting RELA signalling in PDAC.

Bibliography

Agematsu, K., Nagumo, H., Oguchi, Y., Nakazawa, T., Fukushima, K., Yasui, K., Ito, S., Kobata, T., Morimoto, C., and Komiyama, A. (1998). Generation of plasma cells from peripheral blood memory B cells: synergistic effect of interleukin-10 and CD27/CD70 interaction. Blood *91*, 173–180.

Aigner, K., Dampier, B., Descovich, L., Mikula, M., Sultan, A., Schreiber, M., Mikulits, W., Brabletz, T., Strand, D., Obrist, P., et al. (2007). The transcription factor ZEB1 (deltaEF1) promotes tumour cell dedifferentiation by repressing master regulators of epithelial polarity. Oncogene *26*, 6979–6988.

Aksenova, V., Turoverova, L., Khotin, M., Magnusson, K.-E., Tulchinsky, E., Melino, G., Pinaev, G.P., Barlev, N., and Tentler, D. (2013). Actin-binding protein α-actinin 4 (ACTN4) is a transcriptional co-activator of RelA/p65 sub-unit of NF-kB. Oncotarget *4*, 362–372.

Albahde, M.A.H., Abdrakhimov, B., Li, G.-Q., Zhou, X., Zhou, D., Xu, H., Qian, H., and Wang, W. (2021). The Role of Microtubules in Pancreatic Cancer: Therapeutic Progress. Front. Oncol. *11*, 640863.

Alcamo, E., Mizgerd, J.P., Horwitz, B.H., Bronson, R., Beg, A.A., Scott, M., Doerschuk, C.M., Hynes, R.O., and Baltimore, D. (2001). Targeted Mutation of TNF Receptor I Rescues the RelA-Deficient Mouse and Reveals a Critical Role for NF-κB in Leukocyte Recruitment. J. Immunol. *167*, 1592–1600.

Alcamo, E., Hacohen, N., Schulte, L.C., Rennert, P.D., Hynes, R.O., and Baltimore, D. (2002). Requirement for the NF-κB family member RelA in the development of secondary lymphoid organs. J. Exp. Med. *195*, 233–244.

Alexopoulou, L., Holt, A.C., Medzhitov, R., and Flavell, R.A. (2001). Recognition of double-stranded RNA and activation of NF-κB by Toll-like receptor 3. Nature *413*, 732–738.

Allfrey, V.G., Faulkner, R., and Mirsky, A.E. (1964). Acetylation and methylation of histones and their possible role in the regulation of RNA synthesis. Proc. Natl. Acad. Sci. U. S. A. *51*, 786–794.

Almoguera, C., Shibata, D., Forrester, K., Martin, J., Arnheim, N., and Perucho, M. (1988). Most human carcinomas of the exocrine pancreas contain mutant c-K-ras genes. Cell *53*, 549–554.

Alves, C.C., Carneiro, F., Hoefler, H., and Becker, K.-F. (2009). Role of the epithelial-mesenchymal transition regulator Slug in primary human cancers. Front. Biosci. Landmark Ed. *14*, 3035–3050.

Amarante-Mendes, G.P., Finucane, D.M., Martin, S.J., Cotter, T.G., Salvesen, G.S., and Green, D.R. (1998). Anti-apoptotic oncogenes prevent caspase-dependent and independent commitment for cell death. Cell Death Differ. *5*, 298–306.

Amato, C.M., Hintzsche, J.D., Wells, K., Applegate, A., Gorden, N.T., Vorwald, V.M., Tobin, R.P., Nassar, K., Shellman, Y.G., Kim, J., et al. (2020). Pre-Treatment Mutational and Transcriptomic Landscape of Responding Metastatic Melanoma Patients to Anti-PD1 Immunotherapy. Cancers *12*, 1943.

Amiri, K.I., Horton, L.W., LaFleur, B.J., Sosman, J.A., and Richmond, A. (2004). Augmenting

chemosensitivity of malignant melanoma tumors via proteasome inhibition: implication for bortezomib (VELCADE, PS-341) as a therapeutic agent for malignant melanoma. Cancer Res. *64*, 4912–4918.

Anastasiadis, P.Z., Moon, S.Y., Thoreson, M.A., Mariner, D.J., Crawford, H.C., Zheng, Y., and Reynolds, A.B. (2000). Inhibition of RhoA by p120 catenin. Nat. Cell Biol. *2*, 637–644.

Andtbacka, R.H.I., Collichio, F., Harrington, K.J., Middleton, M.R., Downey, G., Öhrling, K., and Kaufman, H.L. (2019). Final analyses of OPTiM: a randomized phase III trial of talimogene laherparepvec versus granulocyte-macrophage colony-stimulating factor in unresectable stage III-IV melanoma. J. Immunother. Cancer *7*, 145.

Ankers, J.M., Awais, R., Jones, N.A., Boyd, J., Ryan, S., Adamson, A.D., Harper, C.V., Bridge, L., Spiller, D.G., Jackson, D.A., et al. (2016). Dynamic NF-κB and E2F interactions control the priority and timing of inflammatory signalling and cell proliferation. eLife *5*, e10473.

Annibaldi, A., and Meier, P. (2018). Checkpoints in TNF-Induced Cell Death: Implications in Inflammation and Cancer. Trends Mol. Med. *24*, 49–65.

Annunziata, C.M., Davis, R.E., Demchenko, Y., Bellamy, W., Gabrea, A., Zhan, F., Lenz, G., Hanamura, I., Wright, G., Xiao, W., et al. (2007). Frequent engagement of the classical and alternative NF-κB pathways by diverse genetic abnormalities in multiple myeloma. Cancer Cell *12*, 115–130.

Antwerp, D.J.V., Martin, S.J., Kafri, T., Green, D.R., and Verma, I.M. (1996). Suppression of TNF-α-Induced Apoptosis by NF-κB. Science *274*, 787–789.

Ardito, C.M., Grüner, B.M., Takeuchi, K.K., Lubeseder-Martellato, C., Teichmann, N., Mazur, P.K., Delgiorno, K.E., Carpenter, E.S., Halbrook, C.J., Hall, J.C., et al. (2012). EGF receptor is required for KRAS-induced pancreatic tumorigenesis. Cancer Cell *22*, 304–317.

Arenzana-Seisdedos, F., Turpin, P., Rodriguez, M., Thomas, D., Hay, R.T., Virelizier, J.L., and Dargemont, C. (1997). Nuclear localization of IκBα promotes active transport of NF-κB from the nucleus to the cytoplasm. J. Cell Sci. *110*, 369–378.

Arlt, A., Vorndamm, J., Müerköster, S., Yu, H., Schmidt, W.E., Fölsch, U.R., and Schäfer, H. (2002). Autocrine production of interleukin 1β confers constitutive nuclear factor κB activity and chemoresistance in pancreatic carcinoma cell lines. Cancer Res. *62*, 910–916.

Arlt, A., Gehrz, A., Müerköster, S., Vorndamm, J., Kruse, M.-L., Fölsch, U.R., and Schäfer, H. (2003). Role of NF-κB and Akt/PI3K in the resistance of pancreatic carcinoma cell lines against gemcitabine-induced cell death. Oncogene *22*, 3243–3251.

Aronica, M.A., Mora, A.L., Mitchell, D.B., Finn, P.W., Johnson, J.E., Sheller, J.R., and Boothby, M.R. (1999). Preferential Role for NF-κB/Rel Signaling in the Type 1 But Not Type 2 T Cell-Dependent Immune Response In Vivo. J. Immunol. *163*, 5116–5124.

Ashall, L., Horton, C.A., Nelson, D.E., Paszek, P., Harper, C.V., Sillitoe, K., Ryan, S., Spiller, D.G., Unitt, J.F., Broomhead, D.S., et al. (2009). Pulsatile stimulation determines timing and specificity of NF-κB-dependent transcription. Science *324*, 242–246.

Ashburner, B.P., Westerheide, S.D., and Baldwin, A.S. (2001). The p65 (RelA) Subunit of NF-κB Interacts with the Histone Deacetylase (HDAC) Corepressors HDAC1 and HDAC2 To Negatively Regulate Gene Expression. Mol. Cell. Biol. *21*, 7065–7077.

Aspenström, P., Richnau, N., and Johansson, A.-S. (2006). The diaphanous-related formin DAAM1 collaborates with the Rho GTPases RhoA and Cdc42, CIP4 and Src in regulating

cell morphogenesis and actin dynamics. Exp. Cell Res. *312*, 2180–2194.

Babakov, V.N., Petukhova, O.A., Turoverova, L.V., Kropacheva, I.V., Tentler, D.G., Bolshakova, A.V., Podolskaya, E.P., Magnusson, K.-E., and Pinaev, G.P. (2008). RelA/NF-κB transcription factor associates with α-actinin-4. Exp. Cell Res. *314*, 1030–1038.

Baer, M., Dillner, A., Schwartz, R.C., Sedon, C., Nedospasov, S., and Johnson, P.F. (1998). Tumor necrosis factor α transcription in macrophages is attenuated by an autocrine factor that preferentially induces NF-κB p50. Mol. Cell. Biol. *18*, 5678–5689.

Baeuerle, P.A., and Baltimore, D. (1988a). Activation of DNA-binding activity in an apparently cytoplasmic precursor of the NF-κB transcription factor. Cell *53*, 211–217.

Baeuerle, P.A., and Baltimore, D. (1988b). IκB: a specific inhibitor of the NF-κB transcription factor. Science *242*, 540–546.

Baeuerle, P.A., and Baltimore, D. (1989). A 65-kD subunit of active NF-κB is required for inhibition of NF-κB by IκB. Genes Dev. *3*, 1689–1698.

Baeuerle, P.A., and Henkel, T. (1994). Function and activation of NF-κB in the immune system. Annu. Rev. Immunol. *12*, 141–179.

Bagnall, J., Boddington, C., Boyd, J., Brignall, R., Rowe, W., Jones, N.A., Schmidt, L., Spiller, D.G., White, M.R.H., and Paszek, P. (2015). Quantitative dynamic imaging of immune cell signalling using lentiviral gene transfer. Integr. Biol. Quant. Biosci. Nano Macro *7*, 713–725.

Bakal, C., Aach, J., Church, G., and Perrimon, N. (2007). Quantitative morphological signatures define local signaling networks regulating cell morphology. Science *316*, 1753–1756.

Balkwill, F. (2009). Tumour necrosis factor and cancer. Nat. Rev. Cancer *9*, 361–371.

Bannister, A.J., and Kouzarides, T. (1996). The CBP co-activator is a histone acetyltransferase. Nature *384*, 641–643.

Bargou, R.C., Emmerich, F., Krappmann, D., Bommert, K., Mapara, M.Y., Arnold, W., Royer, H.D., Grinstein, E., Greiner, A., Scheidereit, C., et al. (1997). Constitutive nuclear factor-κB-RelA activation is required for proliferation and survival of Hodgkin's disease tumor cells. J. Clin. Invest. *100*, 2961–2969.

Barkett, M., and Gilmore, T.D. (1999). Control of apoptosis by Rel/NF-κB transcription factors. Oncogene *18*, 6910–6924.

Barnes, M.J., Krebs, P., Harris, N., Eidenschenk, C., Gonzalez-Quintial, R., Arnold, C.N., Crozat, K., Sovath, S., Moresco, E.M., Theofilopoulos, A.N., et al. (2009). Commitment to the regulatory T cell lineage requires CARMA1 in the thymus but not in the periphery. PLoS Biol. *7*, e51.

Barr, A.R., and Bakal, C. (2015). A sensitised RNAi screen reveals a ch-TOG genetic interaction network required for spindle assembly. Sci. Rep. *5*, 10564.

Barr, A.R., Cooper, S., Heldt, F.S., Butera, F., Stoy, H., Mansfeld, J., Novák, B., and Bakal, C. (2017). DNA damage during S-phase mediates the proliferation-quiescence decision in the subsequent G1 via p21 expression. Nat. Commun. *8*, 1–17.

Bar-Sagi, D., and Hall, A. (2000). Ras and Rho GTPases: A Family Reunion. Cell *103*, 227–238.

Barton, E.S., Forrest, J.C., Connolly, J.L., Chappell, J.D., Liu, Y., Schnell, F.J., Nusrat, A., Parkos, C.A., and Dermody, T.S. (2001). Junction Adhesion Molecule Is a Receptor for Reovirus. Cell *104*, 441–451.

Bash, J., Zong, W.X., and Gélinas, C. (1997). c-Rel arrests the proliferation of HeLa cells and affects critical regulators of the G1/S-phase transition. Mol. Cell. Biol. *17*, 6526–6536.

Batchelor, E., Loewer, A., Mock, C., and Lahav, G. (2011). Stimulus-dependent dynamics of p53 in single cells. Mol. Syst. Biol. *7*, 488.

Batlle, E., Sancho, E., Francí, C., Domínguez, D., Monfar, M., Baulida, J., and García de Herreros, A. (2000). The transcription factor Snail is a repressor of E-cadherin gene expression in epithelial tumour cells. Nat. Cell Biol. *2*, 84–89.

Bazan-Peregrino, M., Garcia-Carbonero, R., Laquente, B., Álvarez, R., Mato-Berciano, A., Gimenez-Alejandre, M., Morgado, S., Rodríguez-García, A., Maliandi, M.V., Riesco, M.C., et al. (2021). VCN-01 disrupts pancreatic cancer stroma and exerts antitumor effects. J. Immunother. Cancer *9*, e003254.

Beatty, G.L., Chiorean, E.G., Fishman, M.P., Saboury, B., Teitelbaum, U.R., Sun, W., Huhn, R.D., Song, W., Li, D., Sharp, L.L., et al. (2011). CD40 agonists alter tumor stroma and show efficacy against pancreatic carcinoma in mice and humans. Science *331*, 1612–1616.

Beg, A.A., and Baltimore, D. (1996). An Essential Role for NF-κB in Preventing TNF-α-Induced Cell Death. Science *274*, 782–784.

Beg, A.A., Ruben, S.M., Scheinman, R.I., Haskill, S., Rosen, C.A., and Baldwin, A.S. (1992). IκB interacts with the nuclear localization sequences of the subunits of NF-κB: a mechanism for cytoplasmic retention. Genes Dev. *6*, 1899–1913.

Beg, A.A., Sha, W.C., Bronson, R.T., Ghosh, S., and Baltimore, D. (1995a). Embryonic lethality and liver degeneration in mice lacking the RelA component of NF-κB. Nature *376*, 167–170.

Beg, A.A., Sha, W.C., Bronson, R.T., and Baltimore, D. (1995b). Constitutive NF-κB activation, enhanced granulopoiesis, and neonatal lethality in IκBα-deficient mice. Genes Dev. *9*, 2736–2746.

Beggs, A.H., Byers, T.J., Knoll, J.H., Boyce, F.M., Bruns, G.A., and Kunkel, L.M. (1992). Cloning and characterization of two human skeletal muscle α-actinin genes located on chromosomes 1 and 11. J. Biol. Chem. *267*, 9281–9288.

Bendall, H.H., Sikes, M.L., Ballard, D.W., and Oltz, E.M. (1999). An intact NF-κB signaling pathway is required for maintenance of mature B cell subsets. Mol. Immunol. *36*, 187–195.

Bengtsson, A., Andersson, R., and Ansari, D. (2020). The actual 5-year survivors of pancreatic ductal adenocarcinoma based on real-world data. Sci. Rep. *10*, 16425.

Berg, S., Kutra, D., Kroeger, T., Straehle, C.N., Kausler, B.X., Haubold, C., Schiegg, M., Ales, J., Beier, T., Rudy, M., et al. (2019). ilastik: interactive machine learning for (bio)image analysis. Nat. Methods *16*, 1226–1232.

Berger, A.K., and Danthi, P. (2013). Reovirus Activates a Caspase-Independent Cell Death Pathway. MBio *4*, e00178-13.

Berger, A.K., Hiller, B.E., Thete, D., Snyder, A.J., Perez, E., Upton, J.W., and Danthi, P. (2017). Viral RNA at Two Stages of Reovirus Infection Is Required for the Induction of Necroptosis. J. Virol. *91*, e02404-16.

Berghe, W.V., Bosscher, K.D., Boone, E., Plaisance, S., and Haegeman, G. (1999). The Nuclear Factor-κB Engages CBP/p300 and Histone Acetyltransferase Activity for Transcriptional Activation of the Interleukin-6 Gene Promoter. J. Biol. Chem. *274*, 32091–32098.

Bharti, A.C., Donato, N., Singh, S., and Aggarwal, B.B. (2003). Curcumin (diferuloylmethane) down-regulates the constitutive activation of nuclear factor–κB and IκBα kinase in human multiple myeloma cells, leading to suppression of proliferation and induction of apoptosis. Blood *101*, 1053–1062.

Biankin, A.V., Waddell, N., Kassahn, K.S., Gingras, M.-C., Muthuswamy, L.B., Johns, A.L., Miller, D.K., Wilson, P.J., Patch, A.-M., Wu, J., et al. (2012). Pancreatic cancer genomes reveal aberrations in axon guidance pathway genes. Nature *491*, 399–405.

Bischoff, J.R., and Samuel, C.E. (1989). Mechanism of interferon action. Activation of the human P1/eIF-2α protein kinase by individual reovirus s-class mRNAs: s1 mRNA is a potent activator relative to s4 mRNA. Virology *172*, 106–115.

Bischoff, J.R., Kirn, D.H., Williams, A., Heise, C., Horn, S., Muna, M., Ng, L., Nye, J.A., Sampson-Johannes, A., Fattaey, A., et al. (1996). An adenovirus mutant that replicates selectively in p53-deficient human tumor cells. Science *274*, 373–376.

Biswas, S.K., and Lewis, C.E. (2010). NF-κB as a central regulator of macrophage function in tumors. J. Leukoc. Biol. *88*, 877–884.

Blank, V., Kourilsky, P., and Israël, A. (1991). Cytoplasmic retention, DNA binding and processing of the NF-κB p50 precursor are controlled by a small region in its C-terminus. EMBO J. *10*, 4159–4167.

du Bois, A., Lück, H.-J., Meier, W., Adams, H.-P., Möbus, V., Costa, S., Bauknecht, T., Richter, B., Warm, M., Schröder, W., et al. (2003). A Randomized Clinical Trial of Cisplatin/Paclitaxel Versus Carboplatin/Paclitaxel as First-Line Treatment of Ovarian Cancer. JNCI J. Natl. Cancer Inst. *95*, 1320–1329.

Bold, R.J., Virudachalam, S., and McConkey, D.J. (2001). Chemosensitization of Pancreatic Cancer by Inhibition of the 26S Proteasome. J. Surg. Res. *100*, 11–17.

Bonizzi, G., and Karin, M. (2004). The two NF-κB activation pathways and their role in innate and adaptive immunity. Trends Immunol. *25*, 280–288.

Borghini, L., Lu, J., Hibberd, M., and Davila, S. (2018). Variation in Genome-Wide NF-κB RELA Binding Sites upon Microbial Stimuli and Identification of a Virus Response Profile. J. Immunol. *201*, 1295–1305.

Borregaard, N., and Cowland, J.B. (1997). Granules of the Human Neutrophilic Polymorphonuclear Leukocyte. Blood *89*, 3503–3521.

Bourgarel-Rey, V., Vallee, S., Rimet, O., Champion, S., Braguer, D., Desobry, A., Briand, C., and Barra, Y. (2001). Involvement of nuclear factor κB in c-Myc induction by tubulin polymerization inhibitors. Mol. Pharmacol. *59*, 1165–1170.

Bours, V., Franzoso, G., Azarenko, V., Park, S., Kanno, T., Brown, K., and Siebenlist, U. (1993). The oncoprotein Bcl-3 directly transactivates through κB motifs via association with DNA-binding p50B homodimers. Cell *72*, 729–739.

Boyce, B.F., Xiu, Y., Li, J., Xing, L., and Yao, Z. (2015). NF-κB-Mediated Regulation of Osteoclastogenesis. Endocrinol. Metab. *30*, 35–44.

Bren, G.D., Solan, N.J., Miyoshi, H., Pennington, K.N., Pobst, L.J., and Paya, C.V. (2001). Transcription of the RelB gene is regulated by NF-κB. Oncogene *20*, 7722–7733.

Brinkley, W. (1997). Microtubules: a brief historical perspective. J. Struct. Biol. *118*, 84–86.

Brown, S.S., and Spudich, J.A. (1981). Mechanism of action of cytochalasin: evidence that it binds to actin filament ends. J. Cell Biol. *88*, 487–491.

Brown, K., Park, S., Kanno, T., Franzoso, G., and Siebenlist, U. (1993). Mutual regulation of the transcriptional activator NF-κB and its inhibitor, IκB-α. Proc. Natl. Acad. Sci. U. S. A. *90*, 2532–2536.

Brummelkamp, T.R., Nijman, S.M.B., Dirac, A.M.G., and Bernards, R. (2003). Loss of the cylindromatosis tumour suppressor inhibits apoptosis by activating NF-κB. Nature *424*, 797–801.

Buerki, C., Rothgiesser, K.M., Valovka, T., Owen, H.R., Rehrauer, H., Fey, M., Lane, W.S., and Hottiger, M.O. (2008). Functional relevance of novel p300-mediated lysine 314 and 315 acetylation of RelA/p65. Nucleic Acids Res. *36*, 1665–1680.

Burkly, L., Hession, C., Ogata, L., Reilly, C., Marconi, L.A., Olson, D., Tizard, R., Cate, R., and Lo, D. (1995). Expression of relB is required for the development of thymic medulla and dendritic cells. Nature *373*, 531–536.

Burridge, K., Fath, K., Kelly, T., Nuckolls, G., and Turner, C. (1988). Focal adhesions: transmembrane junctions between the extracellular matrix and the cytoskeleton. Annu. Rev. Cell Biol. *4*, 487–525.

Buss, H., Dörrie, A., Schmitz, M.L., Hoffmann, E., Resch, K., and Kracht, M. (2004a). Constitutive and Interleukin-1-inducible Phosphorylation of p65 NF-κB at Serine 536 Is Mediated by Multiple Protein Kinases Including IκB Kinase (IKK)-α, IKKβ, IKKε, TRAF Family Member-associated (TANK)-binding Kinase 1 (TBK1), and an Unknown Kinase and Couples p65 to TATA-binding Protein-associated Factor II31-mediated Interleukin-8 Transcription. J. Biol. Chem. *279*, 55633–55643.

Buss, H., Dörrie, A., Schmitz, M.L., Frank, R., Livingstone, M., Resch, K., and Kracht, M. (2004b). Phosphorylation of serine 468 by GSK-3β negatively regulates basal p65 NF-κB activity. J. Biol. Chem. *279*, 49571–49574.

Caamaño, J.H., Rizzo, C.A., Durham, S.K., Barton, D.S., Raventós-Suárez, C., Snapper, C.M., and Bravo, R. (1998). Nuclear factor (NF)-κB2 (p100/p52) is required for normal splenic microarchitecture and B cell-mediated immune responses. J. Exp. Med. *187*, 185–196.

Camps, M., Nichols, A., and Arkinstall, S. (2000). Dual specificity phosphatases: a gene family for control of MAP kinase function. FASEB J. *14*, 6–16.

Cano, A., Pérez-Moreno, M.A., Rodrigo, I., Locascio, A., Blanco, M.J., del Barrio, M.G., Portillo, F., and Nieto, M.A. (2000). The transcription factor Snail controls epithelial–mesenchymal transitions by repressing E-cadherin expression. Nat. Cell Biol. *2*, 76–83.

Cao, Z., Fu, B., Deng, B., Zeng, Y., Wan, X., and Qu, L. (2014). Overexpression of Chemokine (C-X-C) ligand 1 (CXCL1) associated with tumor progression and poor prognosis in hepatocellular carcinoma. Cancer Cell Int. *14*, 86.

Carballo, E., Lai, W.S., and Blackshear, P.J. (1998). Feedback inhibition of macrophage tumor necrosis factor-α production by tristetraprolin. Science *281*, 1001–1005.

Carpenter, A.E., Jones, T.R., Lamprecht, M.R., Clarke, C., Kang, I.H., Friman, O., Guertin, D.A., Chang, J.H., Lindquist, R.A., Moffat, J., et al. (2006). CellProfiler: image analysis software for identifying and quantifying cell phenotypes. Genome Biol. *7*, R100.

Carswell, E.A., Old, L.J., Kassel, R.L., Green, S., Fiore, N., and Williamson, B. (1975). An endotoxin-induced serum factor that causes necrosis of tumors. Proc. Natl. Acad. Sci. *72*, 3666–3670.

Carver, E.A., Jiang, R., Lan, Y., Oram, K.F., and Gridley, T. (2001). The mouse snail gene encodes a key regulator of the epithelial-mesenchymal transition. Mol. Cell. Biol. *21*, 8184–8188.

Chalut, K.J., and Paluch, E.K. (2016). The Actin Cortex: A Bridge between Cell Shape and Function. Dev. Cell *38*, 571–573.

Chandran, K., Walker, S.B., Chen, Y., Contreras, C.M., Schiff, L.A., Baker, T.S., and Nibert, M.L. (1999). In Vitro Recoating of Reovirus Cores with Baculovirus-Expressed Outer-Capsid Proteins μ1 and ς3. J. Virol. *73*, 3941–3950.

Chang, D.W., Xing, Z., Pan, Y., Algeciras-Schimnich, A., Barnhart, B.C., Yaish-Ohad, S., Peter, M.E., and Yang, X. (2002). c-FLIP(L) is a dual function regulator for caspase-8 activation and CD95-mediated apoptosis. EMBO J. *21*, 3704–3714.

Chang, J.-H., Hu, H., and Sun, S.-C. (2015). Survival and maintenance of regulatory T cells require the kinase TAK1. Cell. Mol. Immunol. *12*, 572–579.

Chari, S.T., Kelly, K., Hollingsworth, M.A., Thayer, S.P., Ahlquist, D.A., Andersen, D.K., Batra, S.K., Brentnall, T.A., Canto, M., Cleeter, D.F., et al. (2015). Early Detection of Sporadic Pancreatic Cancer: Summative Review. Pancreas *44*, 693–712.

Chellappan, S.P., Hiebert, S., Mudryj, M., Horowitz, J.M., and Nevins, J.R. (1991). The E2F transcription factor is a cellular target for the RB protein. Cell *65*, 1053–1061.

Chen, D., Frezza, M., Schmitt, S., Kanwar, J., and Dou, Q.P. (2011). Bortezomib as the First Proteasome Inhibitor Anticancer Drug: Current Status and Future Perspectives. Curr. Cancer Drug Targets *11*, 239–253.

Chen, F.E., Huang, D.B., Chen, Y.Q., and Ghosh, G. (1998). Crystal structure of p50/p65 heterodimer of transcription factor NF-κB bound to DNA. Nature *391*, 410–413.

Chen, J., Wang, S., Fu, R., Zhou, M., Zhang, T., Pan, W., Yang, N., and Huang, Y. (2018). RIP3 dependent NLRP3 inflammasome activation is implicated in acute lung injury in mice. J. Transl. Med. *16*, 233.

Chen, L.-W., Egan, L., Li, Z.-W., Greten, F.R., Kagnoff, M.F., and Karin, M. (2003). The two faces of IKK and NF-B inhibition: prevention of systemic inflammation but increased local injury following intestinal ischemia-reperfusion. Nat. Med. *9*, 575–581.

Chen, Y., Song, Y., Zhang, C., Zhang, F., O'Donnell, L., Chrzanowski, W., and Cai, W. (2021). CellTrack R-CNN: A Novel End-To-End Deep Neural Network for Cell Segmentation and Tracking in Microscopy Images. ArXiv210210377 Cs.

Chen, Z., Hagler, J., Palombella, V.J., Melandri, F., Scherer, D., Ballard, D., and Maniatis, T. (1995). Signal-induced site-specific phosphorylation targets IκBα to the ubiquitin-proteasome pathway. Genes Dev. *9*, 1586–1597.

Cheng, C.S., Feldman, K.E., Lee, J., Verma, S., Huang, D.-B., Huynh, K., Chang, M., Ponomarenko, J.V., Sun, S.-C., Benedict, C.A., et al. (2011). The specificity of innate

immune responses is enforced by repression of interferon response elements by NF-κB p50. Sci. Signal. *4*, ra11.

Cheng, Y., Jutooru, I., Chadalapaka, G., Corton, J.C., and Safe, S. (2015). The long non-coding RNA HOTTIP enhances pancreatic cancer cell proliferation, survival and migration. Oncotarget *6*, 10840–10852.

Cheong, R., Rhee, A., Wang, C.J., Nemenman, I., and Levchenko, A. (2011). Information transduction capacity of noisy biochemical signaling networks. Science *334*, 354–358.

Cho, Y., Challa, S., Moquin, D., Genga, R., Ray, T.D., Guildford, M., and Chan, F.K.-M. (2009). Phosphorylation-Driven Assembly of the RIP1-RIP3 Complex Regulates Programmed Necrosis and Virus-Induced Inflammation. Cell *137*, 1112–1123.

Choi, Y., Park, S.-K., Kim, H.M., Kang, J.S., Yoon, Y.D., Han, S.B., Han, J.W., Yang, J.S., and Han, G. (2008). Histone deacetylase inhibitor KBH-A42 inhibits cytokine production in RAW 264.7 macrophage cells and in vivo endotoxemia model. Exp. Mol. Med. *40*, 574–581.

Chu, Z.-L., McKinsey, T.A., Liu, L., Gentry, J.J., Malim, M.H., and Ballard, D.W. (1997). Suppression of tumor necrosis factor-induced cell death by inhibitor of apoptosis c-IAP2 is under NF-κB control. Proc. Natl. Acad. Sci. *94*, 10057–10062.

Chua, H.L., Bhat-Nakshatri, P., Clare, S.E., Morimiya, A., Badve, S., and Nakshatri, H. (2007). NF-κB represses E-cadherin expression and enhances epithelial to mesenchymal transition of mammary epithelial cells: potential involvement of ZEB-1 and ZEB-2. Oncogene *26*, 711–724.

Clarke, P., Meintzer, S.M., Gibson, S., Widmann, C., Garrington, T.P., Johnson, G.L., and Tyler, K.L. (2000). Reovirus-induced apoptosis is mediated by TRAIL. J. Virol. *74*, 8135–8139.

Collart, M.A., Baeuerle, P., and Vassalli, P. (1990). Regulation of tumor necrosis factor α transcription in macrophages: involvement of four κB-like motifs and of constitutive and inducible forms of NF-κB. Mol. Cell. Biol. *10*, 1498–1506.

Compagno, M., Lim, W.K., Grunn, A., Nandula, S.V., Brahmachary, M., Shen, Q., Bertoni, F., Ponzoni, M., Scandurra, M., Califano, A., et al. (2009). Mutations of multiple genes cause deregulation of NF-kB in diffuse large B-cell lymphoma. Nature *459*, 717–721.

Connolly, J.L., Rodgers, S.E., Clarke, P., Ballard, D.W., Kerr, L.D., Tyler, K.L., and Dermody, T.S. (2000). Reovirus-induced apoptosis requires activation of transcription factor NF-κB. J. Virol. *74*, 2981–2989.

Cooper, J.A., Buhle, E.L., Walker, S.B., Tsong, T.Y., and Pollard, T.D. (1983). Kinetic evidence for a monomer activation step in actin polymerization. Biochemistry *22*, 2193–2202.

Cooper, S., Sadok, A., Bousgouni, V., and Bakal, C. (2015). Apolar and polar transitions drive the conversion between amoeboid and mesenchymal shapes in melanoma cells. Mol. Biol. Cell *26*, 4163–4170.

Cooper, S., Barr, A.R., Glen, R., and Bakal, C. (2017). NucliTrack: an integrated nuclei tracking application. Bioinformatics *33*, 3320–3322.

Copeland, S.J., Green, B.J., Burchat, S., Papalia, G.A., Banner, D., and Copeland, J.W. (2007). The diaphanous inhibitory domain/diaphanous autoregulatory domain interaction is able to mediate heterodimerization between mDia1 and mDia2. J. Biol. Chem. *282*, 30120–30130.

Coyle, C., Cafferty, F.H., Rowley, S., MacKenzie, M., Berkman, L., Gupta, S., Pramesh, C.S., Gilbert, D., Kynaston, H., Cameron, D., et al. (2016). ADD-ASPIRIN: A phase III, double-blind, placebo controlled, randomised trial assessing the effects of aspirin on disease recurrence and survival after primary therapy in common non-metastatic solid tumours. Contemp. Clin. Trials *51*, 56–64.

Croghan, G.A., Suman, V.J., Maples, W.J., Albertini, M., Linette, G., Flaherty, L., Eckardt, J., Ma, C., Markovic, S.N., and Erlichman, C. (2010). A study of paclitaxel, carboplatin, and bortezomib in the treatment of metastatic malignant melanoma: a phase 2 consortium study. Cancer *116*, 3463–3468.

Cusack, J.C., Liu, R., Houston, M., Abendroth, K., Elliott, P.J., Adams, J., and Baldwin, A.S. (2001). Enhanced Chemosensitivity to CPT-11 with Proteasome Inhibitor PS-341:: Implications for Systemic Nuclear Factor-κB Inhibition. Cancer Res. *61*, 3535–3540.

Cushing, L., Winkler, A., Jelinsky, S.A., Lee, K., Korver, W., Hawtin, R., Rao, V.R., Fleming, M., and Lin, L.-L. (2017). IRAK4 kinase activity controls Toll-like receptor-induced inflammation through the transcription factor IRF5 in primary human monocytes. J. Biol. Chem. *292*, 18689–18698.

Dahlberg, J.E., and Lund, E. (1998). Functions of the GTPase Ran in RNA export from the nucleus. Curr. Opin. Cell Biol. *10*, 400–408.

D'Amours, D., Desnoyers, S., D'Silva, I., and Poirier, G.G. (1999). Poly(ADP-ribosyl)ation reactions in the regulation of nuclear functions. Biochem. J. *342 (Pt 2)*, 249–268.

D'Anselmi, F., Valerio, M., Cucina, A., Galli, L., Proietti, S., Dinicola, S., Pasqualato, A., Manetti, C., Ricci, G., Giuliani, A., et al. (2011). Metabolism and cell shape in cancer: A fractal analysis. Int. J. Biochem. Cell Biol. *43*, 1052–1058.

Das, J., Chen, C.-H., Yang, L., Cohn, L., Ray, P., and Ray, A. (2001). A critical role for NF-κB in Gata3 expression and TH2 differentiation in allergic airway inflammation. Nat. Immunol. *2*, 45–50.

Davis, R.E., Brown, K.D., Siebenlist, U., and Staudt, L.M. (2001). Constitutive nuclear factor κB activity is required for survival of activated B cell-like diffuse large B cell lymphoma cells. J. Exp. Med. *194*, 1861–1874.

Deer, E.L., Gonzalez-Hernandez, J., Coursen, J.D., Shea, J.E., Ngatia, J., Scaife, C.L., Firpo, M.A., and Mulvihill, S.J. (2010). Phenotype and Genotype of Pancreatic Cancer Cell Lines. Pancreas *39*, 425–435.

DeFelice, M.M., Clark, H.R., Hughey, J.J., Maayan, I., Kudo, T., Gutschow, M.V., Covert, M.W., and Regot, S. (2019). NF-κB signaling dynamics is controlled by a dose-sensing autoregulatory loop. Sci. Signal. *12*, eaau3568.

Dejardin, E., Droin, N.M., Delhase, M., Haas, E., Cao, Y., Makris, C., Li, Z.-W., Karin, M., Ware, C.F., and Green, D.R. (2002). The lymphotoxin-β receptor induces different patterns of gene expression via two NF-κB pathways. Immunity *17*, 525–535.

Dennert, G., and Lennox, E. (1972). Cell Interactions in Humoral and Cell-mediated Immunity. Nature. New Biol. *238*, 114–116.

Desai, A., and Mitchison, T.J. (1997). Microtubule Polymerization Dynamics. Annu. Rev. Cell Dev. Biol. *13*, 83–117.

Desai, N., Trieu, V., Yao, Z., Louie, L., Ci, S., Yang, A., Tao, C., De, T., Beals, B., Dykes, D., et al. (2006). Increased antitumor activity, intratumor paclitaxel concentrations, and

endothelial cell transport of cremophor-free, albumin-bound paclitaxel, ABI-007, compared with cremophor-based paclitaxel. Clin. Cancer Res. *12*, 1317–1324.

Desai, N., Trieu, V., Damascelli, B., and Soon-Shiong, P. (2009). SPARC Expression Correlates with Tumor Response to Albumin-Bound Paclitaxel in Head and Neck Cancer Patients. Transl. Oncol. *2*, 59–64.

Dhawan, P., and Richmond, A. (2002). Role of CXCL1 in tumorigenesis of melanoma. J. Leukoc. Biol. *72*, 9–18.

Dhillon, N., Aggarwal, B.B., Newman, R.A., Wolff, R.A., Kunnumakkara, A.B., Abbruzzese, J.L., Ng, C.S., Badmaev, V., and Kurzrock, R. (2008). Phase II Trial of Curcumin in Patients with Advanced Pancreatic Cancer. Clin. Cancer Res. *14*, 4491–4499.

Diasio, R.B., and Harris, B.E. (1989). Clinical Pharmacology of 5-Fluorouracil. Clin. Pharmacokinet. *16*, 215–237.

DiDonato, J.A., Hayakawa, M., Rothwarf, D.M., Zandi, E., and Karin, M. (1997). A cytokine-responsive IκB kinase that activates the transcription factor NF-κB. Nature *388*, 548–554.

Dobrzanski, P., Ryseck, R.P., and Bravo, R. (1993). Both N- and C-terminal domains of RelB are required for full transactivation: role of the N-terminal leucine zipper-like motif. Mol. Cell. Biol. *13*, 1572–1582.

Dobrzyński, M., Jacques, M.-A., and Pertz, O. (2020). Mining single-cell time-series datasets with Time Course Inspector. Bioinformatics *36*, 1968–1969.

Dogterom, M., and Koenderink, G.H. (2019). Actin–microtubule crosstalk in cell biology. Nat. Rev. Mol. Cell Biol. *20*, 38–54.

Dondelinger, Y., Aguileta, M.A., Goossens, V., Dubuisson, C., Grootjans, S., Dejardin, E., Vandenabeele, P., and Bertrand, M.J.M. (2013). RIPK3 contributes to TNFR1-mediated RIPK1 kinase-dependent apoptosis in conditions of cIAP1/2 depletion or TAK1 kinase inhibition. Cell Death Differ. *20*, 1381–1392.

Doniņa, S., Strēle, I., Proboka, G., Auziņš, J., Alberts, P., Jonsson, B., Venskus, D., and Muceniece, A. (2015). Adapted ECHO-7 virus Rigvir immunotherapy (oncolytic virotherapy) prolongs survival in melanoma patients after surgical excision of the tumour in a retrospective study. Melanoma Res. *25*, 421–426.

Doong, S.L., and Dolnick, B.J. (1988). 5-Fluorouracil substitution alters pre-mRNA splicing in vitro. J. Biol. Chem. *263*, 4467–4473.

Doroshow, D.B., Sanmamed, M.F., Hastings, K., Politi, K., Rimm, D.L., Chen, L., Melero, I., Schalper, K.A., and Herbst, R.S. (2019). Immunotherapy in Non–Small Cell Lung Cancer: Facts and Hopes. Clin. Cancer Res. *25*, 4592–4602.

Dranoff, G. (2004). Cytokines in cancer pathogenesis and cancer therapy. Nat. Rev. Cancer *4*, 11–22.

Driehuis, E., van Hoeck, A., Moore, K., Kolders, S., Francies, H.E., Gulersonmez, M.C., Stigter, E.C.A., Burgering, B., Geurts, V., Gracanin, A., et al. (2019). Pancreatic cancer organoids recapitulate disease and allow personalized drug screening. Proc. Natl. Acad. Sci. *116*, 26580–26590.

Du, C., Fang, M., Li, Y., Li, L., and Wang, X. (2000). Smac, a mitochondrial protein that promotes cytochrome c-dependent caspase activation by eliminating IAP inhibition. Cell *102*,

33–42.

Duncan, M.R., Stanish, S.M., and Cox, D.C. (1978). Differential sensitivity of normal and transformed human cells to reovirus infection. J. Virol. *28*, 444–449.

Duschinsky, R., Pleven, E., and Heidelberger, C. (1957). The Synthesis of 5-Flyoropyrimidines. J. Am. Chem. Soc. *79*, 4559–4560.

Ea, C.-K., Deng, L., Xia, Z.-P., Pineda, G., and Chen, Z.J. (2006). Activation of IKK by TNFα requires site-specific ubiquitination of RIP1 and polyubiquitin binding by NEMO. Mol. Cell *22*, 245–257.

Edlund, C., Jackson, T.R., Khalid, N., Bevan, N., Dale, T., Dengel, A., Ahmed, S., Trygg, J., and Sjögren, R. (2021). LIVECell—A large-scale dataset for label-free live cell segmentation. Nat. Methods *18*, 1038–1045.

Egberts, J.-H., Cloosters, V., Noack, A., Schniewind, B., Thon, L., Klose, S., Kettler, B., Forstner, C. von, Kneitz, C., Tepel, J., et al. (2008). Anti–Tumor Necrosis Factor Therapy Inhibits Pancreatic Tumor Growth and Metastasis. Cancer Res. *68*, 1443–1450.

Eger, A., Aigner, K., Sonderegger, S., Dampier, B., Oehler, S., Schreiber, M., Berx, G., Cano, A., Beug, H., and Foisner, R. (2005). DeltaEF1 is a transcriptional repressor of E-cadherin and regulates epithelial plasticity in breast cancer cells. Oncogene *24*, 2375–2385.

El Mezayen, R., El Gazzar, M., Seeds, M.C., McCall, C.E., Dreskin, S.C., and Nicolls, M.R. (2007). Endogenous signals released from necrotic cells augment inflammatory responses to bacterial endotoxin. Immunol. Lett. *111*, 36–44.

Elosegui-Artola, A., Andreu, I., Beedle, A.E.M., Lezamiz, A., Uroz, M., Kosmalska, A.J., Oria, R., Kechagia, J.Z., Rico-Lastres, P., Le Roux, A.-L., et al. (2017). Force Triggers YAP Nuclear Entry by Regulating Transport across Nuclear Pores. Cell *171*, 1397-1410.e14.

Emamekhoo, H., Patel, S., Rodriguez, E., Riaz, M.K., Giaccone, G., Furqan, M., Sacco, J.J., Bommareddy, P., Raza, S., He, S., et al. (2022). IGNYTE: A Phase 1/2 Multi-Cohort Clinical Trial of RP1 ± Nivolumab in Patients with Non-Small Cell Lung Cancer and Other Solid Tumors. Int. J. Radiat. Oncol. *112*, e12–e13.

Emmerich, F., Meiser, M., Hummel, M., Demel, G., Foss, H.-D., Jundt, F., Mathas, S., Krappmann, D., Scheidereit, C., Stein, H., et al. (1999). Overexpression of IκBα Without Inhibition of NF-κB Activity and Mutations in the IκBα Gene in Reed-Sternberg Cells. Blood *94*, 3129–3134.

Emmerich, F., Theurich, S., Hummel, M., Haeffker, A., Vry, M.S., Döhner, K., Bommert, K., Stein, H., and Dörken, B. (2003). Inactivating IκBε mutations in Hodgkin/Reed–Sternberg cells. J. Pathol. *201*, 413–420.

van Erning, F.N., Mackay, T.M., van der Geest, L.G.M., Groot Koerkamp, B., van Laarhoven, H.W.M., Bonsing, B.A., Wilmink, J.W., van Santvoort, H.C., de Vos-Geelen, J., van Eijck, C.H.J., et al. (2018). Association of the location of pancreatic ductal adenocarcinoma (head, body, tail) with tumor stage, treatment, and survival: a population-based analysis. Acta Oncol. Stockh. Swed. *57*, 1655–1662.

Errington, F., Steele, L., Prestwich, R., Harrington, K.J., Pandha, H.S., Vidal, L., Bono, J. de, Selby, P., Coffey, M., Vile, R., et al. (2008). Reovirus Activates Human Dendritic Cells to Promote Innate Antitumor Immunity. J. Immunol. *180*, 6018–6026.

Eshhar, Z., Waks, T., Gross, G., and Schindler, D.G. (1993). Specific activation and targeting of cytotoxic lymphocytes through chimeric single chains consisting of antibody-binding

domains and the gamma or zeta subunits of the immunoglobulin and T-cell receptors. Proc. Natl. Acad. Sci. U. S. A. *90*, 720–724.

Etoh, T., Himeno, Y., Matsumoto, T., Aramaki, M., Kawano, K., Nishizono, A., and Kitano, S. (2003). Oncolytic viral therapy for human pancreatic cancer cells by reovirus. Clin. Cancer Res. Off. J. Am. Assoc. Cancer Res. *9*, 1218–1223.

Evans, L., Mitchison, T., and Kirschner, M. (1985). Influence of the centrosome on the structure of nucleated microtubules. J. Cell Biol. *100*, 1185–1191.

Fagerlund, R., Kinnunen, L., Köhler, M., Julkunen, I., and Melén, K. (2005). NF-κB Is Transported into the Nucleus by Importin α3 and Importin α4. J. Biol. Chem. *280*, 15942–15951.

Fan, C.M., and Maniatis, T. (1991). Generation of p50 subunit of NF-κB by processing of p105 through an ATP-dependent pathway. Nature *354*, 395–398.

Fan, J., Wang, M.-F., Chen, H.-L., Shang, D., Das, J.K., and Song, J. (2020). Current advances and outlooks in immunotherapy for pancreatic ductal adenocarcinoma. Mol. Cancer *19*, 32.

Fan, Y., Weinstein, J.N., Kohn, K.W., Shi, L.M., and Pommier, Y. (1998). Molecular modeling studies of the DNA-topoisomerase I ternary cleavable complex with camptothecin. J. Med. Chem. *41*, 2216–2226.

Farmer, H., McCabe, N., Lord, C.J., Tutt, A.N.J., Johnson, D.A., Richardson, T.B., Santarosa, M., Dillon, K.J., Hickson, I., Knights, C., et al. (2005). Targeting the DNA repair defect in BRCA mutant cells as a therapeutic strategy. Nature *434*, 917–921.

Ferrajoli, A., Keating, M.J., Manshouri, T., Giles, F.J., Dey, A., Estrov, Z., Koller, C.A., Kurzrock, R., Thomas, D.A., Faderl, S., et al. (2002). The clinical significance of tumor necrosis factor-α plasma level in patients having chronic lymphocytic leukemia. Blood *100*, 1215–1219.

Fitzgerald, K.A., McWhirter, S.M., Faia, K.L., Rowe, D.C., Latz, E., Golenbock, D.T., Coyle, A.J., Liao, S.-M., and Maniatis, T. (2003). IKKε and TBK1 are essential components of the IRF3 signaling pathway. Nat. Immunol. *4*, 491–496.

Flanagan, M.D., and Lin, S. (1980). Cytochalasins block actin filament elongation by binding to high affinity sites associated with F-actin. J. Biol. Chem. *255*, 835–838.

Foerster, F., Braig, S., Moser, C., Kubisch, R., Busse, J., Wagner, E., Schmoeckel, E., Mayr, D., Schmitt, S., Huettel, S., et al. (2014). Targeting the actin cytoskeleton: selective antitumor action via trapping PKCε. Cell Death Dis. *5*, e1398–e1398.

Fong, C.Y.K., Burke, E., Cunningham, D., and Starling, N. (2019). Up-to-Date Tailored Systemic Treatment in Pancreatic Ductal Adenocarcinoma (Hindawi).

François, S., Benna, J.E., Dang, P.M.C., Pedruzzi, E., Gougerot-Pocidalo, M.-A., and Elbim, C. (2005). Inhibition of Neutrophil Apoptosis by TLR Agonists in Whole Blood: Involvement of the Phosphoinositide 3-Kinase/Akt and NF-κB Signaling Pathways, Leading to Increased Levels of Mcl-1, A1, and Phosphorylated Bad. J. Immunol. *174*, 3633–3642.

Franzoso, G., Carlson, L., Xing, L., Poljak, L., Shores, E.W., Brown, K.D., Leonardi, A., Tran, T., Boyce, B.F., and Siebenlist, U. (1997). Requirement for NF-κB in osteoclast and B-cell development. Genes Dev. *11*, 3482–3496.

Franzoso, G., Carlson, L., Poljak, L., Shores, E.W., Epstein, S., Leonardi, A., Grinberg, A.,

Tran, T., Scharton-Kersten, T., Anver, M., et al. (1998). Mice deficient in nuclear factor (NF)-κB/p52 present with defects in humoral responses, germinal center reactions, and splenic microarchitecture. J. Exp. Med. *187*, 147–159.

Frasor, J., Weaver, A., Pradhan, M., Dai, Y., Miller, L.D., Lin, C.-Y., and Stanculescu, A. (2009). Positive cross-talk between estrogen receptor and NF-κB in breast cancer. Cancer Res. *69*, 8918–8925.

Freeman, G.J., Long, A.J., Iwai, Y., Bourque, K., Chernova, T., Nishimura, H., Fitz, L.J., Malenkovich, N., Okazaki, T., Byrne, M.C., et al. (2000). Engagement of the PD-1 immunoinhibitory receptor by a novel B7 family member leads to negative regulation of lymphocyte activation. J. Exp. Med. *192*, 1027–1034.

Frese, K.K., Neesse, A., Cook, N., Bapiro, T.E., Lolkema, M.P., Jodrell, D.I., and Tuveson, D.A. (2012). nab-Paclitaxel potentiates gemcitabine activity by reducing cytidine deaminase levels in a mouse model of pancreatic cancer. Cancer Discov. *2*, 260–269.

Friedman, J.R., Webster, B.M., Mastronarde, D.N., Verhey, K.J., and Voeltz, G.K. (2010). ER sliding dynamics and ER–mitochondrial contacts occur on acetylated microtubules. J. Cell Biol. *190*, 363–375.

Friedmann, E., Hauben, E., Maylandt, K., Schleeger, S., Vreugde, S., Lichtenthaler, S.F., Kuhn, P.-H., Stauffer, D., Rovelli, G., and Martoglio, B. (2006). SPPL2a and SPPL2b promote intramembrane proteolysis of TNFα in activated dendritic cells to trigger IL-12 production. Nat. Cell Biol. *8*, 843–848.

Fujioka, S., Sclabas, G.M., Schmidt, C., Frederick, W.A., Dong, Q.G., Abbruzzese, J.L., Evans, D.B., Baker, C., and Chiao, P.J. (2003a). Function of Nuclear Factor κB in Pancreatic Cancer Metastasis. Clin. Cancer Res. *9*, 346–354.

Fujioka, S., Sclabas, G.M., Schmidt, C., Niu, J., Frederick, W.A., Dong, Q.G., Abbruzzese, J.L., Evans, D.B., Baker, C., and Chiao, P.J. (2003b). Inhibition of constitutive NF-κB activity by IκBαM suppresses tumorigenesis. Oncogene *22*, 1365–1370.

Gastonguay, A., Berg, T., Hauser, A.D., Schuld, N., Lorimer, E., and Williams, C.L. (2012). The role of Rac1 in the regulation of NF-κB activity, cell proliferation, and cell migration in non-small cell lung carcinoma. Cancer Biol. Ther. *13*, 647–656.

Génin, P., Algarté, M., Roof, P., Lin, R., and Hiscott, J. (2000). Regulation of RANTES chemokine gene expression requires cooperativity between NF-κB and IFN-regulatory factor transcription factors. J. Immunol. Baltim. Md 1950 *164*, 5352–5361.

Georgouli, M., Herraiz, C., Crosas-Molist, E., Fanshawe, B., Maiques, O., Perdrix, A., Pandya, P., Rodriguez-Hernandez, I., Ilieva, K.M., Cantelli, G., et al. (2019). Regional Activation of Myosin II in Cancer Cells Drives Tumor Progression via a Secretory Cross-Talk with the Immune Microenvironment. Cell *176*, 757-774.e23.

Gerosa, L., Chidley, C., Fröhlich, F., Sanchez, G., Lim, S.K., Muhlich, J., Chen, J.-Y., Vallabhaneni, S., Baker, G.J., Schapiro, D., et al. (2020). Receptor-Driven ERK Pulses Reconfigure MAPK Signaling and Enable Persistence of Drug-Adapted BRAF-Mutant Melanoma Cells. Cell Syst. *11*, 478-494.e9.

Ghosh, G., van Duyne, G., Ghosh, S., and Sigler, P.B. (1995). Structure of NF-κB p50 homodimer bound to a κB site. Nature *373*, 303–310.

Ghosh, G., Ya-Fan Wang, V., Huang, D.-B., and Fusco, A. (2012). NF-κB Regulation: Lessons from Structures. Immunol. Rev. *246*, 36–58.

Ghosh, S., Gifford, A.M., Riviere, L.R., Tempst, P., Nolan, G.P., and Baltimore, D. (1990). Cloning of the p50 DNA binding subunit of NF-κB: homology to rel and dorsal. Cell *62*, 1019–1029.

Ghoshal, K., and Jacob, S.T. (1994). Specific Inhibition of Pre-Ribosomal RNA Processing in Extracts from the Lymphosarcoma Cells Treated with 5-Fluorouracil. Cancer Res. *54*, 632–636.

Gigant, B., Wang, C., Ravelli, R.B.G., Roussi, F., Steinmetz, M.O., Curmi, P.A., Sobel, A., and Knossow, M. (2005). Structural basis for the regulation of tubulin by vinblastine. Nature *435*, 519–522.

Gilmore, T.D. (2006). Introduction to NF-κB: players, pathways, perspectives. Oncogene *25*, 6680–6684.

Gilmore, T.D., and Wolenski, F.S. (2012). NF-κB: where did it come from and why? Immunol. Rev. *246*, 14–35.

Giridharan, S., and Srinivasan, M. (2018). Mechanisms of NF-κB p65 and strategies for therapeutic manipulation. J. Inflamm. Res. *11*, 407–419.

Goddette, D.W., and Frieden, C. (1986). Actin polymerization. The mechanism of action of cytochalasin D. J. Biol. Chem. *261*, 15974–15980.

Goddette, D.W., Uberbacher, E.C., Bunick, G.J., and Frieden, C. (1986). Formation of actin dimers as studied by small angle neutron scattering. J. Biol. Chem. *261*, 2605–2609.

Gong, J., Sachdev, E., Mita, A.C., and Mita, M.M. (2016). Clinical development of reovirus for cancer therapy: An oncolytic virus with immune-mediated antitumor activity. World J. Methodol. *6*, 25–42.

Goodwin, R.G., Alderson, M.R., Smith, C.A., Armitage, R.J., VandenBos, T., Jerzy, R., Tough, T.W., Schoenborn, M.A., Davis-Smith, T., and Hennen, K. (1993). Molecular and biological characterization of a ligand for CD27 defines a new family of cytokines with homology to tumor necrosis factor. Cell *73*, 447–456.

Görlich, D., Panté, N., Kutay, U., Aebi, U., and Bischoff, F.R. (1996). Identification of different roles for RanGDP and RanGTP in nuclear protein import. EMBO J. *15*, 5584–5594.

Gradishar, W.J., Tjulandin, S., Davidson, N., Shaw, H., Desai, N., Bhar, P., Hawkins, M., and O'Shaughnessy, J. (2005). Phase III trial of nanoparticle albumin-bound paclitaxel compared with polyethylated castor oil-based paclitaxel in women with breast cancer. J. Clin. Oncol. Off. J. Am. Soc. Clin. Oncol. *23*, 7794–7803.

Greten, F.R., Weber, C.K., Greten, T.F., Schneider, G., Wagner, M., Adler, G., and Schmid, R.M. (2002). Stat3 and NF-κB activation prevents apoptosis in pancreatic carcinogenesis. Gastroenterology *123*, 2052–2063.

Greten, F.R., Eckmann, L., Greten, T.F., Park, J.M., Li, Z.-W., Egan, L.J., Kagnoff, M.F., and Karin, M. (2004). IKKβ Links Inflammation and Tumorigenesis in a Mouse Model of Colitis-Associated Cancer. Cell *118*, 285–296.

Grilli, M., Pizzi, M., Memo, M., and Spano, P. (1996). Neuroprotection by Aspirin and Sodium Salicylate Through Blockade of NF-κB Activation. Science *274*, 1383–1385.

Grossmann, M., Metcalf, D., Merryfull, J., Beg, A., Baltimore, D., and Gerondakis, S. (1999). The combined absence of the transcription factors Rel and RelA leads to multiple hemopoietic cell defects. Proc. Natl. Acad. Sci. *96*, 11848–11853.

Grunhagen, D.J., de Wilt, J.H.W., Graveland, W.J., Verhoef, C., van Geel, A.N., and Eggermont, A.M.M. (2006). Outcome and prognostic factor analysis of 217 consecutive isolated limb perfusions with tumor necrosis factor-α and melphalan for limb-threatening soft tissue sarcoma. Cancer *106*, 1776–1784.

Gückel, E., Frey, S., Zaiss, M.M., Schett, G., Ghosh, S., and Voll, R.E. (2011). Cell-Intrinsic NF-κB Activation Is Critical for the Development of Natural Regulatory T Cells in Mice. PLoS ONE *6*, e20003.

Guerra, C., Collado, M., Navas, C., Schuhmacher, A.J., Hernández-Porras, I., Cañamero, M., Rodriguez-Justo, M., Serrano, M., and Barbacid, M. (2011). Pancreatitis-Induced Inflammation Contributes to Pancreatic Cancer by Inhibiting Oncogene-Induced Senescence. Cancer Cell *19*, 728–739.

Gupta, S.C., Patchva, S., Koh, W., and Aggarwal, B.B. (2012). Discovery of Curcumin, a Component of the Golden Spice, and Its Miraculous Biological Activities. Clin. Exp. Pharmacol. Physiol. *39*, 283–299.

Gut, G., Herrmann, M.D., and Pelkmans, L. (2018). Multiplexed protein maps link subcellular organization to cellular states. Science *361*, eaar7042.

Gutschow, M.V., Hughey, J.J., Ruggero, N.A., Bajar, B.T., Valle, S.D., and Covert, M.W. (2013). Single-Cell and Population NF-κB Dynamic Responses Depend on Lipopolysaccharide Preparation. PLOS ONE *8*, e53222.

Guttridge, D.C., Albanese, C., Reuther, J.Y., Pestell, R.G., and Baldwin, A.S. (1999). NF-κB Controls Cell Growth and Differentiation through Transcriptional Regulation of Cyclin D1. Mol. Cell. Biol. *19*, 5785–5799.

Hagemann, T., Lawrence, T., McNeish, I., Charles, K.A., Kulbe, H., Thompson, R.G., Robinson, S.C., and Balkwill, F.R. (2008). “Re-educating” tumor-associated macrophages by targeting NF-κB. J. Exp. Med. *205*, 1261–1268.

Hahn, S.A., Schutte, M., Hoque, A.T., Moskaluk, C.A., da Costa, L.T., Rozenblum, E., Weinstein, C.L., Fischer, A., Yeo, C.J., Hruban, R.H., et al. (1996). DPC4, a candidate tumor suppressor gene at human chromosome 18q21.1. Science *271*, 350–353.

Hall, A. (1998). Rho GTPases and the actin cytoskeleton. Science *279*, 509–514.

Hall, A. (2009). The cytoskeleton and cancer. Cancer Metastasis Rev. *28*, 5–14.

Hall, A., Marshall, C.J., Spurr, N.K., and Weiss, R.A. (1983). Identification of transforming gene in two human sarcoma cell lines as a new member of the ras gene family located on chromosome 1. Nature *303*, 396–400.

Hanson, J., and Huxley, H.E. (1953). Structural basis of the cross-striations in muscle. Nature *172*, 530–532.

Hardacre, J.M., Mulcahy, M., Small, W., Talamonti, M., Obel, J., Krishnamurthi, S., Rocha-Lima, C.S., Safran, H., Lenz, H.-J., and Chiorean, E.G. (2013). Addition of algenpantucel-L immunotherapy to standard adjuvant therapy for pancreatic cancer: a phase 2 study. J. Gastrointest. Surg. Off. J. Soc. Surg. Aliment. Tract *17*, 94–100; discussion p. 100-101.

Harlin, H., Hwang, K.W., Palucki, D.A., Kim, O., Thompson, C.B., Boothby, M., and Alegre, M.-L. (2002). CTLA-4 engagement regulates NF-κB activation in vivo. Eur. J. Immunol. *32*, 2095–2104.

Harrington, K., Freeman, D.J., Kelly, B., Harper, J., and Soria, J.-C. (2019). Optimizing oncolytic virotherapy in cancer treatment. Nat. Rev. Drug Discov. *18*, 689–706.

Harrington, K.J., Puzanov, I., Hecht, J.R., Hodi, F.S., Szabo, Z., Murugappan, S., and Kaufman, H.L. (2015). Clinical development of talimogene laherparepvec (T-VEC): a modified herpes simplex virus type-1-derived oncolytic immunotherapy. Expert Rev. Anticancer Ther. *15*, 1389–1403.

Harrington, K.J., Kong, A., Mach, N., Chesney, J.A., Fernandez, B.C., Rischin, D., Cohen, E.E.W., Radcliffe, H.-S., Gumuscu, B., Cheng, J., et al. (2020). Talimogene Laherparepvec and Pembrolizumab in Recurrent or Metastatic Squamous Cell Carcinoma of the Head and Neck (MASTERKEY-232): A Multicenter, Phase 1b Study. Clin. Cancer Res. Off. J. Am. Assoc. Cancer Res. *26*, 5153–5161.

Harrison, M.L., Obermueller, E., Maisey, N.R., Hoare, S., Edmonds, K., Li, N.F., Chao, D., Hall, K., Lee, C., Timotheadou, E., et al. (2007). Tumor necrosis factor α as a new target for renal cell carcinoma: two sequential phase II trials of infliximab at standard and high dose. J. Clin. Oncol. Off. J. Am. Soc. Clin. Oncol. *25*, 4542–4549.

Hart, M.J., Eva, A., Evans, T., Aaronson, S.A., and Cerione, R.A. (1991). Catalysis of guanine nucleotide exchange on the CDC42Hs protein by the dbloncogene product. Nature *354*, 311–314.

Hashiro, G., Loh, P.C., and Yau, J.T. (1977). The preferential cytotoxicity of reovirus for certain transformed cell lines. Arch. Virol. *54*, 307–315.

Havell, E.A., Fiers, W., and North, R.J. (1988). The antitumor function of tumor necrosis factor (TNF), I. Therapeutic action of TNF against an established murine sarcoma is indirect, immunologically dependent, and limited by severe toxicity. J. Exp. Med. *167*, 1067–1085.

Hayashi, T., Ueno, Y., and Okamoto, T. (1993). Oxidoreductive regulation of nuclear factor κB. Involvement of a cellular reducing catalyst thioredoxin. J. Biol. Chem. *268*, 11380–11388.

Hayden, M.S., West, A.P., and Ghosh, S. (2006). NF-κB and the immune response. Oncogene *25*, 6758–6780.

He, G., Yu, G.-Y., Temkin, V., Ogata, H., Kuntzen, C., Sakurai, T., Sieghart, W., Peck-Radosavljevic, M., Leffert, H.L., and Karin, M. (2010). Hepatocyte IKKβ/NF-κB inhibits tumor promotion and progression by preventing oxidative stress driven STAT3 activation. Cancer Cell *17*, 286–297.

He, L., Long, L.R., Antani, S., and Thoma, G.R. (2012). Histology image analysis for carcinoma detection and grading. Comput. Methods Programs Biomed. *107*, 538–556.

He, S., Wang, L., Miao, L., Wang, T., Du, F., Zhao, L., and Wang, X. (2009). Receptor Interacting Protein Kinase-3 Determines Cellular Necrotic Response to TNF-α. Cell *137*, 1100–1111.

He, Y., Northey, J.J., Primeau, M., Machado, R.D., Trembath, R., Siegel, P.M., and Lamarche-Vane, N. (2011). CdGAP is required for transforming growth factor β- and Neu/ErbB-2-induced breast cancer cell motility and invasion. Oncogene *30*, 1032–1045.

Hecht, J.R., Bedford, R., Abbruzzese, J.L., Lahoti, S., Reid, T.R., Soetikno, R.M., Kirn, D.H., and Freeman, S.M. (2003). A Phase I/II Trial of Intratumoral Endoscopic Ultrasound Injection of ONYX-015 with Intravenous Gemcitabine in Unresectable Pancreatic Carcinoma. Clin. Cancer Res. *9*, 555–561.

Hegerfeldt, Y., Tusch, M., Bröcker, E.-B., and Friedl, P. (2002). Collective cell movement in

primary melanoma explants: plasticity of cell-cell interaction, β1-integrin function, and migration strategies. Cancer Res. *62*, 2125–2130.

Heid, I., Lubeseder-Martellato, C., Sipos, B., Mazur, P.K., Lesina, M., Schmid, R.M., and Siveke, J.T. (2011). Early requirement of Rac1 in a mouse model of pancreatic cancer. Gastroenterology *141*, 719–730, 730.e1-7.

Heidelberger, C., Chaudhuri, N.K., Danneberg, P., Mooren, D., Griesbach, L., Duschinsky, R., Schnitzer, R.J., Pleven, E., and Scheiner, J. (1957). Fluorinated Pyrimidines, A New Class of Tumour-Inhibitory Compounds. Nature *179*, 663–666.

Heinrichs, D.E., Yethon, J.A., and Whitfield, C. (1998). Molecular basis for structural diversity in the core regions of the lipopolysaccharides of Escherichia coli and Salmonella enterica. Mol. Microbiol. *30*, 221–232.

Hemminki, O., dos Santos, J.M., and Hemminki, A. (2020). Oncolytic viruses for cancer immunotherapy. J. Hematol. Oncol.J Hematol Oncol *13*, 84.

Hendrix, M.J., Seftor, E.A., Seftor, R.E., and Trevor, K.T. (1997). Experimental co-expression of vimentin and keratin intermediate filaments in human breast cancer cells results in phenotypic interconversion and increased invasive behavior. Am. J. Pathol. *150*, 483–495.

Herman, J.M., Wild, A.T., Wang, H., Tran, P.T., Chang, K.J., Taylor, G.E., Donehower, R.C., Pawlik, T.M., Ziegler, M.A., Cai, H., et al. (2013). Randomized Phase III Multi-Institutional Study of TNFerade Biologic With Fluorouracil and Radiotherapy for Locally Advanced Pancreatic Cancer: Final Results. J. Clin. Oncol. *31*, 886–894.

Hertel, L.W., Kroin, J.S., Misner, J.W., and Tustin, J.M. (1988). Synthesis of 2-deoxy-2,2-difluoro-D-ribose and 2-deoxy-2,2'-difluoro-D-ribofuranosyl nucleosides. J. Org. Chem. *53*, 2406–2409.

Hettmann, T., DiDonato, J., Karin, M., and Leiden, J.M. (1999). An Essential Role for Nuclear Factor κB in Promoting Double Positive Thymocyte Apoptosis. J. Exp. Med. *189*, 145–158.

Hezel, A.F., Kimmelman, A.C., Stanger, B.Z., Bardeesy, N., and DePinho, R.A. (2006). Genetics and biology of pancreatic ductal adenocarcinoma. Genes Dev. *20*, 1218–1249.

Hilliard, B.A., Mason, N., Xu, L., Sun, J., Lamhamedi-Cherradi, S.-E., Liou, H.-C., Hunter, C., and Chen, Y.H. (2002). Critical roles of c-Rel in autoimmune inflammation and helper T cell differentiation. J. Clin. Invest. *110*, 843–850.

Hinata, K., Gervin, A.M., Jennifer Zhang, Y., and Khavari, P.A. (2003). Divergent gene regulation and growth effects by NF-κB in epithelial and mesenchymal cells of human skin. Oncogene *22*, 1955–1964.

Hinz, M., Krappmann, D., Eichten, A., Heder, A., Scheidereit, C., and Strauss, M. (1999). NF-kB function in growth control: regulation of cyclin D1 expression and G0/G1-to-S-phase transition. Mol. Cell. Biol. *19*, 2690–2698.

Hirotani, T., Lee, P.Y., Kuwata, H., Yamamoto, M., Matsumoto, M., Kawase, I., Akira, S., and Takeda, K. (2005). The nuclear IκB protein IκBNS selectively inhibits lipopolysaccharide-induced IL-6 production in macrophages of the colonic lamina propria. J. Immunol. Baltim. Md 1950 *174*, 3650–3657.

Hiscott, J., Marois, J., Garoufalis, J., D'Addario, M., Roulston, A., Kwan, I., Pepin, N., Lacoste, J., Nguyen, H., and Bensi, G. (1993). Characterization of a functional NF-κB site in the human interleukin 1 β promoter: evidence for a positive autoregulatory loop. Mol. Cell. Biol. *13*, 6231–6240.

Hishima, T., Fukayama, M., Hayashi, Y., Fujii, T., Ooba, T., Funata, N., and Koike, M. (2000). CD70 expression in thymic carcinoma. Am. J. Surg. Pathol. *24*, 742–746.

Hobbs, G.A., Der, C.J., and Rossman, K.L. (2016). RAS isoforms and mutations in cancer at a glance. J. Cell Sci. *129*, 1287–1292.

Hoesel, B., and Schmid, J.A. (2013). The complexity of NF-κB signaling in inflammation and cancer. Mol. Cancer *12*, 86.

Hoffmann, A., and Baltimore, D. (2006). Circuitry of nuclear factor κB signaling. Immunol. Rev. *210*, 171–186.

Hoffmann, A., Levchenko, A., Scott, M.L., and Baltimore, D. (2002). The IκB-NF-κB Signaling Module: Temporal Control and Selective Gene Activation. Science *298*, 1241–1245.

Hoffmann, A., Leung, T.H., and Baltimore, D. (2003). Genetic analysis of NF-κB/Rel transcription factors defines functional specificities. EMBO J. *22*, 5530–5539.

Hoffmann, A., Natoli, G., and Ghosh, G. (2006). Transcriptional regulation via the NF-κB signaling module. Oncogene *25*, 6706–6716.

Hofmann, W.A., Stojiljkovic, L., Fuchsova, B., Vargas, G.M., Mavrommatis, E., Philimonenko, V., Kysela, K., Goodrich, J.A., Lessard, J.L., Hope, T.J., et al. (2004). Actin is part of pre-initiation complexes and is necessary for transcription by RNA polymerase II. Nat. Cell Biol. *6*, 1094–1101.

Hömig-Hölzel, C., Hojer, C., Rastelli, J., Casola, S., Strobl, L.J., Müller, W., Quintanilla-Martinez, L., Gewies, A., Ruland, J., Rajewsky, K., et al. (2008). Constitutive CD40 signaling in B cells selectively activates the noncanonical NF-κB pathway and promotes lymphomagenesis. J. Exp. Med. *205*, 1317–1329.

Honda, K., Yamada, T., Endo, R., Ino, Y., Gotoh, M., Tsuda, H., Yamada, Y., Chiba, H., and Hirohashi, S. (1998). Actinin-4, a Novel Actin-bundling Protein Associated with Cell Motility and Cancer Invasion. J. Cell Biol. *140*, 1383–1393.

Horwitz, B.H., Scott, M.L., Cherry, S.R., Bronson, R.T., and Baltimore, D. (1997). Failure of Lymphopoiesis after Adoptive Transfer of NF-κB–Deficient Fetal Liver Cells. Immunity *6*, 765–772.

Hsu, H., Xiong, J., and Goeddel, D.V. (1995). The TNF receptor 1-associated protein TRADD signals cell death and NF-κB activation. Cell *81*, 495–504.

Hu, X., Li, B., Li, X., Zhao, X., Wan, L., Lin, G., Yu, M., Wang, J., Jiang, X., Feng, W., et al. (2014). Transmembrane TNF-α Promotes Suppressive Activities of Myeloid-Derived Suppressor Cells via TNFR2. J. Immunol. *192*, 1320–1331.

Huang, F.-Y., Li, Y.-N., Mei, W.-L., Dai, H.-F., Zhou, P., and Tan, G.-H. (2012a). Cytochalasin D, a tropical fungal metabolite, inhibits CT26 tumor growth and angiogenesis. Asian Pac. J. Trop. Med. *5*, 169–174.

Huang, F.-Y., Mei, W., Li, Y.-N., Tan, G.-H., Dai, H.-F., Guo, J.-L., Wang, H., Huang, Y.-H., Zhao, H.-G., Zhou, S.-L., et al. (2012b). The antitumour activities induced by pegylated liposomal cytochalasin D in murine models. Eur. J. Cancer *48*, 2260–2269.

Huang, H., Liu, Y., Daniluk, J., Gaiser, S., Chu, J., Wang, H., Li, Z.-S., Logsdon, C.D., and Ji, B. (2013). Activation of nuclear factor-κB in acinar cells increases the severity of pancreatitis in mice. Gastroenterology *144*, 202–210.

Huang, L., Holtzinger, A., Jagan, I., BeGora, M., Lohse, I., Ngai, N., Nostro, C., Wang, R., Muthuswamy, L.B., Crawford, H.C., et al. (2015). Ductal pancreatic cancer modeling and drug screening using human pluripotent stem cell- and patient-derived tumor organoids. Nat. Med. *21*, 1364–1371.

Huang, L., Jansen, L., Balavarca, Y., Molina-Montes, E., Babaei, M., van der Geest, L., Lemmens, V., Van Eycken, L., De Schutter, H., Johannesen, T.B., et al. (2019). Resection of pancreatic cancer in Europe and USA: an international large-scale study highlighting large variations. Gut *68*, 130–139.

Huang, T.T., Kudo, N., Yoshida, M., and Miyamoto, S. (2000). A nuclear export signal in the N-terminal regulatory domain of IκBα controls cytoplasmic localization of inactive NF-κB/IκBα complexes. Proc. Natl. Acad. Sci. U. S. A. *97*, 1014–1019.

Huang, W., Zhang, L., Yang, M., Wu, X., Wang, X., Huang, W., Yuan, L., Pan, H., Wang, Y., Wang, Z., et al. (2021). Cancer-associated fibroblasts promote the survival of irradiated nasopharyngeal carcinoma cells via the NF-κB pathway. J. Exp. Clin. Cancer Res. *40*, 87.

Huber, M.A., Azoitei, N., Baumann, B., Grünert, S., Sommer, A., Pehamberger, H., Kraut, N., Beug, H., and Wirth, T. (2004). NF-κB is essential for epithelial-mesenchymal transition and metastasis in a model of breast cancer progression. J. Clin. Invest. *114*, 569–581.

Huelsmann, S., and Brown, N.H. (2014). Nuclear positioning by actin cables and perinuclear actin. Nucleus *5*, 219–223.

Huxford, T., Huang, D.-B., Malek, S., and Ghosh, G. (1998). The Crystal Structure of the IκBα/NF-κB Complex Reveals Mechanisms of NF-κB Inactivation. Cell *95*, 759–770.

Iademarco, M.F., McQuillan, J.J., Rosen, G.D., and Dean, D.C. (1992). Characterization of the promoter for vascular cell adhesion molecule-1 (VCAM-1). J. Biol. Chem. *267*, 16323–16329.

Ingraham, H.A., Tseng, B.Y., and Goulian, M. (1982). Nucleotide levels and incorporation of 5-fluorouracil and uracil into DNA of cells treated with 5-fluorodeoxyuridine. Mol. Pharmacol. *21*, 211–216.

Inman, W., and Crews, P. (1989). Novel marine sponge-derived amino acids. 8. Conformational analysis of jasplakinolide. J. Am. Chem. Soc. *111*, 2822–2829.

Ip, Y.T., Park, R.E., Kosman, D., Yazdanbakhsh, K., and Levine, M. (1992). dorsal-twist interactions establish snail expression in the presumptive mesoderm of the Drosophila embryo. Genes Dev. *6*, 1518–1530.

Ishizaki, T., Morishima, Y., Okamoto, M., Furuyashiki, T., Kato, T., and Narumiya, S. (2001). Coordination of microtubules and the actin cytoskeleton by the Rho effector mDia1. Nat. Cell Biol. *3*, 8–14.

Isogai, T., van der Kammen, R., and Innocenti, M. (2015). SMIFH2 has effects on Formins and p53 that perturb the cell cytoskeleton. Sci. Rep. *5*, 9802.

Iwanaszko, M., and Kimmel, M. (2015). NF-κB and IRF pathways: cross-regulation on target genes promoter level. BMC Genomics *16*, 307.

Jacinto, A., Martinez-Arias, A., and Martin, P. (2001). Mechanisms of epithelial fusion and repair. Nat. Cell Biol. *3*, E117–E123.

Jacks, K.A., and Koch, C.A. (2010). Differential Regulation of Mitogen- and Stress-activated Protein Kinase-1 and -2 (MSK1 and MSK2) by CK2 following UV Radiation. J. Biol. Chem.

285, 1661–1670.

Jacobs, M.D., and Harrison, S.C. (1998). Structure of an IκBα/NF-κB complex. Cell *95*, 749–758.

Jensen, C., and Teng, Y. (2020). Is It Time to Start Transitioning From 2D to 3D Cell Culture? Front. Mol. Biosci. *7*.

Jiang, H., Hegde, S., Knolhoff, B.L., Zhu, Y., Herndon, J.M., Meyer, M.A., Nywening, T.M., Hawkins, W.G., Shapiro, I.M., Weaver, D.T., et al. (2016). Targeting focal adhesion kinase renders pancreatic cancers responsive to checkpoint immunotherapy. Nat. Med. *22*, 851–860.

Jiang, X., Takahashi, N., Matsui, N., Tetsuka, T., and Okamoto, T. (2003). The NF-κB activation in lymphotoxin-β receptor signaling depends on the phosphorylation of p65 at serine 536. J. Biol. Chem. *278*, 919–926.

Jiang, Z., Ninomiya-Tsuji, J., Qian, Y., Matsumoto, K., and Li, X. (2002). Interleukin-1 (IL-1) receptor-associated kinase-dependent IL-1-induced signaling complexes phosphorylate TAK1 and TAB2 at the plasma membrane and activate TAK1 in the cytosol. Mol. Cell. Biol. *22*, 7158–7167.

Jones, S., Zhang, X., Parsons, D.W., Lin, J.C.-H., Leary, R.J., Angenendt, P., Mankoo, P., Carter, H., Kamiyama, H., Jimeno, A., et al. (2008). Core Signaling Pathways in Human Pancreatic Cancers Revealed by Global Genomic Analyses. Science *321*, 1801–1806.

Jordan, M.A., and Wilson, L. (1998). Microtubules and actin filaments: dynamic targets for cancer chemotherapy. Curr. Opin. Cell Biol. *10*, 123–130.

Jordan, M.A., Toso, R.J., Thrower, D., and Wilson, L. (1993). Mechanism of mitotic block and inhibition of cell proliferation by taxol at low concentrations. Proc. Natl. Acad. Sci. U. S. A. *90*, 9552–9556.

Kajiura, F., Sun, S., Nomura, T., Izumi, K., Ueno, T., Bando, Y., Kuroda, N., Han, H., Li, Y., Matsushima, A., et al. (2004). NF-κB-inducing kinase establishes self-tolerance in a thymic stroma-dependent manner. J. Immunol. Baltim. Md 1950 *172*, 2067–2075.

Kalluri, R., and Weinberg, R.A. (2009). The basics of epithelial-mesenchymal transition. J. Clin. Invest. *119*, 1420–1428.

Kanai, M., Yoshimura, K., Asada, M., Imaizumi, A., Suzuki, C., Matsumoto, S., Nishimura, T., Mori, Y., Masui, T., Kawaguchi, Y., et al. (2011). A phase I/II study of gemcitabine-based chemotherapy plus curcumin for patients with gemcitabine-resistant pancreatic cancer. Cancer Chemother. Pharmacol. *68*, 157–164.

Kanamaru, R., Kakuta, H., Sato, T., Ishioka, C., and Wakui, A. (1986). The inhibitory effects of 5-fluorouracil on the metabolism of preribosomal and ribosomal RNA in L-1210 cells in vitro. Cancer Chemother. Pharmacol. *17*, 43–46.

Kanazawa, T., Hamasaki, T., Endo, T., Tamano, K., Sogabe, K., Seta, Y., Ohgi, T., and Okada, H. (2015). Functional peptide nanocarriers for delivery of novel anti-RelA RNA interference agents as a topical treatment of atopic dermatitis. Int. J. Pharm. *489*, 261–267.

Kane, R.C., Bross, P.F., Farrell, A.T., and Pazdur, R. (2003). Velcade: U.S. FDA approval for the treatment of multiple myeloma progressing on prior therapy. The Oncologist *8*, 508–513.

Kapałczyńska, M., Kolenda, T., Przybyła, W., Zajączkowska, M., Teresiak, A., Filas, V., Ibbs, M., Bliźniak, R., Łuczewski, Ł., and Lamperska, K. (2018). 2D and 3D cell cultures – a

comparison of different types of cancer cell cultures. Arch. Med. Sci. AMS *14*, 910–919.

Kapatai, G., and Murray, P. (2007). Contribution of the Epstein–Barr virus to the molecular pathogenesis of Hodgkin lymphoma. J. Clin. Pathol. *60*, 1342–1349.

Karayiannakis, A.J., Syrigos, K.N., Polychronidis, A., Pitiakoudis, M., Bounovas, A., and Simopoulos, K. (2001). Serum levels of tumor necrosis factor-α and nutritional status in pancreatic cancer patients. Anticancer Res. *21*, 1355–1358.

Karin, M. (2009). NF-κB as a Critical Link Between Inflammation and Cancer. Cold Spring Harb. Perspect. Biol. *1*.

Karlsson, M., Zhang, C., Méar, L., Zhong, W., Digre, A., Katona, B., Sjöstedt, E., Butler, L., Odeberg, J., Dusart, P., et al. (2021). A single–cell type transcriptomics map of human tissues. Sci. Adv.

Karyampudi, L., Lamichhane, P., Krempski, J., Kalli, K.R., Behrens, M.D., Vargas, D.M., Hartmann, L.C., Janco, J.M.T., Dong, H., Hedin, K.E., et al. (2016). PD-1 Blunts the Function of Ovarian Tumor–Infiltrating Dendritic Cells by Inactivating NF-κB. Cancer Res. *76*, 239–250.

Kashii, Y., Giorda, R., Herberman, R.B., Whiteside, T.L., and Vujanovic, N.L. (1999). Constitutive Expression and Role of the TNF Family Ligands in Apoptotic Killing of Tumor Cells by Human NK Cells. J. Immunol. *163*, 5358–5366.

Kashman, Y., Groweiss, A., and Shmueli, U. (1980). Latrunculin, a new 2-thiazolidinone macrolide from the marine sponge latrunculia magnifica. Tetrahedron Lett. *21*, 3629–3632.

Kashyap, T., Argueta, C., Aboukameel, A., Unger, T.J., Klebanov, B., Mohammad, R.M., Muqbil, I., Azmi, A.S., Drolen, C., Senapedis, W., et al. (2016). Selinexor, a Selective Inhibitor of Nuclear Export (SINE) compound, acts through NF-κB deactivation and combines with proteasome inhibitors to synergistically induce tumor cell death. Oncotarget *7*, 78883–78895.

Kashyap, V.K., Wang, Q., Setua, S., Nagesh, P.K.B., Chauhan, N., Kumari, S., Chowdhury, P., Miller, D.D., Yallapu, M.M., Li, W., et al. (2019). Therapeutic efficacy of a novel βIII/βIV-tubulin inhibitor (VERU-111) in pancreatic cancer. J. Exp. Clin. Cancer Res. *38*, 29.

Kato, M., Sanada, M., Kato, I., Sato, Y., Takita, J., Takeuchi, K., Niwa, A., Chen, Y., Nakazaki, K., Nomoto, J., et al. (2009). Frequent inactivation of A20 in B-cell lymphomas. Nature *459*, 712–716.

Kawai, T., and Akira, S. (2007). Signaling to NF-κB by Toll-like receptors. Trends Mol. Med. *13*, 460–469.

Kearns, J.D., Basak, S., Werner, S.L., Huang, C.S., and Hoffmann, A. (2006). IκBε provides negative feedback to control NF-κB oscillations, signaling dynamics, and inflammatory gene expression. J. Cell Biol. *173*, 659–664.

Keats, J.J., Fonseca, R., Chesi, M., Schop, R., Baker, A., Chng, W.-J., Van Wier, S., Tiedemann, R., Shi, C.-X., Sebag, M., et al. (2007). Promiscuous mutations activate the noncanonical NF-κB pathway in multiple myeloma. Cancer Cell *12*, 131–144.

Kelliher, M.A., Grimm, S., Ishida, Y., Kuo, F., Stanger, B.Z., and Leder, P. (1998). The Death Domain Kinase RIP Mediates the TNF-Induced NF-κB Signal. Immunity *8*, 297–303.

Kellogg, R.A., and Tay, S. (2015). Noise Facilitates Transcriptional Control under Dynamic Inputs. Cell *160*, 381–392.

Kellogg, R.A., Tian, C., Lipniacki, T., Quake, S.R., and Tay, S. (2015). Digital signaling decouples activation probability and population heterogeneity. eLife *4*, e08931.

Kerr, J.F.R., Wyllie, A.H., and Currie, A.R. (1972). Apoptosis: A Basic Biological Phenomenon with Wideranging Implications in Tissue Kinetics. Br. J. Cancer *26*, 239–257.

Khoshnan, A., Bae, D., Tindell, C.A., and Nel, A.E. (2000). The Physical Association of Protein Kinase Cθ with a Lipid Raft-Associated Inhibitor of κB Factor Kinase (IKK) Complex Plays a Role in the Activation of the NF-κB Cascade by TCR and CD28. J. Immunol. *165*, 6933–6940.

Khurana, N., Dodhiawala, P.B., Bulle, A., and Lim, K.-H. (2020). Deciphering the Role of Innate Immune NF-κB Pathway in Pancreatic Cancer. Cancers *12*, 2675.

Kiefel, H., Bondong, S., Erbe-Hoffmann, N., Hazin, J., Riedle, S., Wolf, J., Pfeifer, M., Arlt, A., Schäfer, H., Müerköster, S.S., et al. (2010). L1CAM–integrin interaction induces constitutive NF-κB activation in pancreatic adenocarcinoma cells by enhancing IL-1β expression. Oncogene *29*, 4766–4778.

Kieran, M., Blank, V., Logeat, F., Vandekerckhove, J., Lottspeich, F., Le Bail, O., Urban, M.B., Kourilsky, P., Baeuerle, P.A., and Israël, A. (1990). The DNA binding subunit of NF-κB is identical to factor KBF1 and homologous to the rel oncogene product. Cell *62*, 1007–1018.

Kim, H.-J., Litzenburger, B.C., Cui, X., Delgado, D.A., Grabiner, B.C., Lin, X., Lewis, M.T., Gottardis, M.M., Wong, T.W., Attar, R.M., et al. (2007). Constitutively Active Type I Insulin-Like Growth Factor Receptor Causes Transformation and Xenograft Growth of Immortalized Mammary Epithelial Cells and Is Accompanied by an Epithelial-to-Mesenchymal Transition Mediated by NF-κB and Snail. Mol. Cell. Biol.

Kimura, K., Ito, M., Amano, M., Chihara, K., Fukata, Y., Nakafuku, M., Yamamori, B., Feng, J., Nakano, T., Okawa, K., et al. (1996). Regulation of myosin phosphatase by Rho and Rho-associated kinase (Rho-kinase). Science *273*, 245–248.

Kimura, Y., Tsukada, J., Tomoda, T., Takahashi, H., Imai, K., Shimamura, K., Sunamura, M., Yonemitsu, Y., Shimodaira, S., Koido, S., et al. (2012). Clinical and immunologic evaluation of dendritic cell-based immunotherapy in combination with gemcitabine and/or S-1 in patients with advanced pancreatic carcinoma. Pancreas *41*, 195–205.

Klomp, J.E., Lee, Y.S., Goodwin, C.M., Papke, B., Klomp, J.A., Waters, A.M., Stalnecker, C.A., DeLiberty, J.M., Drizyte-Miller, K., Yang, R., et al. (2021). CHK1 protects oncogenic KRAS-expressing cells from DNA damage and is a target for pancreatic cancer treatment. Cell Rep. *37*, 110060.

Knowlton, J.J., Dermody, T.S., and Holm, G.H. (2012). Apoptosis induced by mammalian reovirus is β-interferon (IFN) independent and enhanced by IFN regulatory factor 3- and NF-κB-dependent expression of Noxa. J. Virol. *86*, 1650–1660.

Kominsky, D.J., Bickel, R.J., and Tyler, K.L. (2002). Reovirus-induced apoptosis requires both death receptor- and mitochondrial-mediated caspase-dependent pathways of cell death. Cell Death Differ. *9*, 926–933.

Koo, G.-B., Morgan, M.J., Lee, D.-G., Kim, W.-J., Yoon, J.-H., Koo, J.S., Kim, S.I., Kim, S.J., Son, M.K., Hong, S.S., et al. (2015). Methylation-dependent loss of RIP3 expression in cancer represses programmed necrosis in response to chemotherapeutics. Cell Res. *25*, 707–725.

Kopp, E., and Ghosh, S. (1994). Inhibition of NF-κB by sodium salicylate and aspirin.

Science *265*, 956–959.

Körner, M., Tarantino, N., and Debré, P. (1991). Constitutive activation of NF-κB in human thymocytes. Biochem. Biophys. Res. Commun. *181*, 80–86.

Kovács, M., Tóth, J., Hetényi, C., Málnási-Csizmadia, A., and Sellers, J.R. (2004). Mechanism of Blebbistatin Inhibition of Myosin II. J. Biol. Chem. *279*, 35557–35563.

Kovalenko, A., Chable-Bessia, C., Cantarella, G., Israël, A., Wallach, D., and Courtois, G. (2003). The tumour suppressor CYLD negatively regulates NF-κB signalling by deubiquitination. Nature *424*, 801–805.

Kreuz, S., Siegmund, D., Scheurich, P., and Wajant, H. (2001). NF-κB Inducers Upregulate cFLIP, a Cycloheximide-Sensitive Inhibitor of Death Receptor Signaling. Mol. Cell. Biol.

Krizhevsky, A., Sutskever, I., and Hinton, G.E. (2017). ImageNet classification with deep convolutional neural networks. Commun. ACM *60*, 84–90.

Kuei, J.H., Tashkin, D.P., and Figlin, R.A. (1989). Pulmonary toxicity of recombinant human tumor necrosis factor. Chest *96*, 334–338.

Kulbe, H., Thompson, R., Wilson, J.L., Robinson, S., Hagemann, T., Fatah, R., Gould, D., Ayhan, A., and Balkwill, F. (2007). The Inflammatory Cytokine Tumor Necrosis Factor-α Generates an Autocrine Tumor-Promoting Network in Epithelial Ovarian Cancer Cells. Cancer Res. *67*, 585–592.

Kulwichit, W., Edwards, R.H., Davenport, E.M., Baskar, J.F., Godfrey, V., and Raab-Traub, N. (1998). Expression of the Epstein–Barr virus latent membrane protein 1 induces B cell lymphoma in transgenic mice. Proc. Natl. Acad. Sci. *95*, 11963–11968.

Kunimoto, T., Nitta, K., Tanaka, T., Uehara, N., Baba, H., Takeuchi, M., Yokokura, T., Sawada, S., Miyasaka, T., and Mutai, M. (1987). Antitumor Activity of 7-Ethyl-10-[4-(1-piperidino)-1-piperidino]carbonyloxycamptothecin, a Novel Water-soluble Derivative of Camptothecin, against Murine Tumors. Cancer Res. *47*, 5944–5947.

Kunnumakkara, A.B., Guha, S., Krishnan, S., Diagaradjane, P., Gelovani, J., and Aggarwal, B.B. (2007). Curcumin Potentiates Antitumor Activity of Gemcitabine in an Orthotopic Model of Pancreatic Cancer through Suppression of Proliferation, Angiogenesis, and Inhibition of Nuclear Factor-κB–Regulated Gene Products. Cancer Res. *67*, 3853–3861.

Kunsch, C., and Rosen, C.A. (1993). NF-κB subunit-specific regulation of the interleukin-8 promoter. Mol. Cell. Biol. *13*, 6137–6146.

Kunsch, C., Ruben, S.M., and Rosen, C.A. (1992). Selection of optimal κB/Rel DNA-binding motifs: interaction of both subunits of NF-κB with DNA is required for transcriptional activation. Mol. Cell. Biol. *12*, 4412–4421.

Kurki, P., Vanderlaan, M., Dolbeare, F., Gray, J., and Tan, E.M. (1986). Expression of proliferating cell nuclear antigen (PCNA)/cyclin during the cell cycle. Exp. Cell Res. *166*, 209–219.

Kustermans, G., El Benna, J., Piette, J., and Legrand-Poels, S. (2005). Perturbation of actin dynamics induces NF-κB activation in myelomonocytic cells through an NADPH oxidase-dependent pathway. Biochem. J. *387*, 531–540.

Kuwana, Y., Asakura, Y., Utsunomiya, N., Nakanishi, M., Arata, Y., Itoh, S., Nagase, F., and Kurosawa, Y. (1987). Expression of chimeric receptor composed of immunoglobulin-derived V resions and T-cell receptor-derived C regions. Biochem. Biophys. Res. Commun. *149*,

960–968.

Laevsky, G., and Knecht, D.A. (2003). Cross-linking of actin filaments by myosin II is a major contributor to cortical integrity and cell motility in restrictive environments. J. Cell Sci. *116*, 3761–3770.

Lalle, G., Twardowski, J., and Grinberg-Bleyer, Y. (2021). NF-κB in Cancer Immunity: Friend or Foe? Cells *10*, 355.

Lamarche-Vane, N., and Hall, A. (1998). CdGAP, a novel proline-rich GTPase-activating protein for Cdc42 and Rac. J. Biol. Chem. *273*, 29172–29177.

Lamba, V., and Ghosh, I. (2012). New directions in targeting protein kinases: focusing upon true allosteric and bivalent inhibitors. Curr. Pharm. Des. *18*, 2936–2945.

Lamers, C.H.J., Sleijfer, S., Vulto, A.G., Kruit, W.H.J., Kliffen, M., Debets, R., Gratama, J.W., Stoter, G., and Oosterwijk, E. (2006). Treatment of metastatic renal cell carcinoma with autologous T-lymphocytes genetically retargeted against carbonic anhydrase IX: first clinical experience. J. Clin. Oncol. *24*, e20-2.

Lancaster, O.M., Le Berre, M., Dimitracopoulos, A., Bonazzi, D., Zlotek-Zlotkiewicz, E., Picone, R., Duke, T., Piel, M., and Baum, B. (2013). Mitotic rounding alters cell geometry to ensure efficient bipolar spindle formation. Dev. Cell *25*, 270–283.

Lane, K., Valen, D.V., DeFelice, M.M., Macklin, D.N., Kudo, T., Jaimovich, A., Carr, A., Meyer, T., Pe'er, D., Boutet, S.C., et al. (2017). Measuring Signaling and RNA-Seq in the Same Cell Links Gene Expression to Dynamic Patterns of NF-κB Activation. Cell Syst. *4*, 458-469.e5.

Lao, C.D., Ruffin, M.T., Normolle, D., Heath, D.D., Murray, S.I., Bailey, J.M., Boggs, M.E., Crowell, J., Rock, C.L., and Brenner, D.E. (2006). Dose escalation of a curcuminoid formulation. BMC Complement. Altern. Med. *6*, 10.

Larsen, J.E., Nathan, V., Osborne, J.K., Farrow, R.K., Deb, D., Sullivan, J.P., Dospoy, P.D., Augustyn, A., Hight, S.K., Sato, M., et al. (2016). ZEB1 drives epithelial-to-mesenchymal transition in lung cancer. J. Clin. Invest. *126*, 3219–3235.

Latimer, M., Ernst, M.K., Dunn, L.L., Drutskaya, M., and Rice, N.R. (1998). The N-Terminal Domain of IκBα Masks the Nuclear Localization Signal(s) of p50 and c-Rel Homodimers. Mol. Cell. Biol. *18*, 2640–2649.

Laurila, E., Savinainen, K., Kuuselo, R., Karhu, R., and Kallioniemi, A. (2009). Characterization of the 7q21-q22 amplicon identifies ARPC1A, a subunit of the Arp2/3 complex, as a regulator of cell migration and invasion in pancreatic cancer. Genes. Chromosomes Cancer *48*, 330–339.

Le, H.Q., Ghatak, S., Yeung, C.-Y.C., Tellkamp, F., Günschmann, C., Dieterich, C., Yeroslaviz, A., Habermann, B., Pombo, A., Niessen, C.M., et al. (2016). Mechanical regulation of transcription controls Polycomb-mediated gene silencing during lineage commitment. Nat. Cell Biol. *18*, 864–875.

Leach, D.R., Krummel, M.F., and Allison, J.P. (1996). Enhancement of antitumor immunity by CTLA-4 blockade. Science *271*, 1734–1736.

Lee, H., Herrmann, A., Deng, J.-H., Kujawski, M., Niu, G., Li, Z., Forman, S., Jove, R., Pardoll, D.M., and Yu, H. (2009). Persistently activated Stat3 maintains constitutive NF-κB activity in tumors. Cancer Cell *15*, 283–293.

Lee, H.J., Diaz, M.F., Ewere, A., Olson, S.D., Cox, C.S., and Wenzel, P.L. (2017). Focal adhesion kinase signaling regulates anti-inflammatory function of bone marrow mesenchymal stromal cells induced by biomechanical force. Cell. Signal. *38*, 1–9.

Lee, R.E.C., Walker, S.R., Savery, K., Frank, D.A., and Gaudet, S. (2014). Fold Change of Nuclear NF-κB Determines TNF-Induced Transcription in Single Cells. Mol. Cell *53*, 867–879.

Lee, R.E.C., Qasaimeh, M.A., Xia, X., Juncker, D., and Gaudet, S. (2016). NF-κB signalling and cell fate decisions in response to a short pulse of tumour necrosis factor. Sci. Rep. *6*.

Leek, R.D., Lewis, C.E., Whitehouse, R., Greenall, M., Clarke, J., and Harris, A.L. (1996). Association of Macrophage Infiltration with Angiogenesis and Prognosis in Invasive Breast Carcinoma. Cancer Res. *56*, 4625–4629.

Legembre, P., Schickel, R., Barnhart, B.C., and Peter, M.E. (2004). Identification of SNF1/AMP Kinase-related Kinase as an NF-κB-regulated Anti-apoptotic Kinase Involved in CD95-induced Motility and Invasiveness. J. Biol. Chem. *279*, 46742–46747.

Legrand, A.J., Konstantinou, M., Goode, E.F., and Meier, P. (2019). The Diversification of Cell Death and Immunity: Memento Mori. Mol. Cell *76*, 232–242.

Lemaire, C., Andréau, K., Souvannavong, V., and Adam, A. (1998). Inhibition of caspase activity induces a switch from apoptosis to necrosis. FEBS Lett. *425*, 266–270.

Leonard, N., Chaggar, R., Jones, C., Takahashi, M., Nikitopoulou, A., and Lakhani, S. (2001). Loss of heterozygosity at cylindromatosis gene locus, CYLD, in sporadic skin adnexal tumours. J. Clin. Pathol. *54*, 689–692.

Lesina, M., Wörmann, S.M., Morton, J., Diakopoulos, K.N., Korneeva, O., Wimmer, M., Einwächter, H., Sperveslage, J., Demir, I.E., Kehl, T., et al. (2016). RelA regulates CXCL1/CXCR2-dependent oncogene-induced senescence in murine *Kras*-driven pancreatic carcinogenesis. J. Clin. Invest. *126*, 2919–2932.

Lessard, S.J., Rivas, D.A., So, K., Koh, H.-J., Queiroz, A.L., Hirshman, M.F., Fielding, R.A., and Goodyear, L.J. (2016). The AMPK-related kinase SNARK regulates muscle mass and myocyte survival. J. Clin. Invest. *126*, 560–570.

Leung, T.H., Hoffmann, A., and Baltimore, D. (2004). One Nucleotide in a κB Site Can Determine Cofactor Specificity for NF-κB Dimers. Cell *118*, 453–464.

Li, X., and Nicklas, R.B. (1995). Mitotic forces control a cell-cycle checkpoint. Nature *373*, 630–632.

Li, G., Boucher, J.C., Kotani, H., Park, K., Zhang, Y., Shrestha, B., Wang, X., Guan, L., Beatty, N., Abate-Daga, D., et al. (2018). 4-1BB enhancement of CAR T function requires NF-κB and TRAFs. JCI Insight *3*.

Li, H., Zhu, H., Xu, C.J., and Yuan, J. (1998). Cleavage of BID by caspase 8 mediates the mitochondrial damage in the Fas pathway of apoptosis. Cell *94*, 491–501.

Li, J., Sarosi, I., Yan, X.Q., Morony, S., Capparelli, C., Tan, H.L., McCabe, S., Elliott, R., Scully, S., Van, G., et al. (2000). RANK is the intrinsic hematopoietic cell surface receptor that controls osteoclastogenesis and regulation of bone mass and calcium metabolism. Proc. Natl. Acad. Sci. U. S. A. *97*, 1566–1571.

Li, J.K.-K., Scheible, P.P., Keene, J.D., and Joklik, W.K. (1980). The plus strand of reovirus gene S2 is identical with its in vitro transcript. Virology *105*, 282–286.

Li, M., Wang, Y., Li, M., Wu, X., Setrerrahmane, S., and Xu, H. (2021). Integrins as attractive targets for cancer therapeutics. Acta Pharm. Sin. B *11*, 2726–2737.

Li, N., Wu, X., Holzer, R.G., Lee, J.-H., Todoric, J., Park, E.-J., Ogata, H., Gukovskaya, A.S., Gukovsky, I., Pizzo, D.P., et al. (2013). Loss of acinar cell IKKα triggers spontaneous pancreatitis in mice. J. Clin. Invest. *123*, 2231–2243.

Li, X., Liu, J., Park, J.K., Hamilton, T.A., Rayman, P., Klein, E., Edinger, M., Tubbs, R., Bukowski, R., and Finke, J. (1994). T cells from renal cell carcinoma patients exhibit an abnormal pattern of κB-specific DNA-binding activity: a preliminary report. Cancer Res. *54*, 5424–5429.

Li, X., Zhao, Y., Tian, B., Jamaluddin, M., Mitra, A., Yang, J., Rowicka, M., Brasier, A.R., and Kudlicki, A. (2014). Modulation of Gene Expression Regulated by the Transcription Factor NF-κB/RelA. J. Biol. Chem. *289*, 11927–11944.

Li, Z., Shao, C., Liu, X., Lu, X., Jia, X., Zheng, X., Wang, S., Zhu, L., Li, K., Pang, Y., et al. (2020). Oncogenic ERBB2 aberrations and KRAS mutations cooperate to promote pancreatic ductal adenocarcinoma progression. Carcinogenesis *41*, 44–55.

Liang, M. (2018). Oncorine, the World First Oncolytic Virus Medicine and its Update in China. Curr. Cancer Drug Targets *18*, 171–176.

Libermann, T.A., and Baltimore, D. (1990). Activation of interleukin-6 gene expression through the NF-κB transcription factor. Mol. Cell. Biol. *10*, 2327–2334.

Lieber, M., Mazzetta, J., Nelson-Rees, W., Kaplan, M., and Todaro, G. (1975). Establishment of a continuous tumor-cell line (panc-1) from a human carcinoma of the exocrine pancreas. Int. J. Cancer *15*, 741–747.

Lilienbaum, A., Duc Dodon, M., Alexandre, C., Gazzolo, L., and Paulin, D. (1990). Effect of human T-cell leukemia virus type I tax protein on activation of the human vimentin gene. J. Virol. *64*, 256–263.

Lim, S., Ryu, J., Shin, J.-A., Shin, M.-J., Ahn, Y.K., Kim, J.J., and Han, K.H. (2009). Tumor Necrosis Factor-α Potentiates RhoA-Mediated Monocyte Transmigratory Activity In Vivo at a Picomolar Level. Arterioscler. Thromb. Vasc. Biol. *29*, 2138–2145.

Lin, Y.Z., Yao, S.Y., Veach, R.A., Torgerson, T.R., and Hawiger, J. (1995). Inhibition of nuclear translocation of transcription factor NF-κB by a synthetic peptide containing a cell membrane-permeable motif and nuclear localization sequence. J. Biol. Chem. *270*, 14255–14258.

Ling, J., Kang, Y., Zhao, R., Xia, Q., Lee, D.-F., Chang, Z., Li, J., Peng, B., Fleming, J.B., Wang, H., et al. (2012). KrasG12D-Induced IKK2/β/NF-κB Activation by IL-1α and p62 Feedforward Loops Is Required for Development of Pancreatic Ductal Adenocarcinoma. Cancer Cell *21*, 105–120.

Liou, G.-Y., Döppler, H., Necela, B., Krishna, M., Crawford, H.C., Raimondo, M., and Storz, P. (2013). Macrophage-secreted cytokines drive pancreatic acinar-to-ductal metaplasia through NF-κB and MMPs. J Cell Biol *202*, 563–577.

Liou, H.C., Sha, W.C., Scott, M.L., and Baltimore, D. (1994). Sequential induction of NF-κB/Rel family proteins during B-cell terminal differentiation. Mol. Cell. Biol. *14*, 5349–5359.

Lissbrant, I.F., Stattin, P., Wikstrom, P., Damber, J.E., Egevad, L., and Bergh, A. (2000). Tumor associated macrophages in human prostate cancer: relation to clinicopathological

variables and survival. Int. J. Oncol. *17*, 445–451.

Liu, B.P., Chrzanowska-Wodnicka, M., and Burridge, K. (1998). Microtubule depolymerization induces stress fibers, focal adhesions, and DNA synthesis via the GTP-binding protein Rho. Cell Adhes. Commun. *5*, 249–255.

Liu, J., Kumar, K.S., Yu, D., Molton, S., McMahon, M., Herlyn, M., Thomas-Tikhonenko, A., and Fuchs, S. (2007). Oncogenic BRAF regulates β-Trcp expression and NF-κB activity in human melanoma cells. Oncogene *26*, 1954–1958.

Liu, S.F., Ye, X., and Malik, A.B. (1999). Inhibition of NF-κB Activation by Pyrrolidine Dithiocarbamate Prevents In Vivo Expression of Proinflammatory Genes. Circulation *100*, 1330–1337.

Liu, Y.-J., Le Berre, M., Lautenschlaeger, F., Maiuri, P., Callan-Jones, A., Heuzé, M., Takaki, T., Voituriez, R., and Piel, M. (2015). Confinement and Low Adhesion Induce Fast Amoeboid Migration of Slow Mesenchymal Cells. Cell *160*.

Llambi, F., Moldoveanu, T., Tait, S.W.G., Bouchier-Hayes, L., Temirov, J., McCormick, L.L., Dillon, C.P., and Green, D.R. (2011). A Unified Model of Mammalian BCL-2 Protein Family Interactions at the Mitochondria. Mol. Cell *44*, 517–531.

Lobb, I.T., Morin, P., Martin, K., Thoms, H.C., Wills, J.C., Lleshi, X., Olsen, K.C.F., Duncan, R.R., and Stark, L.A. (2021). A Role for the Autophagic Receptor, SQSTM1/p62, in Trafficking NF-κB/RelA to Nucleolar Aggresomes. Mol. Cancer Res. *19*, 274–287.

Lobert, S., Vulevic, B., and Correia, J.J. (1996). Interaction of Vinca Alkaloids with Tubulin: A Comparison of Vinblastine, Vincristine, and Vinorelbine. Biochemistry *35*, 6806–6814.

Lombardi, L., Ciana, P., Cappellini, C., Trecca, D., Guerrini, L., Migliazza, A., Maiolo, A.T., and Neri, A. (1995). Structural and functional characterization of the promoter regions of the NFKB2 gene. Nucleic Acids Res. *23*, 2328–2336.

Long, B.H., and Fairchild, C.R. (1994). Paclitaxel inhibits progression of mitotic cells to G1 phase by interference with spindle formation without affecting other microtubule functions during anaphase and telephase. Cancer Res. *54*, 4355–4361.

Longley, D.B., Harkin, D.P., and Johnston, P.G. (2003). 5-Fluorouracil: mechanisms of action and clinical strategies. Nat. Rev. Cancer *3*, 330–338.

Loo, Y.-M., Fornek, J., Crochet, N., Bajwa, G., Perwitasari, O., Martinez-Sobrido, L., Akira, S., Gill, M.A., García-Sastre, A., Katze, M.G., et al. (2008). Distinct RIG-I and MDA5 signaling by RNA viruses in innate immunity. J. Virol. *82*, 335–345.

Love, M.I., Huber, W., and Anders, S. (2014). Moderated estimation of fold change and dispersion for RNA-seq data with DESeq2. Genome Biol. *15*, 550.

Lowenfels, A.B., Maisonneuve, P., and Lankisch, P.G. (1999). Chronic pancreatitis and other risk factors for pancreatic cancer. Gastroenterol. Clin. North Am. *28*, 673–685.

Lu, Z., Li, Y., Takwi, A., Li, B., Zhang, J., Conklin, D.J., Young, K.H., Martin, R., and Li, Y. (2011). miR-301a as an NF-κB activator in pancreatic cancer cells. EMBO J. *30*, 57–67.

Lubba, C.H., Sethi, S.S., Knaute, P., Schultz, S.R., Fulcher, B.D., and Jones, N.S. (2019). catch22: CAnonical Time-series CHaracteristics. Data Min. Knowl. Discov. *33*, 1821–1852.

Luchini, C., Pea, A., Lionheart, G., Mafficini, A., Nottegar, A., Veronese, N., Chianchiano, P., Brosens, L.A., Noë, M., Offerhaus, G.J.A., et al. (2017). Pancreatic undifferentiated

carcinoma with osteoclast-like giant cells is genetically similar to, but clinically distinct from, conventional ductal adenocarcinoma. J. Pathol. *243*, 148–154.

Luftig, M., Yasui, T., Soni, V., Kang, M.-S., Jacobson, N., Cahir-McFarland, E., Seed, B., and Kieff, E. (2004). Epstein–Barr virus latent infection membrane protein 1 TRAF-binding site induces NIK/IKKα-dependent noncanonical NF-κB activation. Proc. Natl. Acad. Sci. *101*, 141–146.

Ma, F., Li, X., Ren, J., Guo, R., Li, Y., Liu, J., Sun, Y., Liu, Z., Jia, J., and Li, W. (2019). Downregulation of eukaryotic translation initiation factor 3b inhibited proliferation and metastasis of gastric cancer. Cell Death Dis. *10*, 1–12.

Ma, L., Rohatgi, R., and Kirschner, M.W. (1998). The Arp2/3 complex mediates actin polymerization induced by the small GTP-binding protein Cdc42. Proc. Natl. Acad. Sci. *95*, 15362–15367.

Machesky, L.M., and Hall, A. (1997). Role of actin polymerization and adhesion to extracellular matrix in Rac- and Rho-induced cytoskeletal reorganization. J. Cell Biol. *138*, 913–926.

Madhusudan, S., Foster, M., Muthuramalingam, S.R., Braybrooke, J.P., Wilner, S., Kaur, K., Han, C., Hoare, S., Balkwill, F., Talbot, D.C., et al. (2004). A Phase II Study of Etanercept (Enbrel), a Tumor Necrosis Factor α Inhibitor in Patients with Metastatic Breast Cancer. Clin. Cancer Res. *10*, 6528–6534.

Madhusudan, S., Muthuramalingam, S.R., Braybrooke, J.P., Wilner, S., Kaur, K., Han, C., Hoare, S., Balkwill, F., and Ganesan, T.S. (2005). Study of Etanercept, a Tumor Necrosis Factor-α Inhibitor, in Recurrent Ovarian Cancer. J. Clin. Oncol. *23*, 5950–5959.

Maginnis, M.S., Forrest, J.C., Kopecky-Bromberg, S.A., Dickeson, S.K., Santoro, S.A., Zutter, M.M., Nemerow, G.R., Bergelson, J.M., and Dermody, T.S. (2006). β1 Integrin Mediates Internalization of Mammalian Reovirus. J. Virol. *80*, 2760–2770.

Mahalingam, D., Patel, S., Nuovo, G., Gill, G., Selvaggi, G., Coffey, M., and Nawrocki, S.T. (2015). The combination of intravenous Reolysin and gemcitabine induces reovirus replication and endoplasmic reticular stress in a patient with KRAS-activated pancreatic cancer. BMC Cancer *15*, 513.

Mahalingam, D., Goel, S., Aparo, S., Patel Arora, S., Noronha, N., Tran, H., Chakrabarty, R., Selvaggi, G., Gutierrez, A., Coffey, M., et al. (2018). A Phase II Study of Pelareorep (REOLYSIN®) in Combination with Gemcitabine for Patients with Advanced Pancreatic Adenocarcinoma. Cancers *10*, E160.

Mahalingam, D., Wilkinson, G.A., Eng, K.H., Fields, P., Raber, P., Moseley, J.L., Cheetham, K., Coffey, M., Nuovo, G., Kalinski, P., et al. (2020). Pembrolizumab in Combination with the Oncolytic Virus Pelareorep and Chemotherapy in Patients with Advanced Pancreatic Adenocarcinoma: A Phase Ib Study. Clin. Cancer Res. *26*, 71–81.

Maity, A., and Wollman, R. (2020). Information transmission from NF-κB signaling dynamics to gene expression. PLOS Comput. Biol. *16*, e1008011.

Małecki, J.M., Bentke, A., Ostrowska, B., and Laidler, P. (2010). Cytochalasin D, LY294002 and olomoucine synergize in promoting death of melanoma cells through activation of caspase-3 and apoptosis. Melanoma Res. *20*, 52–58.

Maley, F., and Maley, G.F. (1960). Nucleotide interconversions. II. Elevation of deoxycytidylate deaminase and thymidylate synthetase in regenerating rat liver. J. Biol.

Chem. *235*, 2968–2970.

Malinin, N.L., Boldin, M.P., Kovalenko, A.V., and Wallach, D. (1997). MAP3K-related kinase involved in NF-KB induction by TNF, CD95 and IL-1. Nature *385*, 540–544.

Manna, S.K., and Ramesh, G.T. (2005). Interleukin-8 induces nuclear transcription factor-κB through a TRAF6-dependent pathway. J. Biol. Chem. *280*, 7010–7021.

Manolagas, S.C. (2000). Birth and death of bone cells: basic regulatory mechanisms and implications for the pathogenesis and treatment of osteoporosis. Endocr. Rev. *21*, 115–137.

Mantovani, A., Sica, A., Sozzani, S., Allavena, P., Vecchi, A., and Locati, M. (2004). The chemokine system in diverse forms of macrophage activation and polarization. Trends Immunol. *25*, 677–686.

Margolis, R.L., and Wilson, L. (1978). Opposite end assembly and disassembly of microtubules at steady state in vitro. Cell *13*, 1–8.

Margolis, R.L., and Wilson, L. (1981). Microtubule treadmills--possible molecular machinery. Nature *293*, 705–711.

Martin, A.G., and Fresno, M. (2000). Tumor necrosis factor-α activation of NF-κB requires the phosphorylation of Ser-471 in the transactivation domain of c-Rel. J. Biol. Chem. *275*, 24383–24391.

Martin, E.W., Pacholewska, A., Patel, H., Dashora, H., and Sung, M.-H. (2020). Integrative analysis suggests cell type–specific decoding of NF-κB dynamics. Sci. Signal. *13*, eaax7195.

Martinez, F.O., and Gordon, S. (2014). The M1 and M2 paradigm of macrophage activation: time for reassessment. F1000Prime Rep. *6*, 13.

Mateo, J., Lord, C.J., Serra, V., Tutt, A., Balmaña, J., Castroviejo-Bermejo, M., Cruz, C., Oaknin, A., Kaye, S.B., and Bono, J.S. de (2019). A decade of clinical development of PARP inhibitors in perspective. Ann. Oncol. *30*, 1437–1447.

Matthews, H.K., Ganguli, S., Plak, K., Taubenberger, A.V., Win, Z., Williamson, M., Piel, M., Guck, J., and Baum, B. (2020). Oncogenic Signaling Alters Cell Shape and Mechanics to Facilitate Cell Division under Confinement. Dev. Cell *52*, 563-573.e3.

Maturi, V., Enroth, S., Heldin, C.-H., and Moustakas, A. (2018). Genome–wide binding of transcription factor ZEB1 in triple-negative breast cancer cells. J. Cell. Physiol. *233*, 7113–7127.

Maynard, J., Petersson, K., Wilson, D.H., Adams, E.J., Blondelle, S.E., Boulanger, M.J., Wilson, D.B., and Garcia, K.C. (2005). Structure of an autoimmune T cell receptor complexed with class II peptide-MHC: insights into MHC bias and antigen specificity. Immunity *22*, 81–92.

McCarroll, J.A., Sharbeen, G., Liu, J., Youkhana, J., Goldstein, D., McCarthy, N., Limbri, L.F., Dischl, D., Ceyhan, G.O., Erkan, M., et al. (2014). βIII-Tubulin: A novel mediator of chemoresistance and metastases in pancreatic cancer. Oncotarget *6*, 2235–2249.

McLellan, A., Heldmann, M., Terbeck, G., Weih, F., Linden, C., Bröcker, E.B., Leverkus, M., and Kämpgen, E. (2000). MHC class II and CD40 play opposing roles in dendritic cell survival. Eur. J. Immunol. *30*, 2612–2619.

Medzhitov, R., and Janeway, C.A. (1997). Innate immunity: impact on the adaptive immune response. Curr. Opin. Immunol. *9*, 4–9.

Melisi, D., Niu, J., Chang, Z., Xia, Q., Peng, B., Ishiyama, S., Evans, D.B., and Chiao, P.J. (2009). Secreted interleukin-1α induces a metastatic phenotype in pancreatic cancer by sustaining a constitutive activation of nuclear factor-κB. Mol. Cancer Res. MCR *7*, 624–633.

Mémet, S., Laouini, D., Epinat, J.C., Whiteside, S.T., Goudeau, B., Philpott, D., Kayal, S., Sansonetti, P.J., Berche, P., Kanellopoulos, J., et al. (1999). IκBε-deficient mice: reduction of one T cell precursor subspecies and enhanced Ig isotype switching and cytokine synthesis. J. Immunol. Baltim. Md 1950 *163*, 5994–6005.

Menéndez, M., Rivas, G., Díaz, J.F., and Andreu, J.M. (1998). Control of the Structural Stability of the Tubulin Dimer by One High Affinity Bound Magnesium Ion at Nucleotide N-site. J. Biol. Chem. *273*, 167–176.

Meng, Q., Liang, C., Hua, J., Zhang, B., Liu, J., Zhang, Y., Wei, M., Yu, X., Xu, J., and Shi, S. (2020). A miR-146a-5p/TRAF6/NF-kB p65 axis regulates pancreatic cancer chemoresistance: functional validation and clinical significance. Theranostics *10*, 3967–3979.

Mercurio, F., DiDonato, J.A., Rosette, C., and Karin, M. (1993). p105 and p98 precursor proteins play an active role in NF-κB-mediated signal transduction. Genes Dev. *7*, 705–718.

Mercurio, F., Zhu, H., Murray, B.W., Shevchenko, A., Bennett, B.L., Li, J. wu, Young, D.B., Barbosa, M., Mann, M., Manning, A., et al. (1997). IKK-1 and IKK-2: Cytokine-Activated IκB Kinases Essential for NF-κB Activation. Science.

Meulenaere, A.D., Vermassen, T., Aspeslagh, S., Zwaenepoel, K., Deron, P., Duprez, F., Ferdinande, L., and Rottey, S. (2016). CD70 Expression and Its Correlation with Clinicopathological Variables in Squamous Cell Carcinoma of the Head and Neck. Pathobiology *83*, 327–333.

Meylan, E., Dooley, A.L., Feldser, D.M., Shen, L., Turk, E., Ouyang, C., and Jacks, T. (2009). Requirement for NF-κB signalling in a mouse model of lung adenocarcinoma. Nature *462*, 104–107.

Miagkov, A.V., Kovalenko, D.V., Brown, C.E., Didsbury, J.R., Cogswell, J.P., Stimpson, S.A., Baldwin, A.S., and Makarov, S.S. (1998). NF-κB activation provides the potential link between inflammation and hyperplasia in the arthritic joint. Proc. Natl. Acad. Sci. *95*, 13859–13864.

Micheau, O., and Tschopp, J. (2003). Induction of TNF Receptor I-Mediated Apoptosis via Two Sequential Signaling Complexes. Cell *114*, 181–190.

Milanovic, M., Heise, N., De Silva, N.S., Anderson, M.M., Silva, K., Carette, A., Orelli, F., Bhagat, G., and Klein, U. (2017). Differential requirements for the canonical NF-κB transcription factors c-REL and RELA during the generation and activation of mature B cells. Immunol. Cell Biol. *95*, 261–271.

Mills, C.D., Kincaid, K., Alt, J.M., Heilman, M.J., and Hill, A.M. (2000). M-1/M-2 macrophages and the Th1/Th2 paradigm. J. Immunol. Baltim. Md 1950 *164*, 6166–6173.

Min, C., Eddy, S.F., Sherr, D.H., and Sonenshein, G.E. (2008). NF-κB and epithelial to mesenchymal transition of cancer. J. Cell. Biochem. *104*, 733–744.

Minami, F., Sasaki, N., Shichi, Y., Gomi, F., Michishita, M., Ohkusu-Tsukada, K., Toyoda, M., Takahashi, K., and Ishiwata, T. (2021). Morphofunctional analysis of human pancreatic cancer cell lines in 2- and 3-dimensional cultures. Sci. Rep. *11*, 6775.

Minuk, G.Y., Paul, R.W., and Lee, P.W.K. (1985). The prevalence of antibodies to reovirus

type 3 in adults with idiopathic cholestatic liver disease. J. Med. Virol. *16*, 55–60.

Miralles, F., Posern, G., Zaromytidou, A.-I., and Treisman, R. (2003). Actin Dynamics Control SRF Activity by Regulation of Its Coactivator MAL. Cell *113*, 329–342.

Mitchison, T.J. (1993). Localization of an Exchangeable GTP Binding Site at the Plus End of Microtubules. Science *261*, 1044–1047.

Mitra, A., Venkatachalapathy, S., Ratna, P., Wang, Y., Jokhun, D.S., and Shivashankar, G.V. (2017). Cell geometry dictates TNFα-induced genome response. Proc. Natl. Acad. Sci.

Monaco, C., Andreakos, E., Kiriakidis, S., Mauri, C., Bicknell, C., Foxwell, B., Cheshire, N., Paleolog, E., and Feldmann, M. (2004). Canonical pathway of nuclear factor κB activation selectively regulates proinflammatory and prothrombotic responses in human atherosclerosis. Proc. Natl. Acad. Sci. U. S. A. *101*, 5634–5639.

Moore, R.J., Owens, D.M., Stamp, G., Arnott, C., Burke, F., East, N., Holdsworth, H., Turner, L., Rollins, B., Pasparakis, M., et al. (1999). Mice deficient in tumor necrosis factor-α are resistant to skin carcinogenesis. Nat. Med. *5*, 828–831.

Mora, A.L., Stanley, S., Armistead, W., Chan, A.C., and Boothby, M. (2001). Inefficient ZAP-70 Phosphorylation and Decreased Thymic Selection In Vivo Result from Inhibition of NF-κB/Rel. J. Immunol. *167*, 5628–5635.

Morishita, R., Sugimoto, T., Aoki, M., Kida, I., Tomita, N., Moriguchi, A., Maeda, K., Sawa, Y., Kaneda, Y., Higaki, J., et al. (1997). In vivo transfection of cis element “decoy” against nuclear factor-κB binding site prevents myocardial infarction. Nat. Med. *3*, 894–899.

Morrison, M.D., Reiley, W., Zhang, M., and Sun, S.-C. (2005). An atypical tumor necrosis factor (TNF) receptor-associated factor-binding motif of B cell-activating factor belonging to the TNF family (BAFF) receptor mediates induction of the noncanonical NF-κB signaling pathway. J. Biol. Chem. *280*, 10018–10024.

Mouri, Y., Yano, M., Shinzawa, M., Shimo, Y., Hirota, F., Nishikawa, Y., Nii, T., Kiyonari, H., Abe, T., Uehara, H., et al. (2011). Lymphotoxin signal promotes thymic organogenesis by eliciting RANK expression in the embryonic thymic stroma. J. Immunol. Baltim. Md 1950 *186*, 5047–5057.

Mrowietz, U., Schwenk, U., Maune, S., Bartels, J., Küpper, M., Fichtner, I., Schröder, J.-M., and Schadendorf, D. (1999). The chemokine RANTES is secreted by human melanoma cells and is associated with enhanced tumour formation in nude mice. Br. J. Cancer *79*, 1025–1031.

Mudla, A., Jiang, Y., Arimoto, K., Xu, B., Rajesh, A., Ryan, A.P., Wang, W., Daugherty, M.D., Zhang, D.-E., and Hao, N. (2020). Cell-cycle-gated feedback control mediates desensitization to interferon stimulation. eLife *9*, e58825.

Müller, L., Berkeley, R., Barr, T., Ilett, E., and Errington-Mais, F. (2020). Past, Present and Future of Oncolytic Reovirus. Cancers *12*, E3219.

Mullins, R.D., Heuser, J.A., and Pollard, T.D. (1998). The interaction of Arp2/3 complex with actin: Nucleation, high affinity pointed end capping, and formation of branching networks of filaments. Proc. Natl. Acad. Sci. *95*, 6181–6186.

Murphy, J.M., Rodriguez, Y.A.R., Jeong, K., Ahn, E.-Y.E., and Lim, S.-T.S. (2020). Targeting focal adhesion kinase in cancer cells and the tumor microenvironment. Exp. Mol. Med. *52*, 877–886.

Murphy, T.L., Cleveland, M.G., Kulesza, P., Magram, J., and Murphy, K.M. (1995). Regulation of interleukin 12 p40 expression through an NF-κB half-site. Mol. Cell. Biol. *15*, 5258–5267.

Muta, T., Yamazaki, S., Eto, A., Motoyama, M., and Takeshige, K. (2003). IκB-ζ, a new anti-inflammatory nuclear protein induced by lipopolysaccharide, is a negative regulator for nuclear factor-κB. J. Endotoxin Res. *9*, 187–191.

Nagel, D., Vincendeau, M., Eitelhuber, A.C., and Krappmann, D. (2014). Mechanisms and consequences of constitutive NF-κB activation in B-cell lymphoid malignancies. Oncogene *33*, 5655–5665.

Nakatani, Y., Konishi, H., Vassilev, A., Kurooka, H., Ishiguro, K., Sawada, J., Ikura, T., Korsmeyer, S.J., Qin, J., and Herlitz, A.M. (2005). p600, a unique protein required for membrane morphogenesis and cell survival. Proc. Natl. Acad. Sci. U. S. A. *102*, 15093–15098.

Neagu, M., Constantin, C., Caruntu, C., Dumitru, C., Surcel, M., and Zurac, S. (2019). Inflammation: A key process in skin tumorigenesis. Oncol. Lett. *17*, 4068–4084.

Nelson, D.E., Ihekwaba, A.E.C., Elliott, M., Johnson, J.R., Gibney, C.A., Foreman, B.E., Nelson, G., See, V., Horton, C.A., Spiller, D.G., et al. (2004). Oscillations in NF-κB Signaling Control the Dynamics of Gene Expression. Science *306*, 704–708.

Nelson, G., Paraoan, L., Spiller, D.G., Wilde, G.J.C., Browne, M.A., Djali, P.K., Unitt, J.F., Sullivan, E., Floettmann, E., and White, M.R.H. (2002). Multi-parameter analysis of the kinetics of NF-κB signalling and transcription in single living cells. J. Cell Sci. *115*,

Németh, Z.H., Deitch, E.A., Davidson, M.T., Szabó, C., Vizi, E.S., and Haskó, G. (2004). Disruption of the actin cytoskeleton results in nuclear factor-κB activation and inflammatory mediator production in cultured human intestinal epithelial cells. J. Cell. Physiol. *200*, 71–81.

Newton, K., Sun, X., and Dixit, V.M. (2004). Kinase RIP3 Is Dispensable for Normal NF-κBs, Signaling by the B-Cell and T-Cell Receptors, Tumor Necrosis Factor Receptor 1, and Toll-Like Receptors 2 and 4. Mol. Cell. Biol.

Ngo, K.A., Kishimoto, K., Davis-Turak, J., Pimplaskar, A., Cheng, Z., Spreafico, R., Chen, E.Y., Tam, A., Ghosh, G., Mitchell, S., et al. (2020). Dissecting the Regulatory Strategies of NF-κB RelA Target Genes in the Inflammatory Response Reveals Differential Transactivation Logics. Cell Rep. *30*, 2758-2775.e6.

Niu, J., Li, Z., Peng, B., and Chiao, P.J. (2004). Identification of an autoregulatory feedback pathway involving interleukin-1α in induction of constitutive NF-κB activation in pancreatic cancer cells. J. Biol. Chem. *279*, 16452–16462.

Nketia, T.A., Sailem, H., Rohde, G., Machiraju, R., and Rittscher, J. (2017). Analysis of live cell images: Methods, tools and opportunities. Methods San Diego Calif *115*, 65–79.

Nobes, C.D., and Hall, A. (1995). Rho, Rac, and Cdc42 GTPases regulate the assembly of multimolecular focal complexes associated with actin stress fibers, lamellipodia, and filopodia. Cell *81*, 53–62.

Nogales, E., Wolf, S.G., and Downing, K.H. (1998). Structure of the αβ tubulin dimer by electron crystallography. Nature *391*, 199–203.

Nolan, G.P., Ghosh, S., Liou, H.C., Tempst, P., and Baltimore, D. (1991). DNA binding and IκB inhibition of the cloned p65 subunit of NF-κB, a rel-related polypeptide. Cell *64*, 961–969.

Noonan, A.M., Farren, M.R., Geyer, S.M., Huang, Y., Tahiri, S., Ahn, D., Mikhail, S., Ciombor, K.K., Pant, S., Aparo, S., et al. (2016). Randomized Phase 2 Trial of the Oncolytic Virus Pelareorep (Reolysin) in Upfront Treatment of Metastatic Pancreatic Adenocarcinoma. Mol. Ther. J. Am. Soc. Gene Ther. *24*, 1150–1158.

Norman, K.L., and Lee, P.W.K. (2000). Reovirus as a novel oncolytic agent. J. Clin. Invest. *105*, 1035–1038.

O'Brien, S., Golubovskaya, V.M., Conroy, J., Liu, S., Wang, D., Liu, B., and Cance, W.G. (2014). FAK inhibition with small molecule inhibitor Y15 decreases viability, clonogenicity, and cell attachment in thyroid cancer cell lines and synergizes with targeted therapeutics. Oncotarget *5*, 7945–7959.

Odegard, A.L., Chandran, K., Zhang, X., Parker, J.S.L., Baker, T.S., and Nibert, M.L. (2004). Putative Autocleavage of Outer Capsid Protein μ1, Allowing Release of Myristoylated Peptide μ1N during Particle Uncoating, Is Critical for Cell Entry by Reovirus. J. Virol. *78*, 8732–8745.

Oettle, H., Post, S., Neuhaus, P., Gellert, K., Langrehr, J., Ridwelski, K., Schramm, H., Fahlke, J., Zuelke, C., Burkart, C., et al. (2007). Adjuvant Chemotherapy With Gemcitabine vs Observation in Patients Undergoing Curative-Intent Resection of Pancreatic CancerA Randomized Controlled Trial. JAMA *297*, 267–277.

Office for National Statistics (2017). Cancer Registration Statistics, England, 2017.

Ohta, K., Seo, N., Yoshida, T., Hiraga, K., and Tuboi, S. (1987). Tubulin and high molecular weight microtubule-associated proteins as endogenous substrates for protein carboxymethyltransferase in brain. Biochimie *69*, 1227–1234.

Okada, S., Okusaka, T., Ishii, H., Kyogoku, A., Yoshimori, M., Kajimura, N., Yamaguchi, K., and Kakizoe, T. (1998). Elevated serum interleukin-6 levels in patients with pancreatic cancer. Jpn. J. Clin. Oncol. *28*, 12–15.

Oliver Metzig, M., Tang, Y., Mitchell, S., Taylor, B., Foreman, R., Wollman, R., and Hoffmann, A. (2020). An incoherent feedforward loop interprets NFκB/RelA dynamics to determine TNF-induced necroptosis decisions. Mol. Syst. Biol. *16*, e9677.

Orning, P., Weng, D., Starheim, K., Ratner, D., Best, Z., Lee, B., Brooks, A., Xia, S., Wu, H., Kelliher, M.A., et al. (2018). Pathogen blockade of TAK1 triggers caspase-8 dependent cleavage of Gasdermin D and cell death. Science *362*, 1064–1069.

Orosz, P., Echtenacher, B., Falk, W., Rüschoff, J., Weber, D., and Männel, D.N. (1993). Enhancement of experimental metastasis by tumor necrosis factor. J. Exp. Med. *177*, 1391–1398.

Osborn, L., Kunkel, S., and Nabel, G.J. (1989). Tumor necrosis factor α and interleukin 1 stimulate the human immunodeficiency virus enhancer by activation of the nuclear factor κB. Proc. Natl. Acad. Sci. U. S. A. *86*, 2336–2340.

Ostrem, J.M., Peters, U., Sos, M.L., Wells, J.A., and Shokat, K.M. (2013). K-Ras(G12C) inhibitors allosterically control GTP affinity and effector interactions. Nature *503*, 548–551.

Oyler-Yaniv, J., Oyler-Yaniv, A., Maltz, E., and Wollman, R. (2020). TNF controls a speed-accuracy tradeoff in apoptotic decision to restrict viral spread. BioRxiv 2020.02.20.958942.

Pandol, S.J. (2010). The Exocrine Pancreas (Morgan & Claypool Life Sciences).

Pandol, S., Edderkaoui, M., Gukovsky, I., Lugea, A., and Gukovskaya, A. (2009). Desmoplasia of Pancreatic Ductal Adenocarcinoma. Clin. Gastroenterol. Hepatol. *7*, S44–S47.

Park, B.S., Song, D.H., Kim, H.M., Choi, B.-S., Lee, H., and Lee, J.-O. (2009). The structural basis of lipopolysaccharide recognition by the TLR4-MD-2 complex. Nature *458*, 1191–1195.

Park, J.-G., Collins, J.M., Gazdar, A.F., Allegra, C.J., Steinberg, S.M., Greene, R.F., and Kramer, B.S. (1988). Enhancement of fluorinated Pyrimidine-Induced Cytotoxicity by Leucovorin in Human Colorectal Carcinoma Cell Lines. JNCI J. Natl. Cancer Inst. *80*, 1560–1564.

Park, S.-Y., Kim, M.-J., Kim, Y.J., Lee, Y.-H., Bae, D., Kim, S., Na, Y., and Yoon, H.-G. (2015). Selective PCAF inhibitor ameliorates cognitive and behavioral deficits by suppressing NF-κB-mediated neuroinflammation induced by Aβ in a model of Alzheimer's disease. Int. J. Mol. Med. *35*, 1109–1118.

Parker, D.C. (1993). T cell-dependent B cell activation. Annu. Rev. Immunol. *11*, 331–360.

Parsons, J.T., Martin, K.H., Slack, J.K., Taylor, J.M., and Weed, S.A. (2000). Focal Adhesion Kinase: a regulator of focal adhesion dynamics and cell movement. Oncogene *19*, 5606–5613.

Pascual-Vargas, P., Cooper, S., Sero, J., Bousgouni, V., Arias-Garcia, M., and Bakal, C. (2017). RNAi screens for Rho GTPase regulators of cell shape and YAP/TAZ localisation in triple negative breast cancer. Sci. Data *4*, 170018.

Patel, P., Drayman, N., Liu, P., Bilgic, M., and Tay, S. (2021). Computer vision reveals hidden variables underlying NF-κB activation in single cells. Sci. Adv.

Paul, R.W., Choi, A.H., and Lee, P.W. (1989). The α-anomeric form of sialic acid is the minimal receptor determinant recognized by reovirus. Virology *172*, 382–385.

Pellegrin, S., and Mellor, H. (2005). The Rho family GTPase Rif induces filopodia through mDia2. Curr. Biol. CB *15*, 129–133.

Perez-Moreno, M., Davis, M.A., Wong, E., Pasolli, H.A., Reynolds, A.B., and Fuchs, E. (2006). p120-Catenin Mediates Inflammatory Responses in the Skin. Cell *124*, 631–644.

Perkins, N.D., Felzien, L.K., Betts, J.C., Leung, K., Beach, D.H., and Nabel, G.J. (1997). Regulation of NF-κB by cyclin-dependent kinases associated with the p300 coactivator. Science *275*, 523–527.

Perona, R., Montaner, S., Saniger, L., Sánchez-Pérez, I., Bravo, R., and Lacal, J.C. (1997). Activation of the nuclear factor-κB by Rho, CDC42, and Rac-1 proteins. Genes Dev. *11*, 463–475.

Peterson, J.R., and Mitchison, T.J. (2002). Small Molecules, Big Impact: A History of Chemical Inhibitors and the Cytoskeleton. Chem. Biol. *9*, 1275–1285.

Pflueger, D., Terry, S., Sboner, A., Habegger, L., Esgueva, R., Lin, P.-C., Svensson, M.A., Kitabayashi, N., Moss, B.J., MacDonald, T.Y., et al. (2011). Discovery of non-ETS gene fusions in human prostate cancer using next-generation RNA sequencing. Genome Res. *21*, 56–67.

Phelps, C.B., Sengchanthalangsy, L.L., Malek, S., and Ghosh, G. (2000). Mechanism of κB DNA binding by Rel/NF-κB dimers. J. Biol. Chem. *275*, 24392–24399.

Philipson, B.I., O'Connor, R.S., May, M.J., June, C.H., Albelda, S.M., and Milone, M.C. (2020). 4-1BB costimulation promotes CAR T cell survival through noncanonical NF-κB signaling. Sci. Signal. *13*, eaay8248.

Phillips, A.C., Ernst, M.K., Bates, S., Rice, N.R., and Vousden, K.H. (1999). E2F-1 potentiates cell death by blocking antiapoptotic signaling pathways. Mol. Cell *4*, 771–781.

Phillips, M.B., Stuart, J.D., Rodríguez Stewart, R.M., Berry, J.T., Mainou, B.A., and Boehme, K.W. (2018). Current understanding of reovirus oncolysis mechanisms. Oncolytic Virotherapy *7*, 53–63.

Pikarsky, E., Porat, R.M., Stein, I., Abramovitch, R., Amit, S., Kasem, S., Gutkovich-Pyest, E., Urieli-Shoval, S., Galun, E., and Ben-Neriah, Y. (2004). NF-κB functions as a tumour promoter in inflammation-associated cancer. Nature *431*, 461–466.

Pioli, C., Gatta, L., Frasca, D., and Doria, G. (1999). Cytotoxic T lymphocyte antigen 4 (CTLA-4) inhibits CD28-induced IκBα degradation and RelA activation. Eur. J. Immunol. *29*, 856–863.

Pires, B.R.B., Mencalha, A.L., Ferreira, G.M., de Souza, W.F., Morgado-Díaz, J.A., Maia, A.M., Corrêa, S., and Abdelhay, E.S.F.W. (2017). NF-κB Is Involved in the Regulation of EMT Genes in Breast Cancer Cells. PLoS ONE *12*, e0169622.

Piret, B., and Piette, J. (1996). Topoisomerase poisons activate the transcription factor NF-κB in ACH-2 and CEM cells. Nucleic Acids Res. *24*, 4242–4248.

Porter, M.E., and Sale, W.S. (2000). The 9 + 2 Axoneme Anchors Multiple Inner Arm Dyneins and a Network of Kinases and Phosphatases That Control Motility. J. Cell Biol. *151*, 37–42.

Provenzano, P.P., Cuevas, C., Chang, A.E., Goel, V.K., Von Hoff, D.D., and Hingorani, S.R. (2012). Enzymatic Targeting of the Stroma Ablates Physical Barriers to Treatment of Pancreatic Ductal Adenocarcinoma. Cancer Cell *21*, 418–429.

Pruyne, D., Evangelista, M., Yang, C., Bi, E., Zigmond, S., Bretscher, A., and Boone, C. (2002). Role of formins in actin assembly: nucleation and barbed-end association. Science *297*, 612–615.

Pujol, N., Link, E.M., Liu, L.X., Kurz, C.L., Alloing, G., Tan, M.W., Ray, K.P., Solari, R., Johnson, C.D., and Ewbank, J.J. (2001). A reverse genetic analysis of components of the Toll signaling pathway in Caenorhabditis elegans. Curr. Biol. CB *11*, 809–821.

Qian, W., Xiao, Q., Wang, L., Qin, T., Xiao, Y., Li, J., Yue, Y., Zhou, C., Duan, W., Ma, Q., et al. (2020). Resveratrol slows the tumourigenesis of pancreatic cancer by inhibiting NFκB activation. Biomed. Pharmacother. *127*, 110116.

Raetz, C.R.H., and Whitfield, C. (2002). Lipopolysaccharide Endotoxins. Annu. Rev. Biochem. *71*, 635–700.

Raimondi, S., Lowenfels, A.B., Morselli-Labate, A.M., Maisonneuve, P., and Pezzilli, R. (2010). Pancreatic cancer in chronic pancreatitis; aetiology, incidence, and early detection. Best Pract. Res. Clin. Gastroenterol. *24*, 349–358.

Rajani, K., Parrish, C., Kottke, T., Thompson, J., Zaidi, S., Ilett, L., Shim, K.G., Diaz, R.-M., Pandha, H., Harrington, K., et al. (2016). Combination Therapy With Reovirus and Anti-PD-1 Blockade Controls Tumor Growth Through Innate and Adaptive Immune Responses. Mol. Ther. J. Am. Soc. Gene Ther. *24*, 166–174.

Rajitha, B., Belalcazar, A., Nagaraju, G.P., Shaib, W.L., Snyder, J.P., Shoji, M., Pattnaik, S., Alam, A., and El-Rayes, B.F. (2016). Inhibition of NF-κB translocation by curcumin analogs induces G0/G1 arrest and downregulates thymidylate synthase in colorectal cancer. Cancer Lett. *373*, 227–233.

Ramadass, V., Vaiyapuri, T., and Tergaonkar, V. (2020). Small Molecule NF-κB Pathway Inhibitors in Clinic. Int. J. Mol. Sci. *21*, 5164.

Ramsey, K.M., Chen, W., Marion, J.D., Bergqvist, S., and Komives, E.A. (2019). Exclusivity and Compensation in NF-κB Dimer distributions and IκB inhibition. Biochemistry *58*, 2555–2563.

Rao, C.V., Mohammed, A., Janakiram, N.B., Li, Q., Ritchie, R.L., Lightfoot, S., Vibhudutta, A., and Steele, V.E. (2012). Inhibition of pancreatic intraepithelial neoplasia progression to carcinoma by nitric oxide-releasing aspirin in p48(Cre/+)-LSL-Kras(G12D/+) mice. Neoplasia N. Y. N *14*, 778–787.

Rao, M.V., Chu, P.-H., Hahn, K.M., and Zaidel-Bar, R. (2013). An optogenetic tool for the activation of endogenous diaphanous-related formins induces thickening of stress fibers without an increase in contractility. Cytoskelet. Hoboken NJ *70*, 394–407.

Rapicavoli, N.A., Qu, K., Zhang, J., Mikhail, M., Laberge, R.-M., and Chang, H.Y. (2013). A mammalian pseudogene lncRNA at the interface of inflammation and anti-inflammatory therapeutics. eLife *2*, e00762.

Rashid, M., van der Horst, M., Mentzel, T., Butera, F., Ferreira, I., Pance, A., Rütten, A., Luzar, B., Marusic, Z., de Saint Aubain, N., et al. (2019). ALPK1 hotspot mutation as a driver of human spiradenoma and spiradenocarcinoma. Nat. Commun. *10*, 2213.

Rauhala, H.E., Teppo, S., Niemelä, S., and Kallioniemi, A. (2013). Silencing of the ARP2/3 complex disturbs pancreatic cancer cell migration. Anticancer Res. *33*, 45–52.

Ravelli, R.B.G., Gigant, B., Curmi, P.A., Jourdain, I., Lachkar, S., Sobel, A., and Knossow, M. (2004). Insight into tubulin regulation from a complex with colchicine and a stathmin-like domain. Nature *428*, 198–202.

Ravindran, A., Sawant, K.V., Sarmiento, J., Navarro, J., and Rajarathnam, K. (2013). Chemokine CXCL1 dimer is a potent agonist for the CXCR2 receptor. J. Biol. Chem. *288*, 12244–12252.

Ray Chaudhuri, A., and Nussenzweig, A. (2017). The multifaceted roles of PARP1 in DNA repair and chromatin remodelling. Nat. Rev. Mol. Cell Biol. *18*, 610–621.

Rayment, I., Rypniewski, W.R., Schmidt-Bäse, K., Smith, R., Tomchick, D.R., Benning, M.M., Winkelmann, D.A., Wesenberg, G., and Holden, H.M. (1993). Three-Dimensional Structure of Myosin Subfragment-1: A Molecular Motor. Science.

Razidlo, G.L., Burton, K.M., and McNiven, M.A. (2018). Interleukin-6 promotes pancreatic cancer cell migration by rapidly activating the small GTPase CDC42. J. Biol. Chem. *293*, 11143–11153.

Reader, C.S., Vallath, S., Steele, C.W., Haider, S., Brentnall, A., Desai, A., Moore, K.M., Jamieson, N.B., Chang, D., Bailey, P., et al. (2019). The integrin αvβ6 drives pancreatic cancer through diverse mechanisms and represents an effective target for therapy. J. Pathol. *249*, 332–342.

Reinhard, C., Shamoon, B., Shyamala, V., and Williams, L.T. (1997). Tumor necrosis factor α-induced activation of c-jun N-terminal kinase is mediated by TRAF2. EMBO J. *16*,

1080–1092.

Resnitzky, D., Gossen, M., Bujard, H., and Reed, S.I. (1994). Acceleration of the G1/S phase transition by expression of cyclins D1 and E with an inducible system. Mol. Cell. Biol. *14*, 1669–1679.

Richards, S.A., Carey, K.L., and Macara, I.G. (1997). Requirement of guanosine triphosphate-bound ran for signal-mediated nuclear protein export. Science *276*, 1842–1844.

Richardson, P.G., Barlogie, B., Berenson, J., Singhal, S., Jagannath, S., Irwin, D., Rajkumar, S.V., Srkalovic, G., Alsina, M., Alexanian, R., et al. (2003). A Phase 2 Study of Bortezomib in Relapsed, Refractory Myeloma. N. Engl. J. Med. *348*, 2609–2617.

Rietschel, E.T., Kirikae, T., Schade, F.U., Mamat, U., Schmidt, G., Loppnow, H., Ulmer, A.J., Zähringer, U., Seydel, U., and Di Padova, F. (1994). Bacterial endotoxin: molecular relationships of structure to activity and function. FASEB J. Off. Publ. Fed. Am. Soc. Exp. Biol. *8*, 217–225.

Rivière, Y., Blank, V., Kourilsky, P., and Israël, A. (1991). Processing of the precursor of NF-κB by the HIV-1 protease during acute infection. Nature *350*, 625–626.

Rizvi, S.A., Neidt, E.M., Cui, J., Feiger, Z., Skau, C.T., Gardel, M.L., Kozmin, S.A., and Kovar, D.R. (2009). Identification and Characterization of a Small Molecule Inhibitor of Formin-Mediated Actin Assembly. Chem. Biol. *16*, 1158–1168.

Robert, C., Schachter, J., Long, G.V., Arance, A., Grob, J.J., Mortier, L., Daud, A., Carlino, M.S., McNeil, C., Lotem, M., et al. (2015). Pembrolizumab versus Ipilimumab in Advanced Melanoma. N. Engl. J. Med. *372*, 2521–2532.

Robertson, A.G., Kim, J., Al-Ahmadie, H., Bellmunt, J., Guo, G., Cherniack, A.D., Hinoue, T., Laird, P.W., Hoadley, K.A., Akbani, R., et al. (2017). Comprehensive Molecular Characterization of Muscle-Invasive Bladder Cancer. Cell *171*, 540-556.e25.

Robling, A.G., and Turner, C.H. (2009). Mechanical Signaling for Bone Modeling and Remodeling. Crit. Rev. Eukaryot. Gene Expr. *19*, 319–338.

Rocha, S., Garrett, M.D., Campbell, K.J., Schumm, K., and Perkins, N.D. (2005). Regulation of NF-κB and p53 through activation of ATR and Chk1 by the ARF tumour suppressor. EMBO J. *24*, 1157–1169.

Rodríguez-García, A., Giménez-Alejandre, M., Rojas, J.J., Moreno, R., Bazan-Peregrino, M., Cascalló, M., and Alemany, R. (2015). Safety and Efficacy of VCN-01, an Oncolytic Adenovirus Combining Fiber HSG-Binding Domain Replacement with RGD and Hyaluronidase Expression. Clin. Cancer Res. *21*, 1406–1418.

Rosette, C., and Karin, M. (1995). Cytoskeletal control of gene expression: depolymerization of microtubules activates NF-κB. J. Cell Biol. *128*, 1111–1119.

Rothwarf, D.M., Zandi, E., Natoli, G., and Karin, M. (1998). IKK-gamma is an essential regulatory subunit of the IκB kinase complex. Nature *395*, 297–300.

Roulstone, V., Twigger, K., Zaidi, S., Pencavel, T., Kyula, J.N., White, C., McLaughlin, M., Seth, R., Karapanagiotou, E.M., Mansfield, D., et al. (2013). Synergistic cytotoxicity of oncolytic reovirus in combination with cisplatin-paclitaxel doublet chemotherapy. Gene Ther. *20*, 521–528.

Roulstone, V., Pedersen, M., Kyula, J., Mansfield, D., Khan, A.A., McEntee, G., Wilkinson, M., Karapanagiotou, E., Coffey, M., Marais, R., et al. (2015). BRAF- and MEK-Targeted

Small Molecule Inhibitors Exert Enhanced Antimelanoma Effects in Combination With Oncolytic Reovirus Through ER Stress. Mol. Ther. *23*, 931–942.

Rozenblum, E., Schutte, M., Goggins, M., Hahn, S.A., Panzer, S., Zahurak, M., Goodman, S.N., Sohn, T.A., Hruban, R.H., Yeo, C.J., et al. (1997). Tumor-suppressive pathways in pancreatic carcinoma. Cancer Res. *57*, 1731–1734.

Ruggeri, B.A., Huang, L., Wood, M., Cheng, J.Q., and Testa, J.R. (1998). Amplification and overexpression of the AKT2 oncogene in a subset of human pancreatic ductal adenocarcinomas. Mol. Carcinog. *21*, 81–86.

Ruiz van Haperen, V.W.T., Veerman, G., Vermorken, J.B., and Peters, G.J. (1993). *2′*,*2′*-Difluoro-deoxycytidine (gemcitabine) incorporation into RNA and DNA of tumour cell lines. Biochem. Pharmacol. *46*, 762–766.

Ruksha, K., Mezheyeuski, A., Nerovnya, A., Bich, T., Tur, G., Gorgun, J., Luduena, R., and Portyanko, A. (2019). Over-Expression of βII-Tubulin and Especially Its Localization in Cell Nuclei Correlates with Poorer Outcomes in Colorectal Cancer. Cells *8*, E25.

Ryan, M.C., Kostner, H., Gordon, K.A., Duniho, S., Sutherland, M.K., Yu, C., Kim, K.M., Nesterova, A., Anderson, M., McEarchern, J.A., et al. (2010). Targeting pancreatic and ovarian carcinomas using the auristatin-based anti-CD70 antibody-drug conjugate SGN-75. Br. J. Cancer *103*, 676–684.

Ryo, A., Suizu, F., Yoshida, Y., Perrem, K., Liou, Y.-C., Wulf, G., Rottapel, R., Yamaoka, S., and Lu, K.P. (2003). Regulation of NF-κB Signaling by Pin1-Dependent Prolyl Isomerization and Ubiquitin-Mediated Proteolysis of p65/RelA. Mol. Cell *12*, 1413–1426.

Ryseck, R.P., Bull, P., Takamiya, M., Bours, V., Siebenlist, U., Dobrzanski, P., and Bravo, R. (1992). RelB, a new Rel family transcription activator that can interact with p50-NF-κB. Mol. Cell. Biol. *12*, 674–684.

Sabin, A.B. (1959). Reoviruses: A new group of respiratory and enteric viruses formerly classified as ECHO type 10 is described. Science *130*, 1387–1389.

Saccani, S., Marazzi, I., Beg, A.A., and Natoli, G. (2004). Degradation of Promoter-bound p65/RelA Is Essential for the Prompt Termination of the Nuclear Factor κB Response. J. Exp. Med. *200*, 107–113.

Sachs, K., Perez, O., Pe'er, D., Lauffenburger, D.A., and Nolan, G.P. (2005). Causal Protein-Signaling Networks Derived from Multiparameter Single-Cell Data. Science *308*, 523–529.

Sahai, E., and Marshall, C.J. (2003). Differing modes of tumour cell invasion have distinct requirements for Rho/ROCK signalling and extracellular proteolysis. Nat. Cell Biol. *5*, 711–719.

Sakaguchi, S., Sakaguchi, N., Asano, M., Itoh, M., and Toda, M. (1995). Immunologic self-tolerance maintained by activated T cells expressing IL-2 receptor α-chains (CD25). Breakdown of a single mechanism of self-tolerance causes various autoimmune diseases. J. Immunol. Baltim. Md 1950 *155*, 1151–1164.

Sakamoto, K., Maeda, S., Hikiba, Y., Nakagawa, H., Hayakawa, Y., Shibata, W., Yanai, A., Ogura, K., and Omata, M. (2009). Constitutive NF-κB activation in colorectal carcinoma plays a key role in angiogenesis, promoting tumor growth. Clin. Cancer Res. Off. J. Am. Assoc. Cancer Res. *15*, 2248–2258.

Sakurai, H., Chiba, H., Miyoshi, H., Sugita, T., and Toriumi, W. (1999). IκB kinases

phosphorylate NF-κB p65 subunit on serine 536 in the transactivation domain. J. Biol. Chem. *274*, 30353–30356.

Sakurai, H., Suzuki, S., Kawasaki, N., Nakano, H., Okazaki, T., Chino, A., Doi, T., and Saiki, I. (2003). Tumor Necrosis Factor-α-induced IKK Phosphorylation of NF-κB p65 on Serine 536 Is Mediated through the TRAF2, TRAF5, and TAK1 Signaling Pathway. J. Biol. Chem. *278*, 36916–36923.

Sampattavanich, S., Steiert, B., Kramer, B.A., Gyori, B.M., Albeck, J.G., and Sorger, P.K. (2018). Encoding Growth Factor Identity in the Temporal Dynamics of FOXO3 under the Combinatorial Control of ERK and AKT Kinases. Cell Syst. *6*, 664-678.e9.

Samson, A., Scott, K.J., Taggart, D., West, E.J., Wilson, E., Nuovo, G.J., Thomson, S., Corns, R., Mathew, R.K., Fuller, M.J., et al. (2018). Intravenous delivery of oncolytic reovirus to brain tumor patients immunologically primes for subsequent checkpoint blockade. Sci. Transl. Med. *10*, eaam7577.

Sano, M., Ijichi, H., Takahashi, R., Miyabayashi, K., Fujiwara, H., Yamada, T., Kato, H., Nakatsuka, T., Tanaka, Y., Tateishi, K., et al. (2019). Blocking CXCLs-CXCR2 axis in tumor-stromal interactions contributes to survival in a mouse model of pancreatic ductal adenocarcinoma through reduced cell invasion/migration and a shift of immune-inflammatory microenvironment. Oncogenesis *8*, 8.

Santos, S.D.M., Verveer, P.J., and Bastiaens, P.I.H. (2007). Growth factor-induced MAPK network topology shapes Erk response determining PC-12 cell fate. Nat. Cell Biol. *9*, 324–330.

Sasaki, C.Y., Barberi, T.J., Ghosh, P., and Longo, D.L. (2005). Phosphorylation of RelA/p65 on Serine 536 Defines an IκBα-independent NF-κB Pathway. J. Biol. Chem. *280*, 34538–34547.

Sasaki, Y., Suzuki, M., and Hidaka, H. (2002). The novel and specific Rho-kinase inhibitor (S)-(+)-2-methyl-1-[(4-methyl-5-isoquinoline)sulfonyl]-homopiperazine as a probing molecule for Rho-kinase-involved pathway. Pharmacol. Ther. *93*, 225–232.

Sato, M., Suemori, H., Hata, N., Asagiri, M., Ogasawara, K., Nakao, K., Nakaya, T., Katsuki, M., Noguchi, S., Tanaka, N., et al. (2000). Distinct and essential roles of transcription factors IRF-3 and IRF-7 in response to viruses for IFN-α/β gene induction. Immunity *13*, 539–548.

Sato, S., Stark, H.A., Martinez, J., Beaven, M.A., Jensen, R.T., and Gardner, J.D. (1989). Receptor occupation, calcium mobilization, and amylase release in pancreatic acini: effect of CCK-JMV-180. Am. J. Physiol. *257*, G202-209.

Saung, M.T., and Zheng, L. (2017). Current Standards of Chemotherapy for Pancreatic Cancer. Clin. Ther. *39*, 2125–2134.

Sausen, M., Phallen, J., Adleff, V., Jones, S., Leary, R.J., Barrett, M.T., Anagnostou, V., Parpart-Li, S., Murphy, D., Kay Li, Q., et al. (2015). Clinical implications of genomic alterations in the tumour and circulation of pancreatic cancer patients. Nat. Commun. *6*, 7686.

Scaffidi, P., Misteli, T., and Bianchi, M.E. (2002). Release of chromatin protein HMGB1 by necrotic cells triggers inflammation. Nature *418*, 191–195.

Schaider, H., Oka, M., Bogenrieder, T., Nesbit, M., Satyamoorthy, K., Berking, C., Matsushima, K., and Herlyn, M. (2003). Differential response of primary and metastatic melanomas to neutrophils attracted by IL-8. Int. J. Cancer *103*, 335–343.

Scheibenbogen, C., Möhler, T., Haefele, J., Hunstein, W., and Keilholz, U. (1995). Serum interleukin-8 (IL-8) is elevated in patients with metastatic melanoma and correlates with tumour load. Melanoma Res. *5*, 179–181.

Schiff, P.B., and Horwitz, S.B. (1980). Taxol stabilizes microtubules in mouse fibroblast cells. Proc. Natl. Acad. Sci. U. S. A. *77*, 1561–1565.

Schiff, P.B., Fant, J., and Horwitz, S.B. (1979). Promotion of microtubule assembly in vitro by taxol. Nature *277*, 665–667.

Schindelin, J., Arganda-Carreras, I., Frise, E., Kaynig, V., Longair, M., Pietzsch, T., Preibisch, S., Rueden, C., Saalfeld, S., Schmid, B., et al. (2012). Fiji: an open-source platform for biological-image analysis. Nat. Methods *9*, 676–682.

Schliwa, M. (1982). Action of cytochalasin D on cytoskeletal networks. J. Cell Biol. *92*, 79–91.

Schmidt, U., Weigert, M., Broaddus, C., and Myers, G. (2018). Cell Detection with Star-Convex Polygons. Medical Image Computing and Computer Assisted Intervention – MICCAI 2018, A.F. Frangi, J.A. Schnabel, C. Davatzikos, C. Alberola-López, and G. Fichtinger, eds. (Cham: Springer International Publishing), pp. 265–273.

Schmidt-Supprian, M., Bloch, W., Courtois, G., Addicks, K., Israël, A., Rajewsky, K., and Pasparakis, M. (2000). NEMO/IKK gamma-deficient mice model incontinentia pigmenti. Mol. Cell *5*, 981–992.

Schmitz, M.L., and Baeuerle, P.A. (1991). The p65 subunit is responsible for the strong transcription activating potential of NF-κB. EMBO J. *10*, 3805–3817.

Schneider, W.M., Chevillotte, M.D., and Rice, C.M. (2014). Interferon-stimulated genes: a complex web of host defenses. Annu. Rev. Immunol. *32*, 513–545.

Schoggins, J.W., Wilson, S.J., Panis, M., Murphy, M.Y., Jones, C.T., Bieniasz, P., and Rice, C.M. (2011). A diverse range of gene products are effectors of the type I interferon antiviral response. Nature *472*, 481–485.

Schroeder, R.L., Stevens, C.L., and Sridhar, J. (2014). Small Molecule Tyrosine Kinase Inhibitors of ErbB2/HER2/Neu in the Treatment of Aggressive Breast Cancer. Molecules *19*, 15196–15212.

Schulz, W.L., Haj, A.K., and Schiff, L.A. (2012). Reovirus Uses Multiple Endocytic Pathways for Cell Entry. J. Virol. *86*, 12665–12675.

Schumm, K., Rocha, S., Caamano, J., and Perkins, N.D. (2006). Regulation of p53 tumour suppressor target gene expression by the p52 NF-κB subunit. EMBO J. *25*, 4820–4832.

Schuster, M., Glauben, R., Plaza-Sirvent, C., Schreiber, L., Annemann, M., Floess, S., Kühl, A.A., Clayton, L.K., Sparwasser, T., Schulze-Osthoff, K., et al. (2012). IκBNS Protein Mediates Regulatory T Cell Development via Induction of the Foxp3 Transcription Factor. Immunity *37*, 998–1008.

Schwartz, J.C., Zhang, X., Fedorov, A.A., Nathenson, S.G., and Almo, S.C. (2001). Structural basis for co-stimulation by the human CTLA-4/B7-2 complex. Nature *410*, 604–608.

Sclabas, G.M., Uwagawa, T., Schmidt, C., Hess, K.R., Evans, D.B., Abbruzzese, J.L., and Chiao, P.J. (2005). Nuclear factor κB activation is a potential target for preventing pancreatic carcinoma by aspirin. Cancer *103*, 2485–2490.

Scott, M.L., Fujita, T., Liou, H.C., Nolan, G.P., and Baltimore, D. (1993). The p65 subunit of NF-κB regulates IκB by two distinct mechanisms. Genes Dev. *7*, 1266–1276.

Scutari, M., Graafland, C.E., and Gutierrez, J.M. (2018). Who Learns Better Bayesian Network Structures: Constraint-Based, Score-based or Hybrid Algorithms? Proc. Mach. Learn. Res. *72*, 416–427.

Selby, P., Hobbs, S., Viner, C., Jackson, E., Jones, A., Newell, D., Calvert, A.H., McElwain, T., Fearon, K., Humphreys, J., et al. (1987). Tumour necrosis factor in man: Clinical and biological observations. Br. J. Cancer *56*, 803–808.

Selimkhanov, J., Taylor, B., Yao, J., Pilko, A., Albeck, J., Hoffmann, A., Tsimring, L., and Wollman, R. (2014). Accurate information transmission through dynamic biochemical signaling networks. Science.

Sen, R., and Baltimore, D. (1986). Multiple nuclear factors interact with the immunoglobulin enhancer sequences. Cell *46*, 705–716.

Senftleben, U., Cao, Y., Xiao, G., Greten, F.R., Krähn, G., Bonizzi, G., Chen, Y., Hu, Y., Fong, A., Sun, S.C., et al. (2001a). Activation by IKKα of a second, evolutionary conserved, NF-κB signaling pathway. Science *293*, 1495–1499.

Senftleben, U., Li, Z.-W., Baud, V., and Karin, M. (2001b). IKKβ Is Essential for Protecting T Cells from TNFα-Induced Apoptosis. Immunity *14*, 217–230.

Sero, J.E., and Bakal, C. (2017). Multiparametric Analysis of Cell Shape Demonstrates that β-PIX Directly Couples YAP Activation to Extracellular Matrix Adhesion. Cell Syst. *4*, 84-96.e6.

Sero, J.E., Sailem, H.Z., Ardy, R.C., Almuttaqi, H., Zhang, T., and Bakal, C. (2015). Cell shape and the microenvironment regulate nuclear translocation of NF-κB in breast epithelial and tumor cells. Mol. Syst. Biol. *11*.

Sha, W.C., Liou, H.C., Tuomanen, E.I., and Baltimore, D. (1995). Targeted disruption of the p50 subunit of NF-κB leads to multifocal defects in immune responses. Cell *80*, 321–330.

Shah, S., King, E.M., Chandrasekhar, A., and Newton, R. (2014). Roles for the mitogen-activated protein kinase (MAPK) phosphatase, DUSP1, in feedback control of inflammatory gene expression and repression by dexamethasone. J. Biol. Chem. *289*, 13667–13679.

Shah, S., Mostafa, M.M., McWhae, A., Traves, S.L., and Newton, R. (2016). Negative Feed-forward Control of Tumor Necrosis Factor (TNF) by Tristetraprolin (ZFP36) Is Limited by the Mitogen-activated Protein Kinase Phosphatase, Dual-specificity Phosphatase 1 (DUSP1). J. Biol. Chem. *291*, 110–125.

Shah, S.A., Potter, M.W., McDade, T.P., Ricciardi, R., Perugini, R.A., Elliott, P.J., Adams, J., and Callery, M.P. (2001). 26S proteasome inhibition induces apoptosis and limits growth of human pancreatic cancer. J. Cell. Biochem. *82*, 110–122.

Sharma, S., tenOever, B.R., Grandvaux, N., Zhou, G.-P., Lin, R., and Hiscott, J. (2003). Triggering the interferon antiviral response through an IKK-related pathway. Science *300*, 1148–1151.

Sheehy, A.M., and Schlissel, M.S. (1999). Overexpression of RelA Causes G1 Arrest and Apoptosis in a Pro-B Cell Line. J. Biol. Chem. *274*, 8708–8716.

Shen, X., Mizuguchi, G., Hamiche, A., and Wu, C. (2000). A chromatin remodelling complex

involved in transcription and DNA processing. Nature *406*, 541–544.

Shifrut, E., Carnevale, J., Tobin, V., Roth, T.L., Woo, J.M., Bui, C.T., Li, P.J., Diolaiti, M.E., Ashworth, A., and Marson, A. (2018). Genome-wide CRISPR Screens in Primary Human T Cells Reveal Key Regulators of Immune Function. Cell *175*, 1958-1971.e15.

Shimazu, R., Akashi, S., Ogata, H., Nagai, Y., Fukudome, K., Miyake, K., and Kimoto, M. (1999). MD-2, a Molecule that Confers Lipopolysaccharide Responsiveness on Toll-like Receptor 4. J. Exp. Med. *189*, 1777–1782.

Shinohara, H., Yasuda, T., Aiba, Y., Sanjo, H., Hamadate, M., Watarai, H., Sakurai, H., and Kurosaki, T. (2005). PKCβ regulates BCR-mediated IKK activation by facilitating the interaction between TAK1 and CARMA1. J. Exp. Med. *202*, 1423–1431.

Shirane, M., Hatakeyama, S., Hattori, K., Nakayama, K., and Nakayama, K. (1999). Common pathway for the ubiquitination of IκBα, IκBβ, and IκBε mediated by the F-box protein FWD1. J. Biol. Chem. *274*, 28169–28174.

Shishodia, S., Koul, D., and Aggarwal, B.B. (2004). Cyclooxygenase (COX)-2 Inhibitor Celecoxib Abrogates TNF-Induced NF-κB Activation through Inhibition of Activation of IκBα Kinase and Akt in Human Non-Small Cell Lung Carcinoma: Correlation with Suppression of COX-2 Synthesis. J. Immunol. *173*, 2011–2022.

Shyu, A.-B., Wilkinson, M.F., and van Hoof, A. (2008). Messenger RNA regulation: to translate or to degrade. EMBO J. *27*, 471–481.

Siebenlist, U., Brown, K., and Claudio, E. (2005). Control of lymphocyte development by nuclear factor-κB. Nat. Rev. Immunol. *5*, 435–445.

Singh, S., and Aggarwal, B.B. (1995). Activation of Transcription Factor NF-κB Is Suppressed by Curcumin (Diferuloylmethane). J. Biol. Chem. *270*, 24995–25000.

Slifka, M.K., Antia, R., Whitmire, J.K., and Ahmed, R. (1998). Humoral Immunity Due to Long-Lived Plasma Cells. Immunity *8*, 363–372.

Slowicka, K., Petta, I., Blancke, G., Hoste, E., Dumas, E., Sze, M., Vikkula, H., Radaelli, E., Haigh, J.J., Jonckheere, S., et al. (2020). Zeb2 drives invasive and microbiota-dependent colon carcinoma. Nat. Cancer *1*, 620–634.

Socinski, M.A., Bondarenko, I., Karaseva, N.A., Makhson, A.M., Vynnychenko, I., Okamoto, I., Hon, J.K., Hirsh, V., Bhar, P., Zhang, H., et al. (2012). Weekly nab-paclitaxel in combination with carboplatin versus solvent-based paclitaxel plus carboplatin as first-line therapy in patients with advanced non-small-cell lung cancer: final results of a phase III trial. J. Clin. Oncol. Off. J. Am. Soc. Clin. Oncol. *30*, 2055–2062.

Song, H.Y., Rothe, M., and Goeddel, D.V. (1996). The tumor necrosis factor-inducible zinc finger protein A20 interacts with TRAF1/TRAF2 and inhibits NF-κB activation. Proc. Natl. Acad. Sci. U. S. A. *93*, 6721–6725.

Song, L., Ohnuma, T., Gelman, I.H., and Holland, J.F. (2009). Reovirus infection of cancer cells is not due to activated Ras pathway. Cancer Gene Ther. *16*, 382–382.

Southgate, L., Machado, R.D., Snape, K.M., Primeau, M., Dafou, D., Ruddy, D.M., Branney, P.A., Fisher, M., Lee, G.J., Simpson, M.A., et al. (2011). Gain-of-Function Mutations of ARHGAP31, a Cdc42/Rac1 GTPase Regulator, Cause Syndromic Cutis Aplasia and Limb Anomalies. Am. J. Hum. Genet. *88*, 574–585.

Sparks, H., Kondo, H., Hooper, S., Munro, I., Kennedy, G., Dunsby, C., French, P., and

Sahai, E. (2018). Heterogeneity in tumor chromatin-doxorubicin binding revealed by in vivo fluorescence lifetime imaging confocal endomicroscopy. Nat. Commun. *9*, 2662.

Spencer, C.M., and Faulds, D. (1994). Paclitaxel. Drugs *48*, 794–847.

Spencer, S.L., Gaudet, S., Albeck, J.G., Burke, J.M., and Sorger, P.K. (2009). Non-genetic origins of cell-to-cell variability in TRAIL-induced apoptosis. Nature *459*, 428–432.

Spencer, W., Kwon, H., Crépieux, P., Leclerc, N., Lin, R., and Hiscott, J. (1999). Taxol selectively blocks microtubule dependent NF-κB activation by phorbol ester via inhibition of IκBα phosphorylation and degradation. Oncogene *18*, 495–505.

Spiegelman, B.M., Penningroth, S.M., and Kirschner, M.W. (1977). Turnover of tubulin and the N site GTP in chinese hamster ovary cells. Cell *12*, 587–600.

Stamper, C.C., Zhang, Y., Tobin, J.F., Erbe, D.V., Ikemizu, S., Davis, S.J., Stahl, M.L., Seehra, J., Somers, W.S., and Mosyak, L. (2001). Crystal structure of the B7-1/CTLA-4 complex that inhibits human immune responses. Nature *410*, 608–611.

Steele, C.W., Jamieson, N.B., Evans, T.R.J., McKay, C.J., Sansom, O.J., Morton, J.P., and Carter, C.R. (2013). Exploiting inflammation for therapeutic gain in pancreatic cancer. Br. J. Cancer *108*, 997–1003.

Steele, L., Errington, F., Prestwich, R., Ilett, E., Harrington, K., Pandha, H., Coffey, M., Selby, P., Vile, R., and Melcher, A. (2011). Pro-inflammatory cytokine/chemokine production by reovirus treated melanoma cells is PKR/NF-κB mediated and supports innate and adaptive anti-tumour immune priming. Mol. Cancer *10*, 20.

Stein, S.J., and Baldwin, A.S. (2013). Deletion of the NF-κB subunit p65/RelA in the hematopoietic compartment leads to defects in hematopoietic stem cell function. Blood *121*, 5015–5024.

Stein, B., Cogswell, P.C., and Baldwin, A.S. (1993a). Functional and physical associations between NF-κB and C/EBP family members: a Rel domain-bZIP interaction. Mol. Cell. Biol. *13*, 3964–3974.

Stein, B., Baldwin, A.S., Ballard, D.W., Greene, W.C., Angel, P., and Herrlich, P. (1993b). Cross-coupling of the NF-κB p65 and Fos/Jun transcription factors produces potentiated biological function. EMBO J. *12*, 3879–3891.

Steinman, R.M., and Hemmi, H. (2006). Dendritic cells: translating innate to adaptive immunity. Curr. Top. Microbiol. Immunol. *311*, 17–58.

Stelma, T., and Leaner, V.D. (2017). KPNB1-mediated nuclear import is required for motility and inflammatory transcription factor activity in cervical cancer cells. Oncotarget *8*, 32833–32847.

Stennicke, H.R., Jürgensmeier, J.M., Shin, H., Deveraux, Q., Wolf, B.B., Yang, X., Zhou, Q., Ellerby, H.M., Ellerby, L.M., Bredesen, D., et al. (1998). Pro-caspase-3 Is a Major Physiologic Target of Caspase-8. J. Biol. Chem. *273*, 27084–27090.

Steward, R. (1987). Dorsal, an embryonic polarity gene in Drosophila, is homologous to the vertebrate proto-oncogene, c-rel. Science *238*, 692–694.

Stewart-Ornstein, J., and Lahav, G. (2016). Dynamics of CDKN1A in Single Cells Defined by an Endogenous Fluorescent Tagging Toolkit. Cell Rep. *14*, 1800–1811.

Stoddard, P.R., Williams, T.A., Garner, E., and Baum, B. (2017). Evolution of polymer

formation within the actin superfamily. Mol. Biol. Cell *28*, 2461–2469.

Strong, J.E., and Lee, P.W. (1996). The v-erbB oncogene confers enhanced cellular susceptibility to reovirus infection. J. Virol. *70*, 612–616.

Strong, J.E., Tang, D., and Lee, P.W.K. (1993). Evidence That the Epidermal Growth Factor Receptor on Host Cells Confers Reovirus Infection Efficiency. Virology *197*, 405–411.

Strong, J.E., Coffey, M.C., Tang, D., Sabinin, P., and Lee, P.W. (1998). The molecular basis of viral oncolysis: usurpation of the Ras signaling pathway by reovirus. EMBO J. *17*, 3351–3362.

Subramanian, A., Tamayo, P., Mootha, V.K., Mukherjee, S., Ebert, B.L., Gillette, M.A., Paulovich, A., Pomeroy, S.L., Golub, T.R., Lander, E.S., et al. (2005). Gene set enrichment analysis: A knowledge-based approach for interpreting genome-wide expression profiles. Proc. Natl. Acad. Sci. *102*, 15545–15550.

Sun, S.-C. (2011). Non-canonical NF-κB signaling pathway. Cell Res. *21*, 71–85.

Sun, L., Wang, H., Wang, Z., He, S., Chen, S., Liao, D., Wang, L., Yan, J., Liu, W., Lei, X., et al. (2012). Mixed Lineage Kinase Domain-like Protein Mediates Necrosis Signaling Downstream of RIP3 Kinase. Cell *148*, 213–227.

Sun, S.C., Ganchi, P.A., Ballard, D.W., and Greene, W.C. (1993). NF-κB controls expression of inhibitor IκBα: evidence for an inducible autoregulatory pathway. Science *259*, 1912–1915.

Sung, M.-H., Salvatore, L., Lorenzi, R.D., Indrawan, A., Pasparakis, M., Hager, G.L., Bianchi, M.E., and Agresti, A. (2009). Sustained Oscillations of NF-κB Produce Distinct Genome Scanning and Gene Expression Profiles. PLOS ONE *4*, e7163.

Sung, M.-H., Li, N., Lao, Q., Gottschalk, R.A., Hager, G.L., and Fraser, I.D.C. (2014). Switching of the relative dominance between feedback mechanisms in lipopolysaccharide-induced NF-κB signaling. Sci. Signal. *7*, ra6.

Suwa, H., Yoshimura, T., Yamaguchi, N., Kanehira, K., Manabe, T., Imamura, M., Hiai, H., and Fukumoto, M. (1994). K-ras and p53 alterations in genomic DNA and transcripts of human pancreatic adenocarcinoma cell lines. Jpn. J. Cancer Res. Gann *85*, 1005–1014.

Suzuki, N., Suzuki, S., Duncan, G.S., Millar, D.G., Wada, T., Mirtsos, C., Takada, H., Wakeham, A., Itie, A., Li, S., et al. (2002). Severe impairment of interleukin-1 and Toll-like receptor signalling in mice lacking IRAK-4. Nature *416*, 750–756.

Svitkina, T. (2018). The Actin Cytoskeleton and Actin-Based Motility. Cold Spring Harb. Perspect. Biol. *10*, a018267.

Takada, Y., Singh, S., and Aggarwal, B.B. (2004). Identification of a p65 peptide that selectively inhibits NF-κB activation induced by various inflammatory stimuli and its role in down-regulation of NF-κB-mediated gene expression and up-regulation of apoptosis. J. Biol. Chem. *279*, 15096–15104.

Tamatani, M., Che, Y.H., Matsuzaki, H., Ogawa, S., Okado, H., Miyake, S., Mizuno, T., and Tohyama, M. (1999). Tumor Necrosis Factor Induces Bcl-2 and Bcl-x Expression through NFκB Activation in Primary Hippocampal Neurons. J. Biol. Chem. *274*, 8531–8538.

Tang, D., Strong, J.E., and Lee, P.W.K. (1993). Recognition of the Epidermal Growth Factor Receptor by Reovirus. Virology *197*, 412–414.

Tangutur, A.D., Kumar, D., Krishna, K.V., and Kantevari, S. (2017). Microtubule Targeting

Agents as Cancer Chemotherapeutics: An Overview of Molecular Hybrids as Stabilizing and Destabilizing Agents. Curr. Top. Med. Chem. *17*, 2523–2537.

Tascilar, M., Skinner, H.G., Rosty, C., Sohn, T., Wilentz, R.E., Offerhaus, G.J., Adsay, V., Abrams, R.A., Cameron, J.L., Kern, S.E., et al. (2001). The SMAD4 protein and prognosis of pancreatic ductal adenocarcinoma. Clin. Cancer Res. Off. J. Am. Assoc. Cancer Res. *7*, 4115–4121.

Tato, C.M., Villarino, A., Caamaño, J.H., Boothby, M., and Hunter, C.A. (2003). Inhibition of NF-κB Activity in T and NK Cells Results in Defective Effector Cell Expansion and Production of IFN-γ Required for Resistance to Toxoplasma gondii. J. Immunol. *170*, 3139–3146.

Taunton, J., Hassig, C.A., and Schreiber, S.L. (1996). A mammalian histone deacetylase related to the yeast transcriptional regulator Rpd3p. Science *272*, 408–411.

Tay, S., Hughey, J.J., Lee, T.K., Lipniacki, T., Quake, S.R., and Covert, M.W. (2010). Single-cell NF-κB dynamics reveal digital activation and analog information processing in cells. Nature *466*, 267–271.

Tcherkezian, J., Triki, I., Stenne, R., Danek, E.I., and Lamarche-Vane, N. (2006). The human orthologue of CdGAP is a phosphoprotein and a GTPase-activating protein for Cdc42 and Rac1 but not RhoA. Biol. Cell *98*, 445–456.

Tenorio, R., Fernández de Castro, I., Knowlton, J.J., Zamora, P.F., Sutherland, D.M., Risco, C., and Dermody, T.S. (2019). Function, Architecture, and Biogenesis of Reovirus Replication Neoorganelles. Viruses *11*, 288.

Tesselaar, K., Xiao, Y., Arens, R., Schijndel, G.M.W. van, Schuurhuis, D.H., Mebius, R.E., Borst, J., and Lier, R.A.W. van (2003). Expression of the Murine CD27 Ligand CD70 In Vitro and In Vivo. J. Immunol. *170*, 33–40.

Thirukkumaran, C., Shi, Z.-Q., Thirukkumaran, P., Luider, J., Kopciuk, K., Spurrell, J., Elzinga, K., and Morris, D. (2017). PUMA and NF-kB Are Cell Signaling Predictors of Reovirus Oncolysis of Breast Cancer. PLOS ONE *12*, e0168233.

Thirukkumaran, C.M., Shi, Z.Q., Luider, J., Kopciuk, K., Gao, H., Bahlis, N., Neri, P., Pho, M., Stewart, D., Mansoor, A., et al. (2013). Reovirus modulates autophagy during oncolysis of multiple myeloma. Autophagy *9*, 413–414.

Thomas, R.K., Wickenhauser, C., Tawadros, S., Diehl, V., Küppers, R., Wolf, J., and Schmitz, R. (2004). Mutational analysis of the IκBα gene in activated B cell-like diffuse large B-cell lymphoma. Br. J. Haematol. *126*, 50–54.

Tian, B., Nowak, D.E., and Brasier, A.R. (2005). A TNF-induced gene expression program under oscillatory NF-κB control. BMC Genomics *6*, 137.

Tian, B., Patrikeev, I., Ochoa, L., Vargas, G., Belanger, K.K., Litvinov, J., Boldogh, I., Ameredes, B.T., Motamedi, M., and Brasier, A.R. (2017). NF-κB Mediates Mesenchymal Transition, Remodeling, and Pulmonary Fibrosis in Response to Chronic Inflammation by Viral RNA Patterns. Am. J. Respir. Cell Mol. Biol. *56*, 506–520.

Tinevez, J.-Y., Perry, N., Schindelin, J., Hoopes, G.M., Reynolds, G.D., Laplantine, E., Bednarek, S.Y., Shorte, S.L., and Eliceiri, K.W. (2017). TrackMate: An open and extensible platform for single-particle tracking. Methods *115*, 80–90.

Ting, A.T., and Bertrand, M.J.M. (2016). More to Life than NF-κB in TNFR1 Signaling. Trends Immunol. *37*, 535–545.

Tjomsland, V., Spångeus, A., Välilä, J., Sandström, P., Borch, K., Druid, H., Falkmer, S., Falkmer, U., Messmer, D., and Larsson, M. (2011). Interleukin 1α Sustains the Expression of Inflammatory Factors in Human Pancreatic Cancer Microenvironment by Targeting Cancer-Associated Fibroblasts. Neoplasia N. Y. N *13*, 664–675.

Tobacman, L.S., and Korn, E.D. (1983). The kinetics of actin nucleation and polymerization. J. Biol. Chem. *258*, 3207–3214.

Tomita, K., Bokhoven, A. van, Leenders, G.J.L.H. van, Ruijter, E.T.G., Jansen, C.F.J., Bussemakers, M.J.G., and Schalken, J.A. (2000). Cadherin Switching in Human Prostate Cancer Progression. Cancer Res. *60*, 3650–3654.

Tong, L., and Tergaonkar, V. (2014). Rho protein GTPases and their interactions with NFκB: crossroads of inflammation and matrix biology. Biosci. Rep. *34*, e00115.

Tong, A.-J., Liu, X., Thomas, B.J., Lissner, M.M., Baker, M.R., Senagolage, M.D., Allred, A.L., Barish, G.D., and Smale, S.T. (2016). A Stringent Systems Approach Uncovers Gene-Specific Mechanisms Regulating Inflammation. Cell *165*, 165–179.

Totzke, G., Essmann, F., Pohlmann, S., Lindenblatt, C., Jänicke, R.U., and Schulze-Osthoff, K. (2006). A novel member of the IκB family, human IκB-ζ, inhibits transactivation of p65 and its DNA binding. J. Biol. Chem. *281*, 12645–12654.

Traenckner, E.B., Pahl, H.L., Henkel, T., Schmidt, K.N., Wilk, S., and Baeuerle, P.A. (1995). Phosphorylation of human IκB-α on serines 32 and 36 controls IκB-α proteolysis and NF-κB activation in response to diverse stimuli. EMBO J. *14*, 2876–2883.

Tran, P.T., Marsh, L., Doye, V., Inoué, S., and Chang, F. (2001). A Mechanism for Nuclear Positioning in Fission Yeast Based on Microtubule Pushing. J. Cell Biol. *153*, 397–412.

Trendowski, M. (2015). Using Cytochalasins to Improve Current Chemotherapeutic Approaches. Anticancer Agents Med. Chem. *15*, 327–335.

Turner, D.A., Paszek, P., Woodcock, D.J., Nelson, D.E., Horton, C.A., Wang, Y., Spiller, D.G., Rand, D.A., White, M.R.H., and Harper, C.V. (2010). Physiological levels of TNFα stimulation induce stochastic dynamics of NF-κB responses in single living cells. J. Cell Sci. *123*, 2834–2843.

Twigger, K., Vidal, L., White, C.L., De Bono, J.S., Bhide, S., Coffey, M., Thompson, B., Vile, R.G., Heinemann, L., Pandha, H.S., et al. (2008). Enhanced in vitro and in vivo cytotoxicity of combined reovirus and radiotherapy. Clin. Cancer Res. Off. J. Am. Assoc. Cancer Res. *14*, 912–923.

Twigger, K., Roulstone, V., Kyula, J., Karapanagiotou, E.M., Syrigos, K.N., Morgan, R., White, C., Bhide, S., Nuovo, G., Coffey, M., et al. (2012). Reovirus exerts potent oncolytic effects in head and neck cancer cell lines that are independent of signalling in the EGFR pathway. BMC Cancer *12*, 368.

Tyanova, S., and Cox, J. (2018). Perseus: A Bioinformatics Platform for Integrative Analysis of Proteomics Data in Cancer Research. Methods Mol. Biol. Clifton NJ *1711*, 133–148.

Tyanova, S., Temu, T., Sinitcyn, P., Carlson, A., Hein, M.Y., Geiger, T., Mann, M., and Cox, J. (2016). The Perseus computational platform for comprehensive analysis of (prote)omics data. Nat. Methods *13*, 731–740.

Ueda, Y., and Richmond, A. (2006). NF-κB activation in melanoma. Pigment Cell Res. Spons. Eur. Soc. Pigment Cell Res. Int. Pigment Cell Soc. *19*, 112–124.

Ungefroren, H., Groth, S., Sebens, S., Lehnert, H., Gieseler, F., and Fändrich, F. (2011). Differential roles of Smad2 and Smad3 in the regulation of TGF-β1-mediated growth inhibition and cell migration in pancreatic ductal adenocarcinoma cells: control by Rac1. Mol. Cancer *10*, 67.

Vaira, S., Johnson, T., Hirbe, A.C., Alhawagri, M., Anwisye, I., Sammut, B., O'Neal, J., Zou, W., Weilbaecher, K.N., Faccio, R., et al. (2008). RelB is the NF-κB subunit downstream of NIK responsible for osteoclast differentiation. Proc. Natl. Acad. Sci. *105*, 3897–3902.

Vallabhapurapu, S., Matsuzawa, A., Zhang, W., Tseng, P.-H., Keats, J.J., Wang, H., Vignali, D.A.A., Bergsagel, P.L., and Karin, M. (2008). Nonredundant and complementary functions of TRAF2 and TRAF3 in a ubiquitination cascade that activates NIK-dependent alternative NF-κB signaling. Nat. Immunol. *9*, 1364–1370.

Vallenius, T., Vaahtomeri, K., Kovac, B., Osiceanu, A.-M., Viljanen, M., and Mäkelä, T.P. (2011). An association between NUAK2 and MRIP reveals a novel mechanism for regulation of actin stress fibers. J. Cell Sci. *124*, 384–393.

Vandewalle, C., Comijn, J., De Craene, B., Vermassen, P., Bruyneel, E., Andersen, H., Tulchinsky, E., Van Roy, F., and Berx, G. (2005). SIP1/ZEB2 induces EMT by repressing genes of different epithelial cell–cell junctions. Nucleic Acids Res. *33*, 6566–6578.

Vane, J.R. (1971). Inhibition of prostaglandin synthesis as a mechanism of action for aspirin-like drugs. Nature. New Biol. *231*, 232–235.

Vartiainen, M.K., Guettler, S., Larijani, B., and Treisman, R. (2007). Nuclear actin regulates dynamic subcellular localization and activity of the SRF cofactor MAL. Science *316*, 1749–1752.

Vasquez, R.J., Howell, B., Yvon, A.M., Wadsworth, P., and Cassimeris, L. (1997). Nanomolar concentrations of nocodazole alter microtubule dynamic instability in vivo and in vitro. Mol. Biol. Cell *8*, 973–985.

Vermeulen, L., De Wilde, G., Van Damme, P., Vanden Berghe, W., and Haegeman, G. (2003). Transcriptional activation of the NF-κB p65 subunit by mitogen- and stress-activated protein kinase-1 (MSK1). EMBO J. *22*, 1313–1324.

Vimalachandran, D., Greenhalf, W., Thompson, C., Lüttges, J., Prime, W., Campbell, F., Dodson, A., Watson, R., Crnogorac-Jurcevic, T., Lemoine, N., et al. (2005). High Nuclear S100A6 (Calcyclin) Is Significantly Associated with Poor Survival in Pancreatic Cancer Patients. Cancer Res. *65*, 3218–3225.

Vincent, A., Herman, J., Schulick, R., Hruban, R.H., and Goggins, M. (2011). Pancreatic cancer. Lancet Lond. Engl. *378*, 607–620.

van de Vis, R.A.J., Moustakas, A., and van der Heide, L.P. (2021). NUAK1 and NUAK2 Fine-Tune TGF-β Signaling. Cancers *13*, 3377.

Vogl, A.W., and Guttman, J.A. (2018). An Introduction to Actin and Actin-Rich Structures. Anat. Rec. *301*, 1986–1990.

Voll, R.E., Jimi, E., Phillips, R.J., Barber, D.F., Rincon, M., Hayday, A.C., Flavell, R.A., and Ghosh, S. (2000). NF-κB Activation by the Pre-T Cell Receptor Serves as a Selective Survival Signal in T Lymphocyte Development. Immunity *13*, 677–689.

Von Hoff, D.D., Ervin, T., Arena, F.P., Chiorean, E.G., Infante, J., Moore, M., Seay, T., Tjulandin, S.A., Ma, W.W., Saleh, M.N., et al. (2013). Increased Survival in Pancreatic Cancer with nab-Paclitaxel plus Gemcitabine. N. Engl. J. Med. *369*, 1691–1703.

Vyas, O., Leung, K., Ledbetter, L., Kaley, K., Rodriguez, T., Garcon, M.C., and Saif, M.W. (2015). Clinical outcomes in pancreatic adenocarcinoma associated with BRCA-2 mutation. Anticancer. Drugs *26*, 224–226.

Wachsmann, M.B., Pop, L.M., and Vitetta, E.S. (2012). Pancreatic Ductal Adenocarcinoma: A Review of Immunologic Aspects. J. Investig. Med. Off. Publ. Am. Fed. Clin. Res. *60*, 643–663.

Waddell, N., Pajic, M., Patch, A.-M., Chang, D.K., Kassahn, K.S., Bailey, P., Johns, A.L., Miller, D., Nones, K., Quek, K., et al. (2015). Whole genomes redefine the mutational landscape of pancreatic cancer. Nature *518*, 495–501.

Walczak, C.E., and Heald, R. (2008). Chapter Three - Mechanisms of Mitotic Spindle Assembly and Function. International Review of Cytology, K.W. Jeon, ed. (Academic Press), pp. 111–158.

Wang, C., Deng, L., Hong, M., Akkaraju, G.R., Inoue, J., and Chen, Z.J. (2001). TAK1 is a ubiquitin-dependent kinase of MKK and IKK. Nature *412*, 346–351.

Wang, C.-Y., Mayo, M.W., and Baldwin, A.S. (1996). TNF- and Cancer Therapy-Induced Apoptosis: Potentiation by Inhibition of NF-κB. Science *274*, 784–787.

Wang, C.-Y., Mayo, M.W., Korneluk, R.G., Goeddel, D.V., and Albert S. Baldwin, J. (1998). NF-κB Antiapoptosis: Induction of TRAF1 and TRAF2 and c-IAP1 and c-IAP2 to Suppress Caspase-8 Activation. Science.

Wang, H., Wang, H.-S., Zhou, B.-H., Li, C.-L., Zhang, F., Wang, X.-F., Zhang, G., Bu, X.-Z., Cai, S.-H., and Du, J. (2013). Epithelial–Mesenchymal Transition (EMT) Induced by TNF-α Requires AKT/GSK-3β-Mediated Stabilization of Snail in Colorectal Cancer. PLOS ONE *8*, e56664.

Wang, J., Wang, X., Hussain, S., Zheng, Y., Sanjabi, S., Ouaaz, F., and Beg, A.A. (2007). Distinct Roles of Different NF-κB Subunits in Regulating Inflammatory and T Cell Stimulatory Gene Expression in Dendritic Cells. J. Immunol. *178*, 6777–6788.

Wang, L., Du, F., and Wang, X. (2008). TNF-α Induces Two Distinct Caspase-8 Activation Pathways. Cell *133*, 693–703.

Wang, N., Liu, W., Zheng, Y., Wang, S., Yang, B., Li, M., Song, J., Zhang, F., Zhang, X., Wang, Q., et al. (2018). CXCL1 derived from tumor-associated macrophages promotes breast cancer metastasis via activating NF-κB/SOX4 signaling. Cell Death Dis. *9*, 1–18.

Wang, W., Abbruzzese, J.L., Evans, D.B., Larry, L., Cleary, K.R., and Chiao, P.J. (1999). The Nuclear Factor-κB RelA Transcription Factor Is Constitutively Activated in Human Pancreatic Adenocarcinoma Cells. Clin. Cancer Res. *5*, 119–127.

Wang, X.W., Tan, N.S., Ho, B., and Ding, J.L. (2006). Evidence for the ancient origin of the NF-κB/IκB cascade: Its archaic role in pathogen infection and immunity. Proc. Natl. Acad. Sci. *103*, 4204–4209.

Wani, M.C., and Horwitz, S.B. (2014). Nature as a Remarkable Chemist: A Personal Story of the Discovery and Development of Taxol. Anticancer. Drugs *25*, 482–487.

Waters, A.M., and Der, C.J. (2018). KRAS: The Critical Driver and Therapeutic Target for Pancreatic Cancer. Cold Spring Harb. Perspect. Med. *8*, a031435.

Wathelet, M.G., Lin, C.H., Parekh, B.S., Ronco, L.V., Howley, P.M., and Maniatis, T. (1998). Virus infection induces the assembly of coordinately activated transcription factors on the

IFN-β enhancer in vivo. Mol. Cell *1*, 507–518.

Webster, G.A., and Perkins, N.D. (1999). Transcriptional Cross Talk between NF-κB and p53. Mol. Cell. Biol. *19*, 3485–3495.

Weichert, W., Boehm, M., Gekeler, V., Bahra, M., Langrehr, J., Neuhaus, P., Denkert, C., Imre, G., Weller, C., Hofmann, H.-P., et al. (2007). High expression of RelA/p65 is associated with activation of NF-κB-dependent signaling in pancreatic cancer and marks a patient population with poor prognosis. Br. J. Cancer *97*, 523–530.

Weil, R., Schwamborn, K., Alcover, A., Bessia, C., Di Bartolo, V., and Israël, A. (2003). Induction of the NF-κB Cascade by Recruitment of the Scaffold Molecule NEMO to the T Cell Receptor. Immunity *18*, 13–26.

Weisenberg, R.C., Broisy, G.G., and Taylor, E.William. (1968). Colchicine-binding protein of mammalian brain and its relation to microtubules. Biochemistry *7*, 4466–4479.

Weiss, S.A., Wolchok, J.D., and Sznol, M. (2019). Immunotherapy of Melanoma: Facts and Hopes. Clin. Cancer Res. *25*, 5191–5201.

Welch, M.D., Iwamatsu, A., and Mitchison, T.J. (1997). Actin polymerization is induced by Arp 2/3 protein complex at the surface of Listeria monocytogenes. Nature *385*, 265–269.

Wen, C., Miura, T., Voleti, V., Yamaguchi, K., Tsutsumi, M., Yamamoto, K., Otomo, K., Fujie, Y., Teramoto, T., Ishihara, T., et al. (2021). 3DeeCellTracker, a deep learning-based pipeline for segmenting and tracking cells in 3D time lapse images. eLife *10*, e59187.

Werner, J., Combs, S.E., Springfeld, C., Hartwig, W., Hackert, T., and Büchler, M.W. (2013). Advanced-stage pancreatic cancer: therapy options. Nat. Rev. Clin. Oncol. *10*, 323–333.

Werner, S.L., Barken, D., and Hoffmann, A. (2005). Stimulus Specificity of Gene Expression Programs Determined by Temporal Control of IKK Activity. Science *309*, 1857–1861.

Werner, S.L., Kearns, J.D., Zadorozhnaya, V., Lynch, C., O'Dea, E., Boldin, M.P., Ma, A., Baltimore, D., and Hoffmann, A. (2008). Encoding NF-κB temporal control in response to TNF: distinct roles for the negative regulators IκBα and A20. Genes Dev. *22*, 2093–2101.

Wertz, I.E., O'Rourke, K.M., Zhou, H., Eby, M., Aravind, L., Seshagiri, S., Wu, P., Wiesmann, C., Baker, R., Boone, D.L., et al. (2004). De-ubiquitination and ubiquitin ligase domains of A20 downregulate NF-κB signalling. Nature *430*, 694–699.

Wiese, C., and Zheng, Y. (2000). A new function for the γ -tubulin ring complex as a microtubule minus-end cap. Nat. Cell Biol. *2*, 358–364.

Wilhelmsen, K.C., and Temin, H.M. (1984). Structure and dimorphism of c-rel (turkey), the cellular homolog to the oncogene of reticuloendotheliosis virus strain T. J. Virol.

Willems, M., Dubois, N., Musumeci, L., Bours, V., and Robe, P.A. (2016). IκBζ: an emerging player in cancer. Oncotarget *7*, 66310–66322.

Williams, C.S., Mann, M., and DuBois, R.N. (1999). The role of cyclooxygenases in inflammation, cancer, and development. Oncogene *18*, 7908–7916.

Witkiewicz, A.K., McMillan, E.A., Balaji, U., Baek, G., Lin, W.-C., Mansour, J., Mollaee, M., Wagner, K.-U., Koduru, P., Yopp, A., et al. (2015). Whole-exome sequencing of pancreatic cancer defines genetic diversity and therapeutic targets. Nat. Commun. *6*, 6744.

Wolff, B., and Naumann, M. (1999). INK4 cell cycle inhibitors direct transcriptional

inactivation of NF-κB. Oncogene *18*, 2663–2666.

Wood, L.D., and Richmond, A. (1995). Constitutive and cytokine-induced expression of the melanoma growth stimulatory activity/GRO α gene requires both NF-κB and novel constitutive factors. J. Biol. Chem. *270*, 30619–30626.

Woodrum, D.T., Rich, S.A., and Pollard, T.D. (1975). Evidence for biased bidirectional polymerization of actin filaments using heavy meromyosin prepared by an improved method. J. Cell Biol. *67*, 231–237.

Woynarowski, J.M., Faivre, S., Herzig, M.C.S., Arnett, B., Chapman, W.G., Trevino, A.V., Raymond, E., Chaney, S.G., Vaisman, A., Varchenko, M., et al. (2000). Oxaliplatin-Induced Damage of Cellular DNA. Mol. Pharmacol. *58*, 920–927.

Wu, C., Fernandez, S.A., Criswell, T., Chidiac, T.A., Guttridge, D., Villalona-Calero, M., and Bekaii-Saab, T.S. (2013). Disrupting cytokine signaling in pancreatic cancer: a phase I/II study of etanercept in combination with gemcitabine in patients with advanced disease. Pancreas *42*, 813–818.

Wu, H., Liu, J., Li, W., Liu, G., and Li, Z. (2016). LncRNA-HOTAIR promotes TNF-α production in cardiomyocytes of LPS-induced sepsis mice by activating NF-κB pathway. Biochem. Biophys. Res. Commun. *471*, 240–246.

Wu, L., D'Amico, A., Winkel, K.D., Suter, M., Lo, D., and Shortman, K. (1998). RelB is essential for the development of myeloid-related CD8α- dendritic cells but not of lymphoid-related CD8α+ dendritic cells. Immunity *9*, 839–847.

Wu, L., Timmers, C., Maiti, B., Saavedra, H.I., Sang, L., Chong, G.T., Nuckolls, F., Giangrande, P., Wright, F.A., Field, S.J., et al. (2001). The E2F1–3 transcription factors are essential for cellular proliferation. Nature *414*, 457–462.

Wu, L., Nakano, H., and Wu, Z. (2006). The C-terminal activating region 2 of the Epstein-Barr virus-encoded latent membrane protein 1 activates NF-κB through TRAF6 and TAK1. J. Biol. Chem. *281*, 2162–2169.

Wu, M., Lee, H., Bellas, R.E., Schauer, S.L., Arsura, M., Katz, D., FitzGerald, M.J., Rothstein, T.L., Sherr, D.H., and Sonenshein, G.E. (1996). Inhibition of NF-κB/Rel induces apoptosis of murine B cells. EMBO J. *15*, 4682–4690.

Wu, P.-H., Phillip, J.M., Khatau, S.B., Chen, W.-C., Stirman, J., Rosseel, S., Tschudi, K., Van Patten, J., Wong, M., Gupta, S., et al. (2015). Evolution of cellular morpho-phenotypes in cancer metastasis. Sci. Rep. *5*, 18437.

Wuerzberger-Davis, S.M., Chang, P.-Y., Berchtold, C., and Miyamoto, S. (2005). Enhanced G2-M arrest by nuclear factor-κB-dependent p21waf1/cip1 induction. Mol. Cancer Res. MCR *3*, 345–353.

Wulf, E., Deboben, A., Bautz, F.A., Faulstich, H., and Wieland, T. (1979). Fluorescent phallotoxin, a tool for the visualization of cellular actin. Proc. Natl. Acad. Sci. *76*, 4498–4502.

Xiao, G., Harhaj, E.W., and Sun, S.C. (2001). NF-κB-inducing kinase regulates the processing of NF-κB2 p100. Mol. Cell *7*, 401–409.

Xie, T.-X., Xia, Z., Zhang, N., Gong, W., and Huang, S. (2010). Constitutive NF-κB activity regulates the expression of VEGF and IL-8 and tumor angiogenesis of human glioblastoma. Oncol. Rep. *23*, 725–732.

Xiong, Y., Connolly, T., Futcher, B., and Beach, D. (1991). Human D-type cyclin. Cell *65*,

691–699.

Xu, Y., Davidson, L., Alt, F.W., and Baltimore, D. (1996). Deletion of the Igκ Light Chain Intronic Enhancer/Matrix Attachment Region Impairs but Does Not Abolish VκJκ Rearrangement. Immunity *4*, 377–385.

Yachida, S., White, C.M., Naito, Y., Zhong, Y., Brosnan, J.A., Macgregor-Das, A.M., Morgan, R.A., Saunders, T., Laheru, D.A., Herman, J.M., et al. (2012). Clinical significance of the genetic landscape of pancreatic cancer and implications for identification of potential long-term survivors. Clin. Cancer Res. Off. J. Am. Assoc. Cancer Res. *18*, 6339–6347.

Yamaguchi, K., Shirakabe, K., Shibuya, H., Irie, K., Oishi, I., Ueno, N., Taniguchi, T., Nishida, E., and Matsumoto, K. (1995). Identification of a member of the MAPKKK family as a potential mediator of TGF-β signal transduction. Science *270*, 2008–2011.

Yamamoto, H., Kishimoto, T., and Minamoto, S. (1998). NF-κB activation in CD27 signaling: involvement of TNF receptor-associated factors in its signaling and identification of functional region of CD27. J. Immunol. Baltim. Md 1950 *161*, 4753–4759.

Yamamoto, H., Takashima, S., Shintani, Y., Yamazaki, S., Seguchi, O., Nakano, A., Higo, S., Kato, H., Liao, Y., Asano, Y., et al. (2008). Identification of a novel substrate for TNFα-induced kinase NUAK2. Biochem. Biophys. Res. Commun. *365*, 541–547.

Yamamoto, M., Yamazaki, S., Uematsu, S., Sato, S., Hemmi, H., Hoshino, K., Kaisho, T., Kuwata, H., Takeuchi, O., Takeshige, K., et al. (2004). Regulation of Toll/IL-1-receptor-mediated gene expression by the inducible nuclear protein IκBζ. Nature *430*, 218–222.

Yamashita, M., and Passegué, E. (2019). TNF-α Coordinates Hematopoietic Stem Cell Survival and Myeloid Regeneration. Cell Stem Cell *25*, 357-372.e7.

Yamazaki, K., Masugi, Y., Effendi, K., Tsujikawa, H., Hiraoka, N., Kitago, M., Shinoda, M., Itano, O., Tanabe, M., Kitagawa, Y., et al. (2014). Upregulated SMAD3 promotes epithelial–mesenchymal transition and predicts poor prognosis in pancreatic ductal adenocarcinoma. Lab. Invest. *94*, 683–691.

Yan, B., Wang, H., Rabbani, Z.N., Zhao, Y., Li, W., Yuan, Y., Li, F., Dewhirst, M.W., and Li, C.-Y. (2006). Tumor necrosis factor-α is a potent endogenous mutagen that promotes cellular transformation. Cancer Res. *66*, 11565–11570.

Yang, C.H., Gonzalez-Angulo, A.M., Reuben, J.M., Booser, D.J., Pusztai, L., Krishnamurthy, S., Esseltine, D., Stec, J., Broglio, K.R., Islam, R., et al. (2006). Bortezomib (VELCADE) in metastatic breast cancer: pharmacodynamics, biological effects, and prediction of clinical benefits. Ann. Oncol. Off. J. Eur. Soc. Med. Oncol. *17*, 813–817.

Yang, D., Zhao, X., and Lin, X. (2021). Bcl10 is required for the development and suppressive function of Foxp3+ regulatory T cells. Cell. Mol. Immunol. *18*, 206–218.

Yang, J., Liao, X., Agarwal, M.K., Barnes, L., Auron, P.E., and Stark, G.R. (2007). Unphosphorylated STAT3 accumulates in response to IL-6 and activates transcription by binding to NF-κB. Genes Dev. *21*, 1396–1408.

Yang, L., Cohn, L., Zhang, D.-H., Homer, R., Ray, A., and Ray, P. (1998). Essential Role of Nuclear Factor κB in the Induction of Eosinophilia in Allergic Airway Inflammation. J. Exp. Med. *188*, 1739–1750.

Yang, X., Yao, L., Fu, X., Mukherjee, R., Xia, Q., Jakubowska, M.A., Ferdek, P.E., and Huang, W. (2020). Experimental Acute Pancreatitis Models: History, Current Status, and

Role in Translational Research. Front. Physiol. *11*, 1685.

Yardley, D.A. (2013). nab-Paclitaxel mechanisms of action and delivery. J. Controlled Release *170*, 365–372.

Yatim, N., Jusforgues-Saklani, H., Orozco, S., Schulz, O., Barreira da Silva, R., Reis e Sousa, C., Green, D.R., Oberst, A., and Albert, M.L. (2015). RIPK1 and NF-κB signaling in dying cells determines cross-priming of $CD8^+$ T cells. Science *350*, 328–334.

Yeo, T.P., and Lowenfels, A.B. (2012). Demographics and epidemiology of pancreatic cancer. Cancer J. Sudbury Mass *18*, 477–484.

Yeung, T., Georges, P.C., Flanagan, L.A., Marg, B., Ortiz, M., Funaki, M., Zahir, N., Ming, W., Weaver, V., and Janmey, P.A. (2005). Effects of substrate stiffness on cell morphology, cytoskeletal structure, and adhesion. Cell Motil. Cytoskeleton *60*, 24–34.

Yin, M.-J., Yamamoto, Y., and Gaynor, R.B. (1998). The anti-inflammatory agents aspirin and salicylate inhibit the activity of IκB kinase-β. Nature *396*, 77–80.

Yin, Z., Sadok, A., Sailem, H., McCarthy, A., Xia, X., Li, F., Garcia, M.A., Evans, L., Barr, A.R., Perrimon, N., et al. (2013). A screen for morphological complexity identifies regulators of switch-like transitions between discrete cell shapes. Nat. Cell Biol. *15*, 860–871.

Ying, H., Kimmelman, A.C., Lyssiotis, C.A., Hua, S., Chu, G.C., Fletcher-Sananikone, E., Locasale, J.W., Son, J., Zhang, H., Coloff, J.L., et al. (2012). Oncogenic Kras maintains pancreatic tumors through regulation of anabolic glucose metabolism. Cell *149*, 656–670.

Yoshimura, H., Matsuda, Y., Yamamoto, M., Michishita, M., Takahashi, K., Sasaki, N., Ishikawa, N., Aida, J., Takubo, K., Arai, T., et al. (2018). Reduced expression of the H19 long non-coding RNA inhibits pancreatic cancer metastasis. Lab. Invest. *98*, 814–824.

Yoshimura, S., Bondeson, J., Foxwell, B.M., Brennan, F.M., and Feldmann, M. (2001). Effective antigen presentation by dendritic cells is NF-κB dependent: coordinate regulation of MHC, co-stimulatory molecules and cytokines. Int. Immunol. *13*, 675–683.

Younes, A., Nowakowski, G., Rosenthal, A.C., Leslie, L.A., Tun, H.W., Lunning, M.A., Isufi, I., Martell, R., and Patel, K. (2019). Phase 1 Dose-Finding Study Investigating CA-4948, an IRAK4 Kinase Inhibitor, in Patients with R/R NHL: Report of Initial Efficacy and Updated Safety Information. Blood *134*, 5327.

Young, K.G., and Copeland, J.W. (2010). Formins in cell signaling. Biochim. Biophys. Acta BBA - Mol. Cell Res. *1803*, 183–190.

Yu, G., Wang, L.-G., Han, Y., and He, Q.-Y. (2012). clusterProfiler: an R Package for Comparing Biological Themes Among Gene Clusters. OMICS J. Integr. Biol. *16*, 284–287.

Yu, J.H., Lim, J.W., Namkung, W., Kim, H., and Kim, K.H. (2002). Suppression of cerulein-induced cytokine expression by antioxidants in pancreatic acinar cells. Lab. Investig. J. Tech. Methods Pathol. *82*, 1359–1368.

Yu, J.W., Jeffrey, P.D., and Shi, Y. (2009). Mechanism of procaspase-8 activation by c-FLIPL. Proc. Natl. Acad. Sci. U. S. A. *106*, 8169–8174.

Yuan, W.-C., Pepe-Mooney, B., Galli, G.G., Dill, M.T., Huang, H.-T., Hao, M., Wang, Y., Liang, H., Calogero, R.A., and Camargo, F.D. (2018). NUAK2 is a critical YAP target in liver cancer. Nat. Commun. *9*, 4834.

Yunis, A.A., Arimura, G.K., and Russin, D.J. (1977). Human pancreatic carcinoma (MIA

PaCa-2) in continuous culture: sensitivity to asparaginase. Int. J. Cancer *19*, 128–135.

Zambrano, S., De Toma, I., Piffer, A., Bianchi, M.E., and Agresti, A. (2016). NF-κB oscillations translate into functionally related patterns of gene expression. eLife *5*.

Zarnegar, B.J., Wang, Y., Mahoney, D.J., Dempsey, P.W., Cheung, H.H., He, J., Shiba, T., Yang, X., Yeh, W.-C., Mak, T.W., et al. (2008). Noncanonical NF-κB activation requires coordinated assembly of a regulatory complex of the adaptors cIAP1, cIAP2, TRAF2 and TRAF3 and the kinase NIK. Nat. Immunol. *9*, 1371–1378.

Zatulovskiy, E., Zhang, S., Berenson, D.F., Topacio, B.R., and Skotheim, J.M. (2020). Cell growth dilutes the cell cycle inhibitor Rb to trigger cell division. Science *369*, 466–471.

Zhang, Z., and Rigas, B. (2006). NF-κB, inflammation and pancreatic carcinogenesis: NF-κB as a chemoprevention target. Int. J. Oncol. *29*, 185–192.

Zhang, D., Li, L., Jiang, H., Knolhoff, B., Lockhart, A.C., Wang-Gillam, A., DeNardo, D.G., Ruzinova, M.B., and Lim, K.-H. (2017a). Constitutive IRAK4 Activation Underlies Poor Prognosis and Chemoresistance In Pancreatic Ductal Adenocarcinoma. Clin. Cancer Res. Off. J. Am. Assoc. Cancer Res. *23*, 1748–1759.

Zhang, D., Li, L., Jiang, H., Li, Q., Wang-Gillam, A., Yu, J., Head, R., Liu, J., Ruzinova, M.B., and Lim, K.-H. (2018a). Tumor-Stroma IL1β-IRAK4 Feedforward Circuitry Drives Tumor Fibrosis, Chemoresistance, and Poor Prognosis in Pancreatic Cancer. Cancer Res. *78*, 1700–1712.

Zhang, J.Y., Green, C.L., Tao, S., and Khavari, P.A. (2004). NF-κB RelA opposes epidermal proliferation driven by TNFR1 and JNK. Genes Dev. *18*, 17–22.

Zhang, Q., Gupta, S., Schipper, D.L., Kowalczyk, G.J., Mancini, A.E., Faeder, J.R., and Lee, R.E.C. (2017b). NF-κB Dynamics Discriminate between TNF Doses in Single Cells. Cell Syst. *5*, 638-645.e5.

Zhang, X., Ren, D., Wu, X., Lin, X., Ye, L., Lin, C., Wu, S., Zhu, J., Peng, X., and Song, L. (2018b). miR-1266 Contributes to Pancreatic Cancer Progression and Chemoresistance by the STAT3 and NF-κB Signaling Pathways. Mol. Ther. Nucleic Acids *11*, 142–158.

Zhao, K., Wang, W., Rando, O.J., Xue, Y., Swiderek, K., Kuo, A., and Crabtree, G.R. (1998). Rapid and phosphoinositol-dependent binding of the SWI/SNF-like BAF complex to chromatin after T lymphocyte receptor signaling. Cell *95*, 625–636.

Zhao, X., Fan, W., Xu, Z., Chen, H., He, Y., Yang, G., Yang, G., Hu, H., Tang, S., Wang, P., et al. (2016). Inhibiting tumor necrosis factor-α diminishes desmoplasia and inflammation to overcome chemoresistance in pancreatic ductal adenocarcinoma. Oncotarget *7*, 81110–81122.

Zhong, H., SuYang, H., Erdjument-Bromage, H., Tempst, P., and Ghosh, S. (1997). The transcriptional activity of NF-κB is regulated by the IκB-associated PKAc subunit through a cyclic AMP-independent mechanism. Cell *89*, 413–424.

Zhong, H., Voll, R.E., and Ghosh, S. (1998). Phosphorylation of NF-κB p65 by PKA Stimulates Transcriptional Activity by Promoting a Novel Bivalent Interaction with the Coactivator CBP/p300. Mol. Cell *1*, 661–671.

Zhong, H., May, M.J., Jimi, E., and Ghosh, S. (2002). The phosphorylation status of nuclear NF-κB determines its association with CBP/p300 or HDAC-1. Mol. Cell *9*, 625–636.

Zhou, B.P., Deng, J., Xia, W., Xu, J., Li, Y.M., Gunduz, M., and Hung, M.-C. (2004). Dual

regulation of Snail by GSK-3β-mediated phosphorylation in control of epithelial–mesenchymal transition. Nat. Cell Biol. *6*, 931–940.

Zhou, L.Z., Johnson, A.P., and Rando, T.A. (2001). NF-κB and AP-1 mediate transcriptional responses to oxidative stress in skeletal muscle cells. Free Radic. Biol. Med. *31*, 1405–1416.

Zhu, J., Yamane, H., and Paul, W.E. (2010). Differentiation of Effector CD4 T Cell Populations. Annu. Rev. Immunol. *28*, 445–489.

Zhuang, Z., Ju, H., Aguilar, M., Gocho, T., Li, H., Iida, T., Lee, H., Fan, X., Zhou, H., Ling, J., et al. (2016). IL-1 Receptor Antagonist Inhibits Pancreatic Cancer Growth by Abrogating NF-κB Activation. Clin. Cancer Res. Off. J. Am. Assoc. Cancer Res. *22*, 1432–1444.

Zigmond, S.H., Otto, J.J., and Bryan, J. (1979). Organization of myosin in a submembranous sheath in well-spread human fibroblasts. Exp. Cell Res. *119*, 205–219.

Appendices

Table A1 TNFα-regulated genes in MIA PaCa2 and PANC1 cells

Gene	Cluster	Gene	Cluster	Gene	Cluster
AC145207.3	1	DDIT4	4	PIM3	6
AL662797.1	1	KCTD11	4	PLK3	6
SNX32	1	ZC3H12C	4	B3GNT5	6
AL133415.1	1	ARL5B	4	BTG2	6
AC006064.4	1	TP53BP2	4	NFKBID	6
AC068580.3	1	PATL1	4	NFKBIZ	6
AP003352.1	1	ANKRD10	4	NLRP3	6
VIM-AS1	1	SPPL2B	4	AL135999.1	7
XRCC4	2	PVT1	4	AC138393.1	7
AC010531.6	2	KIAA1109	4	HSF4	7
DNAJC3-AS1	2	TRAF4	4	AC138932.1	7
AL136162.1	2	HMGCS1	4	MPP3	7
AL137845.2	2	CSNK1E	4	DNHD1	7
AC087481.1	2	ERN1	4	PSMA3-AS1	7
CBX8	2	MAP3K8	4	AC087388.1	7
COPZ2	2	MTURN	4	ABCG1	7
FAM222A-AS1	2	ZNF140	4	PABPC1L	7
CCDC163	2	SCARF1	4	HERC2P2	7
KBTBD7	2	THAP2	4	TNFRSF25	7
LCA5L	2	CDK6	4	FAM229A	7
ZC2HC1A	2	ZNRF3	4	ALKBH6	7
AC097359.2	2	GPATCH2L	4	AMH	7
DLGAP1	2	PLEKHG5	4	PAQR6	7
AC023161.2	2	NUP58	4	IDUA	7
AC025171.1	2	FMNL2	4	AC018638.5	7
DNAH3	2	PPP1R15B	4	CCDC57	7
AC026412.1	2	FOXP4	4	LBHD1	7
TIGD4	2	PHLDB1	4	LTB4R	7
AF274858.1	2	BTAF1	4	DDX39B	7
LINC01278	2	PNN	4	AC020916.1	7
LINC01637	2	PLAU	4	AC021078.1	7
HOXA-AS2	2	PNRC1	4	LENG8	7
CMTR2	2	NBPF19	4	AL390728.4	7
FLVCR1-AS1	2	NEURL4	4	AL390728.6	7
TMEM140	2	NOCT	4	RTEL1-TNFRSF6B	7
STOML1	2	BTG1	4	CCNL1	7
TMEM182	2	GORAB	4	CCNL2	7
SEC62	2	NFE2L2	4	LINC-PINT	7

PPP1R7	2	SYNGAP1	4	MAMDC4	7
BHLHB9	2	SETD5	4	ADIRF-AS1	7
PNPO	2	NFKBIB	4	ASMTL-AS1	7
MET	2	GCNT2	4	ZGPAT	7
C9orf78	2	ULK3	4	TRIM36	7
RHPN1-AS1	2	SLC25A37	4	AGAP6	7
TACO1	2	GGA3	4	SAT1	7
SLC29A3	2	GIGYF1	4	ZNF136	7
SNAI2	2	REL	4	FER1L4	7
AL138724.1	3	RNF207	4	CLUHP3	7
TNFAIP3	3	ROBO3	4	EGLN2	7
ARHGAP31	3	SH3D21	4	AHSA2P	7
TRAF1	3	CATSPER2	5	AC126755.1	7
TIFA	3	AC093525.8	5	SCNN1D	7
CD70	3	AC022400.5	5	CYP27B1	7
CD83	3	ZMIZ1-AS1	5	PGGHG	7
CXCL1	3	CXCL8	5	PILRB	7
IRF1	3	LINC02340	5	MDN1	7
PLEKHF1	3	AC009549.1	5	MIR17HG	7
BCL3	3	CARD9	5	BTBD19	7
NUAK2	3	RANP2	5	MIR222HG	7
BIRC3	3	MIR29B2CHG	5	PI4KAP1	7
NFKB2	3	NFKBIA	5	GOLGA8A	7
NFKBIE	3	JUNB	6	GOLGA8B	7
RELB	3	IER3	6	NBPF26	7
ZNF267	4	DUSP1	6	NBPF8	7
CNTNAP1	4	DUSP8	6	UBR4	7
FAM126B	4	KDM6B	6	GABBR1	7
ZNF276	4	MAFF	6	NPIPB2	7
CEP95	4	LIF	6	SLFNL1-AS1	7
DCP1A	4	ZFP36	6	RNASEK	7
TNFRSF10B	4	CD274	6	SMG1	7
DCUN1D3	4	N4BP3	6		
PANK3	4	BBC3	6		

Table A2 Divergent genes between MIA PaCa2 and PANC1 cells

Gene	Fold Change (log_2) > 0 upregulated in MIA PaCa2 < 0 upregulated in PANC1	Gene	Fold Change (log_2) > 0 upregulated in MIA PaCa2 < 0 upregulated in PANC1	Gene	Fold Change (log_2) > 0 upregulated in MIA PaCa2 < 0 upregulated in PANC1
ABCA10	5.42204289	FRMD3	-3.5855772	PLEKHA5	-4.5062285
ABCA4	-4.6872622	FRMD4A	-2.7365615	PLEKHA7	-4.7443014
ABCC1	-2.9772113	FRMD5	-2.9714745	PLEKHG1	-6.2846633
ABCC2	6.18535406	FSCN1	-8.5839853	PLEKHG2	-5.9401795
ABCC3	-7.0623556	FTH1P3	4.26318256	PLEKHG4B	-4.8506882
ABHD6	-3.0797646	FUCA1	-3.4045003	PLEKHH2	-4.2764307
ABHD8	-2.6194032	FXYD6	5.67750459	PLEKHO1	2.75948816
ABLIM3	-5.7640354	FZD4	2.96398267	PLK2	2.9235442
AC004816.1	-4.2420483	FZD7	-2.8073116	PLPP7	-3.4119386
AC006064.4	4.18679424	FZD8	5.03140147	PLTP	3.10985763
AC007842.1	-4.0829884	G6PD	-2.5344335	PMEPA1	-2.6093306
AC008556.1	-2.5260047	GAB3	-4.4392694	PODNL1	3.61674833
AC009118.2	3.16477021	GABBR2	-4.3075048	PODXL	6.21234183
AC009120.2	2.88530096	GALC	-2.6848414	POLN	-3.5970235
AC009831.1	2.64163648	GALNT18	-5.0230183	PPFIBP2	-2.9147592
AC010735.2	2.58417385	GALNT6	-3.8377403	PPP1R13L	-3.5391821
AC015712.6	-3.055898	GALNT7	-9.1555738	PPP1R26-AS1	4.0833557
AC016027.1	3.00096642	GAS1	7.94903946	PPP1R3G	3.4438583
AC017100.1	-3.0983136	GATA3	-3.2509672	PPP2R2C	-3.9501748
AC020928.1	-2.7191143	GCHFR	-7.1966344	PPP3CA	-4.9089654
AC020928.2	-2.7283841	GCLM	2.69186036	PPP4R4	2.72995837
AC021218.1	2.86007933	GCNA	-2.6102216	PRDM1	-4.0124297
AC026250.1	-4.3573077	GDF15	-9.6808495	PRDM8	4.02888138
AC026471.3	3.00759405	GGT1	2.52193117	PREX1	-6.0660095
AC037459.3	2.94221987	GGT5	-4.3508213	PRICKLE1	4.23219918
AC068282.1	-3.9606133	GGT7	-3.2512618	PRKAA2	-4.6123915
AC078923.1	5.29530851	GINS4	5.35910296	PRKAR2B	8.27490023
AC080112.1	-2.7207742	GJB2	-7.1931665	PRKCG	-2.9834413
AC092807.3	-3.0478205	GJB3	3.48458738	PROB1	-2.5270387
AC092919.2	-3.3904576	GLDN	-2.893302	PROCR	-2.7227449

AC096537.1	2.93363735	GLIPR1	-3.1565672	PRR5L	3.97243881
AC103702.2	-3.1891315	GLIS2	-2.9347971	PRRG4	4.6295603
AC104794.2	-3.3952735	GMFG	-2.6343657	PRSS33	-3.7274792
AC106820.1	-4.4158949	GMPR	-3.9151868	PSD3	3.38238996
AC110079.1	-3.9872594	GNA12	-3.0829576	PSD4	3.26645673
AC116351.2	-2.6642651	GNAL	4.55971896	PSMB8	-3.4912274
AC134878.2	-2.9386153	GNB3	2.99033751	PSMB9	-3.702158
AC142472.1	2.90200104	GOLGA2P7	-2.7145143	PSMC4	-4.072147
AC145098.2	2.77474876	GOLGA7	2.57552307	PTGER4	-4.2941364
AC241952.1	2.67814787	GOLGA7B	-3.391938	PTGIS	-4.1050749
ACAP1	-3.6112452	GPC2	-2.7923476	PTK6	-2.7527111
ADA	-3.018904	GPR1	5.51736031	PTPN6	-6.4530563
ADAM19	-6.9722504	GPR146	2.58782523	PTPRE	4.35446085
ADAM22	3.21218673	GPR161	2.94705263	PTPRH	-2.7230226
ADAM23	5.19265613	GPR39	-4.4176844	PTX3	-5.293923
ADAMTS6	-5.0742886	GPRASP1	-4.4156562	PWAR5	-3.2259388
ADAMTS7	2.81048248	GPRC5B	-2.8741761	PWAR6	-3.5943762
ADAMTSL4	-2.8489902	GPRC5C	-4.827246	PWP2	3.38408984
ADCY5	2.57774467	GRAMD2B	2.82921415	PXK	-3.253793
ADGRG1	-2.5528102	GRIK2	-2.671071	RAB11FIP4	-3.1554967
ADHFE1	-2.5040587	GRIN2D	-3.1518789	RAB26	-8.0310726
ADM	-6.3154921	GRIN3B	-3.5512569	RAB27B	4.98982442
ADORA1	3.73741585	GSC	3.47898443	RAB3IP	-2.5671943
ADRB1	-4.093657	GSE1	-2.5740252	RAC2	5.22762771
AFAP1	-2.9330029	GSTT2B	3.00645395	RAI14	4.81558714
AFAP1L2	-3.6848143	GTF2H2B	3.39144998	RALGPS2	3.0744394
AGAP7P	-3.3055201	GUCA1B	-2.865186	RAP2B	2.57793066
AIG1	-3.6437155	GULP1	-4.593623	RAPGEF3	-2.763809
AK4	5.38361603	H19	-6.0352061	RARRES3	-3.2659793
AK5	3.74548538	H2AFY2	4.58737823	RASD1	-5.0767744
AKAP12	-5.3028239	HAP1	-4.3622348	RASD2	-5.8614692
AKT2	-4.0892489	HAPLN3	-6.1161177	RASGEF1A	-3.1634073
AL109976.1	-3.2660319	HAR1A	-3.1514978	RASL10B	4.170497
AL133415.1	4.36979239	HAS3	-3.5366065	RASSF2	5.22018405
AL160408.1	3.53653037	HBEGF	2.52619451	RBM44	-2.500506

AL161431.1	3.50104326	HDAC9	3.10916302	RBM47	3.49210738
AL353150.1	3.38619565	HECTD2	-3.0523267	RCN3	-4.7782821
AL365181.2	4.67295918	HECW1	4.65734023	RECQL	2.57694085
AL365181.3	3.33728422	HECW2	-2.7398504	REEP1	3.71483655
AL365203.2	-2.8024225	HEG1	-3.3242043	RFTN1	2.98089212
AL365356.5	2.70887881	HES1	-3.2059986	RGPD8	-4.5954249
AL390719.1	-2.9412814	HES2	-3.9165939	RGS2	-4.1596702
AL450998.1	-4.6169114	HES7	-4.2292504	RGS5	3.11678791
AL512488.1	7.27892331	HEYL	-3.4894493	RHBDL2	-4.287252
AL590666.2	2.65429632	HHIPL1	-6.9606636	RHBDL3	3.04824166
AL591846.1	4.99966306	HID1	-3.9785293	RHOBTB2	2.9727583
AL592494.3	3.34531736	HIPK2	-2.9533197	RHPN2	-3.7562406
ALDH1L2	-2.8217549	HIST1H1B	2.6758521	RIMKLA	-2.9222162
ALS2CL	-3.0058486	HIVEP2	-2.7279003	RIPK4	-3.4229929
ALX4	-2.7168614	HK2	2.55335557	RNF128	3.59219803
AMOTL1	4.23767293	HOXB-AS3	-3.6975542	RNF208	-2.6155366
ANGPTL6	-2.6765934	HOXB4	-3.3038378	RNF217	-5.1750661
ANKEF1	-6.3690667	HOXB8	2.50713609	ROBO1	-6.7810992
ANKRD2	-3.4234184	HOXC6	-4.6325947	ROR1	-4.1842011
ANKRD31	2.60433642	HPDL	4.16834781	ROR2	-4.7078463
ANO1	7.25721668	HPSE	-4.7576833	RPL10P13	2.68040439
ANTXR1	-2.6351317	HR	-3.7492231	RPS16	-4.0716673
AOX1	-5.2481988	HSD17B14	-3.182023	RPS28P7	2.74849178
AP001062.1	3.07471143	HSD17B8	-3.2190987	RPS6KA2	-7.0034218
AP002478.1	3.42483714	HSPA2	-4.119823	RPS6KL1	-2.9191765
AP006621.5	-2.690288	HSPG2	-4.2696701	RPSAP58	-3.1451184
AP1S3	-3.43048	HTR6	5.47359193	RRAD	-4.3089449
APBB1	2.53984996	HTR7P1	2.81531111	RRAGD	2.68785663
APLF	-3.4236618	IER3	-2.5537248	RSPO4	4.83134112
APLN	3.09683275	IFITM3	-4.9296237	RTL8B	-4.1779428
APOE	-8.4024562	IGF2	-3.7579323	RTN4RL2	2.80230012
AREG	7.29682805	IGFBP2	-9.0077386	RUNDC3A	-2.5538824
ARHGAP26	-4.2987269	IGFBP6	6.0238922	RUNX1	2.73909751
ARHGAP4	-6.8237625	IL11	-5.6909408	RUNX2	-3.8311179
ARHGAP42	-7.7021524	IL11RA	-2.6567317	S100A1	-2.7956854

ARHGAP45	-3.8170941	IL15RA	-2.9044164	SAMD11	-5.3440502
ARHGAP5-AS1	3.80955813	IL17D	2.52989648	SAMD14	-2.5525423
ARHGEF6	-3.6122396	IL17RB	-4.8769312	SAMD4B	-2.9335642
ARL10	-3.2025429	IL18	-8.9498822	SAMD5	2.61217611
ARSJ	-3.1631599	IL31RA	-6.4668111	SARS2	-3.123373
ATF7IP2	-2.7963994	IL6R	-2.9894155	SCARA3	3.39651008
ATP10D	-3.6058892	INHBB	-6.7137861	SCG2	5.81736758
ATP1B1	-2.5543095	INTS6L	-5.2556519	SCRN1	-3.1686882
ATP2A3	-7.2878276	IQCA1	7.58610643	SDHAF1	-3.0913243
ATP6V0D2	5.60325778	IQCD	-4.034799	SEL1L3	2.73470523
B3GNT5	-4.1863207	IQGAP2	6.2276157	SEMA3A	6.85302405
B4GALT6	-3.8204823	IRAK2	-4.0482064	SEMA3F	-3.8370619
BACH2	-2.5460659	IRS2	3.46171436	SEMA4B	-4.406706
BAIAP2L1	-3.7157218	ISL2	4.2961413	SENCR	2.58881306
BARX2	6.25116032	ISYNA1	-2.6053551	SERINC2	-3.526752
BCAM	-4.2115243	ITGA1	-3.3586633	SERPINB8	5.25618091
BCAR3	2.99324421	ITGAV	-2.5954754	SERPINB9	4.05234862
BCL2	5.7460875	ITGB5	-4.1014702	SERPINE1	-4.5153416
BCL7A	-2.5930832	ITGB6	3.87556509	SERPINF1	2.89311351
BDNF	4.36003525	ITPKB	-5.7621308	SERPINI1	-3.2094454
BEST1	3.87130157	JCAD	-2.5497218	SFN	-6.7734326
BEX2	-5.8317545	JHY	-2.8008375	SFR1	2.88597959
BICDL1	-3.0911627	JUP	-5.6545046	SFRP1	-5.9208428
BMF	-3.9022874	KCNC1	-4.3190532	SGK1	5.13675885
BMP6	-6.587276	KCNK5	4.06453662	SH2D3C	-2.5304635
BMS1P8	-2.8286865	KCTD12	-4.0798774	SH3BGRL2	-4.1440244
BNIP3L	2.5130534	KHDRBS3	-2.5473652	SH3BP4	-3.6466534
BOLA3-AS1	-3.257133	KIAA1217	-4.5726163	SH3RF3	-3.5640182
BTC	4.88988182	KIAA1755	6.27968853	SH3TC2	7.08809728
BTNL9	-4.6237655	KIF17	-3.2381577	SH3YL1	-2.5378454
BX322562.1	-4.5910768	KIF1A	-3.8145366	SHC3	3.64490123
C17orf107	-3.8136252	KIF9-AS1	-2.6804164	SHH	-2.896883
C19orf57	-2.9329515	KLF14	-3.7782438	SHTN1	-2.6057259
C1QL1	-3.7673151	KLF2	4.56059109	SIK1B	2.82967099
C1QTNF12	-6.8162696	KLF9	3.73376331	SIX2	-4.5712134

C1S	3.64354031	KLHDC7B	-2.9313623	SKIDA1	-3.0308525
C21orf33	3.64896952	KLHL29	-4.9496869	SKIL	-3.6151621
C3orf80	2.90117543	KLHL4	-4.6784092	SLC16A3	-2.7658046
C7orf31	-3.381356	KPNA7	-3.0598584	SLC1A1	2.67691449
C8orf37	-2.7666742	KREMEN2	-3.0158552	SLC22A15	-2.5207184
C8orf46	2.68631822	KRT7	-4.2271551	SLC22A23	-2.519621
C8orf49	-2.5331067	KRT80	-2.5339323	SLC2A8	-4.6173185
C9orf3	-3.6411841	KRT81	-2.8692976	SLC30A3	2.82582223
CA5B	-2.6297068	L1CAM	-4.6335325	SLC39A8	-2.8936341
CABLES1	-2.9552644	LAMA2	3.21497282	SLC3A1	-4.9600978
CACNA1D	-6.3845934	LAMA5	-4.4143831	SLC43A1	3.31176661
CACNA2D1	-8.0689514	LAMB1	-4.0255869	SLC48A1	-3.1392057
CACNG7	-6.0532625	LAMB2	-2.6300221	SLC4A11	-3.8775477
CACNG8	-4.3714482	LAMC3	-5.5578473	SLC4A7	-2.501446
CALB2	7.43173493	LAMP3	-4.8687443	SLC6A6	-2.6066788
CAMK2B	3.775586	LAPTM5	4.82069356	SLC9A2	-3.1105554
CAMK2N1	3.61469222	LARGE1	4.84145861	SLC9A3-AS1	2.66100223
CAPN12	-5.9940319	LBX1	3.72158466	SLCO4A1	3.10736629
CARD10	-2.8580419	LCA5	-3.1675178	SLFNL1-AS1	-2.6569024
CARD6	4.16906993	LCTL	4.5160645	SLIT1	-3.1316764
CARS2	2.63510598	LFNG	-3.4772579	SMAD3	-3.1847601
CBR3	2.80451299	LGR4	-4.6482913	SMAD6	-5.7107426
CBSL	6.03070701	LHFPL6	-2.8800501	SMAD7	-4.7296652
CCDC136	2.60540484	LHX1	3.5006464	SMARCA4	3.99912916
CCDC15	3.13051609	LHX1-DT	3.69406913	SNAI2	3.37516583
CCDC68	4.36433973	LINC00511	-3.9553712	SNHG14	-2.8917219
CCDC73	2.65894091	LINC00665	-4.2611843	SNRPN	-2.5045167
CCDC80	4.06595871	LINC00704	4.55390142	SOBP	-3.1790534
CCDC88C	-3.1007839	LINC00886	-5.1212088	SOCS2	-5.0995086
CCNJL	-4.6243448	LINC01123	-3.0156185	SORBS1	-2.5375973
CCNO	4.46056513	LINC01152	-2.9002401	SOWAHC	-2.5162346
CCT6B	3.44422005	LINC01503	-3.2041954	SOX4	-4.4828837
CD22	5.54839277	LINC01588	4.29345497	SPARC	-10.559227
CD24	-10.539253	LINC01833	-2.8267539	SPINT2	-10.581976
CD274	5.37394255	LINC02086	-4.905616	SPNS2	-6.3470163

CD40	-3.0863055	LLGL2	-2.9958928	SPOCD1	4.26172564
CD55	-4.6402852	LMNTD2	-3.1123785	SPOCK2	-2.5996837
CD70	-7.9178875	LMO7	-2.8818409	SPSB1	-2.8922101
CDA	3.67373154	LMTK3	-4.9705345	SQOR	-3.9815747
CDC42EP5	-4.9976409	LOXL4	-7.859931	SRGN	12.0712659
CDH3	-3.7818532	LPAR2	-2.6389144	SSC5D	-5.7306791
CELF5	-3.5145163	LPXN	4.53457167	SSPO	-3.1597771
CERKL	3.26532377	LRP5	-2.6620676	ST3GAL1	-4.9306474
CFAP53	2.51215958	LRRC1	-3.9518678	ST6GALNAC2	-3.2054961
CFP	2.67882772	LRRC37A4P	5.21886849	STAP2	-5.4361841
CGN	-2.7826703	LRRC56	-3.2390493	STOM	-3.1470777
CGNL1	-3.7982582	LRRN2	-3.6206296	STS	3.02611442
CHDH	-2.6081586	LTBP1	-3.2234438	STXBP2	-6.1149037
CHRNB1	-3.5591271	LTBP2	-6.4137868	SUGCT	-3.120701
CHST2	3.84918368	LTBP4	-3.2692385	SUPT5H	-3.9033481
CITED4	-3.0012817	LTBR	8.22730284	SUSD2	-3.9550864
CKB	-4.66152	LYNX1	-3.8623908	SUSD4	5.71188953
CKMT1A	-2.5214125	LYPD3	-3.5269122	SYNGR3	-2.7276647
CLCF1	3.08280967	MAFK	-3.0438173	SYNM	-2.8642703
CLCN4	-2.7998161	MAML3	-5.3056753	SYNPO	-7.2190516
CLDN11	6.8422197	MAMLD1	-3.8614822	SYT12	-2.5743874
CLDN23	-3.2933427	MAMSTR	-2.8963335	SYT5	-3.8307784
CLDN4	-3.0067472	MAP2	-3.0984109	SYTL1	-4.1860507
CLIP3	-4.6613046	MAP2K6	-3.9119881	SYTL2	-5.1771226
CLN8	-4.1290835	MAP3K10	-4.3557069	TAGLN	4.11998219
CNIH3	4.44904417	MAP3K15	-2.6910286	TAGLN2P1	-2.7394287
CNN3	-4.740644	MAP3K9	-2.934246	TBC1D2	5.005197
CNTNAP3	-3.3576362	MAP4K1	-4.2362248	TBC1D30	-6.2941003
COL13A1	5.0468057	MAPK13	-3.9006037	TBC1D8	-5.0183971
COL16A1	-4.3908439	MAPK15	-3.5101756	TCEA3	-4.5887995
COL18A1	-3.201085	MAPT	2.87279244	TCN2	-5.6135381
COL26A1	-5.7414418	MATK	3.53956583	TERT	-2.865122
COL5A1	-5.9225026	MCAM	-7.5942968	TEX15	4.91983301
COL6A3	5.90407999	MCIDAS	3.06486717	TFAP2E	-2.7841979
COL7A1	-3.6422128	MCPH1-AS1	2.55655884	TFCP2L1	-2.6377748

COLEC11	3.57990863	MDK	-5.9435354	TGFBI	-4.3935659
COX20P1	4.36529492	ME3	-6.8739805	TGFBR3	2.67687762
CPEB2	-2.7243536	MED29	-4.1819889	TGM2	3.30334859
CPPED1	-4.4152308	MERTK	-3.9209008	THSD4	-7.3402704
CRABP2	-10.272287	MET	-4.463093	TIAF1	3.12896971
CRLF1	2.58934835	METRN	-3.1030746	TIAM2	-3.3637279
CROT	-2.7618985	METTL25	-3.1459211	TIMM50	-4.1599848
CTGF	-4.9389766	MEX3C	2.79672422	TIMP2	2.72149834
CUBN	4.72746835	MFGE8	-4.6768972	TLN2	-2.7817834
CXADR	-6.1826578	MGLL	-2.5406536	TLR5	3.70875283
CXCL1	3.74438619	MGST1	2.64089897	TM4SF18	2.50799193
CXCL5	6.33446034	MICB	-4.2394012	TMC6	-2.8643646
CXCL8	7.84865661	MID1	-8.0795997	TMEM102	-6.1626323
CYBRD1	3.87596207	MIPOL1	-2.7530922	TMEM132A	-2.6097675
CYP1B1	-6.7700938	MIR100HG	-4.4550659	TMEM140	-2.8362575
CYR61	-3.1058493	MIR4767	2.75349213	TMEM145	-2.8062819
CYS1	-3.6493021	MISP	-3.7852154	TMEM150C	-3.3387032
DAAM1	-3.7045495	MITF	-3.5018222	TMEM151A	-4.9105338
DCBLD1	-2.7770572	MMP17	-4.6381477	TMEM158	2.65569648
DCDC2	8.85442407	MMP25	-4.1994549	TMEM173	-2.5500213
DCHS1	-2.80739	MMRN2	3.31727276	TMEM184A	-5.1092339
DDN-AS1	-3.8552394	MN1	2.80052475	TMEM200B	-3.1827687
DDR2	6.22621967	MOK	4.70352803	TMEM217	-3.0957793
DDTL	2.88766804	MRPS12	-2.671275	TMEM25	-6.6133635
DDX60	-2.5319464	MSX2	-3.7385488	TMEM255B	-2.5930253
DEF6	7.66696428	MT1M	2.56160818	TMEM40	-3.2357787
DENND3	-3.521323	MT1X	2.53652022	TMEM56	3.81138663
DEPTOR	-4.8423776	MUC1	-2.5375437	TMEM63C	-3.152277
DHRS3	-3.6155647	MUC3A	-7.9891809	TMEM65	-3.8942987
DKK3	-7.4157369	MX2	2.84185168	TMEM9B-AS1	-3.4099865
DLG1	3.39176114	MXRA8	-11.408444	TMIE	-4.5347968
DLL3	-6.2552735	MYH16	5.43674605	TMTC2	2.96594298
DMKN	-3.4954587	MYO15B	-2.8478957	TNFRSF11A	-6.2359442
DMTN	6.1804796	NAP1L4P1	2.65034301	TNFSF9	-3.3446691
DNAJA4	8.17282415	NAPRT	-3.1192375	TNIK	-3.0115356

DNER	7.15287542	NAV3	-5.4904281	TNNC1	-3.1032707
DNM1	-3.2672551	NEBL	-6.4321654	TP53INP1	-3.0938634
DOC2B	-2.7763533	NECAB2	4.01352727	TP63	7.86200697
DOCK11	5.09437307	NECTIN3	5.30236633	TPBG	-5.2420395
DOCK4	-4.8778015	NEDD4L	3.79257422	TPCN1	-2.897502
DPY19L2	-3.8122861	NES	-7.7146782	TPM1	-4.7926346
DPYD	3.61201532	NEU4	-5.2955045	TPPP3	-2.5168713
DPYSL2	2.72466467	NEXN	-5.4960488	TRABD2A	4.89545522
DPYSL4	-4.6465709	NFASC	-5.8975369	TRAF3IP2	-3.0287697
DPYSL5	5.78832486	NFATC2	-6.336956	TRIB1	-2.8751256
DSEL	-4.433472	NFIA	-4.6975601	TRIM36	3.76304012
DUSP6	-3.2247532	NFKBIB	-3.0345448	TRIM46	-3.4846247
DYRK1B	-7.310527	NGFR	5.30118059	TRIM55	9.58402785
E2F5	-2.6036288	NKILA	-2.5677083	TRIP6	8.75179093
EBF3	4.45700417	NLRP3	4.72252722	TRNP1	-4.8754431
ECH1	-3.9891633	NMRK1	-5.0376324	TRPM8	-2.9814277
EDARADD	-3.9759672	NNT	-4.7150033	TRPV2	-3.3180786
EEPD1	-3.3560829	NOMO3	-4.1722872	TRPV4	2.86008803
EFEMP2	-4.8822721	NOTUM	-2.703701	TSPAN13	-7.6420285
EFNB2	6.37743954	NPW	-5.4481715	TSPAN15	-4.2968158
EFR3B	-2.6260426	NR2F1	2.82340503	TSPAN31	-2.8524801
EGFLAM	-4.7995239	NRP1	-5.4601472	TSPAN5	-8.7973836
EI24P2	3.56682674	NRROS	2.88419093	TTLL6	-2.7268839
EID2	-3.5381573	NUAK1	-4.4648557	TUBB2A	3.66241045
EIF3K	-3.1864349	NUAK2	-4.6830617	TXNIP	2.93133498
ELF3	-3.8926244	NUDT11	-5.5416743	TYMP	-6.3578836
ELOVL2	-5.568612	NUDT7	-2.7997798	UBA7	-3.2747403
EMILIN2	-2.7287606	NUP210	-2.5430556	UBASH3B	-2.8360151
EML6	-2.5764342	NUPR1	-8.2712593	UBE2FP1	2.55453322
ENHO	-2.6207939	NXN	-3.7926584	UNC13D	-3.8492157
ENPP1	-3.6372985	NXPE3	-2.8373175	UNC5A	3.18497136
EOMES	-3.7361275	NYAP1	-2.5160632	UPK3B	-3.3457784
EPAS1	-3.8164145	OAS1	-3.5813378	UPP1	-6.0719153
EPB41L4B	-5.538091	OAS3	-3.3190614	USP53	-5.5457338
EPHX4	3.25207809	OASL	-3.5194306	UST	4.97515961

EPS8L1	-5.6321346	OGDHL	4.57230427	VASN	-3.3462194
EREG	7.50998967	OLFML2A	-3.4857308	VEPH1	5.95191684
ESCO2	2.53171109	ONECUT2	4.07900967	VILL	-2.9136981
ESRP2	-7.0708438	OPN3	-6.3599984	VIM-AS1	2.86755476
ETS2	-6.2650495	OSBPL3	2.64005448	VPS35L	-4.418209
EVA1C	-3.9325801	OSCAR	-6.9545266	VWA5A	-2.5798117
F11R	-5.7515632	OTUB2	-2.7663215	VWA7	-3.4340284
F2RL1	-6.7593714	OXSM	5.77699579	WASF3	-6.0480562
FAAH	-4.4403659	P2RX6	3.35227354	WDR66	-4.4376113
FABP5	-6.7460318	P3H2	-3.6514534	WDR90	-4.2601425
FADS2	-3.0971623	P4HTM	-2.8851358	WDR97	-2.8125763
FAM102A	-3.4179355	PACSIN1	3.16387042	WFIKKN1	-2.7855553
FAM107B	-5.552402	PAF1	-4.6857892	WLS	-5.6926848
FAM135A	-4.3153156	PANX2	2.7695144	WNT10A	-5.9328918
FAM171B	-3.9453498	PARD6B	-4.714338	WNT5B	-4.8138927
FAM174B	-4.6614921	PARD6G-AS1	2.65807544	WNT6	-3.8094636
FAM198B	4.97993205	PARP10	-3.5254416	WNT9A	-2.693381
FAM43A	-3.8432959	PAX2	-2.6511061	WT1	-3.2188081
FAM46B	-3.5799112	PAX6	4.82019461	WWC1	-3.0749665
FAM46C	-4.9372423	PCAT6	-2.5772879	XPO7	2.66615111
FAM57B	-2.7676058	PCDH1	4.19611551	ZBTB42	-3.8237714
FAM71D	-6.3041602	PCDH18	-3.7076664	ZDHHC2	-3.4889126
FAM72C	3.47577882	PCDHAC2	-3.315273	ZDHHC8P1	2.56710899
FAM86DP	-3.8656758	PCDHGB2	-3.7363804	ZFAND4	-2.6001556
FANK1	-4.0733457	PCGF5	-2.7717231	ZFP36	-4.9575082
FAT4	-4.7525898	PCOTH	3.47628634	ZFYVE28	-3.1378889
FBL	-4.005727	PDE3B	-3.1713246	ZG16B	-5.0333301
FBLL1	-6.0095361	PDE4A	-5.7000009	ZHX2	3.04288146
FBLN5	2.61710629	PDE9A	3.68542864	ZMAT1	-2.5775314
FBXO17	-3.2011733	PDGFB	-4.57401	ZMYND10	-2.7633337
FBXO27	-3.2368824	PDLIM1	-6.8129358	ZNF185	-3.08115
FBXO32	-6.5497169	PDX1	-4.2148757	ZNF22	4.72113381
FCER1G	2.9728668	PERP	-3.1748847	ZNF395	2.66107594
FCGBP	-4.808896	PGM2L1	-3.5056993	ZNF467	-2.8439613
FERMT1	5.18341133	PHEX	3.13539866	ZNF469	-4.4131325

FEZ1	3.14178431	PHLPP1	4.52895447	ZNF503	4.44489198
FGD4	-3.3896528	PI4KAP1	2.52869278	ZNF528	3.04508
FGF1	4.36530514	PIK3C3	2.50708148	ZNF546	-5.1303795
FHL2	-3.7050169	PITPNC1	-3.0808245	ZNF568	-3.542797
FHOD3	-5.888968	PIWIL4	-3.3789768	ZNF594	3.42705134
FKBP1B	-4.4929364	PKD1P5	3.24739213	ZNF641	-3.8036237
FLI1	5.09721072	PLAT	-2.6247176	ZNF697	-2.6898677
FLNC	-8.4631887	PLAUR	4.28275316	ZNF713	-2.6659304
FLVCR2	-2.5227117	PLB1	3.49420027	ZNF714	4.71932373
FMN1	2.94784227	PLCD4	-3.2982291	ZNF761	-2.6431433
FN1	3.53080897	PLCE1	-3.9730298	ZNF780A	-4.0369996
FOXL1	-4.6349856	PLCG1-AS1	3.15027166	ZNF780B	-3.596839
FOXL2NB	-5.3051407	PLCL2	-4.3267358	ZNF860	-3.697906
FOXQ1	-5.2316776	PLD1	-4.9470665	ZNF888	-2.6324709
FRG1EP	-2.5159643	PLEKHA1	-2.9044957	ZSWIM5	-3.8553287

Appendix 3 PDAC prognosis according to NUAK2 expression

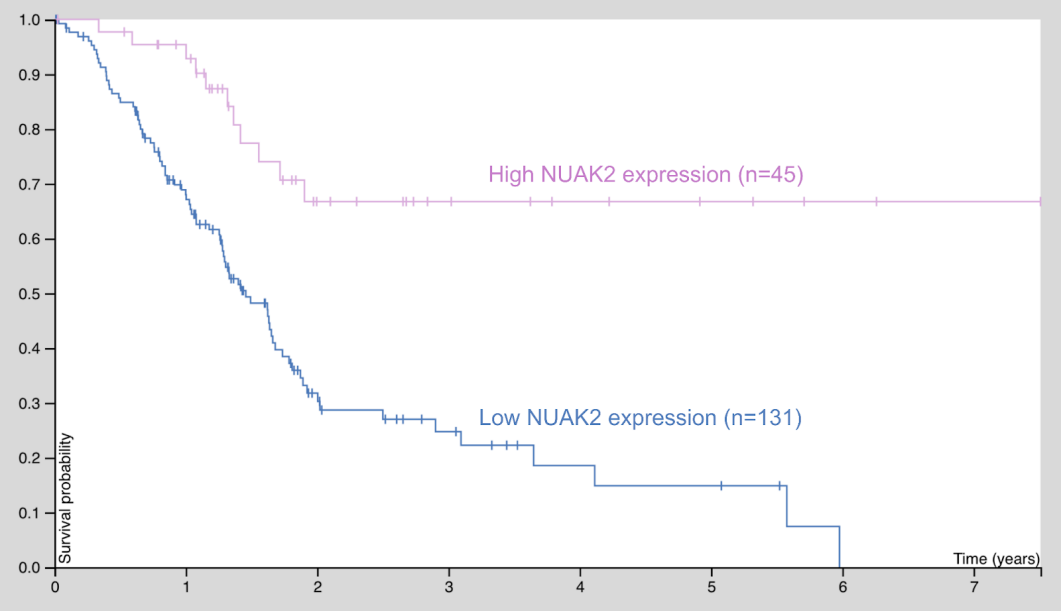

The Human Protein Atlas analysis of survival probability in pancreatic patients with high (n = 45) or low (n = 131) NUAK2 expression.